

Design and Development of Chiral Catalysts for Highly Enantioselective
Hydrogenation of Amides via Dynamic Kinetic Resolution Under Low Pressure at
Room Temperature

by

Loorthuraja Rasu

A thesis submitted in partial fulfillment of the requirements for the degree of

Doctor of Philosophy

Department of Chemistry
University of Alberta

© Loorthuraja Rasu, 2017

Abstract

Amide reduction has a long, important history in pharmaceutical and related chemical industries. Traditional stoichiometric reduction methods suffer from numerous drawbacks such as limited functional group tolerance, poor atom economy, and environmental issues. Over the past two decades, significant effort has been dedicated to the development of greener synthetic approaches to amide reduction. Several transition metal (Ru, Fe, Ir, and Mn), bifunctional, and pincer type catalysts were developed for the hydrogenation of amides. These catalysts typically hydrogenate amides under 10–50 atm H₂ at 80–150 °C in acidic, neutral, or basic conditions to produce C–O, or C–N cleavage products. This dissertation describes three independent projects on amide hydrogenation. Chapter 2 describes a base-free catalytic system containing [Ru(η^3 -C₃H₅)(Ph₂P(CH₂)₂NH₂)₂]BF₄ and NaBH₄ for the hydrogenation of amides (0.1–1 mol% Ru, 0.2–2 mol% NaBH₄, 50 atm H₂, 100 °C in 24 hours) to produce the corresponding alcohol and amine products of C–N cleavage. A variety of functional groups tolerated the hydrogenation.

Recent mechanistic studies show that Noyori's hydrogenation catalyst, *trans*-RuH₂((*R*)-BINAP)((*R,R*)-dpen), can be deprotonated at the N–H position, and the resulting catalysts are extremely active (–80 °C under ~2 atm H₂) towards the hydrogenation of imide and amide functional groups. These results motivated the development of an enantioselective catalyst for the hydrogenation of amides reported in this dissertation. A detailed study of high throughput rapid screening, lab-scale screening, and optimization are described in Chapter 3. The moderately air

stable, crystalline dichloride precursor *trans*-RuCl₂((*S,S*)-skewphos)((*R,R*)-dpen) was utilized with 2-PrONa as base in the presence of 2-PrOH to hydrogenate racemic α -chiral amides to form chiral primary alcohols in high yields and excellent *ee* (up to 99% yield, 99% *ee*) via dynamic kinetic resolution at room temperature.

An unexpected hydrogenolysis of an sp^3 - sp^2 C-C bond with a phosphine free homogeneous catalysis under mild condition (4 atm H₂, room temperature, 4–24 hours, 1 mol% Ru, 15 mol% KO^tBu in THF) is also described. For example, the catalysts prepared by reacting *cis*-[Ru(η^3 -C₃H₅)(MeCN)₂(COD)]BF₄ with diamine ligands transforms the trifluoroacetamide, 2,2,2-trifluoro-1-(piperidin-1-yl)ethanone into the formylated amine, 1-formylpiperidine, and fluoroform via a catalytic C-C bond hydrogenolysis.

Dedication

I dedicate this dissertation to my father, Sivalai Rasu. You are my role model and a source of inspiration at every moment of life. You never taught me but you showed me how to live. You would have been a proud father at this moment of my success. I cannot thank you enough for what you have done and sacrificed in your life to make me who I am now. You will always be a reason for my success and accomplishments.

“Be careful how you think; your life is shaped by your thoughts”

Proverbs 4:23

Acknowledgements

I would like to convey my sincerest gratitude to all those who have helped me to complete this dissertation successfully. Primarily, I would like to thank my supervisor Prof. Steven Bergens for providing me with challenging projects to work on for my thesis. Also, his guidance, motivation, patience, and constructive comments were invaluable to achieve my goals throughout my Ph.D. career. I would also like to thank my supervisory committee members Prof. Derrick L. J. Clive, Prof. Frederick G. West, Prof. Eric Rivard, Prof. Rylan Lundgren and Prof. Deryn E. Fogg for their support in all stages of my career.

I am extremely thankful to the past and present group members, who have helped me by providing practical and moral support in numerous ways. I would like to remember my colleagues, Dr. Jeremy John, Dr. Sonja Francis, Dr. Elizabeth Corkum, Suneth Kalapugama, Prabin Nepal, Shuai Xu, Chao Wang, Riley Endean, Elanna Stephenson, Ben Rennie, Evan Antoniuk, Sarah Sutherland, and Stephen Langmaid. Working with you all has made my life more enjoyable and productive.

I would also like to give my gratitude to the following people in the Department of Chemistry for their invaluable support in numerous ways for the success of my projects. Mark Miskolzie and Nupur Dabral of the Nuclear Magnetic Resonance Laboratory; Wayne Moffat and staff of the Analytical and Instrumentation Laboratory; Dr. Angie Morales-Izquierdo and staff of the Mass Spectrometry Laboratory; Bernie Hippel, Ryan Lewis, Andrew Yeung, Matthew Kingston and Karlene Lynch of Chemical Stores and Receiving; Dirk Kelm and Paul

Crothers of Machine Fabrication; Kim Do of Electronics Repair; Jason Dibbs of Glassblowing; Scott Stelck, Laura Pham and Ester Moibi of General office; Tyler Peterson of Information Technology; Administrative Assistants Bonnie Gover and Lynne Lechelt; Anita Weiler of Graduate Student Services; Undergraduate Lab Coordinators: Dr. Norman Gee and Dr. Jason Cooke.

I would like to thank my undergraduate professor who taught and helped me in numerous ways, and one of the main reasons for my career in Ph.D. of chemistry. I would also like to thank and remember my friends who were there for me to remind that I am not alone in my tough times. I would like to acknowledge, with gratitude, for the support and love of my father Sivalai Rasu and my mother Loorthamma, who would be very proud of my achievement. I am indebted to my sisters, brothers, and relatives who nurtured me throughout my life. Finally, I would like to thank God the Almighty for being with me and giving me the strength and blessing to accomplish this endeavor.

Table of Contents

Chapter 1: Introduction

Catalysis	1
Catalytic hydrogenation of amides.....	11
Heterogeneous catalytic hydrogenation of amides	12
Homogeneous catalytic amide hydrogenation via C–O cleavage	16
Homogeneous catalytic hydrogenation of amides via C–N cleavage	28
Earth abundant metal based homogeneous catalysts for the hydrogenation of amides via C–N cleavage.....	42
Selectivity for C–O vs. C–N cleavage in catalytic amide hydrogenation.....	49
Asymmetric hydrogenation.....	52
Research objectives	64

Chapter 2: Catalytic hydrogenation of functionalized amides under basic and neutral conditions

Introduction	65
Results and discussion	66
Conclusion.....	74
Materials and methods.....	75

Chapter 3: A highly enantioselective hydrogenation of amides via dynamic kinetic resolution under low pressure and room temperature

Introduction	91
Results and discussion.....	97
Conclusion.....	111
Materials and methods.....	111

Chapter 4: A fortuitous, mild catalytic carbon-carbon bond hydrogenolysis by a phosphine-free catalyst

Introduction	158
Results and discussion.....	161
Conclusion.....	166
Materials and methods.....	166

Chapter 5: Conclusions and future directions

Conclusions.....	184
Future work.....	186

List of Tables

Chapter 1

Table 1.1: Air emission and energy per 1000 kg of material transported 528 km using a diesel-fuel vehicle.....	9
Table 1.2: Relationship between the diastereomeric transition state energies and corresponding ee values.....	59

Chapter 2

Table 2.1: Base-free hydrogenation of <i>N</i> -phenylpyrrolidin-2-one (114) by various Ru-precursors.....	67
Table 2.2: Base-free hydrogenation of simple amides	69
Table 2.3: Base-free vs. base-assisted hydrogenation of functionalized amides	71
Table 2.4: Base-free hydrogenation of <i>N</i> -acyloxazolidinones.....	73

Chapter 3

Table 3.1: Optimization studies for the asymmetric hydrogenation of <i>rac</i> - 133 and <i>rac</i> - 134	102
Table 3.2: Enantioselective hydrogenation of functionalized racemic amides	104
Table 3.3–3.5: Sources, CAS number, and vial numbers for the ligands used in the rapid screening	113

Chapter 4

Table 4.1: Crystallographic experimental details for trans-RuCl₂((*S,S*)-skewphos)((*R,R*)-dpen) (**135**).....176

Table 4.2: Selected interatomic distances (Å) for **135**.....179

Table 4.3: Selected interatomic angles (deg) for **135**.....180

Chapter 5

Table 5.1: Screening studies for the hydrogenation of benzanilide under acidic condition.....187

List of Figures

Chapter 1

Figure 1.1: Illustration of resonance delocalization and overlap of π orbitals in amides.....	3
Figure 1.2: Reaction, work-up, and purification steps in the medium scale reduction of the amide 3 by LiBH_4	7
Figure 1.3: Catalyst system for the hydrogenation of amides via C–O cleavage	16
Figure 1.4: Representatives of chelating, bridging, and monodentate Ru-MSA complexes identified by Cole-Hamilton and coworkers.....	18
Figure 1.5: Variation of concentration of the products over time under hydrogenation conditions of 15 atm, 150 °C, using the catalytic system 8/9/ $\text{Yb}(\text{OTf})_3$	25
Figure 1.6: Catalyst system for the hydrogenation of amides via C–N cleavage	29
Figure 1.7: <i>Homogeneous earth abundant catalyst system available for the hydrogenation of amides via C–N cleavage pathway</i>	42
Figure 1.8: Illustration of possible intermediates from a representative hemiaminal under acidic conditions	50
Figure 1.9: Illustration of possible intermediates formation from a representative hemiaminal under basic condition	51
Figure 1.10: Illustration of energy diagram and reaction scheme for KR.....	57

Figure 1.11: Illustration of energy diagram and reaction scheme for DKR..... 58

Figure 1.12: Illustration of fundamental steps in high throughput screening technology..... 61

Chapter 2

Figure 2.1: $^{31}\text{P}\{^1\text{H}\}$ NMR of trans-[Ru(H)(η^1 -BH₄)(Ph₂CH₂CH₂NH₂)₂] (**61**). The top spectrum shows the product formed after 30 minutes at 60 °C. The bottom spectrum was recorded just after mixing at room temperature. 84

Figure 2.2: ^1H NMR spectrum (δ 6 to 0.4 ppm) of trans-**61** formed by the reaction of **51** and NaBH₄ at ~2 atm H₂ in THF-*d*₈..... 85

Figure 2.3: ^1H NMR spectrum (δ 0.4 to -20 ppm) of trans-**61** formed by the reaction of **51** and NaBH₄ at ~2 atm H₂ in THF-*d*₈..... 86

Figure 2.4: ^1H NMR spectrum showing the products from the hydrogenation of 4-fluorobenzamide..... 87

Figure 2.5: ^1H NMR spectrum showing the product from the hydrogenation of 4-chloro-*N*-methyl-*N*-phenylbenzamide..... 87

Figure 2.6: ^1H NMR spectrum showing the products from the hydrogenation of *N*-(4-fluorophenyl)benzamide..... 87

Figure 2.7: The HRMS (ESI⁺) spectrum showing the product mixture resulting from the hydrogenation of *N*-(4-fluorophenyl)benzamide..... 88

Figure 2.8: ¹ H NMR spectrum showing the products from the hydrogenation of <i>N</i> -(4-bromophenyl)benzamide	88
Figure 2.9: ¹ H NMR spectrum showing the products from the hydrogenation of <i>N</i> -phenyl-2-furancarboxamide.....	88
Figure 2.10: ¹ H NMR spectrum showing products from the hydrogenation of furan-2-yl(piperidin-1-yl)methanone.	89
Figure 2.11: ¹ H NMR spectrum showing the products from the hydrogenation of 2-piperazin-1-yl-1-piperidin-1-yl-ethanone.	89

Chapter 3

Figure 3.1: Strategy for the high throughput screening process	98
Figure 3.2: Putative dihydride catalysts of active category IV and their <i>ee</i> (%) for the hydrogenation of <i>rac</i> - 56 and <i>rac</i> - 133	100
Figure 3.3: Structures of diamine ligands used for catalyst optimization	101
Figure 3.4: Proposed structure of the active catalyst 137 with possible interactions with 2-PrOH, primary alcohol products, etc.	109
Figure 3.5: HPLC retention times of the reactants and products.....	115
Figure 3.6: UV-Vis spectrum of authentic sample, <i>tert</i> -butyl 2-phenoxy propanoate (127) vs. product mixture from rapid screening	116
Figure 3.7: UV-Vis spectrum of authentic sample, diphenylamine vs. product mixture from rapid screening	116

Figure 3.8: UV-Vis spectrum of authentic sample, <i>rac</i> -2-phenoxypropan-1-ol vs. product mixture from rapid screening	117
Figure 3.9: UV-Vis spectrum of authentic sample, <i>N,N</i> -diphenyl-2-phenoxypropionamide (56) vs. product mixture from rapid screening.....	117
Figure 3.10: UV-Vis spectrum obtained from the authentic sample of 2-phenoxypropyl 2-phenoxypropanoate	118
Figure 3.11: Representative UV-Vis spectrum of 2-phenoxypropyl 2-phenoxypropanoate from the rapid screening product mixture.....	118
Figure 3.12: Gas chromatogram of the rapid screening hydrogenation product mixture from the reaction well D7	119
Figure 3.13: Mass spectrum for the peak at 8.794 min showing the presence of <i>tert</i> -butyl 2-phenoxypropanoate in the reaction product mixture.....	119
Figure 3.14: Mass spectrum for the peak at 14.189 minutes showing the presence of 2-phenoxypropyl 2-phenoxypropanoate in the reaction product mixture	120
Figure 3.15: Representative chromatogram of well A2 for Category I ((<i>R,R</i>)-dpen and (<i>R</i>)-3,4,5-MeO-MeOBIPHEP).	120
Figure 3.16: Representative chromatogram of well D7 for Category II ((<i>R,R</i>)-dpen and (<i>R</i>)-BINAP).	121
Figure 3.17: Representative chromatogram of well G3 for Category III (Bis[2-(dicyclohexylphosphino)ethyl]amine).....	121
Figure 3.18: Representative chromatogram of well C12 for Category IV ((<i>R,R</i>)-dpen and (<i>S,S</i>)-BDPP).	122

Figure 3.19: Structures of the ligands in Category I	122
Figure 3.20: Structures of the ligands in Category II.....	125
Figure 3.21: Structures of the ligands in Category III	125
Figure 3.22: Structures of the ligands and <i>ee</i> 's for the hydrogenations of <i>rac</i> - 56 in Category IV	126
Figure 3.23: The δ region from 10 to 1 ppm showing major products obtained from the reduction of isolated 134 by LiAlH ₄	130
Figure 3.24: GC traces of the 2-phenoxypropan-1-ol from the enantioselective hydrogenation of 134 with a reduced amount of base and the reduction of isolated 134 by LiAlH ₄	131
Figure 3.25: The putative dihydride catalysts (128 , 128a-128e) used for the optimization experiments.....	132

Chapter 4

Figure 4.1: Solid state structure of <i>trans</i> - 135 as determined by X-Ray diffraction with 30% probability of non-hydrogen atoms.	163
Figure 4.2: ¹ H NMR spectrum (δ 6.5 to -2.0 ppm) of [Ru(H ₂ NCH(Ph)CH(Ph)NH ⁻)($\eta^{1,5}$ -C ₈ H ₁₂)(η^3 -C ₃ H ₅)]BF ₄ (141) formed by the reaction of 117 , (<i>R,R</i>)-dpen and KO ^t Bu at ~1 atm H ₂ in THF- <i>d</i> ₈ at -80 °C....	170
Figure 4.3a: ¹ H NMR and zTOCSY1D spectrum (δ 6.5 to -2.0 ppm) of 141 formed by the reaction of 117 , (<i>R,R</i>)-dpen, and KO ^t Bu at ~1 atm H ₂ in THF- <i>d</i> ₈ at -80 °C.....	171

Figure 4.3b: ^1H - ^1H gCOSY (vs. zTOCSY1D) spectrum of the product 141 formed by the reaction of 117 , (<i>R,R</i>)-dpen, and KO^tBu at ~ 1 atm H_2 in $\text{THF-}d_8$ at -80°	171
Figure 4.4: ^1H NMR spectrum (δ 6.5 to -2.0 ppm) of the product 142 formed by the reaction between 117 , (<i>R,R</i>)-dpen, and KO^tBu at ~ 1 atm H_2 in $\text{THF-}d_8$ at -20°C	173
Figure 4.5: ^1H NMR spectrum (δ 9.0 to -12.0 ppm) of the product formed by the reaction between 117 , (<i>R,R</i>)-dpen, and KO^tBu at ~ 1 atm H_2 in $\text{THF-}d_8$ at RT.....	173
Figure 4.6: ^1H NMR spectrum (δ 5.0 to 0.0 ppm) of the product formed by the reaction between 117 , (<i>R,R</i>)-dpen, and KO^tBu at ~ 1 atm H_2 in $\text{THF-}d_8$ at RT.	174
Figure 4.7: ^1H NMR and ^1H - ^{15}N NMR of a gHSQC spectrum (δ 6 to -2 ppm) of 141 formed by the reaction of 117 , (<i>R,R</i>)-dpen, and KO^tBu at ~ 1 atm H_2 in $\text{THF-}d_8$ at -80°C	174
Figure 4.8: ^{19}F NMR spectrum (δ -65.0 to -85.0 ppm) of the product formed by the reaction between the catalyst and 10 equivalents of substrate 138 in $\text{THF-}d_8$ at room temperature at different times.	175

List of Schemes

Chapter 1

Scheme 1.1: Reduction of amide products via C–O cleavage (path A) or C–N cleavage (path B)	4
Scheme 1.2: Amide reduction step in the synthesis of verapamil	5
Scheme 1.3: Amide reduction to alcohol using LiBH ₄ hydride reagent.	6
Scheme 1.4: Hydrogenation of amides via C–O cleavage (path A) or C–N cleavage (path B)	12
Scheme 1.5: Proposed reaction pathways and intermediates in the hydrogenation of CyCONH ₂	14
Scheme 1.6: Possible hydrolysis of amide and imine intermediates by excess water	17
Scheme 1.7: Proposed mechanism for the hydrogenation of indole under acidic conditions	20
Scheme 1.8: Proposed mechanism for the hydrogenation of Levulinic acid to γ -velerolactone in acidic conditions	21
Scheme 1.9: Hydrogenation of primary and secondary amides using the neutral catalyst 24	22
Scheme 1.10: Plausible mechanism for the hydrogenation of amides via C–O cleavage under acidic condition	24
Scheme 1.11: Plausible mechanism for the hydrogenation of amides via borrowing hydrogen pathway to produce C–O cleavage products.....	26

Scheme 1.12: Proposed mechanism for the hydrogenation of amides via C–N cleavage using a pincer type catalyst 41	32
Scheme 1.13: The energy barriers for C–N and C–O cleavage during the hydrogenation of <i>N</i> -ethylacetamide by 41	33
Scheme 1.14: Hydrogenation of amides and substrate scope by allylic catalysts 51	34
Scheme 1.15: The role of a base in the bifunctional addition between 50 and 55	36
Scheme 1.16: Top: mono, or di-deprotonation of 50 to form the electron-rich 54-K and 54-Li₂ . Bottom: the products observed for the bifunctional addition of 54-K to 55 and 56	37
Scheme 1.17: Hydrogenation of amides by Saitos' catalyst 62	38
Scheme 1.18: Proposed mechanisms for the hydrogenation of an amide via C–N cleavage products using pincer-type catalyst 66	40
Scheme 1.19: Proposed mechanism for the hydrogenation of an amide to C–N cleavage products using pincer-type catalysts 73 and 74	44
Scheme 1.20: Synthetic route to [(R-PN ^H -P)Fe(X) ₂ (CO)] and [(R-PN ^H -P)Fe(H)(CO)(η ¹ -BH ₄)] complexes.....	45
Scheme 1.21: Resolution of naproxen using <i>N</i> -methyl- <i>D</i> -glucamine as the resolving agent.....	53
Scheme 1.22: Asymmetric hydrogenation and deprotection steps in the synthesis of L-dopa.....	54

Scheme 1.23: Asymmetric hydrogenation of the imine 97 with an Ir-Josiphos catalyst in the synthesis of (<i>S</i>)-Metolachlor	55
Scheme 1.24: Asymmetric hydrogenation of 101 by 104 in the synthesis of 103	56
Scheme 1.25: Asymmetric hydrogenation of 105 to 106 by 108 in the synthesis of Ro 67-8867	60
Scheme 1.26: Asymmetric hydrogenation of 109 to 110 via DKR in the synthesis of active pharmaceutical ingredient 111	62

Chapter 2

No Scheme

Chapter 3

Scheme 3.1: Hydrogenation of amide products via C–O or C–N cleavage pathway.....	91
Scheme 3.2: Products observed for the bifunctional addition of 54-K to the imide 55 and the amide 56 under mild condition	92
Scheme 3.3: Enantioselective hydrogenation of α -arylaldehydes by catalyst 121 via DKR.....	93
Scheme 3.4: Enantioselective hydrogenation of α -aryloxyaldehydes by catalyst 121 via DKR.....	94
Scheme 3.5: Enantioselective hydrogenation of α -arylaldehydes by List's catalyst 122 via DKR.....	95

Scheme 3.6: Enantioselective hydrogenation of <i>rac</i> - α -phenyl- γ -butyrolactone by Ikariya's catalyst 123	95
Scheme 3.7: Enantioselective hydrogenation of racemic α -phenylesters by catalyst 124	96

Chapter 4

Scheme 4.1: Transition metal assisted strain-driven C–C bond activation by oxidative addition.....	158
Scheme 4.2: Catalytic C–C bond hydrogenolysis of 2,2,2-trifluoro-1-(piperidin-1-yl)ethanone (138).....	159
Scheme 4.3: The proposed mechanism for base assisted formylation of amines by CO	161

List of Equations

Chapter 1

Eq. 1.1: Hydrogenation of 4-fluoroacetophenone by [RuCl ₂ ((<i>S</i>)-xyl-PhanePhos)(<i>R,R</i> -dpen)	11
Eq. 1.2: Hydrogenation of dodecanamide by CuCr ₂ O ₄	12
Eq. 1.3: Hydrogenation of butanamide by Ru(acac) ₃ (8)/Triphos ^{Ph} (9)	17
Eq. 1.4: Products obtained upon heating 24 at 140 °C under 45 atm H ₂ in THF- <i>d</i> ₈ solution	23
Eq. 1.5: Hydrogenation of benzanilide by 8/9 /Yb(OTf) ₃ ·H ₂ O	25
Eq. 1.6: A general reaction scheme for the hydrogenation of amides by 16 /TsOH·H ₂ O/BF ₃ ·OEt ₂	27
Eq. 1.7: Hydrogenation of lactams by 35 /MSA system	28
Eq. 1.8: A general reaction scheme for the hydrogenation of amides by iridium-based pincer complex 37	28
Eq. 1.9: Hydrogenation of amides by Cp*RuCl(2-C ₅ H ₄ NCH ₂ NH ₂) (39)	30
Eq. 1.10: Hydrogenation of amides by ruthenium-pincer complex [Ru(H)(CO)(PNN)] (41)	31
Eq. 1.11: Hydrogenation of amides by ruthenium-pincer complex [Ru(H)(CO)(PNN)] (42)	31
Eq. 1.12: A general reaction scheme for the hydrogenation of amides by <i>trans</i> -[Ru(H)(HBH ₃)(Ph ₂ P(CH ₂) ₂ NH ₂) ₂] (61)	38
Eq. 1.13: A general reaction scheme for the hydrogenation of amides by <i>cis</i> -[Ru(OCOCF ₃) ₂ (Ph ₂ P(CH ₂) ₂ NH ₂) ₂] (65)	39

Eq. 1.14: A general reaction scheme for the hydrogenation of amides by ruthenium-pincer complex 66	39
Eq. 1.15: A general reaction scheme for the hydrogenation of primary amides by ruthenium-pincer complex 66 under basic conditions	41
Eq. 1.16: A general reaction scheme for the hydrogenation of simple amides by Ru-PNNP catalyst 70	41
Eq. 1.17: A general reaction scheme for the hydrogenation of activated amides by Fe-PNP catalyst 73	43
Eq. 1.18: A general reaction scheme for the hydrogenation of amides by Fe(H)(η^1 -BH ₄)PNP catalyst 84	45
Eq. 1.19: A general reaction scheme for the hydrogenation amides by Fe(H)(η^1 -BH ₄)PNP catalyst 86	46
Eq. 1.20: Hydrogenation of <i>N</i> -arylformamide by Fe-PNP catalyst 87	47
Eq. 1.21: Hydrogenation of DMF by Fe-PNP catalyst 87	47
Eq. 1.22: A general reaction scheme for the hydrogenation of amides by the catalyst [Mn(PNN)(CO) ₃]Br (89)	48

Chapter 2

Eq. 2.1: Hydrogenation of 114 by 51 under neutral conditions	67
Eq. 2.2: In situ synthesis of 61 from the reaction between NaBH ₄ and 51	74

Chapter 3

Eq. 3.1: Hydrogenation of <i>rac</i> - 56 by <i>trans</i> - 50 under under 4 atm H ₂ at 0 °C in THF.....	97
Eq. 3.2: Products from the reaction between allylic Ru precursors like [Ru(η^3 -C ₃ H ₅)(P-N) ₂]BF ₄ , base, and H ₂	98
Eq. 3.3: Product mixture obtained from the Categories II and III in rapid screening experiments	99
Eq. 3.4: Products from the reaction between <i>rac</i> - 56 and KO ^t Bu in THF	100
Eq. 3.5: Hydrogenation of <i>rac</i> - 133 during the optimization under 4 atm H ₂ at RT in THF.....	101
Eq. 3.6: Hydrogenation of <i>rac</i> - 134 by <i>trans</i> - 135 under 4 atm H ₂ at RT in THF	104
Eq. 3.7: Product obtained from the hydrogenation of 2-phenoxy-2-(2-pyridyl)-1-(1-piperidinyl)-ethanone by <i>trans</i> - 135	107
Eq. 3.8: Equilibrium of the product from the reaction between Ru amides such as 58 and 2-PrOH under basic conditions	107
Eq. 3.9: Equilibrium of 50 in the presence of both RO ⁻ and ROH during hydrogenation.....	108

Chapter 4

Eq. 4.1: Synthesis of formamides by the reaction between amines and chloral	160
---	-----

Eq. 4.2: Synthesis of formamides by the reaction between amines and formic acid.....	160
Eq. 4.3: Base-assisted synthesis of formamides by the reaction between amines and CO.....	160
Eq. 4.4: Fe-pincer catalyzed synthesis of formamides by the reaction between amines, CO ₂ , and H ₂	161
Eq. 4.5: Hydrogenation of 2,2,2-trifluoro-1-(morpholin-4-yl)ethanone (138) by putative dihydride 128	162
Eq. 4.6: Formation of an amido complex 141 from the reaction between 117 and (<i>R,R</i>)-dpen in THF- <i>d</i> ₈ at -80 °C to -40 °C	164
Eq. 4.7: Formation of Ru-H complex 142 upon warming the amido complex 141 at -40 °C to -20 °C	165
Eq. 4.8: Products characterized from the hydrogenation of 138 by the catalysts 128 or 140	165

List of Abbreviations and Symbols

1°	- primary
2°	- secondary
3°	- tertiary
Ac	- acetyl
acac	- acetylacetonate
API	- active pharmaceutical ingredient
aq	- aqueous
BINAP	- 2,2'-bis(diphenylphosphino)-1,1'-binaphthyl bis(diphenylphosphino)butane
Bn	- benzyl
br	- broad
Bu	- butyl
CAS	- Chemical Abstracts Service
COD	- 1,5-cyclooctadiene
Cp*	- 1,2,3,4,5- pentamethylcyclopentadienyl
Cy	- cyclohexyl
d	- doublet
<i>dr</i>	- diastereoisomeric ratio
daipen	- 1,1-bis(4-methoxyphenyl)-3-methyl-1,2-butanediamine
dd	- doublet of doublets
ddd	- doublet of doublets of doublets

DFT	- density functional theory
DIBAL-H	- diisobutylaluminium hydride
DIPAMP	- 1,2-bis[(2-methoxyphenyl)(phenyl)phosphino]ethane
DME	- dimethoxyethane
DMF	- dimethylformamide
dpen	- 1,2-diphenylethylenediamine
dt	- doublet of triplets
<i>ee</i>	- enantiomeric excess
ESI MS	- electrospray ionization mass spectroscopy
Et	- ethyl
FTIR	- Fourier transform infrared
gCOSY	- gradient correlation spectroscopy
GDP	- gross domestic product
gHSQC	- gradient heteronuclear multiple quantum coherence
HPLC	- high pressure liquid chromatography
LA	- levulinic acid
m	- multiplet
Me	- methyl
MeOH	- methanol
min	- minute(s)
m/z	- mass to charge ratio
MS	- molecular sieves
MSA	- methanesulfonic acid

nd	- not determined
NMR	- nuclear magnetic resonance
NMVOC	- non-methane volatile organic compounds
oaTOF	- orthogonal acceleration time of flight
Ph	- phenyl
Pr	- propyl
ⁱ Pr	- <i>iso</i> -propyl
PrOH	- propanol
q	- quartet
RedAl	- sodium bis(2-methoxyethoxy)aluminumhydride
RT	- room temperature
s	- singlet
S/C	- substrate to catalyst ratio
sex	- sextuplet
t	- triplet or time
^t Bu	- <i>tert</i> -butyl
TfOH	- triflic acid
THF	- tetrahydrofuran
TOF	- turnover frequency
TON	- turnover number
TsOH	- tosylic acid
gTOSCY	- total correlation spectroscopy
Triphos ^{Ph}	- 1,1,1-tris(diphenylphosphinomethyl)ethane

- TS – transition state
- tt – triplet of triplets
- Xyl-BINAP – 2,2'-bis[di(3,5-xylyl)phosphino]-1,1'-binaphthyl
- ΔG^{\ddagger} – standard Gibbs free energy of activation

Chapter 1

Introduction

Catalysis is a vital component of the economy and of all life on the planet.¹ Catalysis contributes to over 35% of the global domestic product (GDP),² and it plays a role in the production of 80–90% of industrial chemicals.^{1,3} The term catalysis was introduced by Jons Jacob Berzelius in 1835, who defined catalysis as a process that increases the rate of a chemical reaction using a substance called a catalyst.⁴ In 1895 Ostwald defined catalyst as “a substance that accelerates the rate of a reaction by lowering the activation energy without being consumed in the reaction.”⁵ According to IUPAC, a catalyst is a substance that increases the rate of a reaction without modifying the overall standard Gibbs energy change in the reaction.⁶

Catalysis is a natural phenomenon that is billions of years old. Enzymes are one example of a catalyst, and they are critical for all life on the planet. The earliest form of life on earth is believed to have formed around 3.5–3.7 billion years ago.^{7,8} Thousands of years ago, dating back to 6000 BC or earlier,⁹ the origins are hard to track, human beings used fermentation to produce ethanol. Industrial catalytic processes began in the late nineteenth century.⁴ The development of catalysis is often influenced by political and societal demands. For example, World War I and World War II had a significant impact on catalysis. Among the most significant processes developed during those periods were the Haber-Bosch process,¹⁰ the Fischer-Tropsch process,¹¹ the synthesis of methanol from methane and water,¹² steam reforming,¹³ the catalytic cracking of petroleum,¹⁴ and the large-scale

production of penicillin.¹⁵ Ziegler and Natta's polymerization of olefins,¹⁶ the Wacker Process,¹⁷ and Wilkinson's catalyst for olefin hydrogenation^{5,18} are other significant catalytic discoveries that occurred in the first half of the 20th century.

Green chemistry is a primary focus of present-day catalysis to address the consequences of climate change and pollution. Chemical industry is increasingly being pressured to use and develop new catalytic processes that are environmentally benign.¹⁹ In 2005, the American Chemical Society (ACS), the Green Chemistry Institute (GCI), and several leading pharmaceutical corporations (including AstraZeneca, GlaxoSmithKline, Merck & Co., Inc., Pfizer, Inc., Eli Lilly & Company, and Schering-Plough Corporation) formed the ACS GCI Pharmaceutical Roundtable (ACS GCIPR). The ACS GCIPR identified amide reduction without stoichiometric hydride reagents as one of the key areas of research that required improvement or a greener approach.²⁰

Amides are among the least reactive carboxylic acid derivatives.²¹ The lone pairs on nitrogen donate to the carbonyl carbon, enabling resonance delocalization to share the double bond character between the C–N and C–O bonds. Indeed, the typical length of an amide C–N bond (133 pm)²² is shorter than a C–N single bond (149 pm) and close to a typical C–N bond (127 pm).²³ This effective overlap of the O, C, and N π orbitals restricts the rotation around the C–N bond, and prefers a planar geometry for the amide group.²³

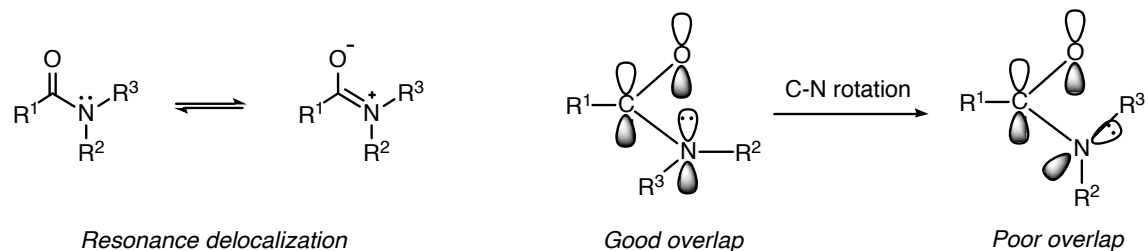
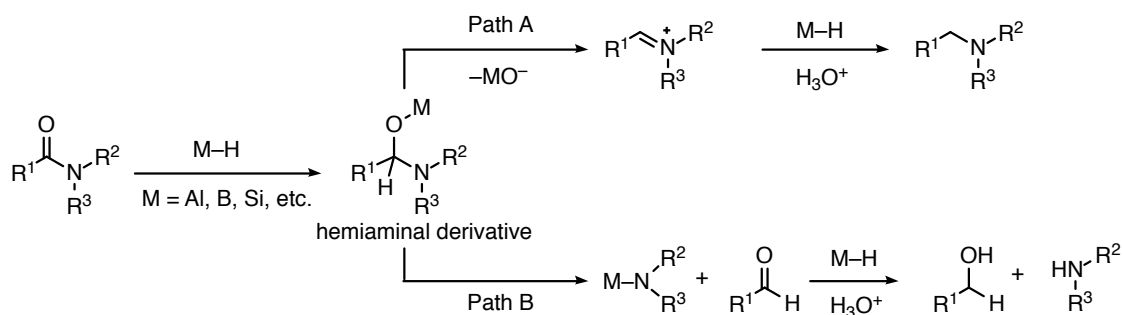


Figure 1.1: Illustration of resonance delocalization and overlap of π orbitals in amides.²¹

The π donation from both oxygen and nitrogen decreases the electrophilic nature of the carbonyl carbon, making it less reactive towards hydridic reducing agents like LiAlH_4 . This delocalization stabilizes the amide carbonyl group more than aldehydes, ketones, and esters.^{21,24}

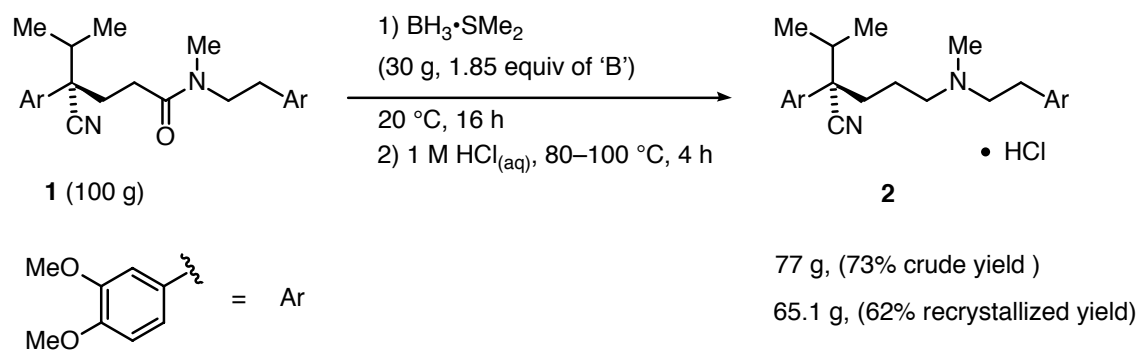
Amide reduction is mostly carried out with stoichiometric amounts of hydride reagents like LiAlH_4 , DIBAL, RedAl, B_2H_6 or silanes. The driving force for these reaction is partially the formation of strong Al–O, B–O, or Si–O bonds. Silanes reduce amides via catalytic hydrosilylation.^{20,21,25} These reducing agents react with the amide carbonyl group to form the corresponding Al, B, or Si oxygen-bonded hemiaminal (Scheme 1.1),²⁵ which can produce a higher amine by breaking the C–O bond (Path A), or it can produce an alcohol as the final product by breaking the C–N bond (Path B). The reduction products depend on the nature of the reducing agent and the substituent groups on the nitrogen.²⁵



Scheme 1.1: Reduction of amide products via C–O cleavage (path A) or C–N cleavage (path B).

In 2006, a survey was conducted to analyze the reaction types used in the synthesis of 128 drug candidates from three pharmaceutical companies, AstraZeneca, GlaxoSmithKline, and Pfizer.²⁶ These complete syntheses required 1039 chemical transformations including 94 reduction steps. Most of the reductions used hydride reagents (42%, e.g., imine to amine, amide to amine, ester to alcohols, alkyne to alkane, etc.) and catalytic hydrogenation over precious metal catalysts (47%, e.g., imine to amine, NO_x to NH_2 , alkene/alkyne to alkane). Notably, the reduction of all the carboxylic acid derivatives was carried out using a stoichiometric amount of hydride reagents alone.

Hydrides are the reagents of choice for small to medium-scale reductions of amides.²⁷ An example is the following synthesis of verapamil (**2**). Verapamil is used to treat cardiovascular ailments. Brookes and coworkers at Celltech-Chiroscience reported a synthesis of **2** in which a stoichiometric amount of $BH_3 \cdot SMe_2$ was used to reduce the functionalized amide **1** to its higher amine via C–O cleavage (Scheme 1.2).²⁸

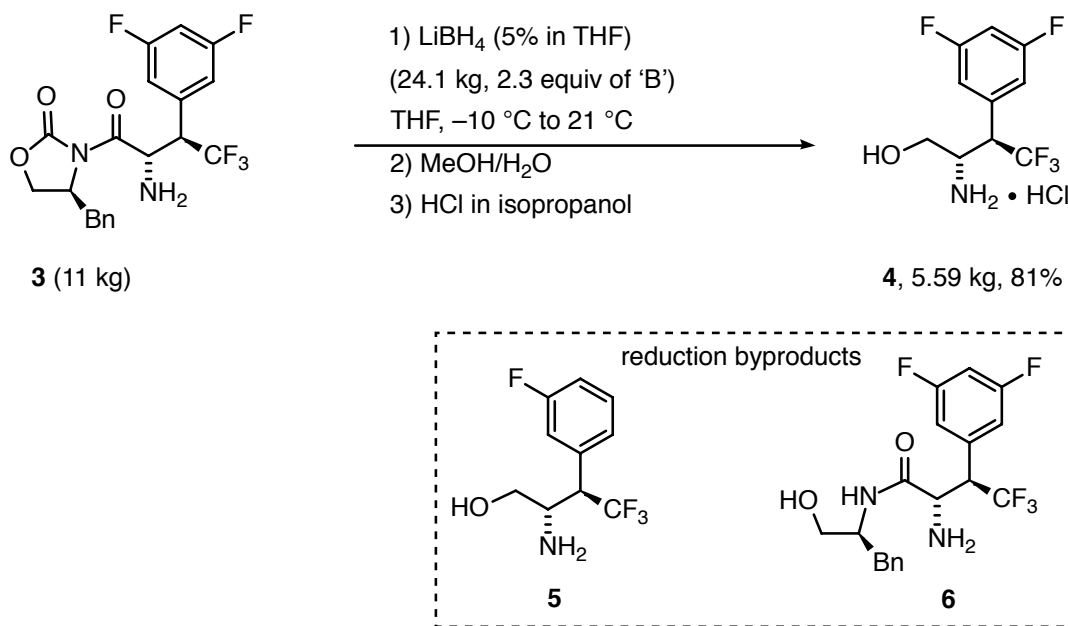


Scheme 1.2: Amide reduction step in the synthesis of verapamil.

The authors stated that the amide reduction was the most challenging step of the synthesis. Extensive optimization was required to find the suitable hydride reagent and work-up procedure for the reduction. Other hydride reagents such as $\text{BH}_3 \cdot \text{THF}$ showed poor selectivity by reducing both the amide and nitrile group, while lithium aluminium hydride tended to cleave the C–N bond. $\text{BH}_3 \cdot \text{SMe}_2$ reduced the amide **1** with minimum side products, but afforded the product as a BH_3 adduct, which required forcing conditions (heating at 80–100 °C in 1 M HCl) to liberate the target verapamil **2**. The authors cautioned that a large-scale reaction is not worthwhile due to the high cost of the $\text{BH}_3 \cdot \text{SMe}_2$ reagent, which also needed specialized handling equipment for large volumes. It is noteworthy that the atom economy of this process is low, and it produces toxic Me_2S .

Recently, Alimardanov and coworkers described a synthesis of the medicinally important trifluoromethyl amino alcohol **4**. In the penultimate synthetic step, a stoichiometric amount of LiBH_4 was used to remove the Evans auxiliary from **3** by reduction (Scheme 1.3).²⁹ This is an example of an amide reduction with C–N cleavage to prepare an active pharmaceutical ingredient (API). The reduction

produced **4** along with the side products **5** and **6**. The authors stated that a significant amount of the mono defluoro impurity **5** formed while adding substrate **3** to a solution of LiBH_4 . However, changing the order of addition, with LiBH_4 added to the substrate **3**, suppressed the formation of **5**.



Scheme 1.3: Amide reduction to alcohol using LiBH_4 hydride reagent.

Limiting the amount of impurity **6** was challenging and important because **6** would react in the final step of the synthetic route to form further side products. Maintaining the temperature between -10 and $0\text{ }^\circ\text{C}$ limited the amount of **6** to between 2–3%.

Although usually effective, the use of hydride reagents and other reducing agents has several disadvantages and creates environmental issues. The metal hydrides produce stoichiometric amounts of inorganic by-products²⁰ (such as aluminium hydroxide, $\text{B}(\text{OH})_n$, etc.), which are hard to separate from the product.

These by-products are either dissolved in water and sent to a waste water treatment plant or they are precipitated out and then sent to a solid waste dump.²⁰ Also, $\text{BH}_3 \cdot \text{SMe}_2$ produces the toxic by-product Me_2S . To illustrate the difficulties in the workup, additional cost, and considerable environmental impact of the use of hydride reagents, it is instructive to discuss in detail the amide reduction involved in the preparation of **4** (Figure 1.2).

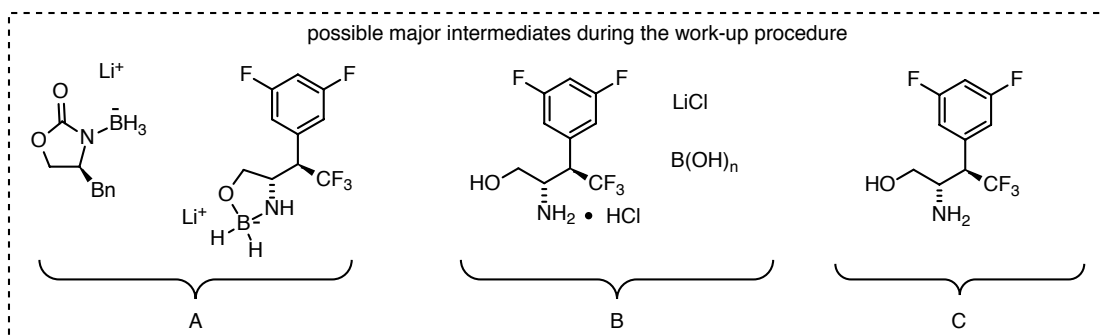
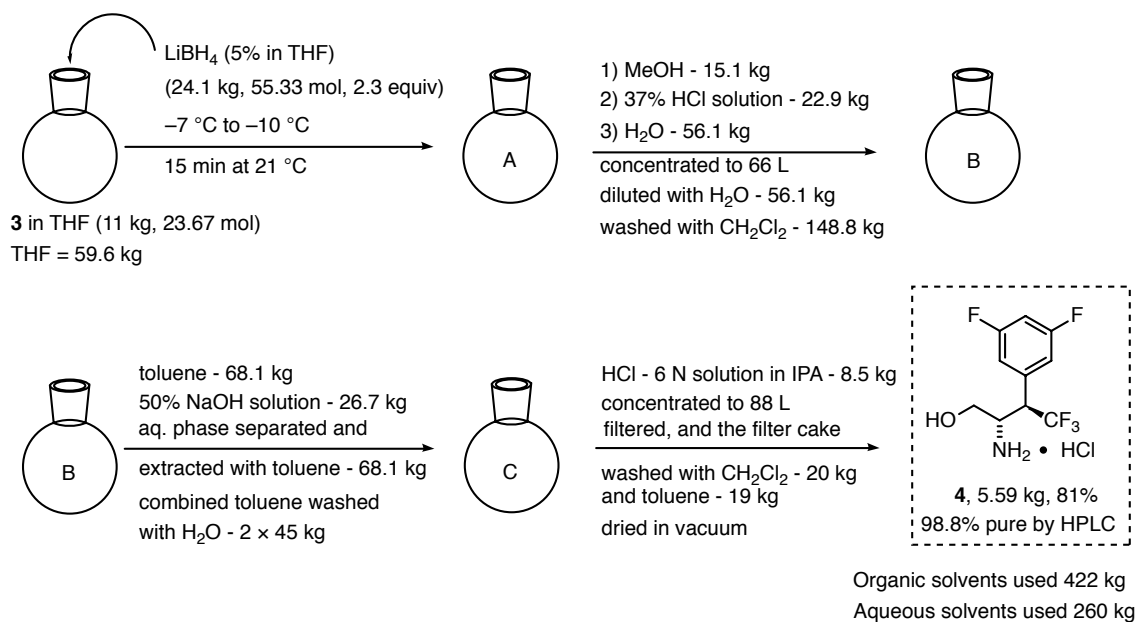


Figure 1.2: Reaction, work-up, and purification steps in the medium scale reduction of the amide **3** by LiBH_4 .

An important concept of green chemistry is that the best solvent for a reaction is no solvent. When there is no alternative, an environmentally friendly solvent should be used. Traditional organic solvents such as chlorinated alkanes (CH_2Cl_2 , CHCl_3 , etc.) and benzene, pose health and safety issues. The solvents used in industry are typically recycled and reused as much as possible, but with a percentage of loss that ends up in the atmosphere or ground water.³⁰ If we assume an upper limit of one percent of solvents is lost during the synthesis of **4**, then about 1.7 kg of CH_2Cl_2 and 1.6 kg of toluene would be released into the environment. The CH_2Cl_2 was likely required to extract the product from the boron-oxide residues. Jimenez-Conzales and coworkers at GlaxoSmithKline studied the Cradle-to-Gate life cycle of active pharmaceutical ingredients. They reported that solvent usage accounts for 75% of the energy used, about 80% of the life cycle mass excluding water, about 70% of the life cycle photochemical ozone creation potential, and about 50% of the greenhouse gases released.³¹ A major requirement for solvents in stoichiometric amide reduction is for the hydrolysis and work-up steps.

Hydride reagents are often flammable and react explosively with water, and so must be transported on the ground using trucks, trains, or ships. Table 1.1 shows the results of a survey by the United States Department of Commerce, Economics, and Statistics Administration on the average transport-related air emissions per 1000 kg of chemicals transported a distance of 528 km.³² It is notable that 33.5 kg of CO_2 , considered to be one of the major causes of global warming, is released to the environment when this much material is transported (Table 1.1, entry 3). Thus transportation not only increases the cost of the API but it also has a negative

environmental impact. Especially considering a multi-ton scale synthesis, which often require that the reagents are transported to the site, and that waste is transported from the site.

Table 1.1: Air emission and energy per 1000 kg of material transported 528 km using a diesel-fuel vehicle.

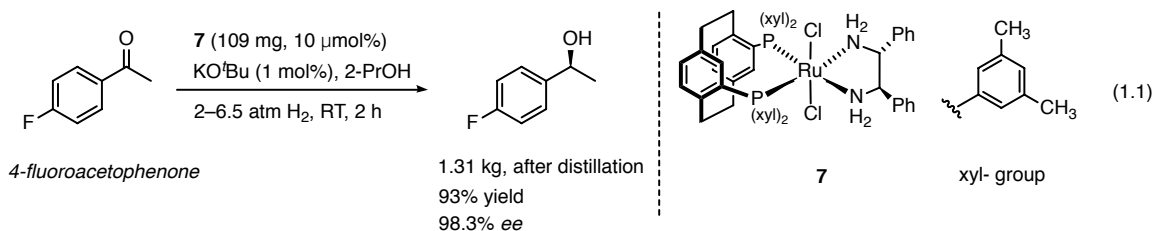
Substances emitted	kg/1000 kg of material transported
CH ₄	0.033
CO	0.185
CO ₂	33.5
Non-methane volatile organic-compounds (NMVOC)	0.216
NO _x	0.627
SO _x	0.043

Another problem with stoichiometric hydride reducing agents is their universal reducing properties, which often results in poor selectivity over unsaturated functional groups. The amide reduction step in the synthesis of **2** is an example where a nitrile group was also reduced with BH₃•THF, while LiAlH₄ led to C–N bond cleavage.

Another green chemistry concept is to prevent waste in the first place, rather than look for remediation. It is obvious that the source of the waste in the synthesis of **4** is not only the hydride reagents, but also the enormous amount of solvents used in the work-up. In fact, to prepare 5.59 kg of **4** required about 422 kg of organic

solvents and 260 kg of aqueous solutions. As well, the hydrolysis of amide reductions often evolves hydrogen gas by an exothermic reaction. In short, it is important to find environmentally benign, safe, and economic methods to reduce amides.

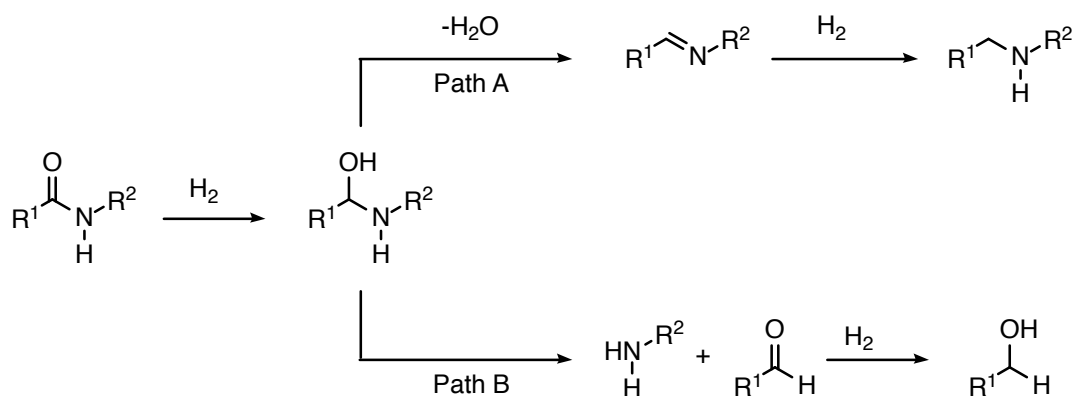
The catalytic reduction of organic functional groups using molecular hydrogen is among the largest-volume human-made chemical reactions in the world.^{33,34} Even though hydrogen gas is flammable and often needs specialized equipment, there are many good reasons to use it in industry. Catalytic hydrogenation is a well-established and reliable reaction.³⁵ It is an atom-economical reaction, with excess H₂ often as the only byproduct, that can be reused or burned to produce useful heat and pure H₂O. Hydrogen also can be produced on site by electrolysis of water. Hydrogen is environmentally benign, and hydrogenations often require minimal work-up, with less solvent required for purification than hydrolysis based work-ups. Hydrogenation also typically affords high turnover numbers (TON) with high purity.³⁵ Two decades ago, the catalytic hydrogenation of ketones was as challenging a reaction as the catalytic hydrogenation of amides is today. Then, a ground-breaking discovery by Noyori and coworkers showed that RuCl₂(diphosphine)(diamine) complexes in the presence of a base are active and selective catalysts for the hydrogenation of ketones.³⁶⁻³⁸ For example, only 109 mg of catalyst [RuCl₂((*S*)-xyl-PhanePhos)(*R,R*)-dppe] (**7**) was required to hydrogenate 1.38 kg of 4-fluoroacetophenone to the corresponding alcohol product in 93% yield with 98.3% *ee* in two hours (Eq. 1.1).³⁹



It is notable that only 3.6 L of 2-PrOH was required for the hydrogenation. After the hydrogenation, the excess base was neutralized using dilute HCl (2 N, ~50 mL). The precipitated potassium chloride was filtered off, and the organic solvent was removed in vacuo to give a crude product. Distillation of the crude product produced (bp 77 °C, 0.33 mbar) 1.31 kg of (*S*)-1-(4-fluorophenyl)ethanol as a clear, colorless liquid.³⁹ There are many examples of commercial asymmetric ketone hydrogenations resulting from Noyori's discovery.^{27,40,41} Attention in the literature is now turning towards the catalytic hydrogenation of amides.

Catalytic hydrogenation of amides

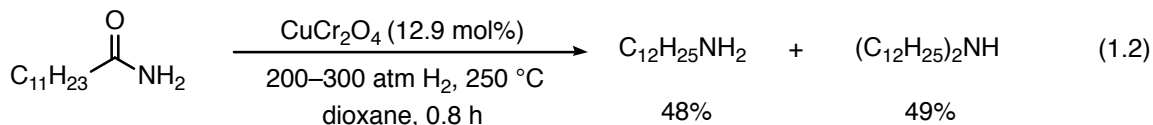
In principle, amide hydrogenation can proceed by C–O or C–N cleavage (Scheme 1.4). The first addition of H₂ to the amide will theoretically form the corresponding hemiaminal. Elimination of H₂O will form the corresponding imine, (Path A) that would be hydrogenated to the higher amine. Elimination of the amine from the hemiaminal would form the corresponding aldehyde, (Path B) that would be hydrogenated to the alcohol. Of course, the actual pathway a particular hydrogenation follows will likely be different from this simple, illustrative model.



Scheme 1.4: Hydrogenation of amides via C–O cleavage (path A) or C–N cleavage (path B).

Heterogeneous catalytic hydrogenation of amides

Although the first reference for an amide hydrogenation dates back to 1908,²¹ the first key development is the pioneering work of Adkins and Wojcik in 1934.^{42,43} Adkins and Wojcik demonstrated that copper-chromium oxide catalyzes the hydrogenation of various of amides under forcing conditions (~6–21 mol% $CuCr_2O_4$ under 200–300 atm H_2 at 250 °C in dioxane).⁴² For example, dodecanamide was hydrogenated to give a mixture of dodecylamine (48% yield, ~4 TON) and didodecylamine (49% yield, ~4 TON) after 0.8 hours (Eq. 1.2).



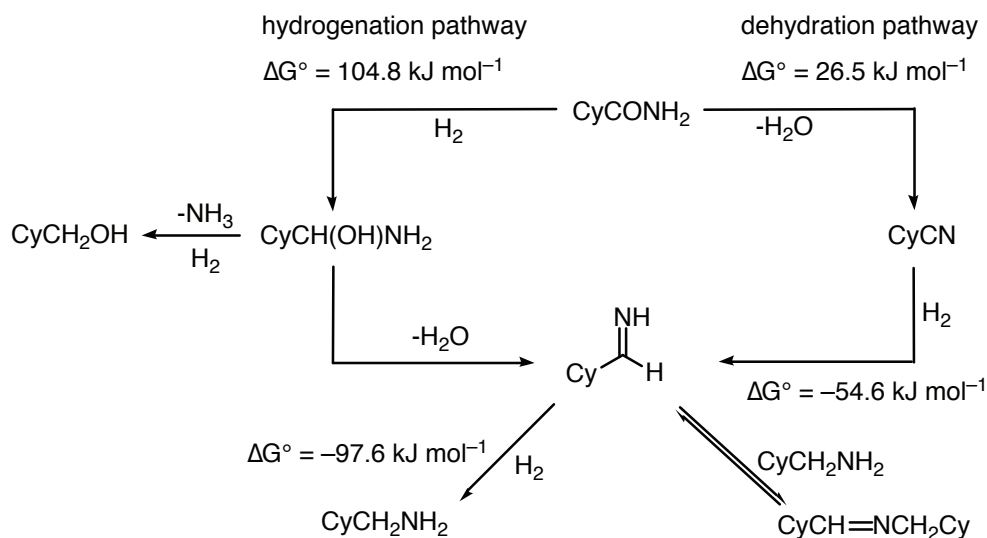
Over the six decades since Adkins and Wojcik's discovery, copper chromite catalysts, with modifications, remained the standard heterogeneous catalysts for the hydrogenation of amides despite the harsh conditions.^{21,44,45} Significant progress

has been made over the past two decades with the use of bimetallic or multimetallic heterogeneous catalysts.⁴⁶⁻⁵³

In 1996, Fuchikami and coworkers published a landmark paper that describes bimetallic catalyst systems consisting of groups 8-10 metals such as $\text{Rh}_6(\text{CO})_{16}$, $\text{Ru}_3(\text{CO})_{12}$, and group 6 or 7 metals such as $\text{Re}_2(\text{CO})_{10}$, $\text{W}(\text{CO})_6$, or $\text{Mo}(\text{CO})_6$.⁴⁶ The hydrogenation occurs with several 2° and 3° amides under less strenuous conditions than the early catalysts, and with 80-92% selectivity for C-O cleavage (TON 33-100 with respect to 'Rh', 75-100% yield, 1-3 mol% 'Rh' 160-180 °C, 100 atm H_2 , 16 h). For example, *N*-acetylmorpholine was hydrogenated to *N*-ethylmorpholine using the bimetallic system $\text{Rh}_6(\text{CO})_{16}$ (1 mol% with respect to Rh) and $\text{Re}_2(\text{CO})_{10}$ (1 mol% with respect to Re) under 100 atm H_2 at 170 °C in quantitative yield in 16 hours. The hydrogenation was highly selective for C-O cleavage with no detectable C-N cleavage product. A side reaction observed with this system is that phenyl rings are hydrogenated to give cyclohexyl rings. The authors did not provide an explanation for the selectivity of these bimetallic catalysts towards C-O cleavage.⁴⁶

Recently, Whyman and coworkers reported a similar series of bimetallic catalysts consisting of Ru/Mo, Rh/Mo, Ru/Re, and Rh/Re metals for the hydrogenation of amides.⁴⁷⁻⁴⁹ These bimetallic catalysts typically operate under 20-100 atm H_2 and at 130-160 °C. A detailed study on the hydrogenation of cyclohexylamide was performed with a variety of Mo:Ru compositions.⁴⁷ The ratio of Mo:Ru was significant for both activity and selectivity towards the hydrogenation. The best activity and selectivity was obtained with Mo:Ru of ~0.5:1. Increasing the

Mo content from this value decreases both the activity and the selectivity towards the C–O cleavage. The active catalyst is believed to be bifunctional with metallic Ru or Rh mixed with Mo or Re oxides. The oxides are believed to act as Lewis acids. A control experiment in which Mo(CO)₆ was heated at 160 °C under 100 atm H₂ in DME (1,2-dimethoxyethane) formed Mo(VI) oxide.⁴⁸ The authors explained high selectivity for C–O cleavage during the hydrogenation of primary amides with the following proposed mechanism (Scheme 1.5).⁴⁹



Scheme 1.5: Proposed reaction pathways and intermediates in the hydrogenation of CyCONH₂.⁴⁹

Based on standard free energies, amide dehydration to form the nitrile (ΔG° 26.5 kJ mol⁻¹) is more favorable (less unfavorable) than amide hydrogenation to form the hemiaminal (ΔG° 104.8 kJ mol⁻¹). The authors suggest that dehydration of the amide to the nitrile is the rate-limiting step, and that the nitrile intermediate rapidly undergoes subsequent hydrogenation to the amine product. The low standing concentration of imine intermediate limits the formation of secondary amine by-

products.⁴⁹ It must be noted that this mechanism is based solely upon standard free energies of the uncoordinated intermediates. They may not represent the actual free energies under reaction conditions and if the intermediates are bonded to the catalyst.

In 2013, Breit and coworkers reported the most versatile heterogeneous catalytic system (Pd/Re (1:5)/graphite, 4 Å sieves) to date.⁵⁰ Out of ~109 secondary and tertiary amides investigated, over 70 were hydrogenated with 100% selectivity for C–O cleavage, with almost 30 of these at >99% conversion [TON 125/Pd, 30 atm H₂, 160 °C, 20 h, 4 Å sieves]. The reaction tolerated ether functional groups. Side reactions included ester, olefin, alkyne, and arene ring hydrogenation. Cole-Hamilton and coworkers recently reported that 4%Pt–4%Re/TiO₂ catalyses the hydrogenation of certain amides in flow reactors.⁵¹ For example, *N*-methylpyrrolidin-2-one in hexane (0.33 M, substrate flow rate 0.06 mL min⁻¹) was hydrogenated in a custom designed flow reactor using 4%Pt–4%Re/TiO₂ as the catalyst at 120 °C under 20 atm H₂ (flow rate of H₂ 190 mL min⁻¹) over 8 hours. 100% selectivity was obtained for *N*-methylpyrrolidine as product (after 8 hours TON 22.6). The authors state that this catalyst is not suitable for substrates containing aromatic functionalities because of arene-ring hydrogenation as a side reaction. Very recently, Rh–Mo/SiO₂/CeO₂⁵² and Pt/Nb₂O₅⁵³ heterogeneous catalysts were reported that operate under 20–80 atm H₂ pressure at 120–200 °C.

Heterogeneous systems have been developed that hydrogenate amides under moderate conditions, with net C–O cleavage. The drawbacks of these heterogeneous catalytic systems are the hydrogenation of aromatic, alkene, and

alkyne groups. Also, it has not been demonstrated that they tolerate a wide variety of functional groups.

Homogeneous catalytic amide hydrogenation via C–O cleavage

There are many reports describing homogeneous catalytic hydrogenations of amides with C–O or C–N cleavage using Ru, Fe, Ir, and Mn-based catalysts. Figure 1.3 shows the homogeneous catalyst system available for the hydrogenation of amides via C–O cleavage pathway.

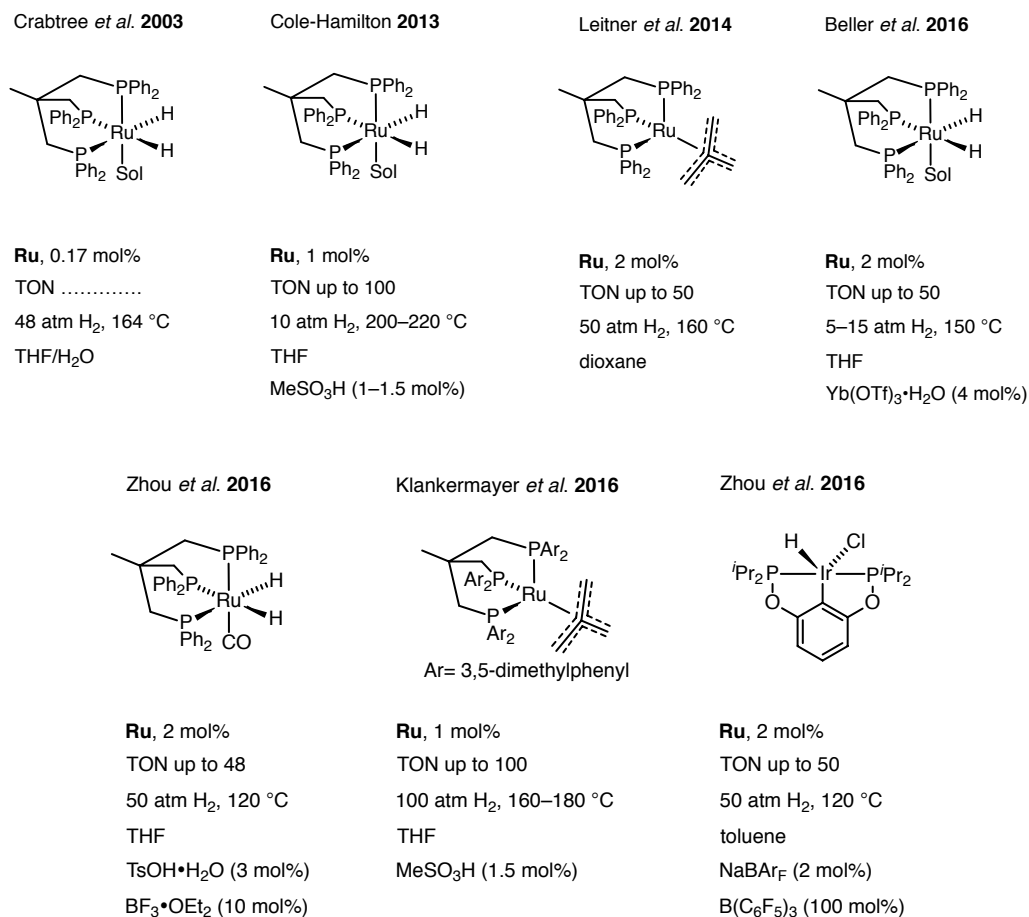
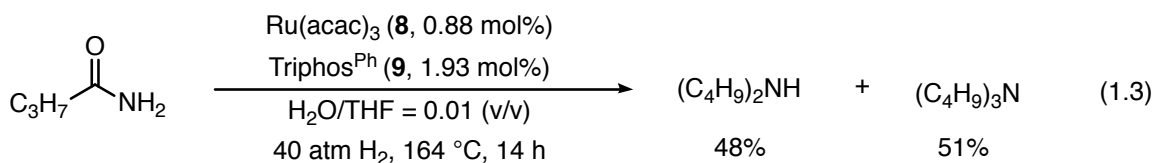
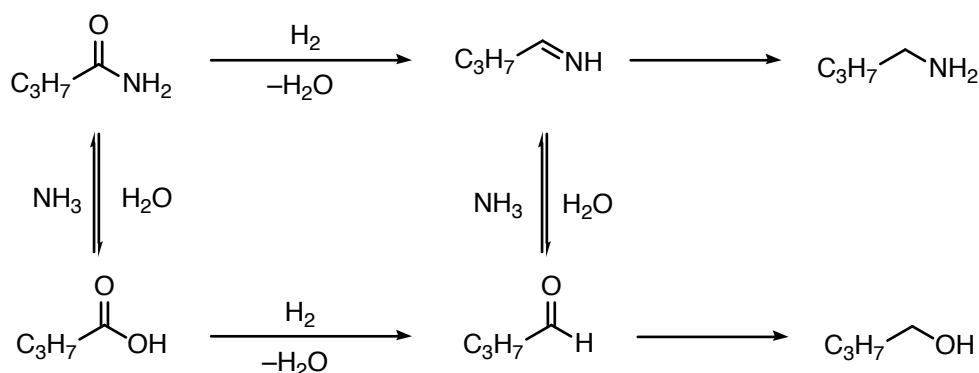


Figure 1.3: Catalyst system for the hydrogenation of amides via C–O cleavage.

The first homogeneous hydrogenation of amides was reported in 2003 by Crabtree and coworkers using $\text{Ru}(\text{acac})_3$ (**8**, acac is acetylacetonate) and $\text{Triphos}^{\text{Ph}}$ (**9**, $\text{Triphos}^{\text{Ph}}$ is 1,1,1-tris(diphenylphosphinomethyl)ethane) in THF under 48 atm H_2 at 164 °C.⁵⁴ Cole-Hamilton reported a similar catalytic system with a 1:2 ratio of **8** to **9**.^{55,56} The hydrogenation of butanamide yielded a ~ 1:1 mixture of $(\text{C}_4\text{H}_9)_2\text{NH}$ and $(\text{C}_4\text{H}_9)_3\text{N}$ under 40 atm H_2 at 164 °C in 14 hours (Eq. 1.3).



The addition of $\text{NH}_4\text{OH}_{(\text{aq})}$ to THF (5 mL of $\text{NH}_4\text{OH}_{(\text{aq})}$ and 10 mL of THF) provided the primary amine, *n*-butylamine, and also *n*-butanol with 85% selectivity. Higher concentrations of $\text{NH}_4\text{OH}_{(\text{aq})}$ increased the amount of water in the reaction, which increased the rate of hydrolysis of the amide and the putative imine intermediate to result in poor selectivity for the *n*-butylamine over *n*-butanol (Scheme 1.6). For example, when the $\text{NH}_4\text{OH}_{(\text{aq})}:\text{THF}$ ratio (10 mL/10 mL) was ~1, only 73% of the primary amine formed along with 25% of alcohol product.



Scheme 1.6: Possible hydrolysis of amide and imine intermediates by excess water.

Breit and coworkers subsequently reported that they were unable to reproduce these results using the conditions reported by Cole-Hamilton and coworkers.⁵⁰ Later, Cole-Hamilton and coworkers reported an amendment to the original report in which the hydrogenation was carried out at 200 °C rather than 164 °C.⁵⁷ Shortly after, these authors reported another catalytic system consisting of **8/9** and catalytic amounts of methane sulfonic acid (MSA).⁵⁸ The hydrogenation of several 2° and 3° amides occurred with 1.0 mol% **8**, 2.0 mol% **9**, and 1.0–1.5 mol% MSA under 10 atm H₂ at 200–220 °C.⁵⁸

The nature of the autoclave determined whether the phenyl rings were hydrogenated. The authors state that Hastolly™ C was ideal, and that use of stainless steel tends to hydrogenate the aromatic rings, which is a common drawback of heterogeneous catalysts. Using a glass liner in a stainless steel autoclave prevented this problem, but there was no explanation for how or why hydrogenation of the arenes occurred. To investigate the nature of the catalyst, the **8/9** system was heated with MSA (1.5 equivalents) in THF at 210 °C under 15 atm H₂ pressure. Many Ru^{II}-triphos complexes with coordinated MSA anions (bridging, monodentate, or chelating) were identified in solution, but none of them contained hydride ligands.

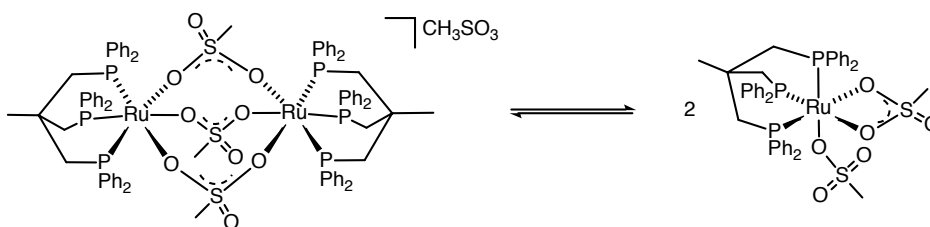
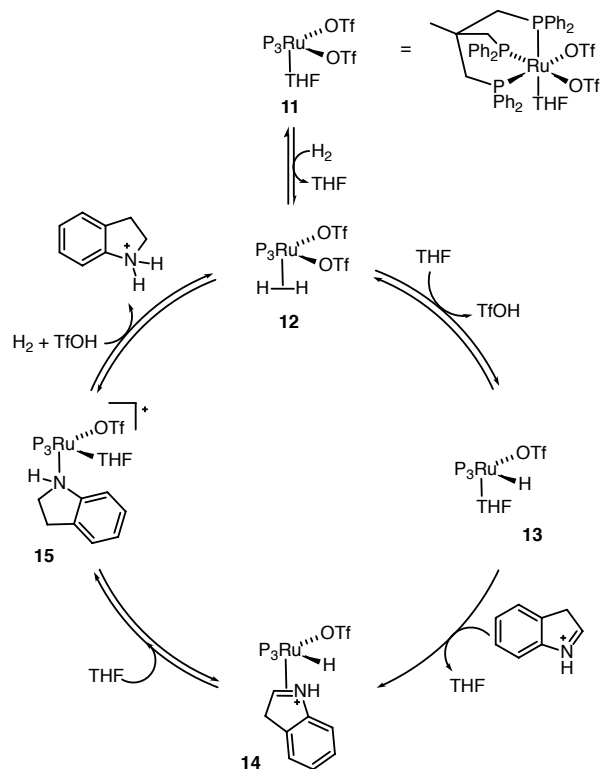


Figure 1.4: Representatives of chelating, bridging, and monodentate Ru-MSA complexes identified by Cole-Hamilton and coworkers.

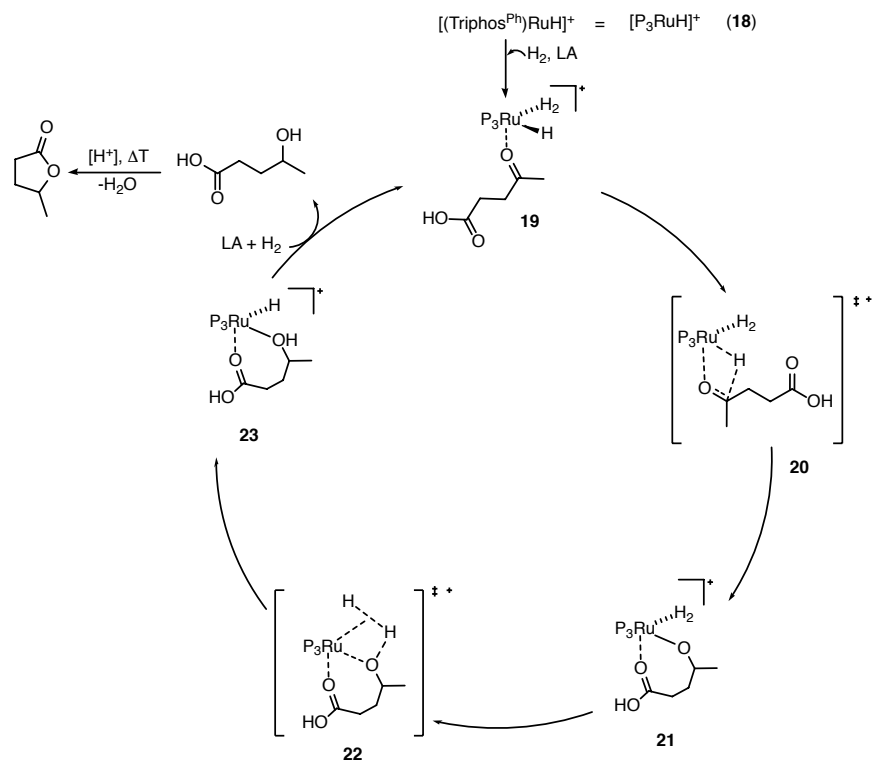
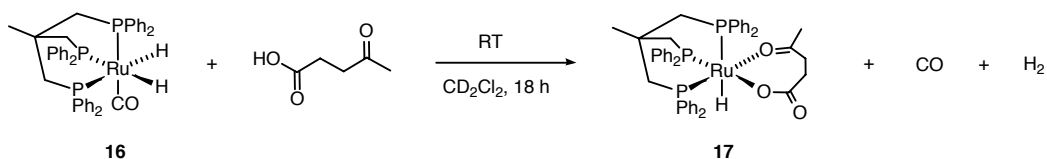
The authors believe these complexes are in equilibrium and are precursors to the active catalysts (Figure 1.4). There are no direct mechanistic investigations of the Cole-Hamilton system in the literature. There are, however studies of related hydrogenations. In 2002, Bianchini and coworkers reported a hydrogenation of indole to indoline using the related catalyst $[\text{Ru}(\text{MeCN})_3(\text{Triphos}^{\text{Ph}})](\text{SO}_3\text{CF}_3)_2$ (**10**) (30 atm H_2 at 60–100 °C in THF) in the presence of triflic acid (TfOH, 10 equivalents).⁵⁹ NMR studies revealed that the MeCN, triflate, and solvent all underwent fast exchange in **10**. Bianchini proposed that ruthenium (II) ions such as $[\text{Ru}(\text{OTf})_2(\text{THF})(\text{Triphos}^{\text{Ph}})]$ (**11**) could be considered as the resting state during the catalysis. This proposal likely relates to Cole-Hamilton's proposed ruthenium-MSA precursor.

Bianchini and coworkers proposed the following mechanism for the hydrogenation of IN (Scheme 1.7). A dihydrogen molecule replaces the THF in **11** to form the ruthenium- $\eta^2\text{-H}_2$ intermediate **12**. The $\eta^2\text{-H}_2$ ligands in Ru(II) complexes like **12** are believed to be acidic,⁶⁰ and the authors proposed that loss of triflic acid forms the hydride intermediate **13**. Protonated indole then replaces the solvent molecule in **13** to generate the intermediate **14**. Hydride insertion leads to **15**, followed by protonolysis of the resulting indolene, and coordination of H_2 to form **12**. The fundamental steps in this mechanism are deprotonation of an acidic $\eta^2\text{-H}_2$ ligand (or proton transfer from an acidic $\eta^2\text{-H}_2$), a substrate-hydride insertion, and protonolysis of the catalyst-product bond to regenerate the catalyst.



Scheme 1.7: Proposed mechanism for the hydrogenation of indole under acidic conditions.

Leitner recently proposed a mechanism with the same fundamental steps for the hydrogenation of levulinic acid (LA)^{54,61-63} using the [(Triphos^{Ph})Ru(CO)(H)₂] (**16**) carbonyl-hydride under acidic conditions.⁶¹ In a control experiment, **16** reacted with LA to form the Ru-carboxylate species **17** by protonolysis of a hydride ligand and loss of CO (Scheme 1.8, top). However, under high pressure, the authors believe that the ruthenium- η^2 -H₂ intermediate **19** provides a more plausible entry into the catalytic cycle (Scheme 1.8, bottom).⁶¹

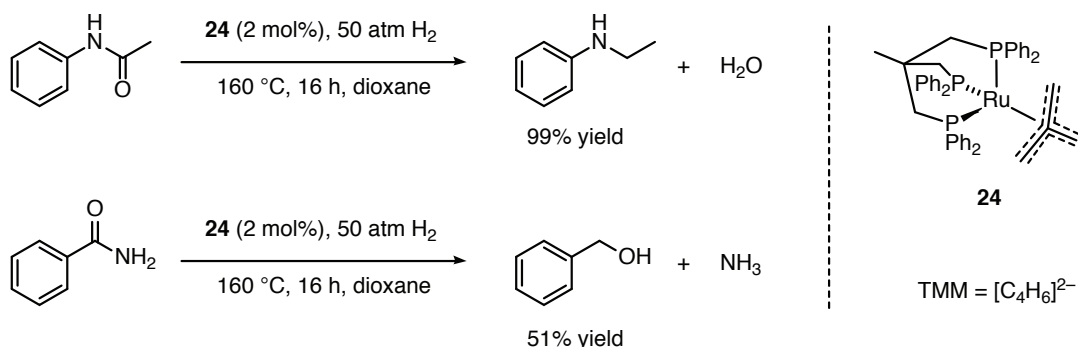


Scheme 1.8: Proposed mechanism for the hydrogenation of levulinic acid to γ -valerolactone in acidic conditions.

Based upon DFT calculations, it is proposed that the ketone-hydride migratory insertion in **19** via transition state **20** eventually leads to the alkoxide **21**. A net protonolysis of the Ru-alkoxide by the η^2 -H₂ ligand generates the product alcohol adduct **23**. The reported mechanisms are not definitive on how the η^2 -H₂ ligand is activated. The likely pathway is by deprotonation of an acidic, σ - η^2 -H₂ ligand.⁶⁴ The transition state **22** illustrates how an intramolecular deprotonation may occur to

generate **23**. Transition state **22** is similar to those proposed for the Sigma-CAM process.⁶⁵

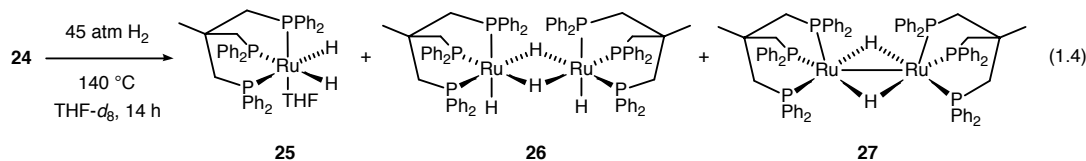
Later, Leitner and coworkers reported a neutral catalyst, [(Triphos^{Ph})Ru(TMM)] (**24**, TMM is trimethylene methane), for the hydrogenation of amides without the use of acid additives.⁶² The secondary amide acetanilide was hydrogenated to *N*-ethylaniline using 2 mol% of **24** under 50 atm H₂ at 160 °C in dioxane with a 99% yield (TON ~50) after 16 hours (Scheme 1.9, top). The primary amide benzamide was hydrogenated to benzyl alcohol via C–N cleavage in 51% yield under the same conditions (Scheme 1.9, bottom).



Scheme 1.9: Hydrogenation of secondary and primary amides using the neutral catalyst **24**.

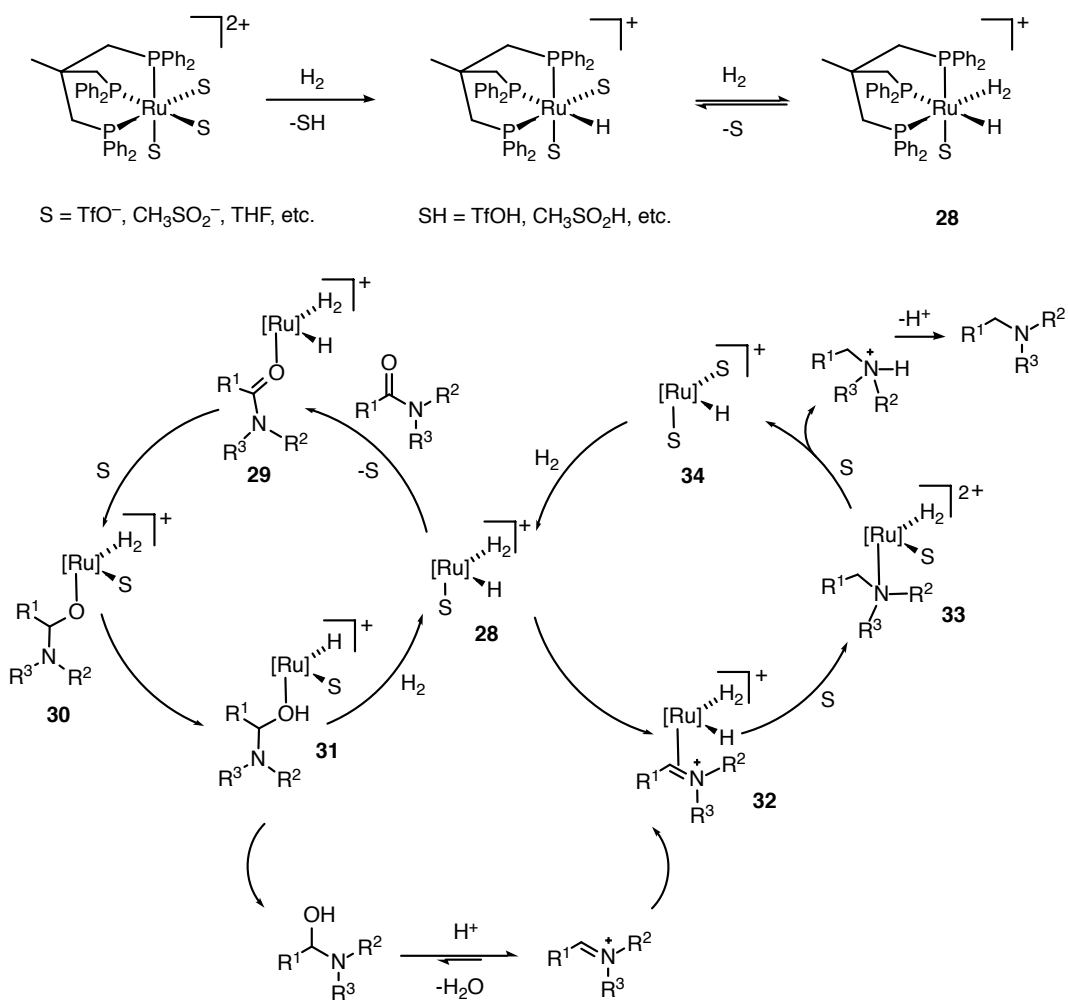
The authors emphasized that more research is required to understand the selectivity for C–N cleavage by this neutral catalyst. In order to investigate any potentially catalytically relevant intermediates, a solution of **24** in THF-*d*₈ was treated under 45 atm H₂ at 140 °C for 14 hours. The ruthenium dihydride [(Triphos^{Ph})Ru(H)₂(THF)] (**25**), and the dimers **26** and **27** formed as a result of

heating (Eq. 1.4). Compound **27** is an unusual Ru(I) species, formally with a Ru–Ru bond.



Complexes **25** and **26** converted into $[(\text{Triphos}^{\text{Ph}})\text{Ru}(\text{CO})(\text{H})_2]$ (**16**) under 9 atm CO at room temperature. Compound **16** is observed during the hydrogenation of amides, and presumably forms by decarbonylation of an aldehyde.⁶⁶ The CO ligand in **16** blocks the coordination site for the neutral hydrogenation mechanism and reduces the catalytic activity. However, acid (HNTf_2) converts **16** to the cationic species $[(\text{Triphos}^{\text{Ph}})\text{Ru}(\text{THF})(\text{H})(\text{H}_2)]^+$ (**28**) which can undergo the cationic catalytic cycle consistent with the previous studies.^{58,61}

Based on these findings it is plausible that the hydrogenation of amides by Ru(Triphos) compounds under acidic conditions proceeds via the Ru(II)-cationic species $[(\text{Triphos}^{\text{Ph}})\text{Ru}(\text{S})_3]^{2+}$ where S is counter anion or solvent. This species generates the ruthenium hydride $[(\text{Triphos}^{\text{Ph}})\text{Ru}(\text{H})(\text{S})_2]^+$ as shown in Scheme 1.10 (top). This ruthenium hydride would be in equilibrium with dihydride **28** under hydrogen (Scheme 1.10, top). These amide hydrogenations then likely proceed by the same fundamental steps as the previous mechanisms: substrate hydride insertion and protonolysis of a catalyst product bond by an acidic $\eta^2\text{-H}_2$ ligand. One proposed mechanism is shown in Scheme 1.10 (bottom).



Scheme 1.10: Plausible mechanism for the hydrogenation of amides via C–O cleavage under acidic condition.

As shown in Scheme 1.10 (bottom), the reaction may involve two catalytic cycles. The first is hydrogenation of the amide to the hemiaminal. The second is dehydration of the hemiaminal followed by hydrogenation of the resulting iminium ion. One function of the added acid would be to catalyze the dehydration of the hemiaminal to iminium species. Protonation of hydroxyl group in the hemiaminal induces the elimination of water and form the corresponding iminium ion.

In a recent report by Beller and coworkers, the Lewis acid $\text{Yb}(\text{OTf})_3 \cdot \text{H}_2\text{O}$ was used as a cocatalyst along with the **8/9** catalytic system to hydrogenate a variety of 2° and 1° amides with net C–O cleavage to the corresponding higher amine in over 95% yield and with 50–100% selectivity (5 atm H_2 , 150 °C, THF).⁶⁷ The authors showed that $\text{Yb}(\text{OTf})_3 \cdot \text{H}_2\text{O}$ performs better than the other cocatalysts including MSA, TfOH, or HNTf_2 .^{58,62} To investigate the mechanism, the hydrogenation of benzanilide was monitored under 15 atm H_2 at 150 °C in THF (Eq. 1.5).

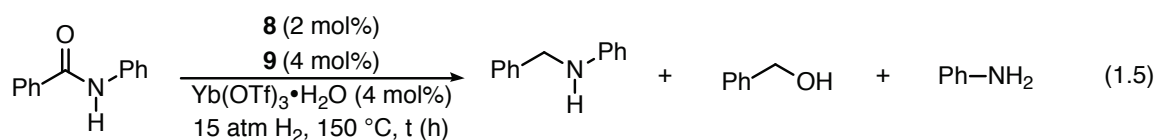


Figure 1.5 shows the change in concentration of hydrogenation products over a period of 25 hours. The C–N cleavage products benzyl alcohol and aniline were produced as the major species at the beginning of the reaction, and reached a maximum in about three hours.

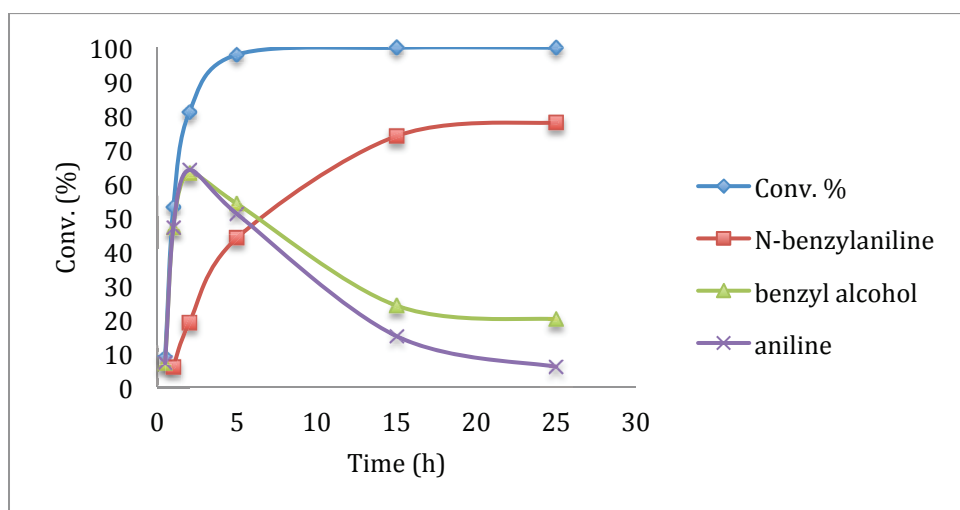
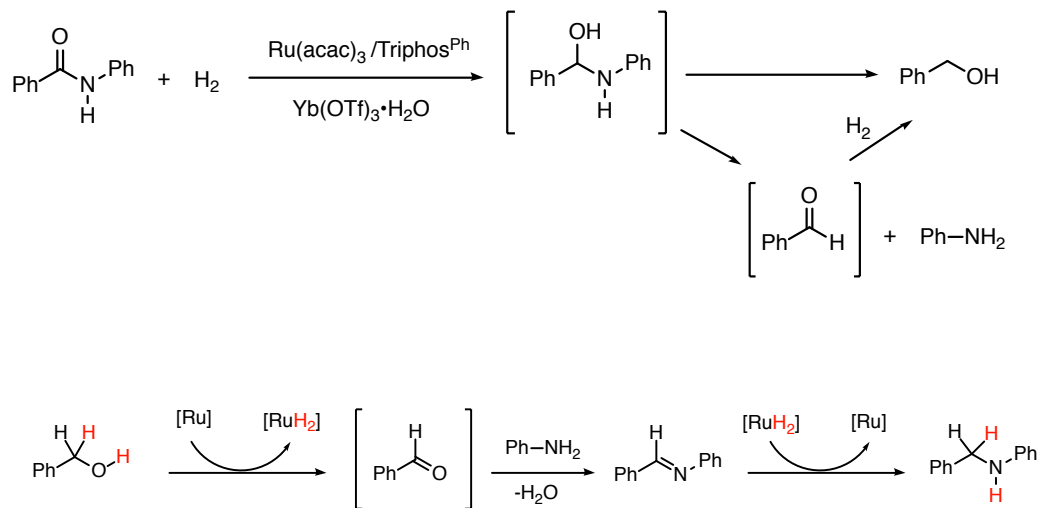


Figure 1.5: Variation of the substrate conversion and yields of the products over time under hydrogenation conditions of 15 atm H_2 , 150 °C, using the catalytic system **8/9**/ $\text{Yb}(\text{OTf})_3$.

The concentrations of these C–N cleavage products then drop, and the concentration of *N*-benzylaniline increases. The complete consumption of the starting material occurs in ~5 hours. These results show that benzyl alcohol and aniline are produced as the initial amide hydrogenation products that are then converted to *N*-benzylaniline.

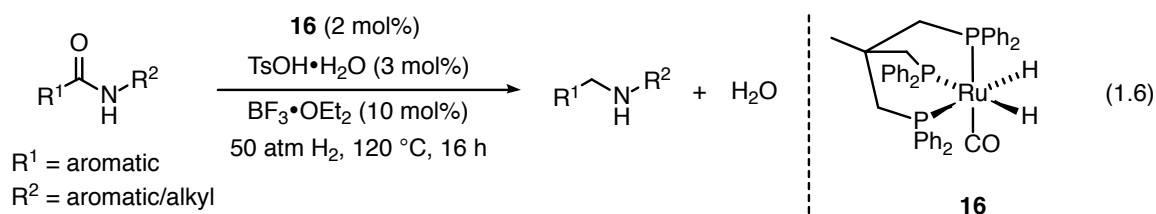
From a series of control experiments, the authors showed that $\text{Yb}(\text{OTf})_3 \cdot \text{H}_2\text{O}$ alone is not able to catalyze this reaction, nor is **8/9**. It is notable that even without hydrogen the benzyl alcohol and aniline are converted into *N*-benzylaniline. Scheme 1.11 shows the mechanism proposed by the authors for these hydrogenations. First, the amide is hydrogenated to generate the hemiaminal, which eliminates H_2O to generate the aldehyde and the non-alkylated amine. Hydrogenation of the aldehyde generates benzyl alcohol. These compounds then produce the higher amine via the borrowing hydrogen pathway outlined in Scheme 1.11 (bottom).



Scheme 1.11: Plausible mechanism for the hydrogenation of amides via borrowing hydrogen pathway to produce C–O cleavage products.

In this mechanism, the alcohol is dehydrogenated to form aldehyde and a dihydride ruthenium species. Condensation of the aldehyde and amine forms the corresponding imine, which is hydrogenated by the ruthenium dihydride to form *N*-benzylaniline. This result raises the possibility that many amide hydrogenations might first proceed through C–N cleavage, and longer reaction times lead eventually to the higher amine.

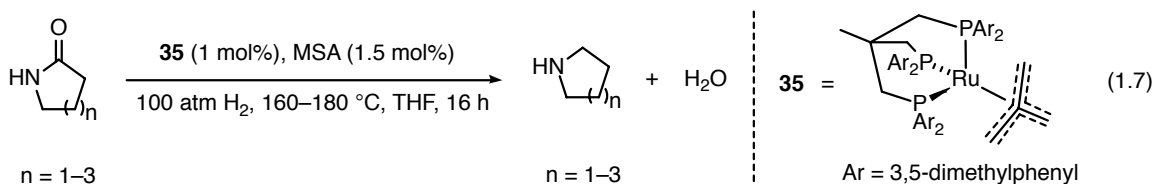
Zhou and coworkers reported the hydrogenation of secondary amides to the corresponding amine using the precursor **16** under 50 atm H₂ at 120 °C in THF in the presence of both a Bronsted acid (TsOH·H₂O) and a Lewis acid (BF₃·OEt₂) (Eq. 1.6).⁶⁸



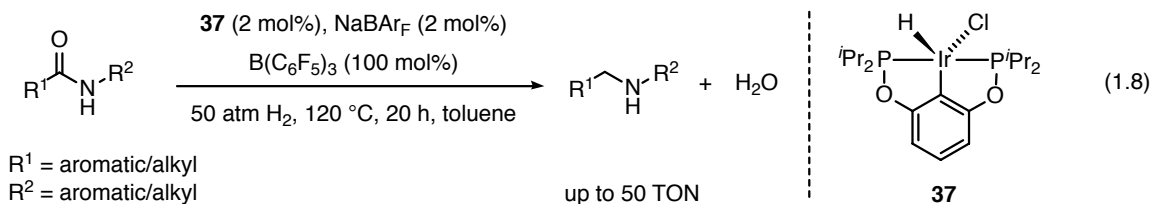
The hydrogenation gives the corresponding higher amine products in 80–95% yield (40–48 TON) with 92–98% selectivity. Halides, alcohols, pyridine, and a furan functional group tolerated the reaction conditions. Interestingly, ethyl/methyl ester functional groups on the aromatic ring were left intact during these hydrogenations. The selectivity towards amides over esters was justified by the formation of an amide-BF₃ adduct that activates the amide carbonyl group in favor of an ester-BF₃ adduct.⁶⁹

More recently, Klankermayer and coworkers reported a catalytic system **35**, containing **8** and a modified version of Triphos, 1,1,1-tris(di(3,5-dimethylphenyl)phosphinomethyl)ethane (**36**). The catalytic system **35** hydrogenates γ , δ , and ϵ -

lactams to corresponding cyclic amines under 100 atm H₂ at 160–180 °C in the presence of MSA (Eq. 1.7).⁷⁰



Recently, Zhou and coworkers reported an iridium-based pincer complex **37** that hydrogenates a variety of secondary amides to the corresponding amines under 50 atm H₂ at 120 °C in toluene in the presence of a catalytic amount of NaBAR_F (BAR_F is tetrakis[3,5-bis(trifluoromethyl)phenyl]borate) and a stoichiometric amount of the Lewis acid B(C₆F₅)₃ (Eq. 1.8).⁷¹ Secondary amides were converted to the corresponding amines by C–O cleavage in a 72–98% yield and with 88–100% selectivity. It is likely that this compound undergoes halide metathesis to generate a cationic Ir catalyst and NaCl precipitate.



Only one tertiary amide was reactive towards this hydrogenation: *N*-phenyl-2-pyrrolidinone was hydrogenated in 29% yield with 100% selectivity for C–O cleavage. Primary amides were inactive.

Homogeneous catalytic hydrogenation of amides via C–N cleavage

A number of homogeneous catalysts have been developed that hydrogenate amides via C–N cleavage to produce the corresponding alcohol and amine products.

Figure 1.6 shows the homogeneous catalyst system available for the hydrogenation of amides via C–N cleavage pathway.

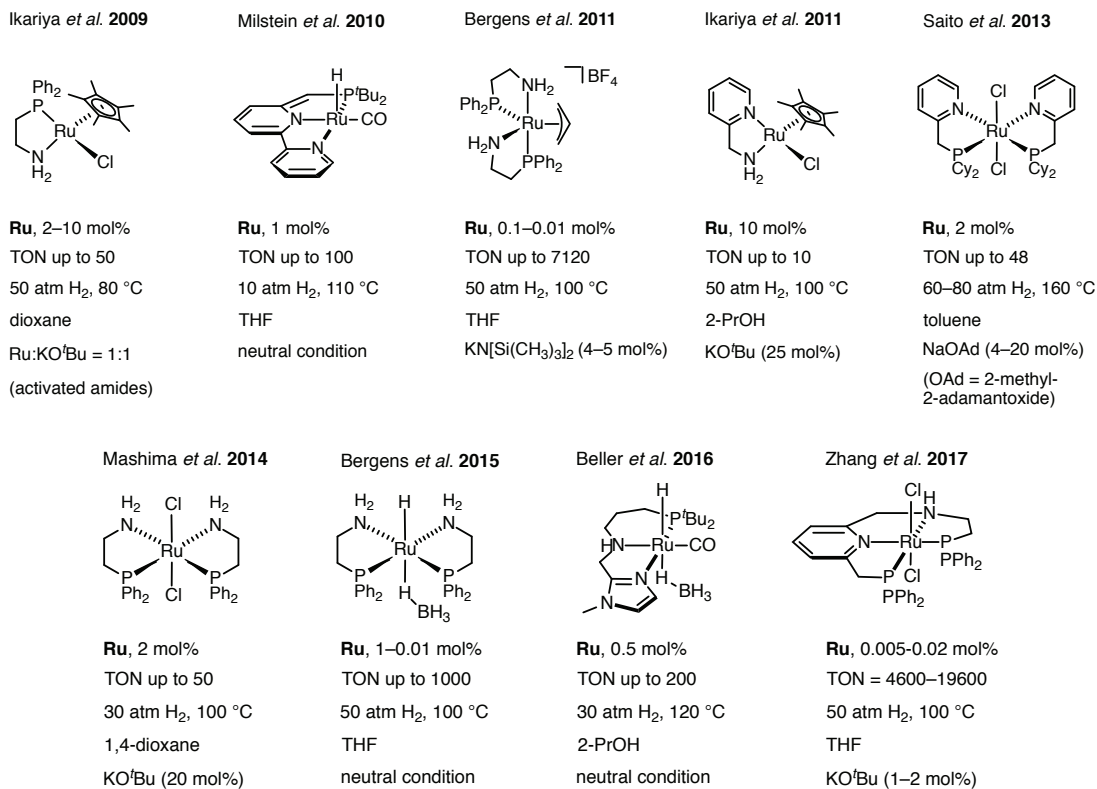
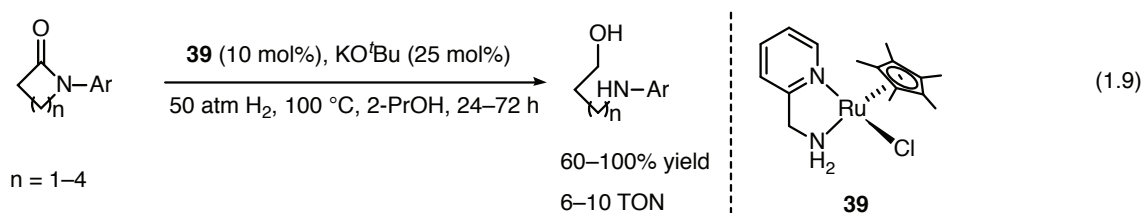


Figure 1.6: Catalyst system for the hydrogenation of amides via C–N cleavage.

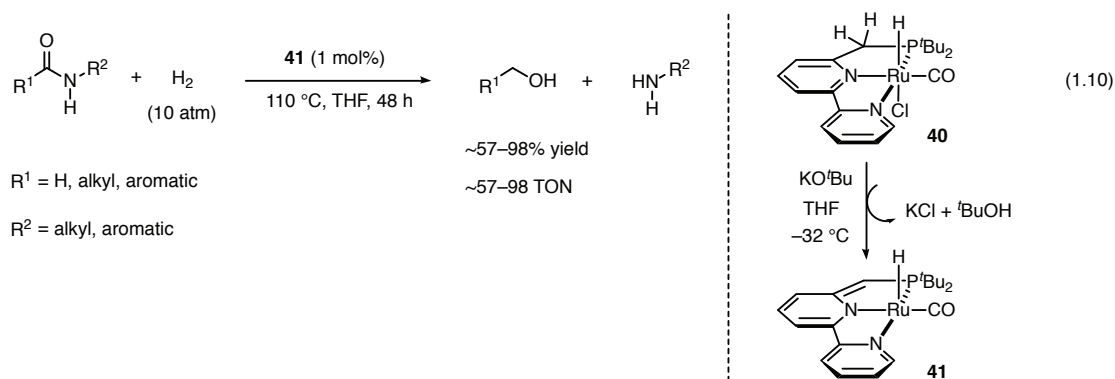
In 2009, Ikariya and coworkers reported the bifunctional homogeneous catalyst Cp*₂RuCl(Ph₂PCH₂CH₂NH₂) (**38**) (Cp* = η⁵-C₅(CH₃)₅) for the hydrogenation of activated amide derivatives such as *N*-acylcarbamates and *N*-acylsulfonamides to the corresponding C–N cleavage products with high catalyst loadings (10 mol% Ru, 30 atm H₂, 80 °C, KO^tBu, *tert*-butanol).⁷² In subsequent work, it was reported that the non-phosphine catalyst Cp*₂RuCl(2-aminomethylpyridine) (**39**) hydrogenates lactams and certain amides to the corresponding C–N cleavage products (50 atm H₂,

100 °C, KO^tBu, 2-propanol) in 60–100% yield, but also with high catalyst loadings (10% of **39**, 6–10 TON) (Eq. 1.9).^{73,74}

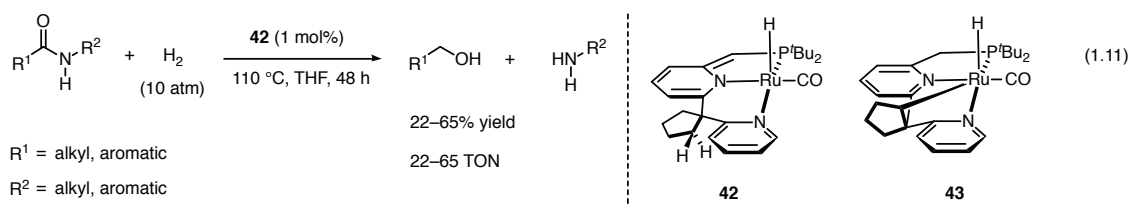


N-Aryl Lactams (β , γ , δ , and ϵ) were hydrogenated to the corresponding amino alcohol products. The simple aromatic amides benzanilide and *N*-methyl-*N*-phenylbenzamide were also hydrogenated to the corresponding amine and alcohol products.

Subsequently, Milstein and coworkers reported that ruthenium pincer complexes hydrogenate amides under neutral conditions.^{75,76} These catalysts were synthesized by reacting [Ru(H)(CO)(Cl)(PNN)] or [Ru(H)(CO)(Cl)(PNP)] (PNN = 6-di-*tert*-butylphosphinomethyl-2,2'-bipyridine, PNP = 2,6-bis(diisopropylphosphino methyl)pyridine) with a stoichiometric amount of the strong base KO^tBu to form the so-called dearomatized compounds such as **41** (Eq. 1.10). The dearomatized pincer complex [Ru(H)(CO)(PNN)] (**41**) operates under 10 atm H₂ at 110 °C in THF to hydrogenate a variety of 2° and 3° amides to form the amine and alcohol products under neutral conditions (Eq. 1.10). Note that 10 atm is the pressure of the reaction used before heating to 110 °C. The operating pressure is higher. It is an unfortunate, common practice to report only the room temperature pressure in the hydrogenation literature.

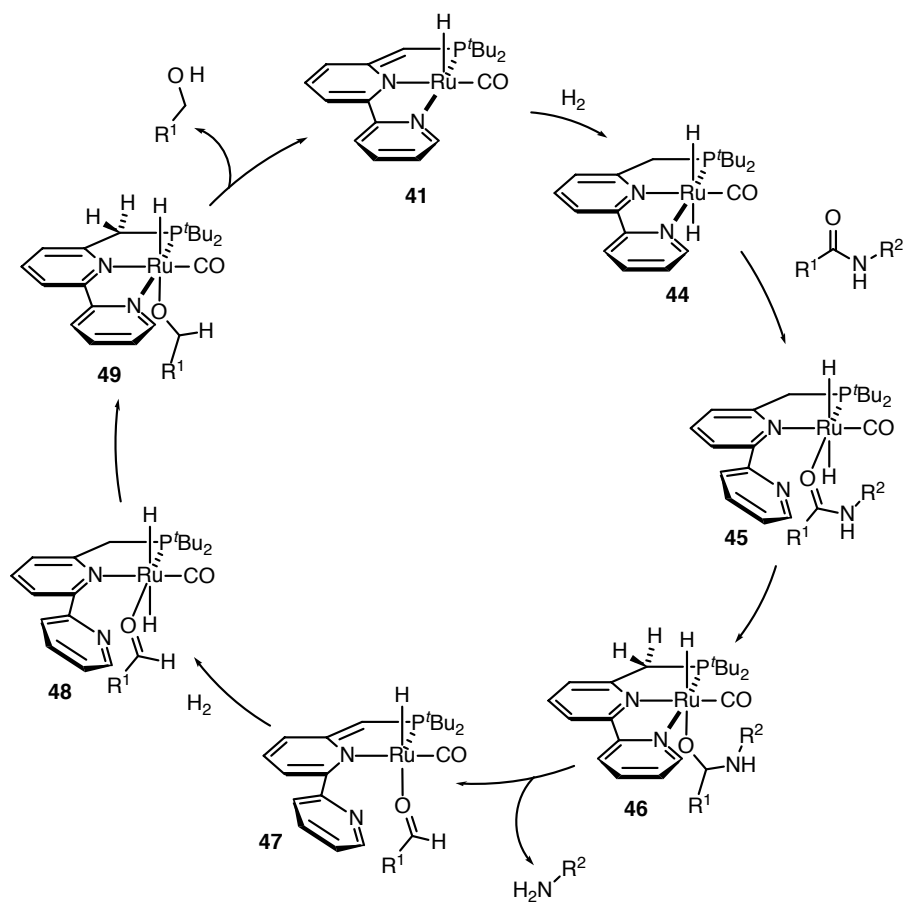


Tertiary amides of the type $\text{RC}(\text{O})\text{NR}'_2$, in which R = H or an alkyl group, and NR'_2 = cyclic amines such as morpholine or pyrrolidine, were hydrogenated to yield the corresponding alcohol and cyclic amine with up to 98 TON. This system was a breakthrough because it was the first homogeneous catalyst that hydrogenates unactivated amides with only 1 mol% catalyst. This system did still require high temperature (110 °C), but low pressures of H_2 . Later, a bridged bipyridine-based ruthenium-PNN catalyst **42** was reported for the hydrogenation of secondary amides under similar conditions (Eq. 1.11).⁷⁷



Catalyst **42** was only moderately active compared to catalyst **41**. The authors attributed the low activity to the cyclometalation of **42** by intramolecular C–H activation to form the sluggish catalyst **43**. Scheme 1.12 shows the mechanism proposed by Milstein and coworkers. Complex **41** undergoes dihydrogen addition by metal-ligand cooperation to a coordinatively saturated *trans* dihydride complex **44**. One hydrogen atom is transferred to the methylene backbone carbon centre

(benzylic arm) during this addition. De-coordination of the pyridyl arm in **44** provides a vacant site to coordinate the amide and form **45**.

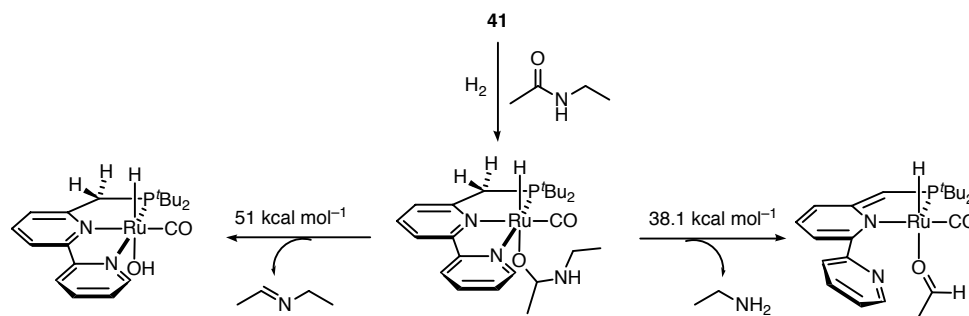


Scheme 1.12: Proposed mechanism for the hydrogenation of amides via C-N cleavage using a pincer type catalyst **41**.

Hydride transfer to the amide carbonyl group leads to the ruthenium-hemiaminoxy intermediate **46**. Milstein then proposed that **46** eliminates amine via a ligand-assisted mechanism to form the dearomatized ruthenium complex **47** bearing the coordinated aldehyde. Addition of dihydrogen to **47**, followed by hydride transfer leads to the aromatized complex **48**, and eventually to the alkoxy intermediate **49**. Deprotonation of the benzylic arm regenerates catalyst **41** along with the alcohol

product. The authors emphasized that the catalytic cycle does not involve the free hemiaminal, thereby avoiding water elimination to give the imine, and the C–O cleavage product.

Cantillo performed DFT calculations to investigate C–O versus C–N cleavage during the hydrogenation *N*-ethylacetamide using **41**. *N*-Ethylacetamide was used as the model substrate because Milstein and coworkers hydrogenated it with the catalyst **41**. The calculated energy barrier for C–O cleavage is ~ 12 kcal mol⁻¹ higher than that for C–N cleavage (Scheme 1.13).⁷⁸

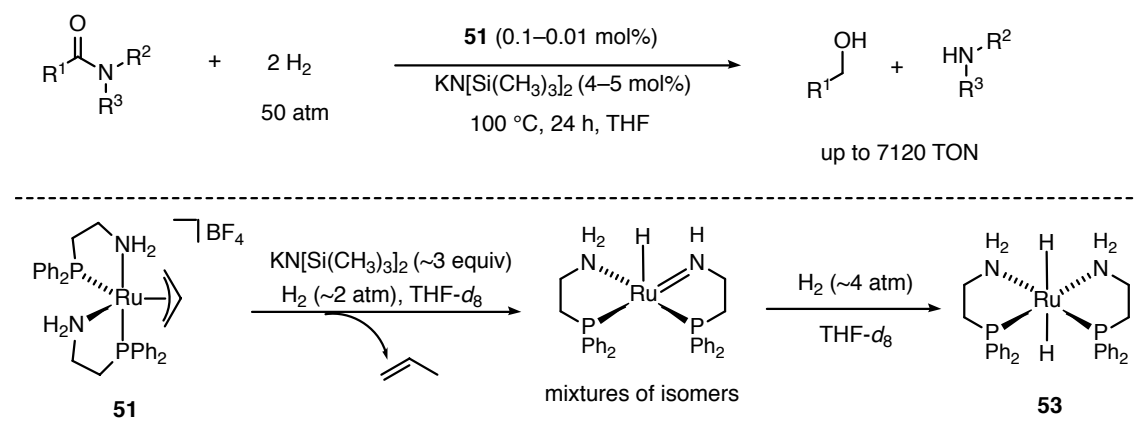


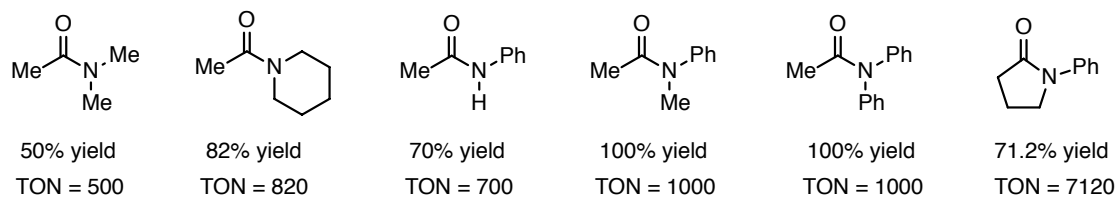
Scheme 1.13: The energy barriers for C–N and C–O cleavage during the hydrogenation of *N*-ethylacetamide by **41**.

Bergens and coworkers studied the use of Noyori's ketone hydrogenation catalyst *trans*-[Ru(H)₂((*R*)-BINAP)((*R,R*)-dppe)] (**50**, BINAP is 2,2'-bis(diphenylphosphino)-1,1'-binaphthyl, dppe is 1,2-diphenyl-1,2-diaminoethane) for the hydrogenation of activated amides (50 atm H₂, 100 °C).^{79,80} The activity of **50** towards amides was lower than expected considering its high activity towards ketones, esters, and imides.^{81–84} The dihydride **50** is unstable at room temperature in the absence of a reactive substrate. In the presence of ketones, for example, **50** rapidly forms the corresponding ruthenium alkoxides by a net ketone-hydride

insertion. These alkoxides are stable at room temperature, essentially providing thermal protection for the catalyst. Amides do not react with **50** in the absence of base at room temperature. It was likely then that **50** decomposed at the 100 °C typically required for amide hydrogenations, perhaps by dissociation of the open ligand. It was hypothesized that introducing a P–N ligand that would maintain catalytic activity at higher temperature by preventing diamine ligand dissociation.

Bergens and coworkers discovered that the catalyst $[\text{Ru}(\eta^3\text{-C}_3\text{H}_5)(\text{Ph}_2\text{P}(\text{CH}_2)_2\text{NH}_2)_2]\text{BF}_4$ (**51**) is highly active for the hydrogenation of amides and lactams under 50 atm H_2 at 100 °C in the presence of the base $\text{KN}[\text{Si}(\text{CH}_3)_3]_2$ (potassium bis(trimethylsilyl)amide) (Scheme 1.14). Turnover numbers up to 7200 were obtained after 24 hours. At the time, these were the highest reported turnovers for amide hydrogenations at moderate temperatures and pressure. Secondary and tertiary amides were hydrogenated with good yield and turnover numbers as well (Scheme 1.14; bottom).

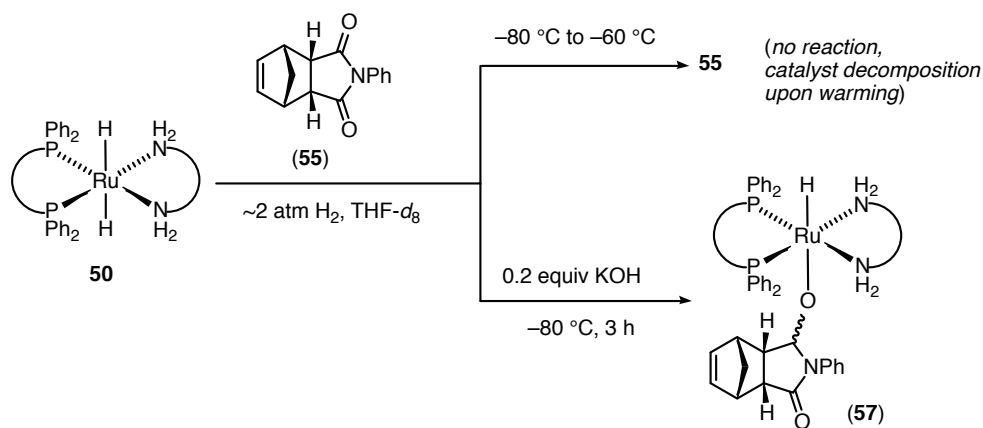




Scheme 1.14: Hydrogenation of amides and substrate scope by catalysts **51**.

In preliminary mechanistic experiments, the allyl precursor **51** was found to react with H₂ (~1–2 atm) at 60 °C with 3 equivalents of KN[Si(CH₃)₃]₂ to form a mixture of Ru-amide monohydrides and propylene. At higher pressures (~4 atm H₂) these amides form the dihydride as the major product, and the active catalyst is proposed to be *trans*-[Ru(H)₂(Ph₂P(CH₂)₂NH₂)₂] (**53**). The dichloride RuCl₂(Ph₂P(CH₂)₂NH₂)₂ (**52**) forms the same ruthenium dihydride under these conditions. Indeed both **51** and **52** hydrogenated the lactam in up to 7200 turnovers under these conditions using sodium methoxide (NaOMe) as base.

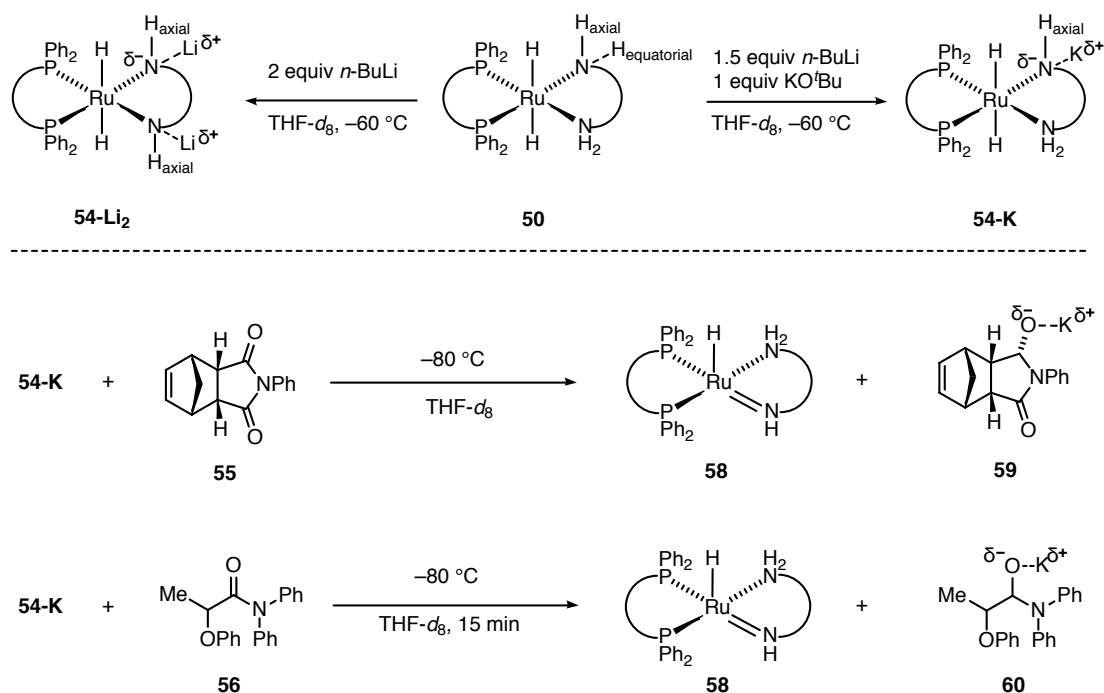
Recently, Bergens and coworkers reported the only experimental mechanistic study on an amide hydrogenation with the active catalyst.⁸⁵ In prior work, the Bergens group showed that the BINAP-dpen catalyst **50** hydrogenates mesocyclic imides by desymmetrization in up to 97% de at 0 °C.⁸⁴ During these investigations it was found that unexpectedly the bifunctional addition between **50** and the imide did not occur in the absence of base. Remarkably, even at –80 °C the presence of trace base (< amount Ru) effectively catalyzed this bifunctional addition (Scheme 1.15).



Scheme 1.15: The role of the base in the bifunctional addition between **50** and **55**.

This is the first example of a base catalyzed stoichiometric bifunctional addition.⁸⁵ This result led them to investigate the actual catalyst involved in the hydrogenation. Eventually they found that mono or di deprotonation of the N–H groups in **50** occurred with excess strong base to form *trans*-M⁺[RuH₂((*R,R*)-BINAP)((*R,R*)-H₂NCH(Ph)CH(Ph)NH⁽⁻⁾)] (**54-M**; where M = K⁺ or Li⁺), or *trans*-(M⁺)₂[Ru(H)₂((*R,R*)-BINAP)((*R,R*)-HN⁽⁻⁾CH(Ph)CH(Ph)NH⁽⁻⁾)] (**54-M₂**; where M = Li⁺), respectively (Scheme 1.16: top).

These deprotonated dihydrides **54-M** and **54-M₂** were highly active towards the bifunctional addition of imides and amides, even at –80 °C. These anions **54-M** and **54-M₂** likely are highly active because the lone pair on the amide N increases the electron density on Ru and thus the nucleophilicity of the Ru–H towards carbonyl compounds. Scheme 1.16 (bottom) outlines the examples for the bifunctional addition of a *meso*-cyclic imide **55** and an amide **56** (**56** is *N,N'*-diphenyl-2-phenoxy propanamide) to **54-K**.

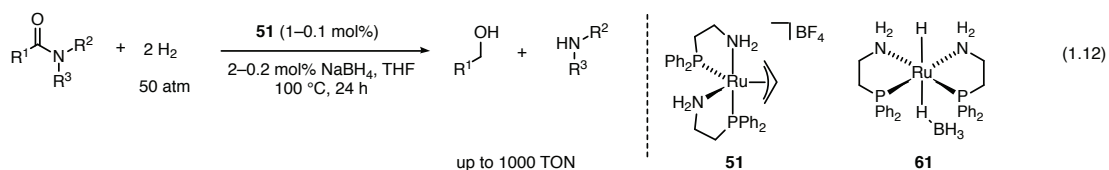


Scheme 1.16: Top: mono, or di-deprotonation of **50** to form the electron-rich **54-K** and **54-Li₂**. Bottom: the products observed for the bifunctional addition of **54-K** to **55** and **56**.

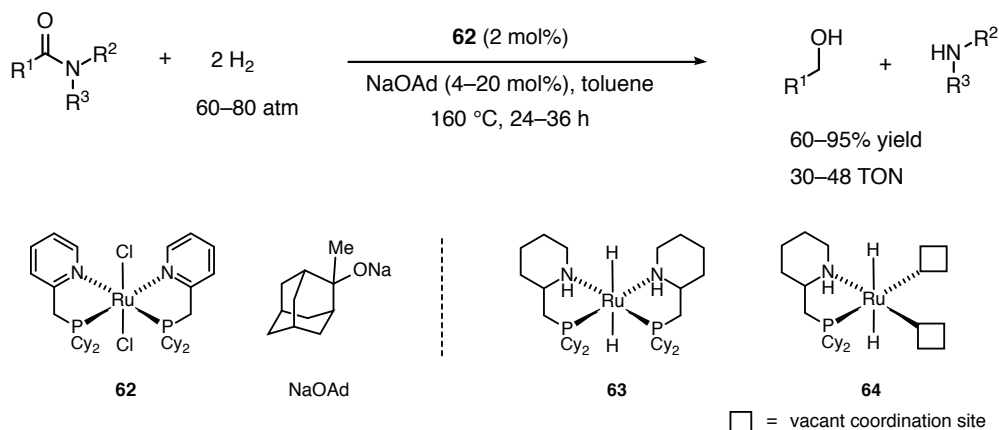
It is notable that the addition of **54-K** to **55** or **56** resulted in the Ru-amide **58**, which is an intermediate proposed in the hydrogenation of ketones by **50**.^{81,82} These results show that an acidic N–H bonded to the metal center of the catalyst can be deprotonated with base to form highly active amide hydrogenation catalysts. This design feature has been incorporated into several base-assisted catalysts in the recent literature (*vide infra*).

The Bergens group developed a base-free version of the catalyst, *trans*-[Ru(H)(η^1 -BH₄)(Ph₂P(CH₂)₂NH₂)₂] (**61**) that was generated *in situ* by the reaction between the allyl-precursor **51** and two equivalents of NaBH₄ (with respect to B) at 60 °C under ~2 atm H₂. This catalyst **61** hydrogenates amides to corresponding

alcohol and the amine at 100 °C under 50 atm H₂ with up to a 100% yield (TON 1000) in THF in the absence of added base. (Eq. 1.12).⁸⁶ This work is detailed in Chapter 2 of this dissertation.



In 2013, Saito and coworkers reported a catalyst system containing RuCl₂(2-C₅H₄NCH₂PPh₂)₂ (**62**) and the bulky base NaOAd (NaOAd is sodium 2-methyl-2-adamantoxide) that hydrogenates unactivated amides to the corresponding alcohols and amines.⁸⁷ Scheme 1.17 shows the general hydrogenation reaction and conditions (60–80 atm H₂, 160 °C, toluene).

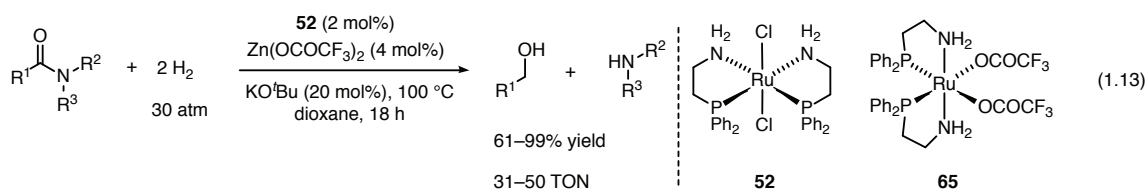


Scheme 1.17: Hydrogenation of amides by Saito's catalyst **62**.

The ³¹P NMR and mass spectrometry data obtained after the optimum induction period for the catalyst showed that the aromatic rings of **62** were hydrogenated to form the complexes **63** and **64**. The authors concluded, along with the negative Hg test, that either **63** or **64** is responsible for the hydrogenation. The hydrogenation of

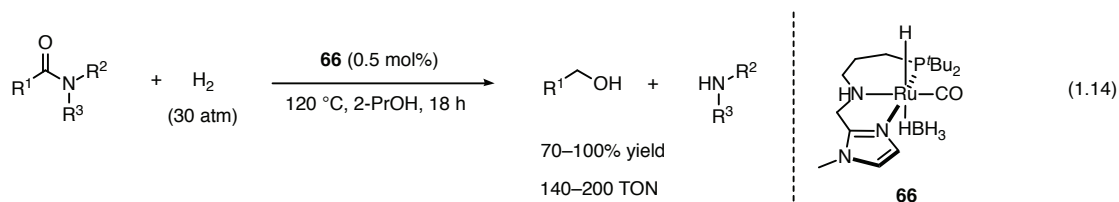
1°, 2°, and 3° amides was demonstrated. Primary amides were less reactive. For example, benzamide was hydrogenated to benzyl alcohol with 87% (TON 44) conversion after 216 hours.

In 2014, Mashima and coworkers described a catalyst system containing **52** and $\text{Zn}(\text{OCOCF}_3)_2$ as an additive. This catalyst system hydrogenates 2° and 3° amides to the corresponding C–N cleavage products under 30 atm H_2 at 100 °C in 18 hours with 31–99% yield (up to 50 TON) in 1,4-dioxane solvent under basic conditions (Eq. 1.13).⁸⁸



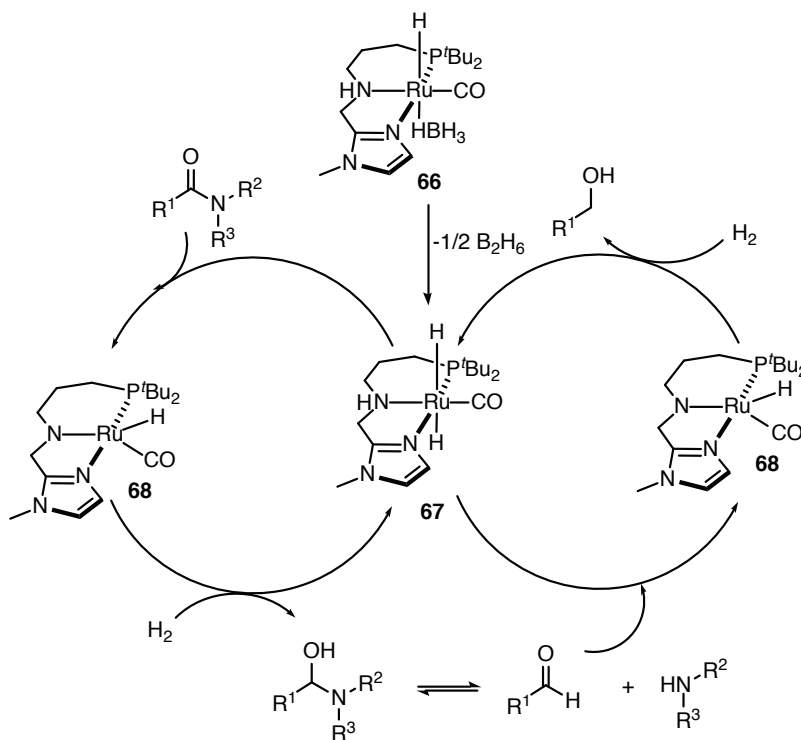
NMR and crystallographic analysis showed that *cis*-[Ru(OCOCF₃)₂(Ph₂P(CH₂)₂NH₂)₂] (**65**) formed when **52** reacted with $\text{Zn}(\text{OCOCF}_3)_2$ in the presence of KO^tBu in 1,4-dioxane-*d*₈.

In 2016, Beller and coworkers reported a ruthenium pincer complex **66**, bearing an imidazolylaminophosphino ligand that hydrogenates secondary and tertiary amides to the corresponding C–N cleavage products (30 atm H_2 , 120 °C, 2-PrOH) under neutral conditions (Eq. 1.14).⁸⁹



Several secondary amides (R^1 = alkyl or aromatic, R^2 = Ph or functionalized aryl) were reduced in quantitative yield (TON 200). However, replacing R^2 with an alkyl

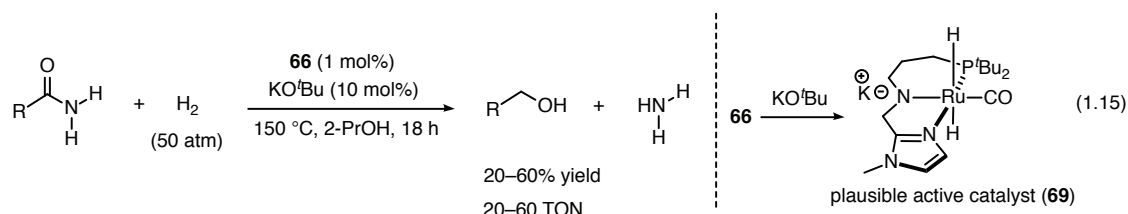
group reduced the conversion to 75–82% (TON 150–162). Tertiary amides were hydrogenated with 92–100% yield (TON 182–200). Scheme 1.18 outlines the proposed mechanism by the authors. The catalytic precursor **66** releases B_2H_6 to form the ruthenium dihydride **67** as the plausible entry into the catalytic cycle.



Scheme 1.18: Proposed mechanisms for the hydrogenation of an amide via C–N cleavage products using pincer-type catalyst **66**.

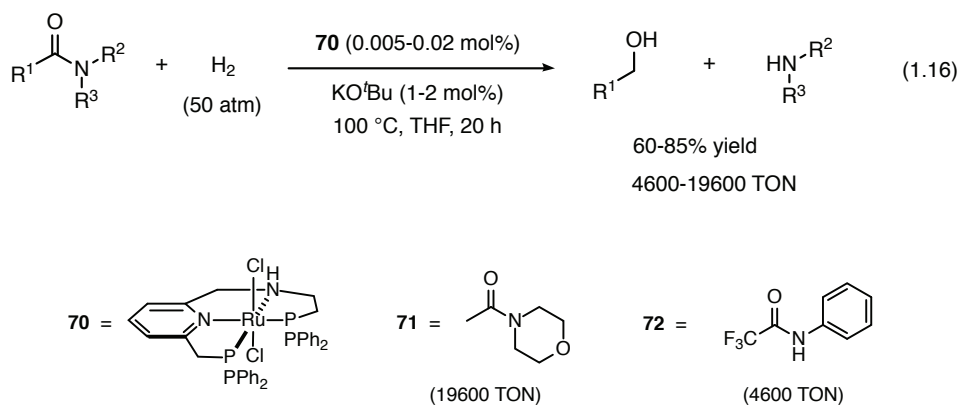
The dihydride then reacts with the amide substrate to form intermediate **68** along with the hemiaminal. Dihydrogen addition to **68** then regenerates the ruthenium dihydride **67**.

Primary amides required forcing conditions and were hydrogenated to the corresponding alcohol and ammonia in 25–60% yield (TON 25–60) (50 atm H₂, 150 °C, IPA) under basic conditions (Eq. 1.15).



The authors emphasized that the use of the base KO^tBu is consistent with the recent work by Bergens and coworkers.⁸⁵ The base increases the nucleophilicity of the coordinated hydride in the ruthenium dihydride **67** by deprotonating the ligand's aliphatic nitrogen.

Zhang and coworkers recently reported an active tetradentate Ru-PNNP catalyst (**70**) that operates under 50 atm H_2 at 100 °C in the presence of KO^tBu to hydrogenate several simple amides to their corresponding alcohol and amide products (Eq. 1.16).⁹⁰



N-aryl acetamides ($\text{R}^1 = \text{CH}_3$, $\text{R}^2 = \text{aryl}$, $\text{R}^3 = \text{H}$) were hydrogenated in 60–98% yield with excellent TONs (6500–19600) regardless of the electronic nature of the substituents on the aryl ring. *N*-alkyl acetamides ($\text{R}^1 = \text{CH}_3$, $\text{R}^2 = \text{alkyl}$, $\text{R}^3 = \text{H}$) were hydrogenated in 60–85% yield (10200–14800 TON). A tertiary amide 4-acetylmorpholine (**71**) was hydrogenated in 98% yield and 19600 TON. 2,2,2-trifluoro-*N*-phenylacetamide (**72**) was hydrogenated in 93% yield and 4600 TON

(0.02 mol% catalyst loading). *N*-Aryl benzamides (R¹ aryl, R² aryl, R³ H) were hydrogenated in 84–99% yield and 8800–15000 TON (0.0067–0.01 mol% catalyst loading). The authors did not discuss the nature of the active catalyst, or any mechanistic insight into the catalytic reaction. This is the most active catalyst reported to date for the hydrogenation of amides in the presence of base. The most active prior to this was the catalyst **51** reported by Bergens and coworkers.

Earth abundant metal based homogeneous catalysts for the hydrogenation of amides via C–N cleavage

There are earth abundant catalysts have been developed for the hydrogenation of amides. Figure 1.7 shows the homogeneous earth abundant catalyst system available for the hydrogenation of amides via C–N cleavage pathway.

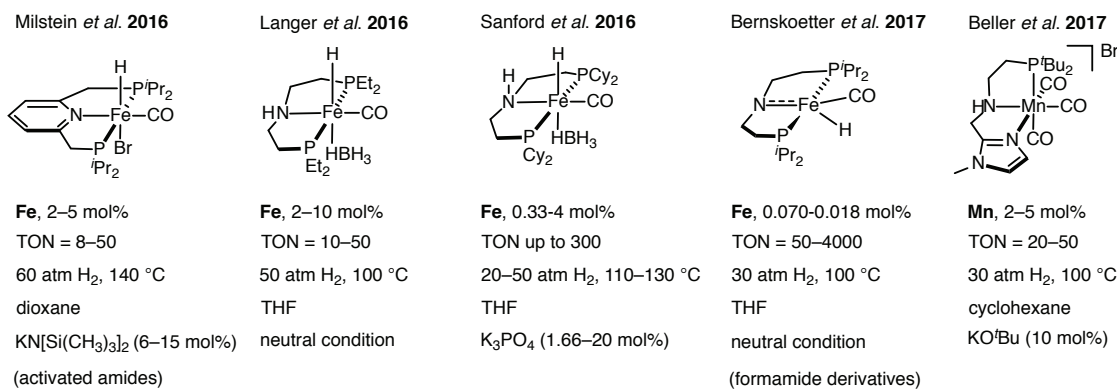
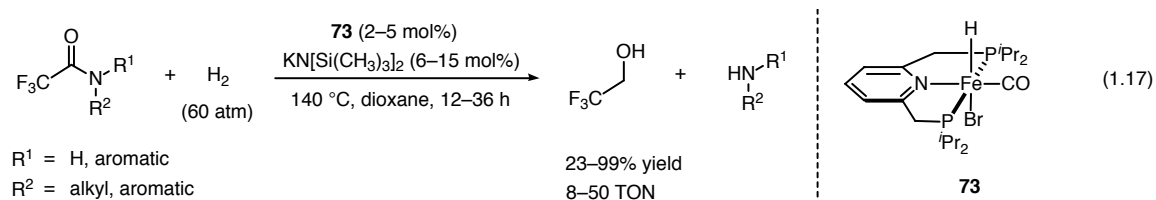


Figure 1.7: Homogeneous earth abundant catalyst system available for the hydrogenation of amides via C–N cleavage pathway.

In early 2016, Milstein and coworkers demonstrated that pyridyl-based PNP iron pincer systems catalyze the hydrogenation of activated trifluoroacetamides.⁹¹ The

Fe-PNP catalyst **73** operates under 60 atm H₂ at 140 °C in dioxane solvent in the presence of a catalytic amount of the strong base KN[Si(CH₃)₃]₂ (Eq. 1.17).

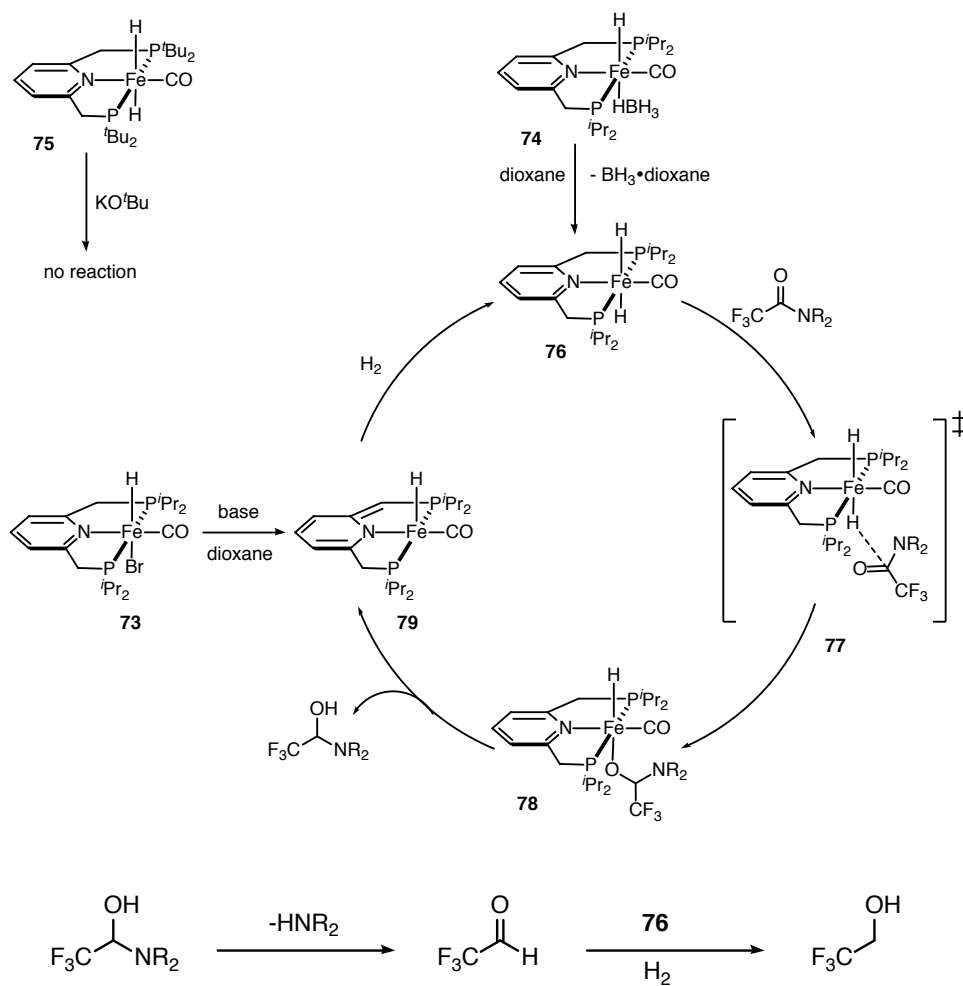


Quantitative conversion (up to 50 TON) was obtained with the *N*-phenyl secondary amide. Placement of *N,N*-dimethyl (58% yield, 29 TON in 12 hours) or a nitro group (25% yield, 13 TON in 36 hours) at the para position of the *N*-phenyl group reduced the activity of the amide. Only one tertiary amide, 2,2,2-trifluoro-*N,N*-diphenylacetamide was hydrogenated. This sole example underwent complete conversion (20 TON) in 36 hours with 5 mol% of the catalyst.

In a control experiment, the hydrogenation of 2,2,2-trifluoro-*N*-phenylacetamide did not occur with the catalyst **73** (5 mol%) in the absence of added base. The dihydride version **74**, however, hydrogenated ~32% (7 TON) of the amide over 24 hours. Complete conversion (50 TON) was obtained with **73** (2 mol%) in the presence of base in only 12 hours, demonstrating the importance of excess base in this reaction.

The authors proposed a mechanism based on NMR analysis, and experimental data from a similar *tert*-butyl version of the Fe-PNP dihydride **75** (Scheme 1.19). The authors stated that **75** did not react with excess KO^{*t*}Bu and suggested that an anionic iron dihydride complex is not involved in the catalytic cycle. So a dihydride such as **76** is a plausible entry to the catalytic cycle, which is generated by removing BH₃ from **74**. The outer-sphere attack by Fe-H in the

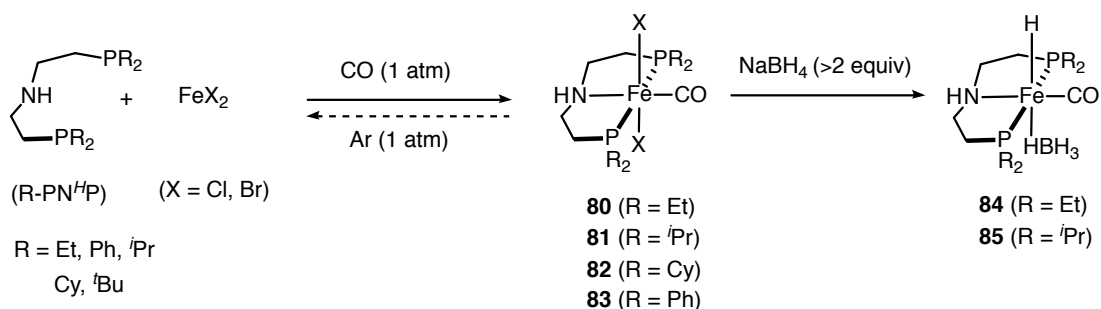
dihydride **76** on the carbonyl of the amide generates the iron-alkoxide intermediate **78** via transition state **77**.



Scheme 1.19: Proposed mechanism for the hydrogenation of an amide to C–N cleavage products using pincer-type catalysts **73** and **74**.

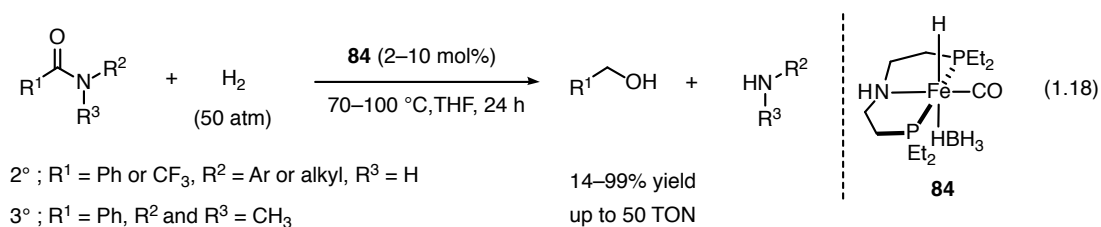
The metal-ligand cooperative (MLC) elimination of the hemiaminal from **78** forms the so-called dearomatized intermediate **79**. The dihydride **76** is then regenerated by a dihydrogen addition to **79** via MLC. The details of these MLC eliminations and additions were not addressed by the authors.

During the same time period, Langer and coworkers reported the synthesis, stability, and catalytic activity of iron pincer complexes of the type $[(R-PN^H-P)Fe(H)(\eta^1-BH_4)(CO)]$, in which R represents ethyl, isopropyl, cyclohexyl, phenyl, or *tert*-butyl groups (Scheme 1.20).⁹² Based upon the results from spectroscopic studies, the authors claimed that the steric demand and electronic nature of the ligands have a strong impact on the stability of these precatalysts in solution.



Scheme 1.20: Synthetic route to $[(R-PN^H-P)Fe(X)_2(CO)]$ and $[(R-PN^H-P)Fe(H)(CO)(\eta^1-BH_4)]$ complexes.

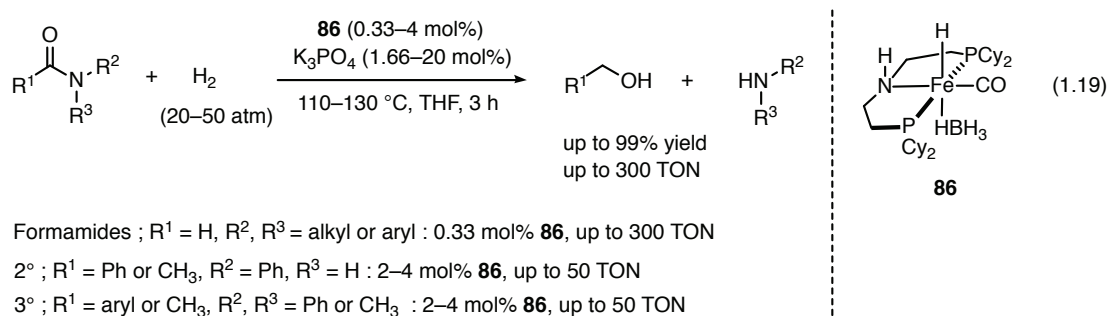
The authors proposed that sterically less demanding, and strong σ -donating ligands would result in the most active catalysts. Compound **84** catalyzed the hydrogenation of secondary and tertiary amides in up to 50 TON under 50 atm H₂ at 100 °C in THF (Eq. 1.18).



A secondary amide *N*-phenylbenzamide was hydrogenated with 99% yield, while *N*-methylbenzamide was hydrogenated in only 14% conversion (1.4 TON) with 10

mol% catalyst. Only one tertiary amide, *N,N*-dimethylbenzamide was hydrogenated. This amide was reduced in 50% yield (5 TON) with 10 mol% catalyst. A six-membered lactam did not react while a five-membered lactam was hydrogenated in 50% conversion with a high catalyst loading.

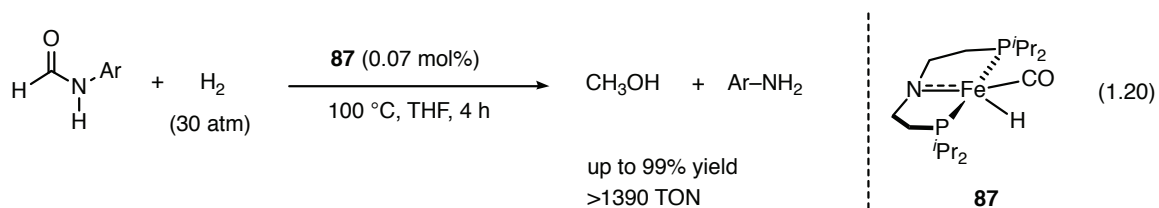
Subsequently, Sanford and coworkers reported improved conditions for the hydrogenation of a variety of 2° and 3° amides to the corresponding C–N cleavage products under mild conditions using the Fe-PNP pincer-type catalyst **86**.⁹³ Langer and coworkers did not consider **86** to be a good choice of an active catalyst. Interestingly, the activities of catalysts **84** and **85** were poor compared to **86**. The catalyst **86** operates under 20–50 atm H₂ at 110–130 °C with up to 300 TON in the presence of K₃PO₄ (Eq. 1.19).⁹³



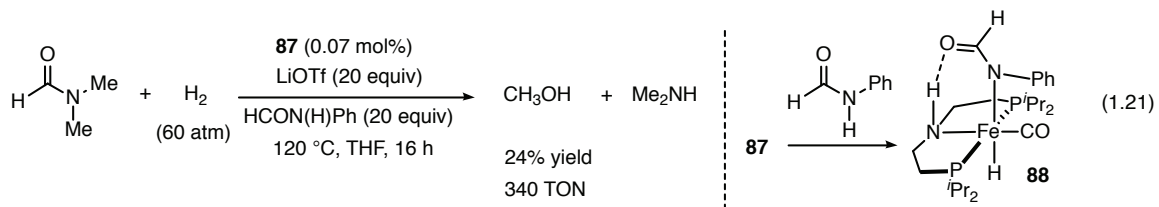
It is notable that the hydrogenation of *N*-formylmorpholine was irreproducible with **86** during the optimization studies. However, switching from ultra-high-purity H₂ (99.999%) to research-grade H₂ (99.9999%) resulted in consistent and reproducible results. During the optimization, K₃PO₄ produced a more active catalyst than other bases such as NaOEt, KO^tBu, and KHMDS. A high TON reaction for the hydrogenation of DMF with 0.038 mol% catalyst under 60 atm H₂ at 110 °C resulted in a 42% conversion (TON = 1080) in 12 hours. Several *N,N*-alkyl, *N,N*-aryl

or *N,N*-alkyl/aryl formamides were hydrogenated with quantitative yield (up to 300 TON) under 20 atm H₂ at 110 °C in 3 hours. Alkyl- and aryl substituted simple amides required forcing conditions (up to 50 TON, 50 atm H₂, 110–130 °C, 3 hours). The authors proposed a mechanism similar to the one reported by Beller and coworkers for the Ru-PNP catalyst **66**.⁸⁹

Very recently, Bernskoetter and coworkers reported a Fe-PNP pincer-type catalyst that operates under 30–60 atm H₂ at 100–120 °C for the hydrogenation of amides in THF.⁹⁴ *N*-arylformamides were hydrogenated by (*i*PrPNP)Fe(H)CO (**87**) in quantitative yield (30 atm H₂, 100 °C) in 4 hours (Eq. 1.20).

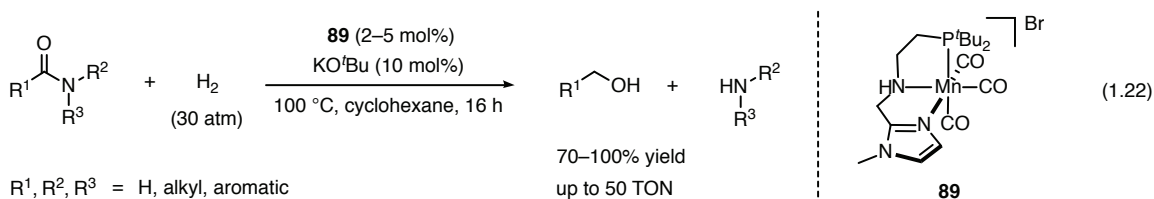


N,N-Diphenylformamide was hydrogenated in 85% yield (TON 1190) but DMF did not react. DMF was hydrogenated, however, under 60 atm H₂ at 120 °C in the presence of lithium triflate (LiOTf) and HCON(H)Ph (20 equivalents each) in 24% yield (Eq. 1.21).



The authors showed that HCON(H)Ph adds across the Fe–N bond in **87** to form the relatively stable compound **88**. The authors believe that **88** is likely the resting state during the hydrogenation.

Recently, Beller and coworkers reported a Mn-based pincer-type catalyst $[\text{Mn}(\text{PNN})(\text{CO})_2]\text{Br}$ (**89**) that operates under 30 atm H_2 at 100 °C to hydrogenate amides in cyclohexane (Eq. 1.22).⁹⁵



A wide variety of 2° and 3° amides with *N*-phenyl groups were hydrogenated in 85–99% yield (TON up to 50). Aliphatic *N*-alkyl amides such as *N,N*-dimethyloctanamide, and *N*-alkyl substituted benzamides did not react. Halogens on the phenyl ring and functional groups including methoxy, naphthyl, and pyridine were tolerated by the reaction. Primary amides were hydrogenated in 50–65% yield (TON 10–12) but required more forcing conditions (50 atm H_2 , 140 °C, and 300 mol% KO^tBu).

Notably, all the catalytic reactions employed an isolated catalyst in crystalline form which was synthesized by reacting commercially available $\text{Mn}(\text{CO})_5\text{Br}$ (**90**) with the PNN ligand. Interestingly, cyclohexane provided the best results compared to other solvents such as THF, EtOH, DCM, and toluene. No explanation was given for the high activity in cyclohexane.

While these early results are promising, the earth abundant amide hydrogenation catalysts reported to date are less active than the ruthenium-based catalysts. An appropriate target for industrial catalysis is 1000 TON or higher.

Selectivity for C–O vs. C–N cleavage in catalytic amide hydrogenation

The origins of the preference for C–O or C–N cleavage have not been fully investigated in catalytic amide hydrogenation. They may partially result from the higher temperatures utilized by the heterogeneous or acidic homogeneous hydrogenations. Higher temperatures promote the elimination of water. The heterogeneous catalysts often possess a Lewis acid cocatalyst. As well, the homogeneous catalysts that favor C–O cleavage also often utilize acid cocatalysts. Figure 1.8 shows possible intermediates and pathways for hemiaminal decomposition in the presence of acid.

They are closely related to the mechanism for the acid-catalyzed imine formation from aldehydes and amines.⁹⁶ Figure 1.8 shows that the putative hemiaminal can be protonated at either nitrogen or oxygen. In reality, the actual cation likely contains a proton H-bonded between nitrogen and oxygen. Protonation at oxygen promotes elimination of water. This pathway is extremely unlikely in the absence of acid, and likely explains why C–N cleavage is favored in base (*vide infra*). Elimination of H₂O forms the iminium cation that would be readily hydrogenated to the protonated higher amine from net C–O cleavage. Conversely, protonation of the hemiaminal at nitrogen would promote the elimination of R²R³NH followed by proton transfer to generate the corresponding aldehyde and the protonated lower amine from net C–N cleavage. Hydrogenation of the aldehyde then produces the alcohol.

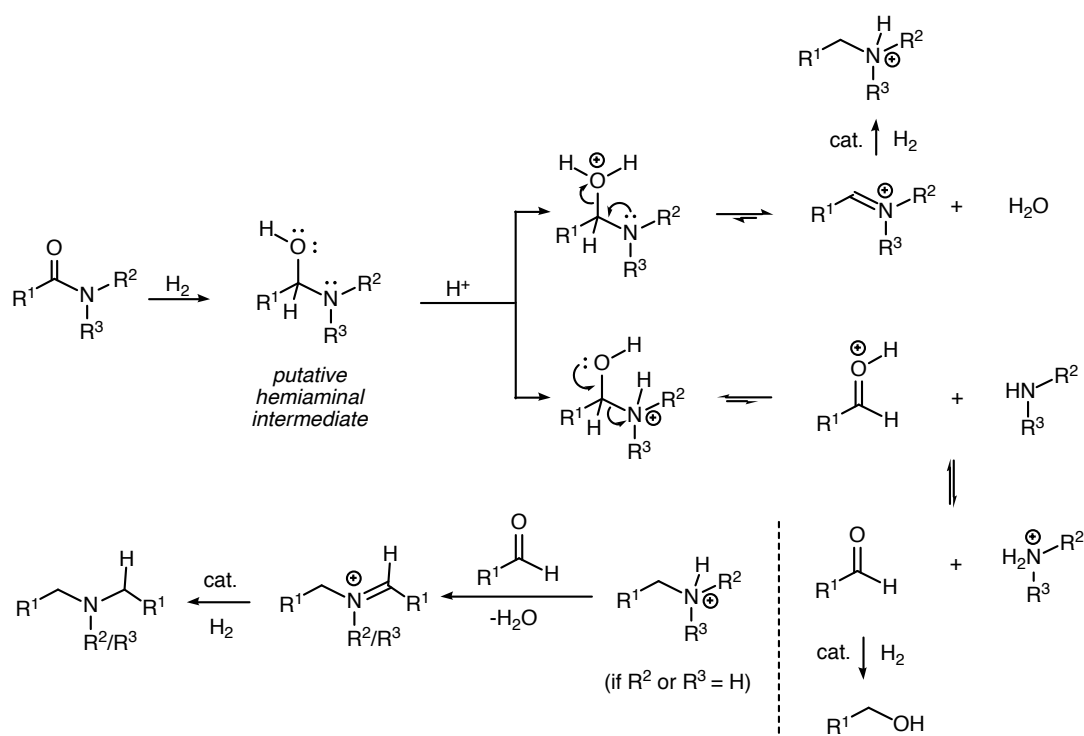


Figure 1.8: Illustration of possible intermediates from a representative hemiaminal under acidic conditions.

As well, C–N cleavage can occur to generate the amine and aldehyde (Figure 1.8 middle). This process can be reversible (See example in Figure 1.5),⁶⁷ or the aldehyde may condense with the higher amine to eventually lead to *N,N*-product (Figure 1.8 bottom pathway).⁵⁸ So it appears then that amide hydrogenations in the presence of acid proceed through a balance of competing equilibria/pathways. The net pathway traversed by a reaction would depend upon the specifics of the reactants, conditions, and catalyst that affect the balance. Figure 1.9 illustrates the possible intermediates under basic conditions. Elimination of hydroxide from the neutral hemiaminal is unlikely (Figure 1.9 top). Conversely, deprotonation of the

hemiaminal at oxygen is favorable, and leads to elimination of $R^2R^3N^{(-)}$ (Figure 1.9 bottom).

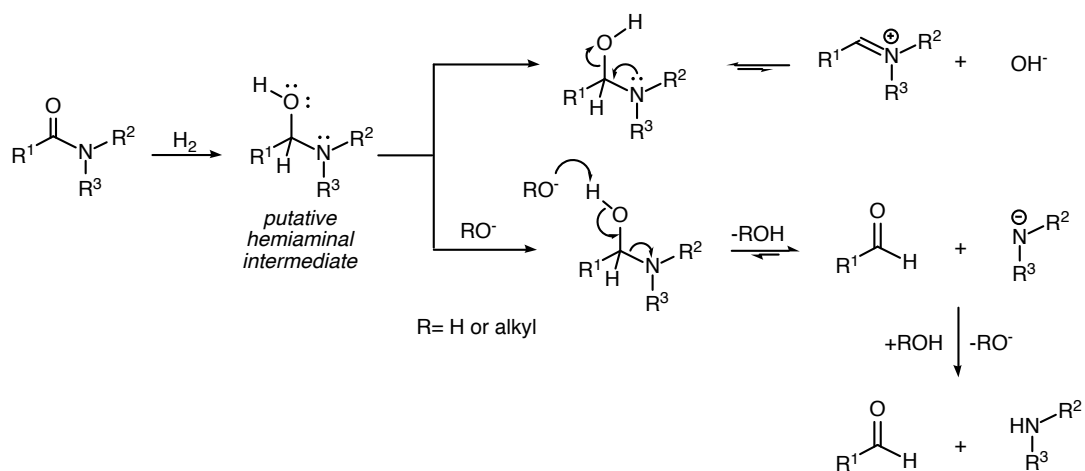


Figure 1.9: Illustration of possible intermediates formation from a representative hemiaminal under basic conditions.

The $R^2R^3N^{(-)}$ would then deprotonate the alcohol to regenerate the alkoxide base and R^2R^3NH . Hydrogenation of the aldehyde then forms the alcohol product from net C–N cleavage. These interpretations serve as general conceptual models for the reported preferences for C–O or C–N cleavage in amide hydrogenations. They predict that base and lower temperatures favor C–N cleavage, and that C–O cleavage is favored by the presence of acid and higher temperatures.

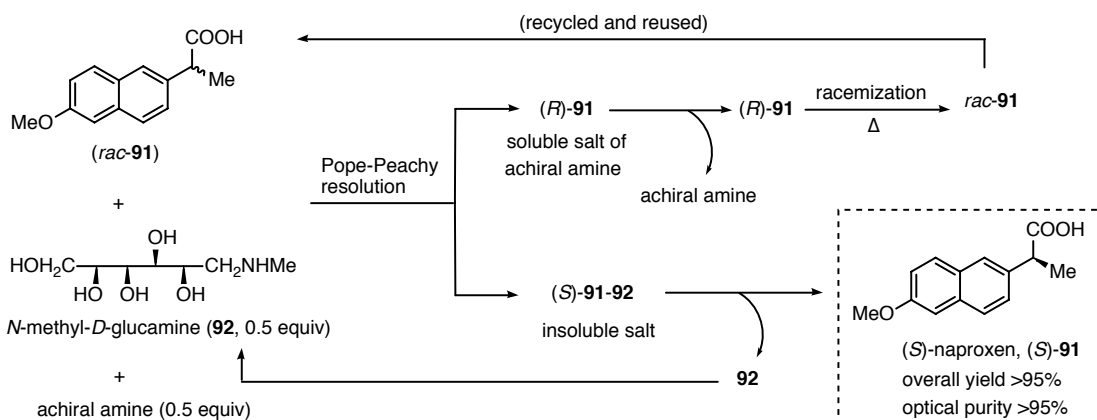
Asymmetric hydrogenation

Louis Pasteur was one of the pioneers who recognized the omnipresence of chirality. Pasteur's separation of racemic tartaric acid into its opposite-handed isomers made it possible to understand enantiomers at the molecular level.⁹⁷ Enantiomers exhibit different chemical and physical properties in a chiral environment and play a prominent role in biological processes. A well-known example is the racemic drug thalidomide, which was prescribed to pregnant women to alleviate morning sickness.⁹⁸ Though one enantiomer had a soothing effect, the other caused severe congenital disabilities. As this case illustrates, there is a strong need to produce enantiopure compounds in the pharmaceutical and related industries.

Currently, the majority of enantiopure compounds are made from the chiral pool or by resolution of racemic mixtures.⁹⁹ For example, 58 of 167 single enantiomer drugs that were introduced between 1985–2004 contained only one stereogenic center. Of these, 26 were produced using natural or unnatural aminoacids or glycidol derivatives. Of the remaining, 27 were prepared by resolution of racemates. The remaining five drugs were prepared by asymmetric synthesis.¹⁰⁰

Resolution is a process in which a racemic mixture is separated into its components enantiomers. Examples include spontaneous resolution (e.g. induced crystallization), resolution by the formation of diastereomers, and resolution by a substrate selective reaction (e.g. kinetic resolution (KR)).¹⁰¹ An industrial example is

the synthesis of (*S*)-naproxen (**91**), which is used to prepare thousands of tons per year (Scheme 1.21).^{101,102}



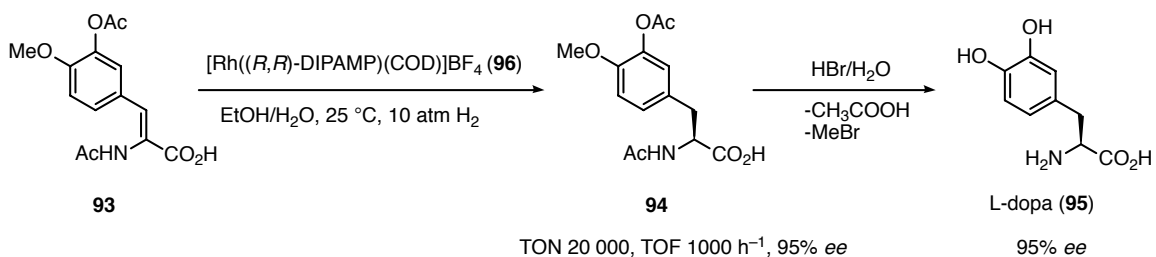
Scheme 1.21: Resolution of naproxen using *N*-methyl-*D*-glucamine as the resolving agent.

In the Pope-Peachy resolution, one equivalent of *racemic* acid is treated with 0.5 equivalent of an achiral amine base and 0.5 equivalent of a chiral base. The (*S*)-acid produces the insoluble salt with the chiral amine, and the (*R*)-acid produces a soluble salt with the achiral amine. The insoluble salt is filtered, and the (*S*)-acid is liberated by reaction with base. The mother liquor is heated to racemize the (*R*)-acid by the achiral amine, and the racemic acid is recycled into the resolution loop.¹⁰²

Though traditional methods are the major approaches to the synthesis of optically pure compounds, they do have many drawbacks. They are inefficient unless the undesired enantiomers can be racemized and reused. Solvent emission is another big concern. For example, the annual emission of methylene chloride from naproxen synthesis is 110 tons.¹⁰² Optically active natural compounds such as amino acids, carbohydrates, terpenes, or steroids are often used as the starting materials to

synthesize targeted molecules.¹⁰³ However, the availability of certain optically pure natural compounds on large scale is limited.^{104,105}

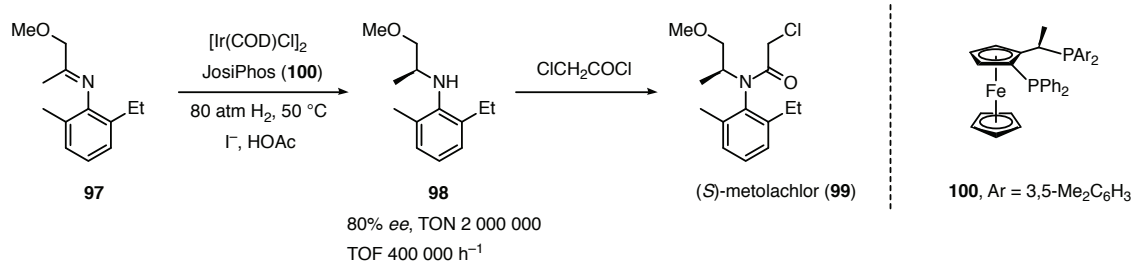
In response to these challenges, it is important to develop new synthetic methods that are efficient, atom economical, environmentally benign, and with a broad substrate scope to obtain the optically pure compounds. In this regard, asymmetric hydrogenation is arguably one of the mature catalytic methodologies. In 1968, the Knowles and Horner groups independently reported the asymmetric hydrogenation of simple prochiral olefins using a rhodium-phosphine catalyst.^{106,107} Eventually, these findings enabled the first commercial application of asymmetric catalytic hydrogenation, the production of L-dopa (**95**) (Scheme 1.22). Knowles developed the L-dopa process at Monsanto in the early 1970s.¹⁰⁸



Scheme 1.22: Asymmetric hydrogenation and deprotection steps in the synthesis of L-dopa.

The key step in the synthesis of **95** is the enantioselective hydrogenation of an enamide intermediate **93** using $[\text{Rh}((R,R)\text{-DIPAMP})(\text{COD})]\text{BF}_4$ as the catalyst (**96**, (*R,R*)-DIPAMP: (*R,R*)-1,2-bis[(2-methoxyphenyl)(phenyl)phosphino]ethane, COD: 1, 5-cyclooctadiene) under 10 atm H₂ at 25 °C in EtOH/H₂O.^{109,110} After hydrogenation, acid promoted hydrolysis produced the target compound **95**.

Another example of an industrial asymmetric hydrogenation is the production of (*S*)-Metolachlor (**99**) in the agrochemical industry. Metolachlor is a grass herbicide sold under the trade names Dual Magnum™ and Dual Gold™.¹¹¹ An *in situ* made Ir-Josiphos catalyst is used to introduce the chirality to an imine substrate (**97**) (Scheme 1.23).^{112,113}



Scheme 1.23: Asymmetric hydrogenation of the imine **97** with an Ir-Josiphos catalyst in the synthesis of (*S*)-Metolachlor.

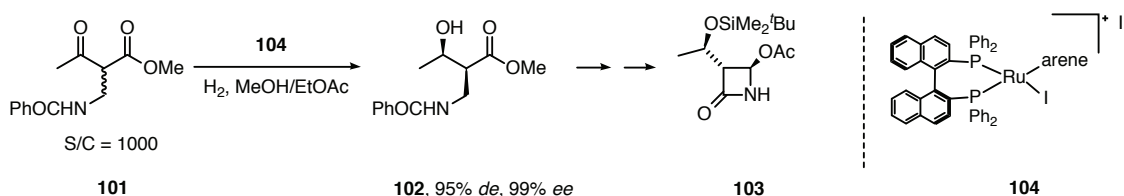
Over 10,000 tons of metolachlor is produced per year. This is the largest scale enantioselective catalytic reaction on the planet. The 80% enantiomeric excess of the metolachlor produced by this hydrogenation provides a strong economic advantage over the use of the racemate.¹¹¹ It is notable that the *S*-configuration at the stereogenic carbon in **99** has more biological activity than *R*. So the use of enantiomerically enriched **99** reduce the loading in the environment.¹¹³ The high catalytic activity (TON 2 000 000, TOF 600 000 h⁻¹) offsets the cost and toxicity of the heavy metal Ir catalyst.¹¹¹

It is notable that an enantiopurity of >80% is often acceptable for agrochemical products unless further enrichment is easy to achieve. In contrast, pharmaceutical products require over >99% enantiopurity.¹¹⁴ An asymmetric hydrogenation catalysts must operate with TON no less than 1000 for high-value

products, and with TON >50 000 for less expensive commodity chemicals to be considered in industrial applications.^{111,114} The cost of the chiral ligand often is higher than the metal centre. All ligands should be considered toxic. Additionally, if a catalyst provides >50, 000 TON in high *ee*, the cost of the catalyst is no longer a significant factor.

The discovery of BINAP by Noyori and coworkers in the beginning of the 1980s is one of the key milestones in catalysis.^{115,116} In 1987, Noyori and coworkers reported the first asymmetric hydrogenation of β -keto esters using the halogen-containing ruthenium complexes of the empirical formula $[\text{RuX}_2(\text{BINAP})]$ (X = Cl, Br, or I).¹¹⁷ In 1995, they discovered that $\text{RuCl}_2(\text{diphosphine})(\text{diamine})$ complexes and a base catalyze the hydrogenation of simple prochiral ketones in high yields and *ee*.³⁶ These types of catalysts are widely used in both academia and industry.

For an example, the potential antibiotic carbapenem is synthesized from the key intermediate 4-acetoxyazetid-2-one (**103**). The synthesis of **103** involves an asymmetric hydrogenation reaction, where the α -substituted β -keto ester **101** is hydrogenated by the $\text{Ru}(\text{I})(\text{BINAP})(\text{arene})$ catalyst **104** via a dynamic kinetic resolution (DKR) to produce two adjacent chiral centers in the drug intermediate **102** (Scheme 1.24).^{118,119} This hydrogenation is carried out on a scale of 120 tons per year.¹¹⁸



Scheme 1.24: Asymmetric hydrogenation of **101** by **104** in the synthesis of **103**.

The catalyst **104** preferentially hydrogenates the pro-*R* face of the ketone group in **101**. Epimerization between *S*-**101** and *R*-**101** is faster than the hydrogenation. This pre equilibrium allows for most of the hydrogenation to proceed through *S*-**101**. This epimerization does not occur in the product, which is no longer a β -keto ester. The hydrogenation of **101** demonstrates an elegant way of utilizing the traditional, extended version of KR along with the asymmetric catalytic hydrogenation reaction to produce two stereocenters in a single step.

The IUPAC definition of KR is “the achievement of partial or complete resolution by virtue of unequal rates of reaction of the enantiomers in a racemate with a chiral agents (reagent, catalyst, solvent, etc.)”.¹²⁰ In the KR, the enantiomers of the racemic substrate ($SM_S : SM_R = 1:1$) interact with the chiral agent leading to two diastereomeric transition states. The difference in free energies between these transition states defines the *ee* of the product (Figure 1.10).¹²¹ The main drawback of KR is that the maximum theoretical yield of the product is 50%.

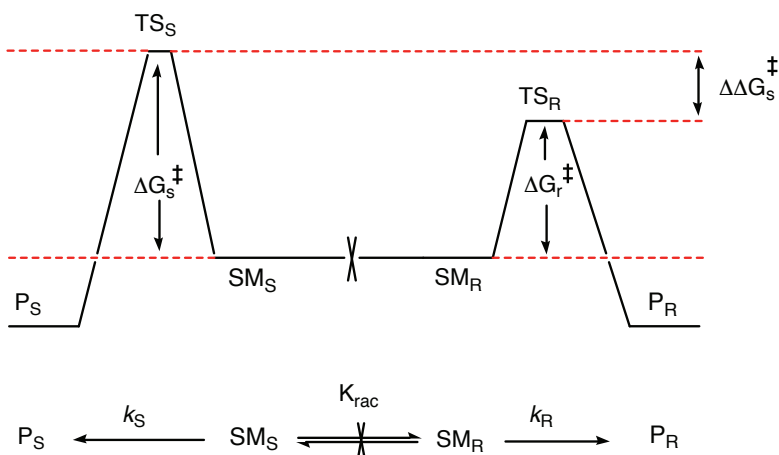


Figure 1.10: Illustration of energy diagram and reaction scheme for KR.

DKR is an extension of KR that theoretically allows for quantitative conversion of a racemate into the desired product enantiomer. In DKR, the enantiomers of the racemate are in rapid pre-equilibrium, so that the faster-reacting enantiomer is converted into an optically pure product at the expense of the slower-reacting enantiomer (Figure 1.11).¹²¹

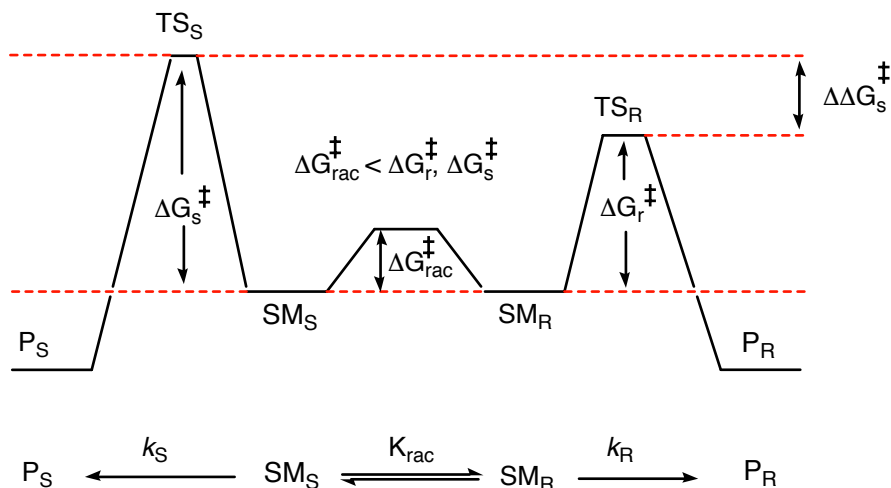


Figure 1.11: Illustration of energy diagram and reaction scheme for DKR.

These are Curtin-Hammett conditions, where the *ee* of the product is determined by the difference in diastereomeric transition state energies.¹²² Table 1.2 shows the equations used for the determination of %*ee* of the product in an enantioselective reaction.^{123,124} Additionally, differences in free energy required for certain *ee* values are also shown.

Table 1.2: Relationship between the diastereomeric transition state energies and their corresponding *ee* values.

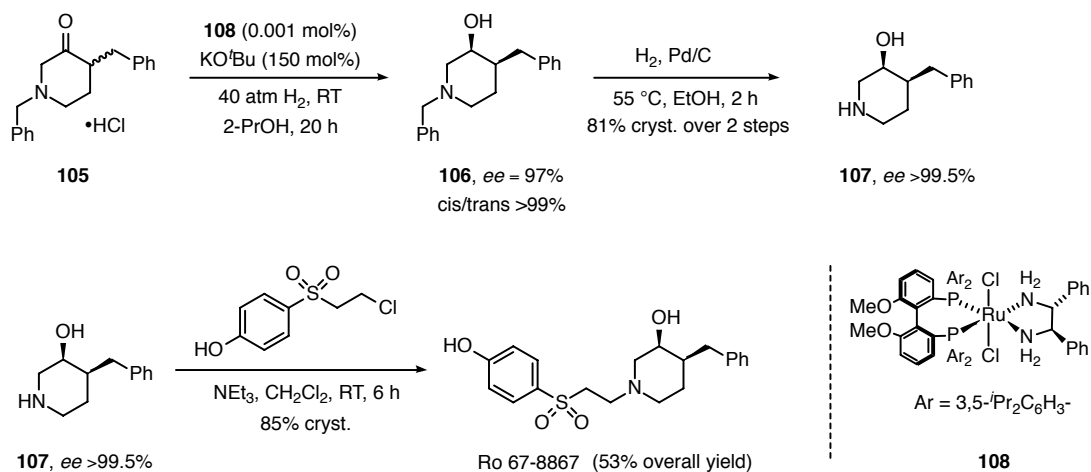
$\Delta\Delta G^\ddagger$ kcal/mol	$\Delta\Delta G^\ddagger$ J/mol	RT at 300K	$\Delta\Delta G^\ddagger / RT$	% <i>ee</i>
1	4184	2494.2	1.6775	68.5
2	8368	2494.2	3.3550	93.3
3	12552	2494.2	5.0325	98.7
4	16736	2494.2	6.7099	99.75
5	20920	2494.2	8.3875	99.954
6	25104	2494.2	10.0649	99.991

$$\%ee = \frac{[P_R] - [P_S]}{[P_R] + [P_S]} \times 100$$

$$\frac{[P_S]}{[P_R]} = \frac{k_S}{k_R} = \frac{-Ae^{-\Delta G_S^\ddagger / RT}}{-Ae^{-\Delta G_R^\ddagger / RT}}$$

$$\%ee = \frac{1 - e^{-\Delta\Delta G^\ddagger / RT}}{1 + e^{-\Delta\Delta G^\ddagger / RT}} \times 100$$

Ro 67-8867 is an *N*-methyl-D-aspartate (NMDA) receptor antagonist. This high-affinity, selective, and activity-dependent antagonist was a proposed treatment for acute ischemic stroke.¹²⁵ The original synthesis involved crystallization of a diastereomeric salt to obtain intermediate **106** from its racemate. This traditional resolution by crystallization yielded only 10–15% of the optically pure intermediate **106** after three to four crystallizations. The poor efficiency of this resolution prevented this reaction from being scaled up for technical development. However, an alternative asymmetric hydrogenation of the ketone **105** via DKR allowed the production of Ro 67-8867 on a multikilogram scale (Scheme 1.25).¹²⁵ The catalyst was the Ru(bisphosphine)(diamine), **108** (0.001 mol%), and 150 mol% of the base KO^tBu to promote both the hydrogenation and DKR of **105**.

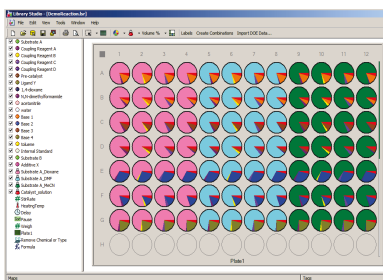


Scheme 1.25: Asymmetric hydrogenation of **105** to **106** by **108** in the synthesis of Ro 67-8867.

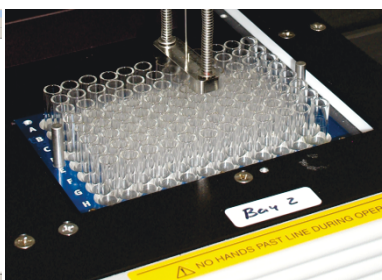
The hydrogenation of **105** via DKR provided the diastereomeric alcohol **106** in 97% *ee* (*cis/trans* >99%). The hydrogenolysis of the benzyl group in **106** and subsequent crystallization provided the intermediate **107** in 81% yield (based on **106**) and in over 99.5% *ee*. In the final step, **107** was coupled with a chlorosulfone to afford the antagonist Ro 67-8867 in 85% yield. The overall yield of this reaction sequences is 53% compared to 3.5% yield with resolution.¹²⁵

Despite enormous progress, the application of asymmetric hydrogenation in the industry is limited. It is believed that only ~20 asymmetric hydrogenation processes are employed at a production scale.^{126,127} The exact number of asymmetric hydrogenation processes at scale is unclear because companies are reluctant to disclose this information.¹¹⁴ In the current era of green chemistry, industries are under pressure to adapt environmentally benign methods. Also, increasing competition between companies forces them to bring products to market faster.¹²⁸

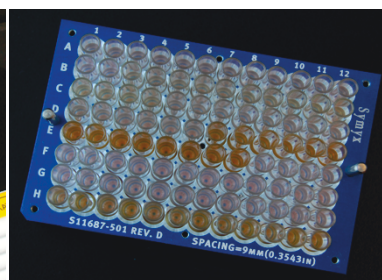
Developing a catalyst is a challenging process, since there is no specific way to design a catalytic system for high *ee*'s beforehand. Instead, a large number of reactions are required to screen for and develop a catalyst. The latest technology in high throughput experimentation (HTE) accelerates the development of a new catalytic systems to save time, money, and other resources.^{129,130} Figure 1.12 shows the fundamental steps in a HTE.



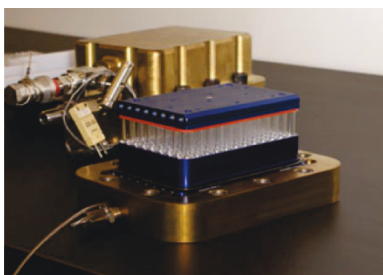
Design the experiments



Dispense reagents using automated freeslate core module



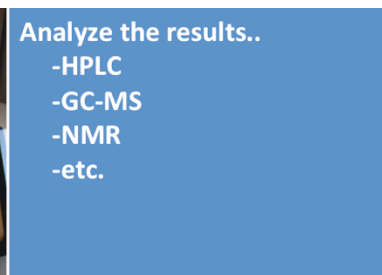
Catalyst preparation, heating and adding substrate, base, solvent, etc.



Encase 96-well plate in a brass reactor block



Run the reactions -hydrogenation



Analyze the results

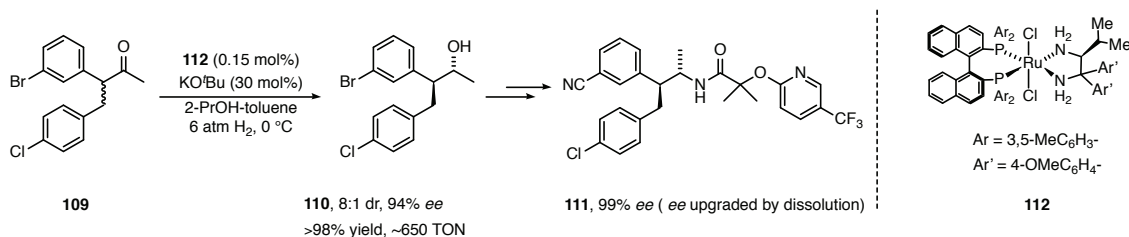
Figure 1.12: Illustration of fundamental steps in high throughput screening technology.

The traditional way to develop a catalytic system involves optimizing one parameter (e.g., temperature, pressure, solvent, etc.) at a time, which requires weeks, months,

or inevitably, years. High throughput screening makes it possible to perform hundreds of reactions under multiple conditions in a matter of days.¹²⁸

For example, the active pharmaceutical ingredient **111** was identified as a potent drug to treat obesity.¹³¹ The original synthesis involved a resolution and an *ee* upgrade by chiral HPLC to obtain the intermediate **110**. Although the original route made it possible to generate a small quantity of the drug, scaling up the reaction was challenging and inefficient. In 2007, Merck reported the development of a new asymmetric catalytic hydrogenation step to improve an existing synthetic route in the production of **111**.¹³¹

High throughput screening succeeded in finding the [RuCl₂(diphosphine)-(diamine)] type catalyst **112** that hydrogenates racemic **109** via DKR to give the chiral intermediate **110** in excellent *ee* (94%), in good diastereoselectivity (dr 8:1), and in over 98% yield (up to 650 TON) (Scheme 1.26).



Scheme 1.26: Asymmetric hydrogenation of **109** to **110** via DKR in the synthesis of active pharmaceutical ingredient **111**.

Notably, hydrogenation of **109** produced **110** with two optically enriched stereogenic centers in a single step. KO^tBu (30 mol%) was used to promote the DKR and the hydrogenation. The hydrogenation time was not provided, but monitoring the hydrogen uptake from a reservoir and HPLC analysis ensured the complete

conversion. The overall yield of the product was 40% (based on **109**). This method enabled the production of **111** on a multikilogram scale.¹²⁶ The authors reported that the diastereoselectivity of **111** was improved during the step converting **110** to **111** but did not provide a final value. The increment of *ee* increased from 94% to 99% in **111** via the dissolution of **111**.

Asymmetric hydrogenation provides a tremendous environmental benefit over traditional synthetic methods. The notable examples are the synthesis of the active pharmaceutical ingredients sitagliptin (Januvia™) and laropiprant (Cordaptive™). Merck modified their existing synthetic route of both APIs by incorporating an asymmetric hydrogenation step.^{126,132} The new synthetic route generated 220 kg less waste and 660 kg less waste, respectively, for each kilogram of sitagliptin^{126,132} and laropiprant.¹²⁶ Remarkably, the new synthetic route in the case of sitagliptin also totally eliminated the aqueous waste.

Research objectives

The development of sustainable and efficient methods for the reduction of amides that avoid hydride reagent are of utmost importance to both academia and industry. Chapter 1 briefly describes the challenges in amide reduction with hydride reagents and greener approaches that employ catalytic hydrogenation. Chapter 2 presents the catalytic hydrogenation of amides under both base-assisted and base-free conditions.

One of the challenges the industry faces in the development of a new catalytic system is that often there is little or no precedent in the literature of asymmetric hydrogenation for a substrate of interest. Without a doubt, developing a new catalytic system or modifying existing reactions with a catalytic system will have many benefits. Recent advances in asymmetric catalytic hydrogenation have made it easy to obtain chiral secondary alcohols from prochiral ketones with excellent yield and selectivity. In contrast, there are only a handful of reports for the enantioselective hydrogenation of α -chiral aldehydes and esters with DKR that provide β -chiral primary alcohols. In Chapter 3, I will discuss the development of a novel catalytic system for the enantioselective hydrogenation of amides to produce chiral primary alcohols via DKR at room temperature and low pressure.

Chapter 2

Catalytic Hydrogenation of Functionalized Amides Under Basic and Neutral Conditions¹

Introduction

As described in Chapter 1, amides are one of the least reactive carboxylic acid derivatives, and their reduction requires forceful conditions or stoichiometric reducing agents that are oxophilic. Amide reductions are typically carried out with stoichiometric hydride reducing agents such as LiAlH_4 , DIBAL, RedAl, B_2H_6 , and silane (catalytic).^{20,21,25} In the current era of green chemistry, amide reduction by catalytic hydrogenation has many environmental and economical advantages over stoichiometric reduction.²⁰ In response, many heterogeneous and homogeneous catalytic systems are being developed for the catalytic hydrogenation of amides. The recent advances in homogeneous amide hydrogenation can be found in Chapter 1. Homogeneous catalytic systems operate under acidic, neutral, or basic conditions. These conditions often control the chemoselectivity of the reaction, and are a deciding factor in which functional groups can tolerate the hydrogenation. In other words, whether the functional groups are acid or base sensitive. In 2011, Bergens and coworkers reported that the cationic allyl precursor $[\text{Ru}(\eta^3\text{-C}_3\text{H}_5)(\text{Ph}_2\text{P}(\text{CH}_2)_2\text{NH}_2)_2]\text{BF}_4$ (**51**) with base in THF hydrogenate a wide variety of

¹ A version of this chapter has been published. John, J. M.; Loorthuraja, R.; Antoniuk, E.; Bergens, S. H. *Catal. Sci. Technol.* **2015**, *5*, 1181-1186.

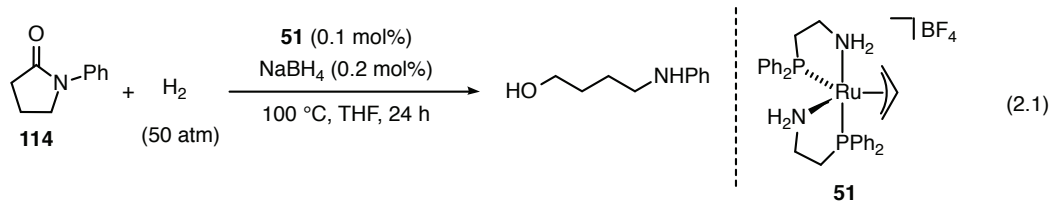
simple amides with C–N cleavage and with high TON's up to ~7200 (100 °C, 50 atm, 4–5 mol% base, 24 h).⁷⁹

The objective of the research described in this chapter was to prepare and evaluate a base-free version of this catalyst. At the time, there were no reports of a high TON (>300), neutral amide hydrogenation catalyst, nor of an amide hydrogenation catalyst that tolerates a wide variety of functional groups. Herein, We report such a neutral catalyst, and demonstrate its functional group tolerance under neutral and basic conditions. We also illustrate the utility of the system as a relatively mild, catalytic method to liberate amines by hydrogenation of the corresponding acetyl amides.

Results and discussion

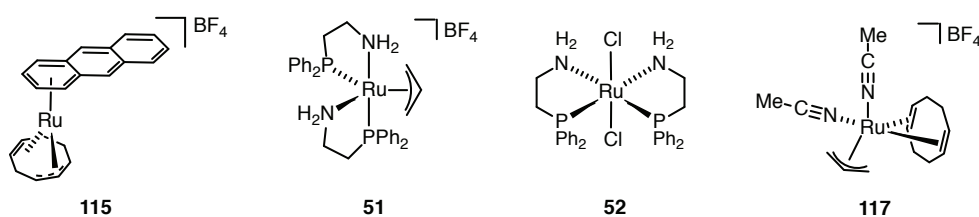
Noyori and coworkers reported that BH_4^- adducts of bifunctional catalysts such as *trans*-[RuH($\eta^1\text{-BH}_4$)]((*S*)-xyl-BINAP)((*S,S*)-dppe)] (**113**; xyl-BINAP: (*S*)-(-)-2,2'-bis[di(3,5-xylyl)phosphino]-1,1'-binaphthyl), are active catalysts for ketone hydrogenations under base-free conditions.^{133,134} Morris,¹³⁵ Milstein,^{136,137} and Kuriyama^{138,139} subsequently reported other bifunctional, and pincer ketone hydrogenation catalysts containing $\eta^1\text{-BH}_4^-$.

For this study, we found that the cationic, η^3 -allyl precursor [Ru($\eta^3\text{-C}_3\text{H}_5$)(Ph₂P(CH₂)₂NH₂)₂]⁺BF₄⁻ (**51**) and 2 equivalents of NaBH₄ react under H₂ in THF (~2 atm, 60 °C, 30 min) to form a catalyst that hydrogenates *N*-phenylpyrrolidin-2-one (**114**) via C–N cleavage under 50 atm H₂, 100 °C with high TON (910) in 24 hours (Eq. 2.1).



Encouraged by this result, the hydrogenation of **114** was repeated with different catalytic precursors under the same conditions. Table 2.1 summarizes the results.

Table 2.1: Base-free hydrogenation of **114** by various Ru-precursors.



entry	Ru-precursors	Ru:NaBH ₄	%conv ^(a)	TON
1 ^(b)	[Ru(η ³ -C ₃ H ₅)(Ph ₂ P(CH ₂) ₂ NH ₂) ₂] ⁺ BF ₄ ⁻ (51)	1:2	91	913
2 ^(c)	[Ru((1-3;5-6-η)-C ₈ H ₁₁)(η ⁶ -anthracene)] ⁺ BF ₄ ⁻ (115) + 2 equiv. Ph ₂ P(CH ₂) ₂ NH ₂ (116)	1:5	71	710
3 ^(c)	[Ru((η ³ -C ₃ H ₅)(COD)(MeCN) ₂)] ⁺ BF ₄ ⁻ (117) + 2 equiv. Ph ₂ P(CH ₂) ₂ NH ₂ (116)	1:5	66	660
4 ^(d)	RuCl ₂ (Ph ₂ P(CH ₂) ₂ NH ₂) ₂ (52)	1:5	76	378

(a) Determined by ¹H NMR Spectroscopy (using the area of non-overlapping CH₂ protons of both **114** and product). (b) **51** reacted with NaBH₄ for 20 min under ~2 atm H₂ at 60 °C. [**114**] 2 M in THF. (c) **115** or **117** reacted with 2 equivalents of **116** (under argon for 30 min) then NaBH₄ (under ~2 atm H₂ for 20 min) at 60 °C. [**114**] 2 M in THF. (d) **52** reacted with NaBH₄ for 20 min under ~2 atm H₂ at 60 °C. [**114**] 1.25 M in THF.

There was no evidence of C–O cleavage, despite the neutral conditions for this hydrogenation. Catalysts prepared by reacting the ruthenium precursors **115** or **117** *in situ* with **116** (2 equivalents), and then with NaBH₄ (5 equivalents) were somewhat less active (entries 2 and 3) than the catalyst prepared from **51**. The dichloride precursor **52** with NaBH₄ was ~66% less active (entry 4). The ratio of Ru:NaBH₄ was increased to 1:5 with **52**, **115**, and **117** to accommodate any uncertainties in the amounts of *in situ* catalyst formed, as well as any potential difficulties in reducing any ligands in these precursors with BH₄⁻. It is likely that the reduced activity of catalysts made from **115** and **117** results from inefficiencies inherent with utilizing two *in situ* reactions to prepare the catalyst: the reaction with **116**, followed by reaction with NaBH₄ and hydrogen. The relatively low reactivity of the dichloride **52** perhaps illustrates the relative ease by which the allyl group in **51** is removed by hydrogenation relative to the reduction of the chloride ligands in **52** by NaBH₄. The nature of the active catalyst formed under these conditions discussed later in this chapter.

Table 2.2 shows the results for the base-free hydrogenations of representative simple amides (**118a–118f**) with **51** (0.1 mol%) and NaBH₄ (NaBH₄/Ru = 2, 100 °C, 50 atm H₂, 24 hours, THF). For comparison, we include the yields reported previously for the same hydrogenations carried out with excess base (4 mol% KN[Si(CH₃)₃]₂).⁷⁹ The *N,N*-diphenyl (entry 1), *N*-phenyl-*N*-methyl (entry 2), and *N*-phenyl acetamides (entry 3) were all hydrogenated in high TON (800–1000, entries 1–3) with both catalyst systems. Interestingly, the 2° *N*-phenyl acetamide (entry 3) was slightly more reactive with the base-free catalyst than with the base-

promoted catalyst. The same order of activity occurs with *N,N*-diphenyl benzamide as substrate (entry 6).

Table 2.2: Base-free hydrogenation of simple amides.^(a,b)

entry	amide	amide structure	%conversion ^(c)		TON	
			Base free ^(a)	Base assisted ^(b)	Base free	Base assisted
1	118a		100	100	1000	1000
2	118b		93	100	930	1000
3	118c		80	70	800	700
4	118d		96	100	960	1000
5 ^(d)	118e		24	50	240	500
6 ^(e)	118f		71	50	710	500

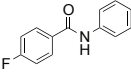
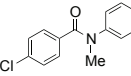
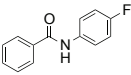
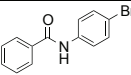
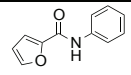
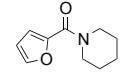
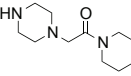
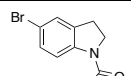
(a) **51** reacted with NaBH₄ for 20 min under ~2 atm H₂ at 60 °C. [**118a–e**] 2.5 M in THF. (b) Results for the base-assisted hydrogenation using 0.1 mol% **51** and 4 mol% KN[Si(CH₃)₃]₂. (c) Determined using ¹H NMR spectroscopy (using the area of non-overlapping alkyl protons). (d) Anthracene used as internal standard. (e) [**118f**] 2 M in THF.

We believe that under basic conditions, 2° amides are deprotonated at nitrogen to form strongly coordinating amidate anions that partially hinder the catalyst. The hydrogenations with BH_4^- are less susceptible to this type of inhibition. The morpholino acetamide **118d** was smoothly hydrogenated under base-free and basic conditions (entry 4), and the stable *N,N*-dimethylacetamide (**118e**), was hydrogenated with appreciable TON (240, entry 5) with the base-free catalyst. The base-promoted system was more active (TON 500). Taken together, the hydrogenations of the *N*-phenyl, *N*-alkyl, and secondary acetamides in Table 2.1 demonstrate that these hydrogenations offer a relatively mild, efficient, and environmentally benign alternative to the stoichiometric methods used to liberate amines that were protected as acetamides.¹⁴⁰ In all cases, only the product alcohol, amine, and starting materials were observed in the product mixtures. As such the %conversion represents the %yield of the alcohol product.

Table 2.3 shows the results from the base-free and base-promoted hydrogenations of functionalized amides (**119a–119h**). Generally, the system with added base was more active for these substrates. The functional groups that tolerated the base-promoted hydrogenation with good TON (400–500) include arene rings, aromatic fluorides (entries 1 and 3), chlorides (entry 2), and bromides (entry 4). The halide can reside on the acyl group (entries 1 and 2), or in the amine of the amide (entries 3 and 4).

Table 2.3: Base-free^(a) vs. base-assisted^(b) hydrogenation of functionalized amides.

$$\begin{array}{c}
 \text{O} \\
 \parallel \\
 \text{R}^1-\text{C}-\text{N}-\text{R}^3 \\
 | \\
 \text{R}^2
 \end{array}
 \xrightarrow[50 \text{ atm H}_2, 100 \text{ }^\circ\text{C, THF, 16-28 h}]{\begin{array}{l} \mathbf{51} (0.1 \text{ mol}\%), \text{NaBH}_4 (0.2 \text{ mol}\%) \text{ or} \\ \mathbf{51} (0.1-1 \text{ mol}\%), \text{inorganic base (4-5 mol}\%) \end{array}}
 \begin{array}{c}
 \text{R}^1-\text{CH}_2-\text{OH} \\
 + \\
 \text{HN}-\text{R}^3 \\
 | \\
 \text{R}^2
 \end{array}$$

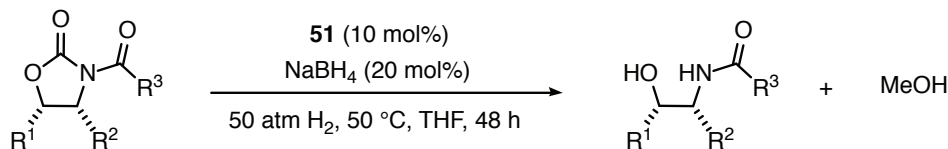
entry	amide	amide structure	t(t) ^(d)	%conversion ^(c)		TON	
				Base free	Base assisted	Base free	Base assisted
1	119a		24(24)	34	89 ^(e)	34	442
2	119b		24(21)	0	50 ^(f)	0	50
3	119c		19(28)	69	100 ^(g,h)	69	500
4	119d		-(24)	nd	100	-	100
5 ^(e)	119e		16(24)	32	88 ^(e)	32	438
6	119f		-(24)	nd	100 ^(e,h)	-	500
7	119g		24(24)	5	86	5	86
8	119h		24(24)	100	100	100	500
			-(24)	nd	100 ⁽ⁱ⁾	-	500

(a) **51** (1 mol%) reacted with NaBH₄ (2 mol%) for 20 min under ~2 atm H₂ at 60 °C. [amide] 0.25 M in THF. nd not determined. (b) **51** (1 mol%) reacted with KO^tBu (4 mol%). [amide] 0.25 M in THF. (c) Determined using ¹H NMR spectroscopy (area of CH₂ protons of the product alcohol and non-overlapping aromatic protons were used). (d) Time for base-assisted hydrogenations denoted in parenthesis. (e) Ru:KO^tBu:amide 1:20:500. (f) Ru:KO^tBu:amide 1:5:100. (g) Proceeded with 8% C–O cleavage. (h) Ferrocene used as internal standard. (i) Reaction performed at 10 atm H₂ pressure.

Interestingly, and for reasons unknown at this time, the base-assisted hydrogenation of the *N*-(4-fluorophenyl)benzamide (**119c**, entry 3) proceeded quantitatively (TON = 500) with 92% net C–N cleavage and ~8% net C–O cleavage. The origin of this C–O cleavage product are unknown at this time. The aromatic chloride **119b** (entry 2) was less reactive than the fluoride (entry 1). Importantly, furans (**119e**, **119f**) are not hydrogenated and do not hinder catalysis (entries 5 and 6, TON = 400–500), demonstrating that amides can be selectively hydrogenated in the presence of furans. Amides containing 2° *N*-heterocycles (**119g**) can also be hydrogenated, albeit with lower, but useful TON (86, entry 7). The halogenated heterocyclic amine 5-bromoindoline (**119h**) was deprotected by the neutral and base-promoted hydrogenations of 1-acetyl-5-bromoindoline (entry 8). Significantly, the base-promoted hydrogenation of **119h** (entry 8) was carried out under 10 atm reaction pressure to give 500 turnovers in 24 hours, demonstrating that this catalytic system is active towards certain amides under lower pressures. The hydrogenation also tolerates ethers (see Table 2.2, entry 4), as well as alcohols and amines as these are the products of the hydrogenation.

N-Acylloxazolidinones are typically harder to reduce than amides. We prepared the diastereomerically pure (2-benzyl)propanamide oxazolidinones **120a** and **120b** by benzylation of the parent enolates.^{141a} Hydrogenation of **120a** and **120b** under base-free conditions with 10 mol% **51** proceeded with quantitative reduction of the endocyclic C–N bond to furnish only the corresponding hydroxyl amides and methanol. Table 2.4 summarizes the results.

Table 2.4. Base-free hydrogenation of *N*-acyloxazolidinones.



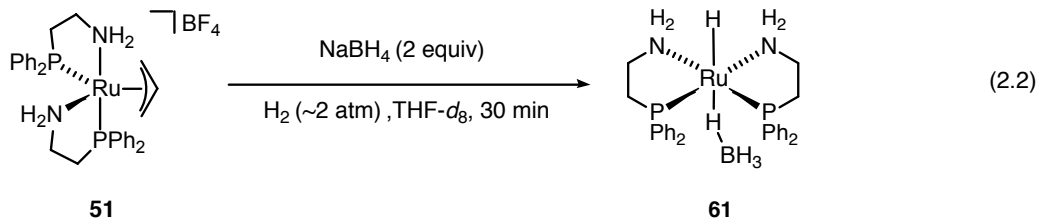
entry	substrate	R ¹	R ²	R ³	%conv ^(a)	dr ^(c)	TON
1 ^(b)	120a	Ph	Me	CMe(H)Bn	100	99:1	10
2 ^(b)	120b	H	<i>i</i> Pr	CMe(H)Bn	100	99:1	10

(a) Determined using ¹H NMR spectroscopy (using the area of non-overlapping CH₂ protons). (b) **51** (10 mol%) reacted with NaBH₄ (20 mol%) for 10 min under ~2 atm H₂ at 60 °C. Reaction conditions: 50 atm H₂ at 50 °C for 24 hours. [**120a** or **120b**] 25 mM in THF. (c) Determined using ¹H NMR spectroscopy.

The diastereomeric ratio of the product was (>99:1) for both these hydrogenations, showing epimerization did not occur. Steric crowding around the exocyclic amide bond likely drives the preference for hydrogenation of the oxazolidinone carbonyl. In contrast, the hydrogenation of **120a** with **51** in the presence of base (10 mol% **51**, 20 mol% KO^tBu) also occurred with near exclusive endocyclic C–N cleavage, but the products consisted of a mixture of diastereomeric hydroxyl amides resulting from base-catalyzed epimerization of the (2-benzyl)propanamide group. These results demonstrate that the base-free hydrogenation will preserve the stereochemistry at enolizable carbon centers. Ikariya and coworkers reported that hydrogenation of **120a** using 3 mol% Cp**Ru*Cl(Ph₂P(CH₂)₂NH₂) (**38**) and KO^tBu (Ru:base 1:1) under 30 atm H₂ at 80 °C for 20 h in 2-PrOH proceeding exclusively with exocyclic C–N cleavage resulting from hydrogenation of the acyl carbonyl.⁷² We believe the active

catalyst generated from **51** and BH_4^- is more susceptible to steric crowding than the catalyst **38** described by Ikariya and coworkers.

Control experiments were performed to investigate the identity of the active catalyst. The use of Ru black as catalyst resulted only in the hydrogenation of the arene ring in **114**. It is therefore unlikely that Ru nanoparticles are the active catalyst in these amide hydrogenations. In control NMR experiments, I found that **51** reacts with 2 equivalents of NaBH_4 after 30 min at 60 °C under ~ 2 atm H_2 to form in 95% yield *trans*- $\text{Ru}(\text{H})(\eta^1\text{-BH}_4)(\text{Ph}_2\text{P}(\text{CH}_2)_2\text{NH}_2)_2$ (**61**) (Eq. 2.2).



Propylene and excess NaBH_4 were also present. The *trans*- H-Ru-BH_4 complex was identified using ^1H , $^1\text{H}\{^{31}\text{P}\}$, ^{31}P , ^{11}B , $^1\text{H}\text{-}^{15}\text{N}$ HSQC, gTOCSY, gCOSY NMR experiments. Based upon this observation, we propose that the catalyst generated under base-free conditions is *trans*- $\text{Ru}(\text{H})_2(\text{Ph}_2\text{P}(\text{CH}_2)_2\text{NH}_2)_2$ (**53**), made from *trans*- $\text{Ru}(\text{H})(\eta^1\text{-BH}_4)(\text{Ph}_2\text{P}(\text{CH}_2)_2\text{NH}_2)_2$ (**61**). Related $\eta^1\text{-BH}_4$ compounds have been reported in the literature before¹³⁴ and after this research was published.^{89,91-93}

Conclusions

The new base-free catalyst system and the base-promoted catalyst system hydrogenate a synthetically useful variety of functionalized and heterocyclic amides. The absolute configurations are preserved at stereogenic carbon centres in groups

attached to nitrogen, and in groups alpha to the carbonyl group under base-free conditions. Certain olefins tolerate the hydrogenation, and the system is a catalytic, clean method to deprotect amines from acetyl amides.

Materials and methods

All pressurized reactions were carried out in a steel pressure reactor (50 atm H₂) equipped with a magnetic stir bar. Deuterated solvents were obtained from Aldrich and Cambridge Isotope Laboratories. Common laboratory solvents were dried over appropriate drying agents before each experiment. For example CH₂Cl₂, THF and 2-PrOH were distilled over CaH₂, Na/benzophenone and anhydrous Mg, respectively. 2-Oxazolidinone, 4*S*-(-)-isopropyl-2-oxazolidinone, 4-chlorobenzoyl chloride, 4-fluorobenzoyl chloride, 2-furoyl chloride and 1-phenyl-pyrrolidin-2-one (**114**) were obtained from Alfa Aesar. Acetyl chloride, benzoyl chloride, 4-fluoroaniline, 4-chloroaniline, aniline, potassium bis(trimethylsilyl)amide, lithium bis(trimethylsilyl)amide, (4*S*,5*R*)-(-)-4-methyl-5-phenyl-2-oxazolidinone, morpholine, propionyl chloride, 2-piperazin-1-yl-1-piperidin-1-yl-ethanone, tris(triphenylphosphine) ruthenium(II) dichloride and *N*-phenylbenzamide (**118f**) were obtained from Aldrich. *N,N*-Diphenylacetamide (**118a**), *N*-methylacetanilide (**118b**) and *N,N*-dimethylacetamide (**118e**), were obtained from TCI America. 2-(Diphenylphosphino)ethylamine (**116**) and sodium borohydride were obtained from Strem and BDH Chemicals, respectively. ¹H, ¹³C, and ³¹P NMR spectra were recorded using 400 and 600 MHz Varian Inova, and 500 MHz Varian DirectDrive spectrometers. ¹H and ¹³C NMR chemical shifts are reported in parts per million (δ)

relative to TMS with the deuterated solvent as the internal reference. ^{31}P chemical shifts are reported in parts per million (δ) relative to 85% H_3PO_4 as the external references. NMR peak assignments were made using ^1H - ^1H gCOSY, ^1H - ^{13}C gHSQC, ^1H - ^{15}N gHSQC and TOSCY NMR experiments. Abbreviations used for NMR spectra are s (singlet), d (doublet), dd (doublet of doublet), ddd (doublet of doublet of doublet), dt (doublet of triplet), t (triplet), tt (triplet of triplet), q (quartet), m (multiplet) and br (broad). High-resolution mass spectra were recorded using an Agilent 6220 oa TOF Mass Spectrometer. Elemental analysis data were obtained using a Carlo Erba CHNS-O EA1108 elemental analyzer.

General procedures used to synthesize amides^{141b}

The amine (76.0 mmol) was dissolved in 150 mL of CH_2Cl_2 and cooled to 0 °C using an ice bath. NEt_3 (83.6 mmol, 1.1 equivalents) was added to the amine solution followed by the corresponding acid chloride (76.0 mmol, 1.0 equivalent) drop-wise over 30 min. Then the mixture was stirred for 3–24 hours at RT. The mixture was then poured into a separatory funnel and washed with 3 \times 40 mL of saturated $\text{NaHCO}_3(\text{aq})$ followed by washing with 50 mL of saturated $\text{NaCl}(\text{aq})$. The organic layer was then dried over anhydrous Na_2SO_4 , filtered and concentrated *in vacuo*. The crude amide was obtained in 90–98% yield. The product suitable for hydrogenation was obtained from distillation (liquid amides), trituration in *n*-hexanes or from recrystallization using EtOH as a recrystallization solvent (solid amides).

Spectroscopic identification of amides

All amide substrates are known. The ^1H NMR chemical shift information is reproduced here for convenience.

1-phenyl-pyrrolidin-2-one (commercial sample, **114**): White powder: ^1H NMR (499.815 MHz, CDCl_3 , 27 °C): δ 2.15 (2H, d, J 7.2 Hz, CH_2), 2.60 (2H, t, J 8.0 Hz, CH_2), 3.86 (2H, t, J 7.0 Hz, CH_2), 7.13 (1H, t, J 7.5 Hz, aromatic CH), 7.36 (2H, t, J 7.5 Hz, 2 aromatic CH), 7.60 (2H, d, J 8.0 Hz, 2 aromatic CH).

N,N-diphenylacetamide (commercial sample, **118a**): White powder: ^1H NMR (499.815 MHz, CDCl_3 , 27 °C): δ 2.09 (3H, s, CH_3), 7.29 (4H, d, J 8.0 Hz, 4 aromatic CH), 7.10-7.50 (6H, m, 6 aromatic CH).

N-methylacetanilide (commercial sample, **118b**): Colorless crystals: ^1H NMR (498.122 MHz, CDCl_3 , 27 °C): δ 1.86 (3H, s, CH_3), 3.26 (3H, s, CH_3), 7.18 (2H, d, J 7.8 Hz, 2 aromatic CH), 7.33 (1H, t, J 7.5 Hz, aromatic CH), 7.42 (2H, t, J 7.2 Hz, 2 aromatic CH).

acetanilide (**118c**): Colorless crystals: ^1H NMR (499.815 MHz, CDCl_3 , 27 °C): δ 2.18 (3H, s, CH_3), 7.10 (1H, t, J 7.5 Hz, aromatic CH), 7.15 (1H, br, NH), 7.32 (2H, t, J 8.0 Hz, 2 aromatic CH), 7.49 (2H, d, J 7.5 Hz, 2 aromatic CH).⁵⁰

1-morpholinoethanone (**118d**): Colorless oil: ^1H NMR (399.794 MHz, CDCl_3 , 27 °C): δ 2.10 (3H, s, CH_3), 3.46 (2H, t, J 4.5 Hz, CH_2), 3.60 (2H, t, J 4.5 Hz, CH_2), 3.68-3.65 (4H, m, 2 CH_2).⁵⁰

N,N-dimethylacetamide (commercial sample, **118e**): Colorless liquid: ^1H NMR (498.122 MHz, CDCl_3 , 27 °C): δ 2.05 (3H, s, CH_3), 2.91 (3H, s, CH_3), 2.98 (3H, s, CH_3).

benzanilide (**118f**): Off-white powder: ^1H NMR (499.815 MHz, CDCl_3 , 27 °C): δ 7.16 (1H, t, J 7.2 Hz, aromatic CH), 7.38 (2H, t, J 7.8 Hz, 2 aromatic CH), 7.49 (2H, t, J 7.5 Hz, 2 aromatic CH), 7.55 (1H, t, J 7.5 Hz, aromatic CH), 7.64 (2H, d, J 8.2 Hz, 2 aromatic CH), 7.82 (1H, br, NH), 7.86 (2H, d, J 7.0 Hz, 2 aromatic CH).⁷⁹

4-fluorobenzanilide (**119a**): White powder: ^1H NMR (498.118 MHz, CDCl_3 , 27 °C): δ 7.19 (3H, t, J 8.5 Hz, 3 aromatic CH), 7.40 (2H, t, J 7.6 Hz, 2 aromatic CH), 7.64 (2H, d, J 7.6 Hz, 2 aromatic CH), 7.77 (1H, br, NH), 7.89-7.92 (2H, m, aromatic 2 CH).^{141c}

4-chloro-*N*-methyl-*N*-phenylbenzamide (**119b**): White powder ^1H NMR (399.794 MHz, CDCl_3 , 27 °C): δ 3.50 (3H, s, CH_3), 7.04 (2H, d, J 7.3 Hz, aromatic CH), 7.13-7.19 (3H, m, aromatic CH), 7.23-7.28 (4H, m, 4 aromatic CH).^{141d}

N-(4-fluorophenyl)benzamide (**119c**): White powder: ^1H NMR (399.984 MHz, CDCl_3 , 27 °C): δ 7.07 (2H, t, J 8.6 Hz, 2 aromatic CH), 7.49 (2H, t, J 7.1 Hz, 2 aromatic CH), 7.55-7.62 (3H, m, 3 aromatic CH), 7.79 (1H, br, NH), 7.87 (2H, d, J 8.6 Hz, 2 aromatic CH).^{141c}

N-(4-bromophenyl)benzamide (**119d**): Colorless crystals: ^1H NMR (498.118 MHz, CDCl_3 , 27 °C): δ 7.49-7.53 (4H, m, 4 aromatic CH), 7.56-7.61 (3H, m, 3 aromatic CH), 7.80 (1H, br, NH), 7.88 (2H, d, J 7.9 Hz, 2 aromatic CH).^{141c}

N-phenyl-2-furancarboxamide (**119e**): Colorless crystals: ^1H NMR (499.118 MHz, CDCl_3 , 27 °C): δ 6.58 (1H, dd, J 3.5, 1.7 Hz, furan CH), 7.17 (1H, t, J 7.4 Hz, aromatic CH), 7.27 (1H, d, J 3.5 Hz, furan CH), 7.39 (2H, t, J 7.4 Hz, 2 aromatic CH), 7.54 (1H, d, J 1.7 Hz, furan CH), 7.67 (2H, d, J 7.5 Hz, aromatic CH).^{141e}

furan-2-yl(piperidin-1-yl)methanone (**119f**): Colorless crystals: ^1H NMR (498.118 MHz, CDCl_3 , 27 °C): δ 1.62-1.72 (6H, m, CH_2 and CH_3 overlapping), 3.71 (4H, br, CH_2),

6.47 (1H, dd, J 3.5, 1.7 Hz, furan CH), 6.93 (1H, d, J 3.5 Hz, furan CH), 7.47 (1H, d, J 1.7 Hz, furan CH).^{141f}

2-piperazin-1-yl-1-piperidin-1-yl-ethanone (commercial sample, **119g**): White powder: ¹H NMR (498.118 MHz, CDCl₃, 27 °C): δ 1.50-1.67 (7H, m, CH₂, CH₃ and NH overlapping), 2.48 (4H, br, CH₂), 2.91 (4H, t, J 4.7 Hz, CH₂), 3.16 (2H, s, CH₂), 3.52-3.57 (4H, m, CH₂).

General procedures used to synthesize N-acyloxazolidinones

The chiral *N*-acyloxazolidinones **120a** and **120b** were prepared according to a procedure reported by Evans and coworkers.^{141a}

120a: Viscous oil: ¹H NMR (498.118 MHz, CDCl₃, 27 °C): δ 0.62 (3H, d, J 6.8 Hz, CH₃), 0.85 (3H, d, J 7.0 Hz, CH₃), 1.18 (3H, d, J 6.8 Hz, CH₃), 2.18 (1H, m, CH), 2.65 (1H, dd, J 7.4, 6.6 Hz, CH), 3.14 (1H, dd, J 7.6, 6.6 Hz, CH), 4.12-4.27 (1H, m, CH), 4.45 (1H, m, CH), 7.2 (1H, m, aromatic CH), 7.27 (4H, m, 4 aromatic CH).

120b: Viscous oil: ¹H NMR (498.118 MHz, CDCl₃, 27 °C): δ 0.75 (3H, d, J 6.5 Hz, CH₃), 1.21 (3H, d, J 6.5 Hz, CH₃), 2.68 (1H, dd, J 7.8, 6.8 Hz, CH), 3.14 (1H, dd, J 7.0, 6.9 Hz, CH), 4.17 (1H, m, CH), 4.78 (1H, m, CH), 5.65 (1H, d, J 7.0 Hz, CH), 7.18-7.44 (10H, m, 10 aromatic CH).

General procedures used to synthesize ruthenium precursors

[Ru(η^3 -C₃H₅)(Ph₂P(CH₂)₂NH₂)₂]BF₄ (**51**) was prepared according to our original procedure.⁷⁹ ³¹P{¹H} NMR - (201.643 MHz, CD₂Cl₂, 27 °C): δ 48.5 (*minor*, s), 51.9 (*major*, d, ² J_{P-P} 29.6 Hz), 69.9 (*major*, d, ² J_{P-P} 30.2 Hz).

$\text{RuCl}_2(\text{Ph}_2\text{P}(\text{CH}_2)_2\text{NH}_2)_2$ (**52**) was prepared according to a procedure reported by Morris and coworkers.¹⁴² $^{31}\text{P}\{^1\text{H}\}$ NMR - (161.839 MHz, CD_2Cl_2 , 27 °C): δ 55.4 (*trans*, d, $^2J_{\text{P-P}}$ 32.0 Hz), 61.8 (*cis*, s), 66.8 (*trans*, d, $^2J_{\text{P-P}}$ 32.0 Hz).

$[\text{Ru}((1\text{-}3;5\text{-}6\text{-}\eta)\text{-C}_8\text{H}_{11})(\eta^6\text{-anthracene})]\text{BF}_4$ (**115**) was prepared¹⁴³ via a modification of a procedure reported by Komiya and coworkers.¹⁴⁴

Catalyst preparation

General procedure for base-assisted hydrogenations using 51 and KO^tBu.

51 (6.8–13.8 mg, 10.0–20.0 μmol) and KO^tBu (9.0–44.8 mg, 80.0–400.0 μmol , 4.0–5.0 mol%) were weighed out into two respective NMR tubes in a glove box. Freshly distilled THF (1.0 mL) was then added by cannula under argon pressure into the tube containing **51**. This yellow solution was then cannulated into the NMR tube containing KO^tBu under ~ 2 atm H₂ pressure. It was then heated at 60 °C for 20 min with occasional mixing. This mixture turned orange/red during this time and was then used for the base-assisted amide hydrogenations described in the next section (Method A or B).

General procedure for base-free hydrogenations using 51 or 52 and NaBH₄

51 or **52** (13.8 mg **51** or 12.6 mg **52**, 20.0 μmol respectively) and NaBH₄ (1.5 mg, 2.0 equivalents based on **51**, 40.0 μmol , or 3.8 mg, 5.0 equivalents based on **52**, 100 μmol) were weighed out into two respective NMR tubes in a glove box. THF (1.0 mL) was then added by cannula under argon pressure into the NMR tube containing the Ru-precursor at room temperature. This solution (or mixture) was then transferred by cannula using ~ 2 atm H₂ pressure into the NMR tube containing NaBH₄ at room

temperature. The mixture was then heated at 60 °C for 20 min under ~2 atm H₂ with periodic mixing. The mixture turned orange/brown during this time and was then used for the base-free amide hydrogenations described in the next section (Method A or B).

*General procedure for base-free hydrogenations using in situ prepared catalysts derived from **115** or **117**, 2 equivalents of Ph₂P(CH₂)₂NH₂ (**116**) and 5 equivalents of NaBH₄*

115 or **117** (8.4 mg, 20 μmol **115** or 9.7 mg, 20 μmol **117**) and NaBH₄ (3.8 mg, 0.10 mmol, 5.0 equivalents based on Ru) were weighed out into two respective NMR tubes in a glove box. THF (1.0 mL) was then added by cannula under argon pressure to the NMR tube containing the Ru-precursor at room temperature. **116** (7.8 μL, 40 μmol, 2.0 equivalents based on Ru) was then added to the THF solution of Ru-precursors. The contents of the NMR tube were then heated at 60 °C for 0.5 hours under argon with periodic mixing. This solution was then transferred by cannula under ~2 atm H₂ pressure at room temperature into the NMR tube containing the 5.0 equivalents of NaBH₄. The mixture was then heated at 60 °C for 20 min with periodic shaking. The mixture turned orange/brown during this time and was then used for the base-free amide hydrogenation described in the next section (Method A).

General procedures for hydrogenation

Method A: Solid amides

The amide (2.0–20.0 mmol, 100–1000 equivalents) was added to a stainless steel autoclave equipped with a magnetic stir bar. The autoclave was then purged with H₂ for 10 min at room temperature. 4.0–5.0 mL of THF was then added to the autoclave using a gas tight syringe. The catalyst/NaBH₄ or catalyst/base mixture, prepared above, was then added by cannula under H₂ pressure followed by a 2.0–4.0 mL THF wash. The autoclave was then pressurized to 50 atm H₂. The reaction mixture was stirred at 50–100 °C for 23 hours. The autoclave was then allowed to cool over the course of 1 hour before venting at room temperature. The percent conversions were determined by ¹H NMR spectroscopy. The yields were confirmed with an internal standard.

Method B: Liquid amide or N-acyloxazolidinones (120a and 120b)

The atmosphere of a stainless steel autoclave was purged with H₂ for 10 min at room temperature. A solution of the amide or N-acyloxazolidinone (0.2–20 mmol, 10–1000 equivalents) in THF (1.0 mL), prepared under argon, was then added by a cannula under H₂ pressure followed by a 4.0 mL THF wash. The catalyst/NaBH₄ mixture, prepared above, was then added by cannula under H₂ pressure followed by a 2.0 mL THF wash. The autoclave was then pressurized to 50 atm H₂. The reaction mixture was stirred at 50–100 °C for 23–47 hours. The autoclave was then allowed to cool over the course of 1 hour before venting at room temperature. The percent conversions were determined by ¹H NMR spectroscopy. The yields were confirmed with an internal standard.

Control experiments

*Nanoparticle mediated hydrogenation:*⁷⁹ 14.5 mg of ruthenium black (10.0 μmol assuming 7% of ruthenium atoms are on the surface) and 100 μmol (10.0 equivalents) of **114** were added to a stainless steel autoclave equipped with a magnetic stir bar. The autoclave was then purged with H_2 for 10 min at room temperature. THF (8.0 mL) was then added to the autoclave using a gas tight syringe. The autoclave was then pressurized to 50 atm H_2 . The reaction mixture was stirred at 100 $^\circ\text{C}$ for 17 hours. The autoclave was then allowed to cool over the course of 1 hour before venting at room temperature. The percent conversion was determined by ^1H NMR spectroscopy. Compound **114** was converted into *N*-cyclohexylpyrrolidin-2-one with TON 1.

NMR study of the reaction between $[\text{Ru}(\eta^3\text{-C}_3\text{H}_5)(\text{Ph}_2\text{P}(\text{CH}_2)_2\text{NH}_2)_2]\text{BF}_4$ (**51**), NaBH_4 , and H_2 .

51 (0.02 mmol, 13.5 mg) and NaBH_4 (0.04 mmol, 1.6 mg) were weighed into two separate NMR tubes inside the glove box. Distilled $\text{THF-}d_8$ (0.7 mL) added to **51** by cannula under argon and ^1H NMR and $^{31}\text{P}\{^1\text{H}\}$ NMR were recorded. Then the solution containing **51** was transferred to the tube containing NaBH_4 under H_2 (~2 atm). The ^1H and $^{31}\text{P}\{^1\text{H}\}$ NMR spectra were recorded at room temperature. Then the resulting solution was heated at 60 $^\circ\text{C}$ for 30 minutes inside the NMR probe. The ^1H and $^{31}\text{P}\{^1\text{H}\}$ NMR spectra showed the reaction was complete, generating *trans*- $\text{Ru}(\text{H})(\eta^1\text{-BH}_4)(\text{Ph}_2\text{CH}_2\text{CH}_2\text{NH}_2)_2$ as the major product (95% spectroscopic yield). The product was identified using ^1H , $^{31}\text{P}\{^1\text{H}\}$, $^{13}\text{C}\{^1\text{H}\}$, $^{11}\text{B}\{^1\text{H}\}$ ^1H - ^{15}N HSQC, gTOCSY,

gCOSY and $^1\text{H}\{^{31}\text{P}\}$ NMR experiments in THF- d_8 . ^1H NMR (399.949 MHz, THF- d_8 , 27 °C): δ -15.67 (1H, t, J 25.0 Hz, Ru-H), -2.63 to -1.56 (4H, br, HBH_3), 2.19-2.30 (2H, m, CH_2), 2.35-2.45 (2H, m, CH_2), 2.52-2.66 (2H, m, CH_2), 3.03-3.20 (2H, m, CH_2), 3.65-3.75 (2H, br, NH), 4.00-4.10 (2H, br, NH), 6.93-7.02 (8H, m, aromatic CH), 7.03-7.12 (4H, m, aromatic CH), 7.23-7.28 (4H, m, aromatic CH), 7.30-7.38 (4H, m, aromatic CH). $^{13}\text{C}\{^1\text{H}\}$ NMR (125.691 MHz, THF- d_8 , 27 °C): δ 41.3 (CH_2), 48.45 (CH_2), 132.2 (aromatic), 133.3 (aromatic), 138.3 (m, aromatic), 145.6 (m, aromatic), 147.2 (m, aromatic), $^{31}\text{P}\{^1\text{H}\}$ NMR - (161.902 MHz, THF- d_8 , 27 °C): δ 29.1 (*minor*, s), 80.3 (*major*, s), $^{11}\text{B}\{^1\text{H}\}$ NMR - (128.319 MHz, THF- d_8 , 27 °C): δ -30.54 to -27.10 (br, BH_4)

Figure 2.1: $^{31}\text{P}\{^1\text{H}\}$ NMR of *trans*- $[\text{Ru}(\text{H})(\eta^1\text{-BH}_4)(\text{Ph}_2\text{CH}_2\text{CH}_2\text{NH}_2)_2]$ (**61**). The top spectrum shows the product formed after 30 minutes at 60 °C. The bottom spectrum was recorded just after mixing at room temperature.

Peak assigned to *trans*-**61** are labeled with (*). The peaks assigned to **51** are labeled with (■).

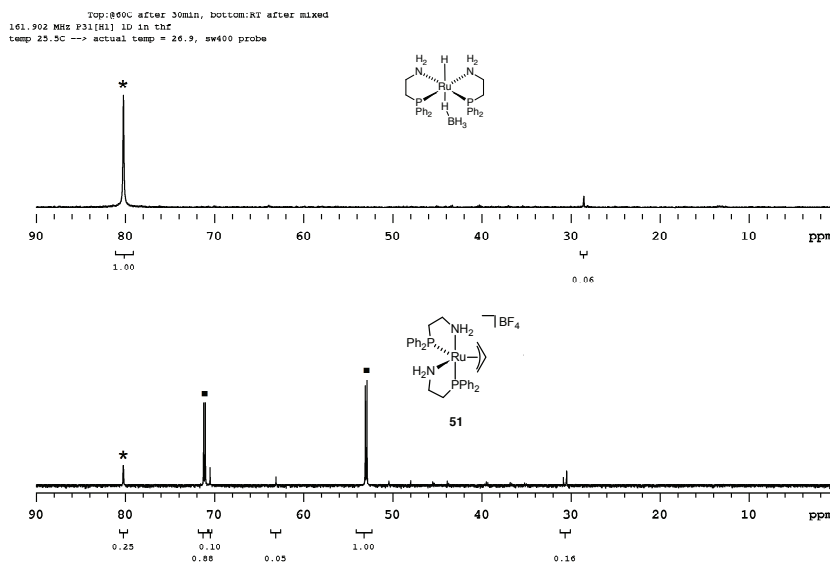


Figure 2.2: ^1H NMR spectrum (δ 6 to 0.4 ppm) of *trans*-**61** formed by the reaction of **51** and NaBH_4 in ~ 2 atm H_2 in THF-d_8 .

Residual solvent = δ ; ligand **116**; $\text{NH} = \text{l}^*$; $\text{CH} = \text{l}^*$; propylene = ϕ ; Free hydrogen gas = H .

Top: ^1H NMR; middle: ^1H - ^{15}N HSQC as 1D trace; bottom: zTOCSY1D, sel.excite @ 2.24 ppm (Coordinated ligand, **116**).

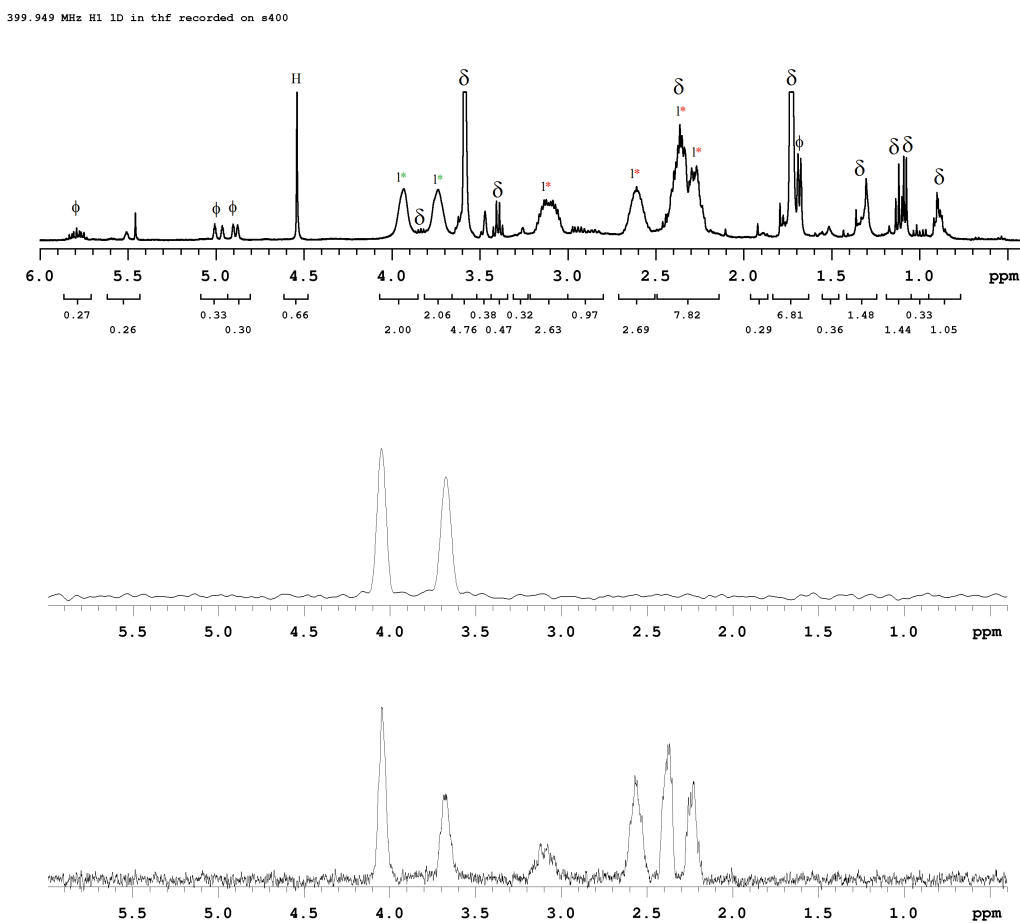
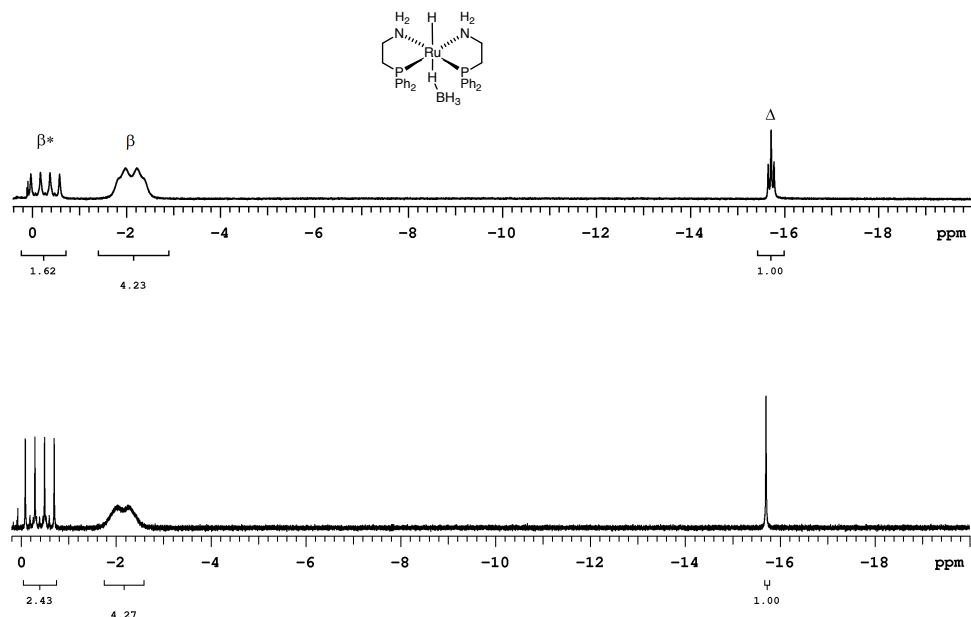


Figure 2.3: ^1H NMR spectrum (δ 0.4 to -20 ppm) of *trans*-**61** formed by the reaction of **51** and NaBH_4 in ~ 2 atm H_2 in THF-d_8 . (Top: ^1H NMR of *trans*-**61**; bottom: ^1H $\{^{31}\text{P}\}$ NMR of *trans*-**61**).

Ruthenium hydride = Δ ; BH_4 bonded to ruthenium = β ; free BH_4^- = β^* .



Spectroscopic identification of products

All hydrogenation products except from **120a** and **120b** are known and will not be reproduced here. The product ^1H NMR spectra for the base-assisted hydrogenation of functionalized amides are reproduced here for convenience.

alcohol product denoted by (*); amine product denoted by (■); starting material denoted by (+); internal standard denoted by (IS); C–O cleavage product denoted by (x)

Figure 2.4: The δ region from 8 to 4 ppm of ^1H NMR spectrum showing the products from the hydrogenation of 4-fluorobenzamide (**119a**) under base-assisted conditions.

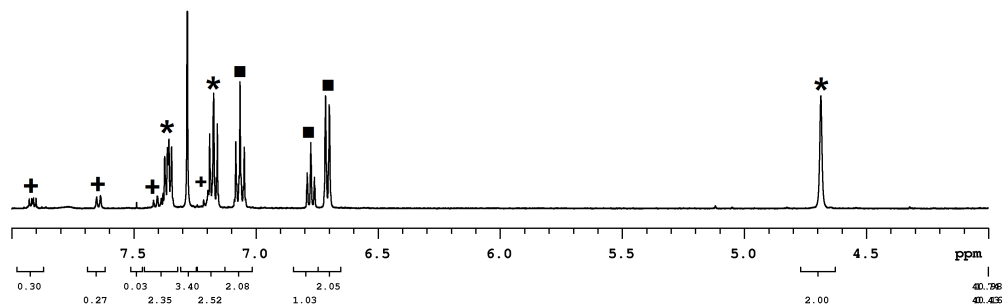


Figure 2.5: The δ region from 7.5 to 3.0 ppm of ^1H NMR spectrum showing the products from the hydrogenation of 4-chloro-*N*-methyl-*N*-phenylbenzamide (**119b**) under base-assisted conditions.

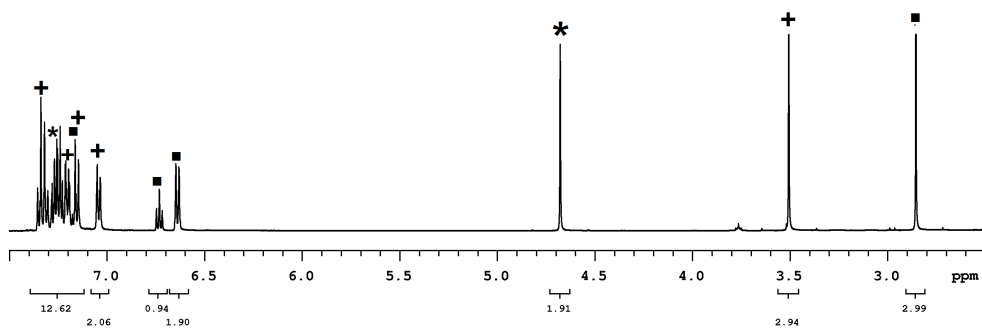


Figure 2.6: The δ region from 8 to 4 ppm of ^1H NMR spectrum showing the products from the hydrogenation of *N*-(4-fluorophenyl)benzamide (**119c**) under base-assisted conditions.

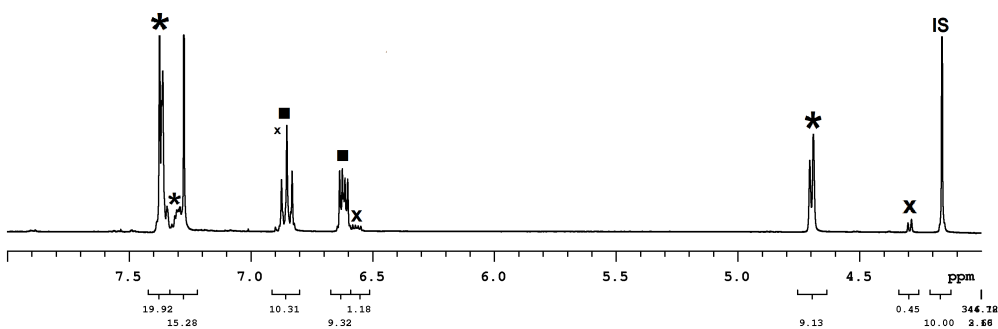


Figure 2.7: The HRMS (ESI+) spectrum showing the product mixture resulting from the hydrogenation of *N*-(4-fluorophenyl)benzamide (**119c**) under base-assisted conditions.

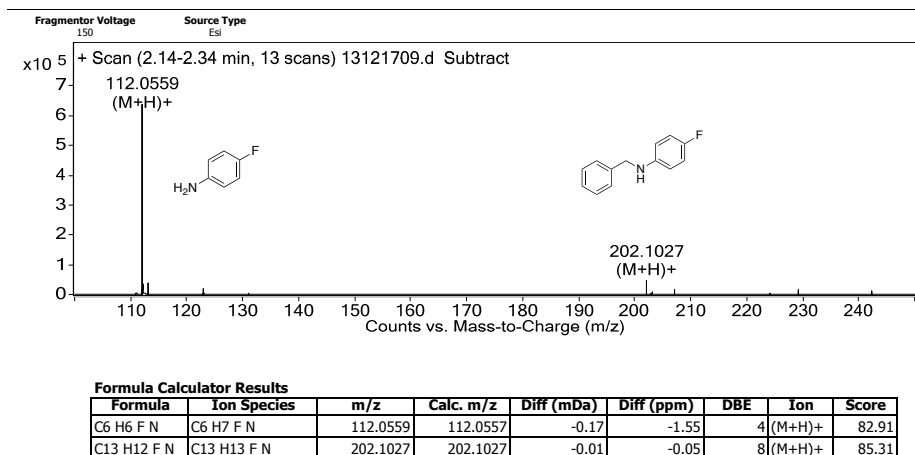


Figure 2.8: The δ region from 8 to 4 ppm of ^1H NMR spectrum showing the products from the hydrogenation of *N*-(4-bromophenyl)benzamide (**119d**) under base-assisted conditions.

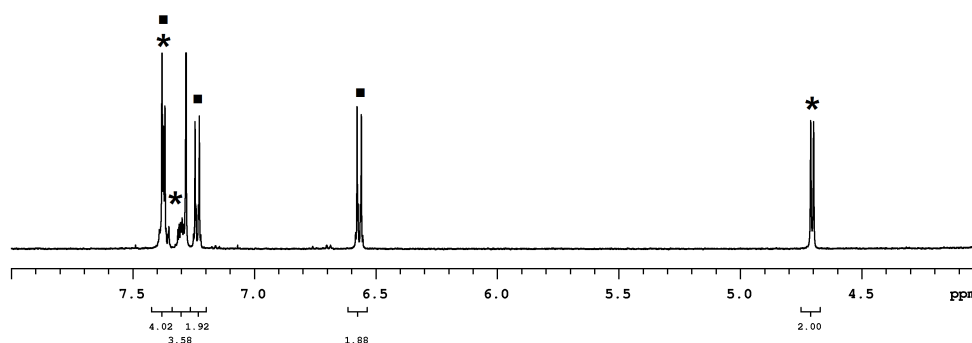


Figure 2.9: The δ region from 8 to 1 ppm of ^1H NMR spectrum showing the products from the hydrogenation of *N*-phenyl-2-furancarboxamide (**119e**) under base-assisted conditions.

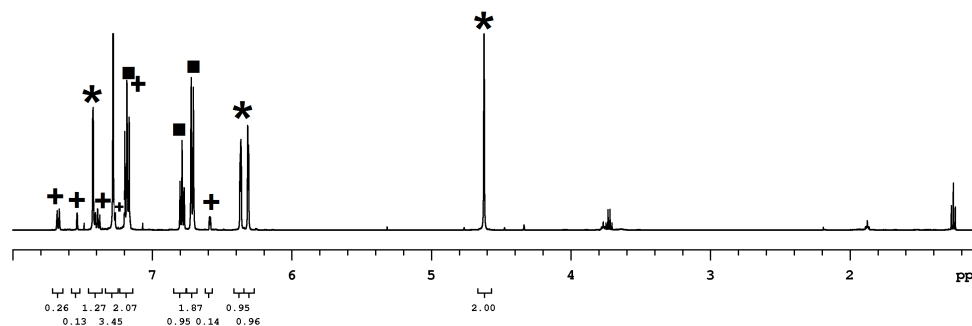


Figure 2.10: The δ region from 8 to 1 ppm of ^1H NMR spectrum showing the products from the hydrogenation of furan-2-yl(piperidin-1-yl)methanone (**119f**) under base-assisted conditions.

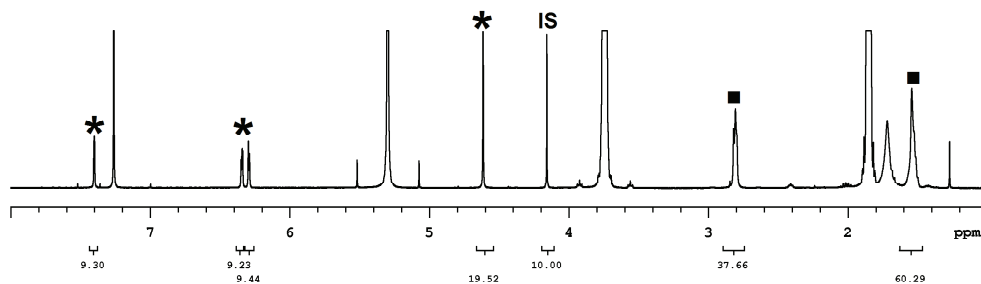
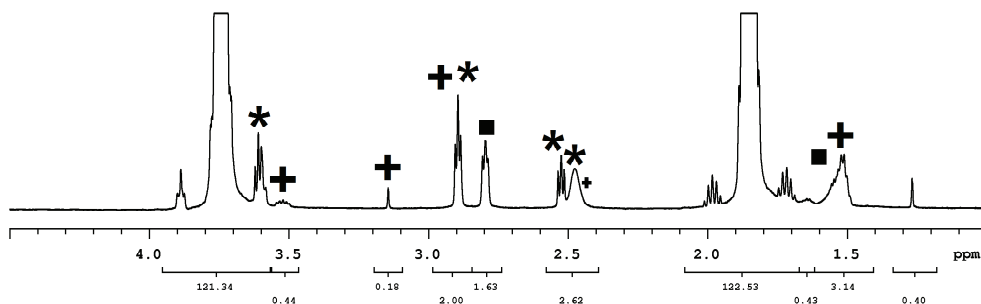


Figure 2.11: The δ region from 4.5 to 1.0 ppm of ^1H NMR spectrum showing the products from the hydrogenation of 2-piperazin-1-yl-1-piperidin-1-yl-ethanone (**119g**) under base-assisted conditions.



The hydrogenation product from **120a**: ^1H NMR (599. 926 MHz, CDCl_3 , 27 $^\circ\text{C}$): δ 0.71 (3H, d, J 7.0 Hz, CH_3), 0.78 (3H, d, J 6.5 Hz, CH_3), 1.21 (3H, d, J 6.0 Hz, CH_3), 1.73 (1H, m, CH), 2.53 (1H, m, CH), 2.70 (1H, m, CH), 2.95 (1H, m, CH), 3.23 (1H, br, OH), 3.60 (3H, m, 3 CH), 5.72 (1H, br, NH), 7.17-7.26 (5H, m, 5 aromatic CH). $^{13}\text{C}\{^1\text{H}\}$ NMR (175.969 MHz, CDCl_3 , 27 $^\circ\text{C}$): δ 17.9 (CH), 18.5 (CH), 19.2 (CH), 28.6 (CH), 40.4 (CH), 43.9 (CHNH), 56.9 (aromatic), 63.6 (CHOH), 126.2 (aromatic), 128.3

(aromatic), 128.8 (aromatic), 139.7 (aromatic), 176.5 (C O). ^1H - ^{15}N HSQC (498.117 MHz, CDCl_3 , 27 °C): δ 123. HRMS (ESI⁺) m/z: Calcd for $\text{C}_{15}\text{H}_{24}\text{NO}_2$ (M+H)⁺ 250.1807; Found 250.1802. Difference (ppm): 0.75. The hydrogenation product of **120a** is not stable for prolonged periods in solution.

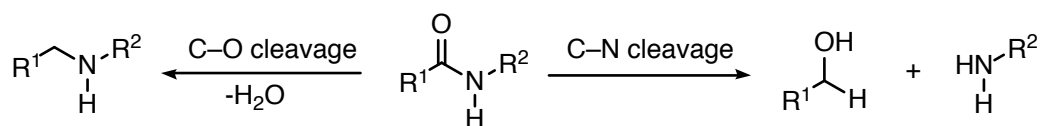
The hydrogenation product from **120b**: ^1H NMR (599.926 MHz, CDCl_3 , 27 °C): δ 0.79 (3H, d, J 7.2 Hz, CH_3), 1.21 (3H, d, J 6.6 Hz, CH_3), 2.43 (1H, sex, J 6.6 Hz, CH), 2.70 (1H, dd, J 6.6, 6.5 Hz, CH), 2.93 (1H, dd, J 9.0, 8.4 Hz, CH), 3.91 (1H, br, OH), 4.19 (1H, m, CH), 4.75 (1H, br, NH), 5.38 (1H, d, J 7.8 Hz, CH), 7.15-7.33 (10H, m, 10 aromatic CH). $^{13}\text{C}\{^1\text{H}\}$ NMR (150.868 MHz, CDCl_3 , 27 °C): δ 14.5 (CH), 17.7 (CH), 40.5 (CH), 43.8 (CH), 50.9 (CHNH), 76.7 (CHOH), 126.3 (aromatic), 126.4 (aromatic), 127.4 (aromatic), 128.0 (aromatic), 128.4 (aromatic), 128.9 (aromatic), 139.7 (aromatic), 140.7 (aromatic), 176.4 (C O). ^1H - ^{15}N HSQC (599.925 MHz, CDCl_3 , 27 °C): δ 127. HRMS (ESI⁺) m/z: Calcd for $\text{C}_{19}\text{H}_{23}\text{NO}_2$ (M+Na)⁺ 320.1621; Found 320.1621. Difference (ppm): 0.01.

Chapter 3

A Highly Enantioselective Hydrogenation of Amides via Dynamic Kinetic Resolution Under Low Pressure and Room Temperature²

Introduction

Catalytic hydrogenations are an atom-economic and efficient alternative to stoichiometric reducing agents. The Chapter 1 reviewed the recent advances in homogeneous catalytic hydrogenation of amides. Depending on the conditions, amide reduction proceeds to give the C–O cleavage product or the C–N cleavage product (Scheme 3.1).



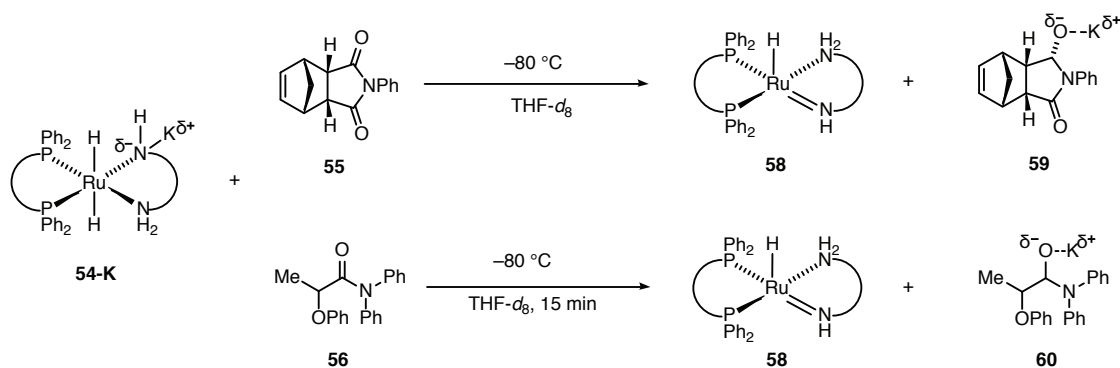
Scheme 3.1: Hydrogenation of amides via C–O cleavage or C–N cleavage pathway

As discussed in detail in Chapter 1, heterogeneous and acidic catalytic systems favor C–O cleavage, while neutral and basic homogeneous systems favor C–N cleavage.

Recently Bergens and coworkers reported a mechanistic investigation into the desymmetrization of cyclic imides using Noyori's hydrogenation catalyst, *trans*-RuH₂((*R*)-BINAP)((*R,R*)-dppe) (**50**). During this study they found that mono or di

² A version of this chapter has been published. Loorthuraja, R.; John, J. M.; Elanna, S.; Riley, E.; Suneth, K.; Roxane, C.; Bergens, S. H. *J. Am. Chem. Soc.* **2017**, *139*, 3065–3071.

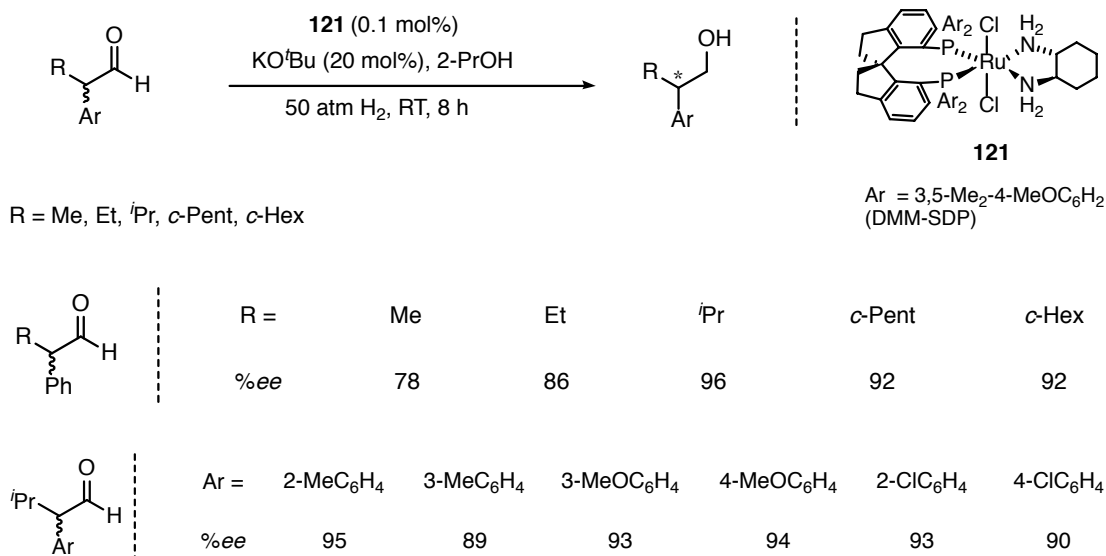
deprotonation at N–H groups of the **50** occurred with excess base to form *trans*- $M^+[\text{RuH}_2((R)\text{-BINAP})(R,R)\text{-H}_2\text{NCH(Ph)CH(Ph)NH}^{(-)}]$ (**54-M**; where **M** = K or Li), or *trans*- $(M^+)_2[\text{RuH}_2((R)\text{-BINAP})(R,R)\text{-HN}^{(-)}\text{CH(Ph)CH(Ph)NH}^{(-)}]$ (**54-M**₂; where **M** = Li), respectively.⁸⁵ They also showed that the **54-K** is extremely active towards the stoichiometric reduction of an imide and an amide substrate with the additions occurring as low as $-80\text{ }^\circ\text{C}$ (Scheme 3.2).⁸⁵



Scheme 3.2: Products observed for the bifunctional addition of **54-K** to **55** and amide **56** under mild condition.

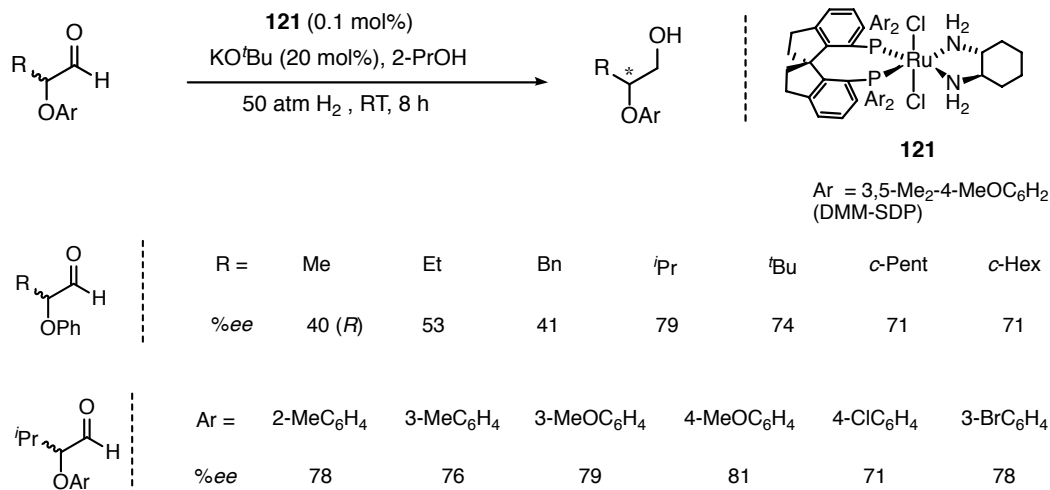
These results suggested that a racemic α -chiral amide (with an acidic hydrogen at the α - position) could be hydrogenated at low temperature and pressures in the presence of a large excess of base. The large excess of base may form species similar to **54-K**. As well, the excess base would racemize the α -chiral amide during the hydrogenation allowing for DKR. Enantioselective hydrogenation of β -ketoesters via DKR is well known.^{97,145–147} In contrast; there are only a handful of reports for the enantioselective hydrogenation of aldehydes^{148–150} and esters^{74,151} with DKR. There are no reports of the hydrogenation of amides via DKR.

In 2007, Zhou and coworkers reported a bifunctional catalyst [RuCl₂((*S*)-DMM-SDP)((*R,R*)-DACH)] (**121**, DACH is 1,2-diaminocyclohexane) for the enantioselective hydrogenation of racemic α -chiral aldehydes.¹⁴⁸ The catalyst **121** hydrogenates several α -arylaldehydes at room temperature under 50 atm H₂ pressure in 2-PrOH to give chiral primary alcohols with quantitative yields (TON up to 1000) and in 78–96% *ee* after 8 hours (Scheme 3.3).



Scheme 3.3: Enantioselective hydrogenation of α -arylaldehydes by catalyst **121** via DKR.

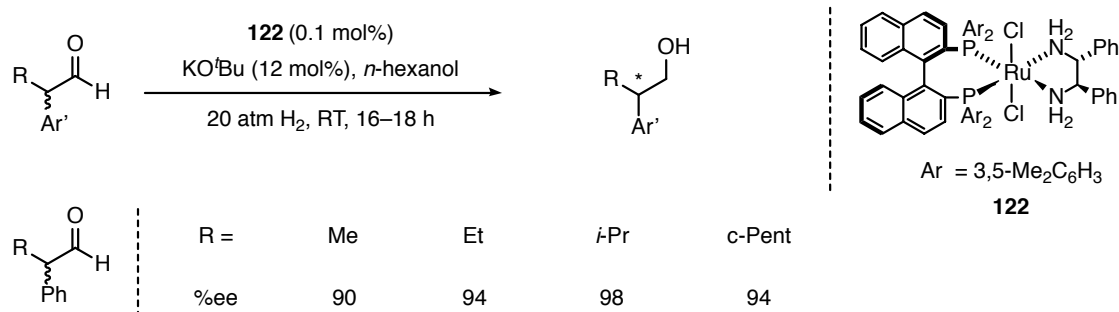
Placement of methyl and ethyl groups at the α -position gave 78% and 86% *ee*, respectively, while an isopropyl group provided 96% *ee* of the corresponding primary alcohol product. The electronic nature and position of substituents on the aryl ring did not significantly affect the *ee*. In 2009, Zhou and coworkers reported another enantioselective hydrogenation of α -aryloxy type aldehydes via DKR using the same bifunctional catalyst **121** under the conditions in his previous report (Scheme 3.4).¹⁴⁹



Scheme 3.4: Enantioselective hydrogenation of α -aryloxyaldehydes by catalyst **121** via DKR.

The hydrogenation of α -aryloxy aldehydes produced chiral β -aryloxy primary alcohols with 92–98% yield and with reasonably good *ee*'s ranging 40–81%. The electronic property or position of substituents on the aryl ring did not affect the *ee* significantly. Placement of a methyl or ethyl group at the α -position gave low *ee*'s (40% and 53% respectively) while bulky alkyl groups gave higher *ee*'s ranging from 71–81%.

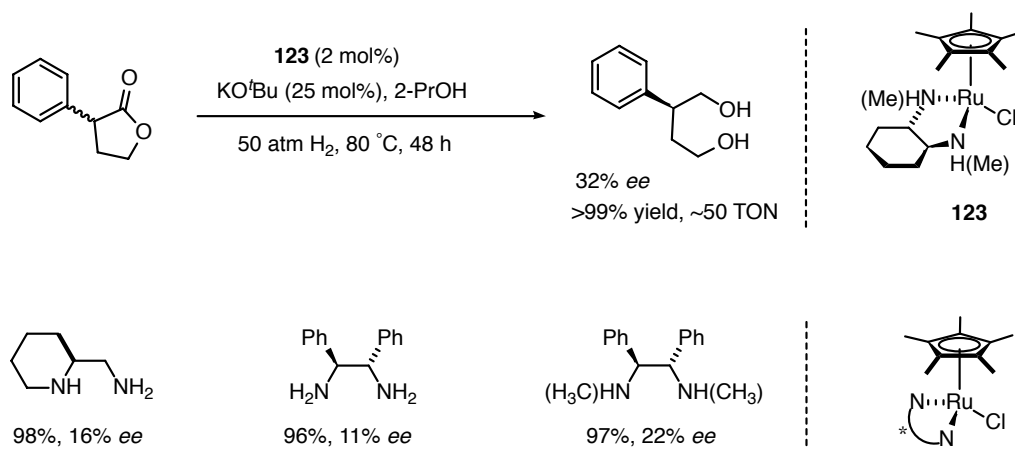
List and coworkers reported the hydrogenation of α -arylaldehydes using [RuCl₂((*R*)-xyl-BINAP)((*R,R*)-dpen)] (**122**, xyl-BINAP is 2,2'-Bis[di(3,5-xylyl)phosphino]-1,1'-binaphthyl) under 20 atm H₂ in *n*-hexanol with 20 mol% KO^tBu at room temperature (Scheme 3.5).¹⁵⁰



Scheme 3.5: Enantioselective hydrogenation of α -arylaldehydes by List's **122** via DKR.

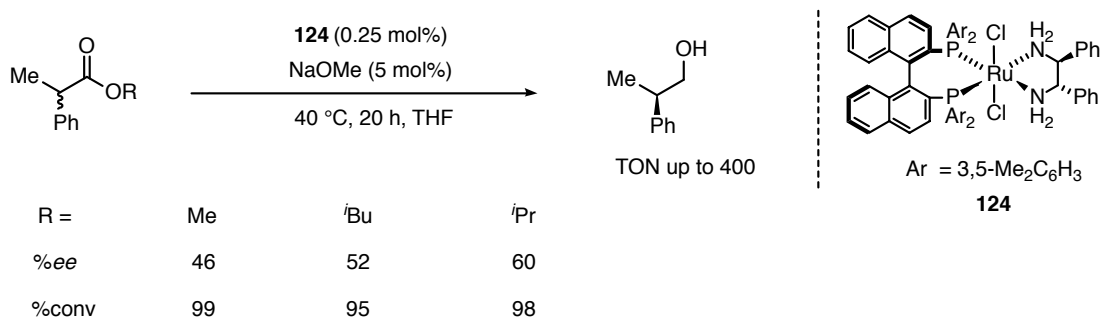
In most cases, the results followed the trends reported previously by Zhou and coworkers.¹⁴⁸ For example, the enantioselectivity of the catalyst increased with the size of the alkyl group at the α -position.

Ikariya and coworkers reported the DKR hydrogenation of the lactone, *rac*- α -phenyl- γ -butyrolactone using the Cp**Ru*Cl(diamine) catalyst **123** at 80 °C under 50 atm H₂ to give (*S*)-2-phenylpropane-1, 3-diol in up to 32% *ee* with quantitative yield (Scheme 3.6).⁷⁴



Scheme 3.6: Enantioselective DKR hydrogenation of *rac*- α -phenyl- γ -butyrolactone by Ikariya's catalyst **123**.

The authors also tested three other chiral diamine ligands that were less enantioselective than **123**. A preliminary result in a book chapter describes the hydrogenation of alkyl 2-phenylpropanoate (alkyl: methyl, isobutyl and isopropyl) by catalyst [RuCl₂((*R*)-xyl-BINAP)((*S,S*)-dpen)] (**124**) at 40 °C in THF (Scheme 3.7).¹⁵¹



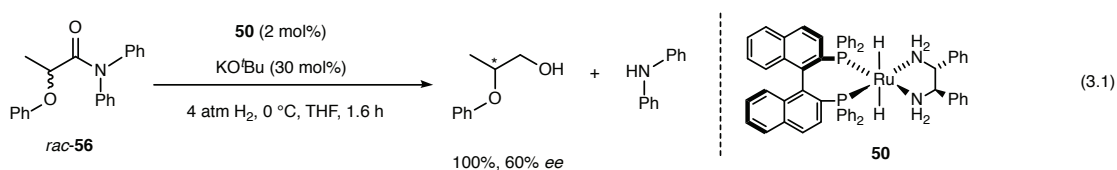
Scheme 3.7: Enantioselective hydrogenation of α -phenylesters by catalyst **124**.

The primary alcohol product, (*R*)-2-phenylpropan-1-ol, was obtained in near quantitative yield with *ee*'s ranging from 46 to 60% for methyl, isobutyl and isopropyl ester substituents respectively. It is notable that the authors did not provide the hydrogen pressure for these hydrogenations.¹⁵¹

There are no reports of the asymmetric hydrogenation of amides. Herein, I report the use of high throughput rapid screening to develop the highly enantioselective hydrogenation of racemic α -phenoxy amides via DKR under mild conditions.

Results and discussion

The amide used for the rapid screening was racemic *N,N*-diphenyl-2-phenoxypropanamide (**56**). The hydrogenation of **56** by *trans*-**50** in THF⁸² occurred under only 4 atm H₂ at 0 °C, in the presence of high amounts of base, to give diphenylamine and 2-phenoxypropan-1-ol in 60% *ee* in quantitative yield (TON = 50, Eq. 3.1). For this reaction, the catalyst **50** was made beforehand by the reaction between [RuH((*R*)-BINAP)((*R,R*)-dpen)(THF)]BF₄, KO^{*t*}Bu (~2 equiv), and H₂ (~2 atm) at -78 °C.⁸² Based upon our earlier studies,⁸⁵ we predict that the catalyst is the active reducing agent *trans*-K⁺[RuH₂((*R,R*)-H₂NCH(Ph)CH(Ph)NH⁽⁻⁾)(*R*)-BINAP)] (**54-K**) in the presence of a large excess KO^{*t*}Bu.



This is the first example of an amide hydrogenation with DKR. High throughput screening was used to develop a catalyst with high yield and enantioselectivity towards this reaction. Monophosphine (P), diphosphine (P-P), dpen and multivalent ligands (P-N, P-N-P, and P-N-N-P) were screened for the hydrogenation (See the complete list of the ligands and their structures on pages 117–122). The catalysts were prepared with our standard catalytic precursor, *cis*-[Ru(η^3 -C₃H₅)(MeCN)₂(COD)]BF₄ (**117**) in a THF/CH₂Cl₂ solution (Figure 3.1).

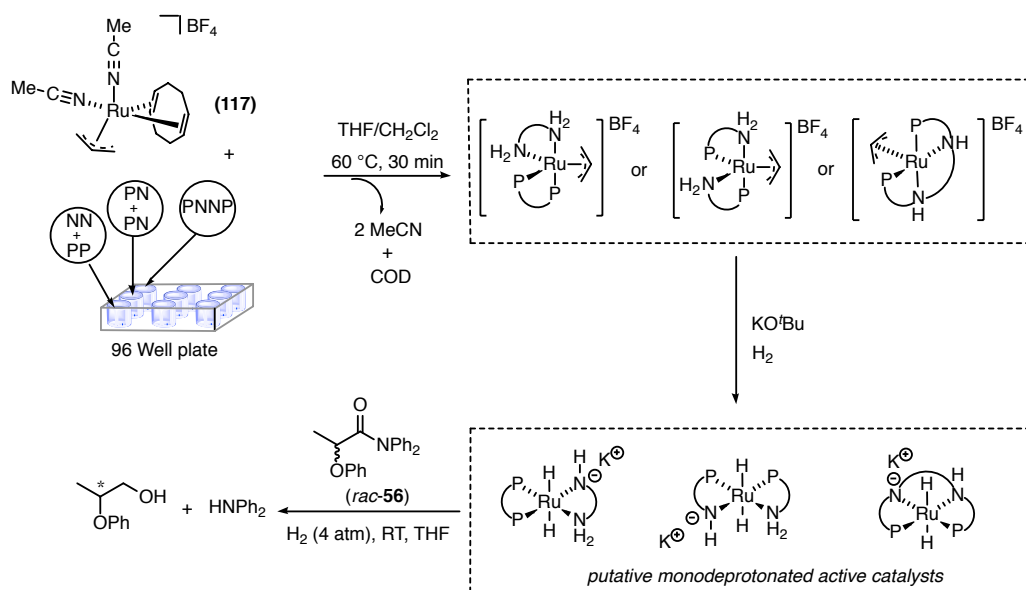
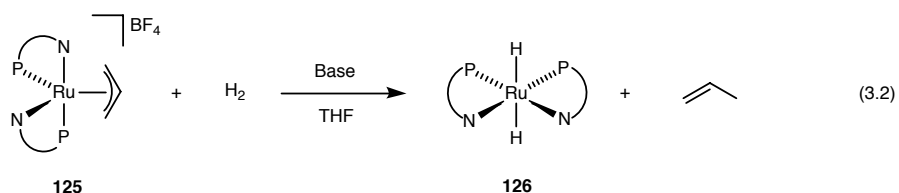


Figure 3.1: Strategy for the high throughput screening process; *in-situ* catalyst preparation (structures shown inside the square-bracket are proposed), and hydrogenation of **56**.

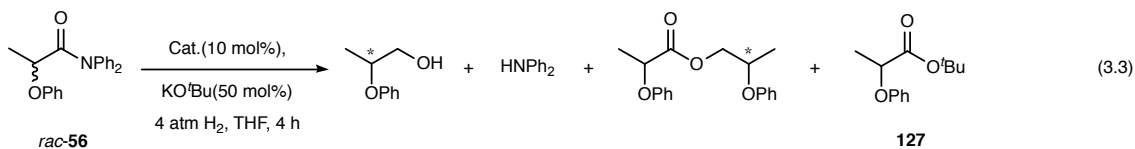
Solutions of **117**, 1 equivalent of a P–P ligand, and (*R,R*)-dpen were allowed to react for 30 min at 60 °C to displace the MeCN and COD ligands before the hydrogenations.^{79,152} Solutions of **117**, P–N (2 equivalents) or P–N–P (1 equivalent), or P–N–N–P (1 equivalent) ligands were allowed to react in the absence of (*R,R*)-dpen. The resulting allylic-Ru precursors were then mixed at room temperature with KO^tBu (5 equivalents), the *rac*-**56** (10 equivalents), and placed under 4 atm H₂ for 4 hours. Bergens and coworkers previously reported that allylic Ru precursors like [Ru(η^3 -C₃H₅)(P–N)₂]⁺BF₄[–], (**125**) react with H₂ and base in THF to form the dihydride catalysts *trans*-RuH₂(P–N)₂ (**126**) and propylene (Eq. 3.2).⁷⁹



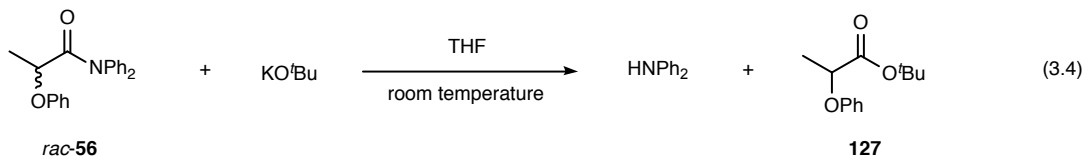
The large excess of KO^tBu ensured that **56** underwent rapid tautomerization and that the putative catalysts, like **126**, were activated by deprotonation of the N–H groups. The results from the rapid screening are arranged into four categories.

- I. Ligands showing little or no activity for the hydrogenation (38 ligands).
- II. Those with moderate to low amounts of starting materials remaining (12 ligands).
- III. No starting materials remaining but varying amounts of products and side products (7 ligands).
- IV. Complete conversion to diphenylamine and 2-phenoxypropan-1-ol (17 ligands).

It was noteworthy that the amide **56** was present as a racemic mixture in the wells with starting material remaining, showing that the hydrogenations proceeded via dynamic kinetic resolution.¹⁵³ The products in categories II and III were mixtures of the expected diphenylamine and 2-phenoxypropan-1-ol, but to our surprise, the ^tBu- and 2-phenoxyprop-1-yl esters (4 diastereomers) of the parent amide **56** were also formed (Eq. 3.3).



A control reaction between **56** and KO^tBu in THF resulted in exchange of diphenylamine to form the ^tBu ester *rac*-CH₃(PhO)CHCO₂^tBu (**127**) on the timescale of the hydrogenation (Eq. 3.4).



Thus the rapid screening occurred to some extent via hydrogenation of the esters formed by the reaction between **56** and KO^tBu or the alkoxide of the product alcohol KOCH₂CH(OPh)CH₃. Indeed, the ^tBu ester **127** and diphenylamine were present to some extent in the reactions that did not go to completion. The results from the screening are therefore indicative and not definitive.

The catalysts in category IV produced only 2-phenoxypropan-1-ol and diphenylamine. Figure 3.2 shows the catalysts (**128–132**) from category IV that were the most enantioselective. They consisted of (P–P)(N–N), (P–N)₂, and (P–N–N–P) catalyst systems, and formed the product with *ee*'s ranging from 17 to ~60%. The hydrogenation was then optimized with these category IV catalysts on larger scale individual reactions.

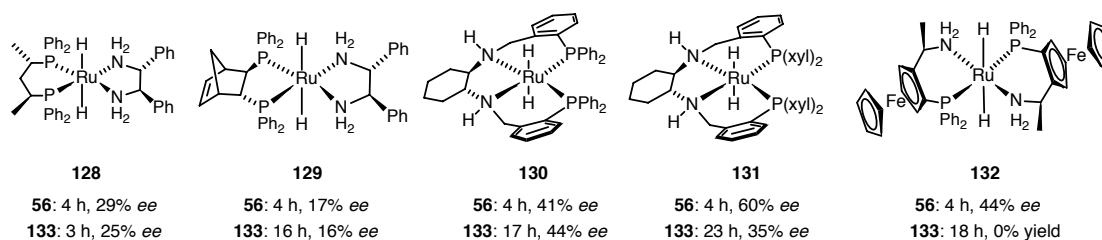
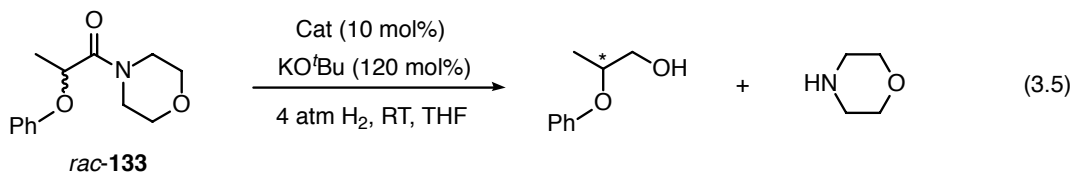


Figure 3.2: Putative dihydride catalysts of active category IV (with 100% conversion) and their *ee* (%) for the hydrogenation of *rac*-**56** and *rac*-**133**.

We employed *rac*-2-phenoxy-1-(morpholine)-1-propanone (**133**) to minimize displacement of the amine group by alkoxides. In control NMR experiments, *rac*-**133** did not undergo displacement of the morpholine by either KO^tBu or *rac*-

KOCH₂CH(OPh)CH₃ under the hydrogenation conditions. Figure 3.2 also shows the activity and selectivity of **128–132** towards the hydrogenation of *rac*-**133**. This *N,N*-dialkyl amide was less reactive than the *N,N*-diphenyl amide **56**, and 12 equivalents of KO^tBu (per Ru) were required to hydrogenate *rac*-**133** at room temperature under 4 atm H₂ (Eq. 3.5).



Catalyst **132** was inactive under these conditions. The dioxyl-(**131**), and diphenylphosphino-(**130**) (*R,R*)-(P–N–N–P) catalysts required 23 and 17 hours, respectively, to form 2-phenoxypropan-1-ol in 35 and 44% *ee*. The (*R,R*)-norphos/(*R,R*)-dpen catalyst **129** also required a similar amount of time (16 hours), but was less enantioselective (16%). The (*S,S*)-skewphos/(*R,R*)-dpen catalyst **128** was significantly more active and the reaction went to completion after 3 hours with 25% *ee*. In all cases, esters and aldehydes could not be detected by NMR. The most active phosphine, (*S,S*)-skewphos in catalyst **128**, was used for subsequent optimizations with the diamines shown in Figure 3.3.

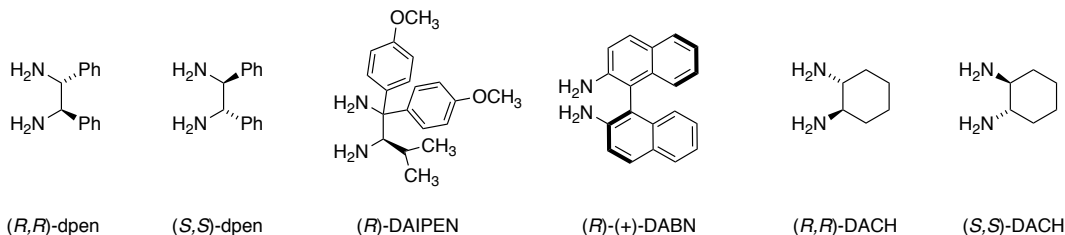
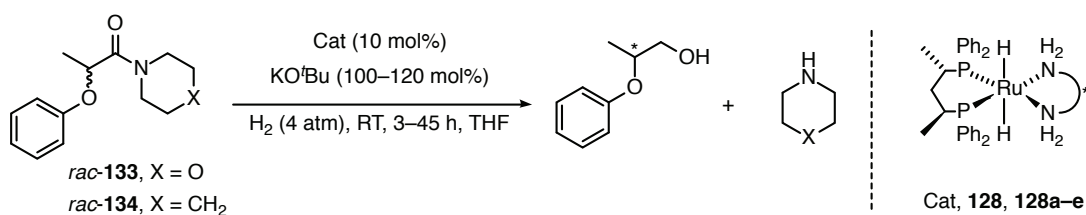


Figure 3.3: Structures of diamine ligands used for catalyst optimization.

During these optimization studies, we found that a piperidine amide, *rac*-2-phenoxy-1-(piperidine)-1-propanone (**134**) gave higher *ee* than *rac*-**133**. Table 3.1

summarizes the results. The reaction time was optimized for >95 % yield, unless the reaction was very slow (entries 4, 7).

Table 3.1: Optimization studies for the asymmetric hydrogenation of *rac*-133 and *rac*-134.^(a)



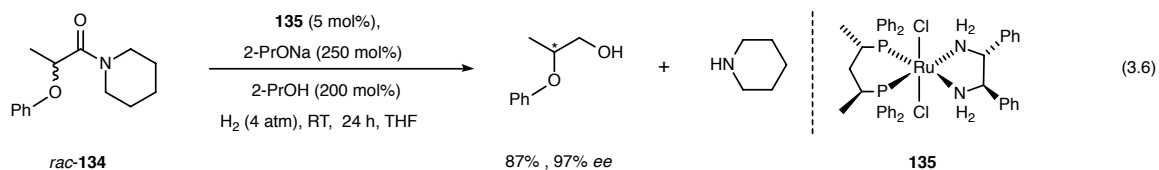
entry	cat	diamine ligand	time (h)	yield (%) ^(b)	<i>ee</i> (%) ^(c)
1	128	(<i>R,R</i>)-dpen	3	100	25
2	128a	(<i>S,S</i>)-dpen	16.5	100	12
3	128b	(<i>R</i>)-DAIPEN	42	100	18
4	128c	(<i>R</i>)-(+)-DABN	16	0	-
5	128d	(<i>R,R</i>)-DACH	45	96	58
6	128e	(<i>S,S</i>)-DACH	41	98	29
7 ^(d, e)	128d	(<i>R,R</i>)-DACH	21	8.3	56
8 ^(d, e)	128	(<i>R,R</i>)-dpen	3.5	96	44
9 ^(d, f)	128	(<i>R,R</i>)-dpen	20	14	88
10 ^(d, g)	128	(<i>R,R</i>)-dpen	24	89	93

(a) Ru:KO^tBu:**133** or **134** 1:12:10, [**133** or **134**] 0.06 M in THF. [KO^tBu] 0.072 M in THF. (b) Determined using ¹H NMR spectroscopy. (c) Determined using HPLC with a Daicel CHIRALPAK IB (4.6 mm i.d. × 250 mm) chiral column. (d) For entry 7–10, **134** was used as the substrate. (e) Ru:KO^tBu:**134** 1:10:10, [KO^tBu] 0.06 M in

THF. (f) Ru:KO^tBu:**134** 1:1.1:10, [KO^tBu] 0.0065 M in THF. (g) Ru:KO^tBu:**134**:2-PrOH 1:30:20:100.

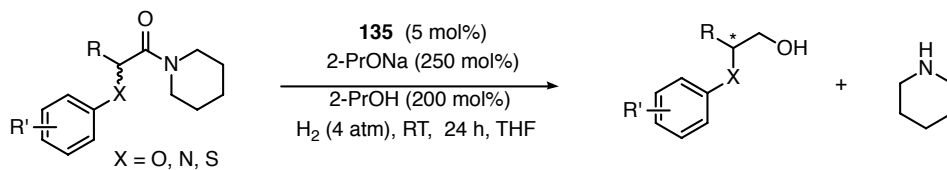
The opposite hand of dpen, (*S,S*)-, decreased both activity and *ee* of the catalyst (Table 1, entry 2). The highest *ee* with this substrate (58% *ee*, 45 hours, entry 5) was obtained with (*R,R*)-*trans*-1,2-diaminocyclohexane ((*R,R*)-DACH). The (*S,S*)-DACH was found to be less enantioselective (entry 6). The piperidine amide, *rac*-**134** was hydrogenated with 56% *ee* with the (*R,R*)-DACH catalyst, but in only 8.3% yield (21 hours, entry 7). The (*R,R*)-dpen catalyst **128** was more active towards **134**, giving 96% yield after 3.5 hours in comparable *ee* (44% *ee*, entry 8). With **128** as the catalyst, reducing the amount of KO^tBu from 10 to 1.1 equivalents reduced the yield (14%, 20 hours), but increased the *ee* to 88% (entry 9). This *ee* indicates that the kinetic selectivity of **128** between the enantiomers of **134** is high. The theoretical *ee* of the remaining **134** would be 6.6% in the opposite direction if racemization did not occur during this hydrogenation. The measured *ee* of isolated **134** was 5%, and in the opposite direction, confirming that racemization was relatively slow in the absence of excess KO^tBu. Satisfyingly, addition of 2-PrOH (100 equivalents) and KO^tBu (30 equivalents) enabled the dynamic kinetic resolution to occur with 20 equivalents of substrate in 93% *ee* and 89% yield (entry 10).

In the final improvement, the convenient, moderately air stable, pure dichloride precursor *trans*-RuCl₂((*S,S*)-skewphos)((*R,R*)-dpen) (**135**) was utilized with 2-PrONa as base (50 equivalents) in the presence of 2-PrOH (40 equivalents), to hydrogenate 20 equivalents of **134** under 4 atm H₂ to form 2-phenoxy-1-propanol in 87% yield and in 97% *ee* (Eq. 3.6).



The potassium alkoxide, 2-PrOK, is more difficult to prepare, and its use did not improve the performance of the hydrogenation compared to 2-PrONa under these conditions. Table 3.2 shows the amides that were hydrogenated under our optimized conditions. Most of the phenoxy amides were hydrogenated in yields that ranged from 87 to 99%. The *ee*'s of the product 2-aryloxy-1-propanols ranged from 95 to >99%.

Table 3.2: Enantioselective hydrogenation of functionalized racemic amides.^(a)



entry	structure of substrate	% yield ^(b)	% ee ^(c)
1		87	97 (<i>R</i>) ⁽ⁱ⁾
2		87 (92.6) ^(d)	96 (95) ^(d)
3		91.7	>99 (<i>R</i>) ⁽ⁱ⁾
4		94	>99
5		78.1	97

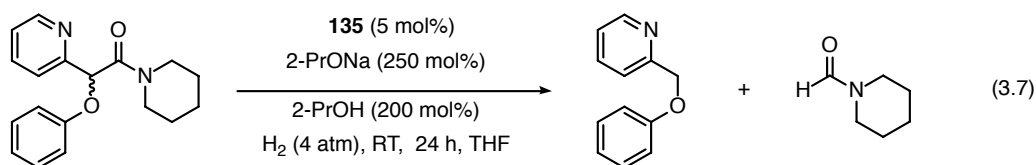
6		84	97
7		99 (95) ^(h)	96
8		93.5	90
9		91.7	84
10		60	95
11		66	46
12 ^(e)		47.5 (71, (69)) ^(f)	74 (72) ^(f)
13		100	---
14 ^(g)		16	74

(a) Reaction conditions (unless otherwise noted) **135**:2-PrONa:amide:2-PrOH 1:50:20:40, [amide] 0.6 M in THF. (b) Determined using ¹H NMR spectroscopy. (c) Determined using chiral GC-MS or HPLC. (d) **135**:2-PrONa:amide:2-PrOH 1:250:100:100, [amide] 0.6 M in THF, reaction carried at 50 atm H₂ pressure. (e) KO^tBu used as the base. (f) Reaction performed at 50 atm H₂ pressure at 0 °C, 69% yield with respect to internal standard. (g) **135**:KO^tBu:amide 1:5:20, reaction performed at 30 atm H₂ pressure. (h) Isolated yield by flash chromatography on silica gel. (i) [α]_D²² -29.3 @ 97% ee (c 1.87, CHCl₃); lit. [α]_D²⁰ -12.1 @ 40% ee

(c 1.0, CHCl₃).¹⁴⁹ (j) [α]_D²² -33.1 @ >99% *ee* (c 1.11, CHCl₃); lit. [α]_D²⁵ -35.1 @ >99% *ee* (c 1.0, CHCl₃).¹⁵⁴

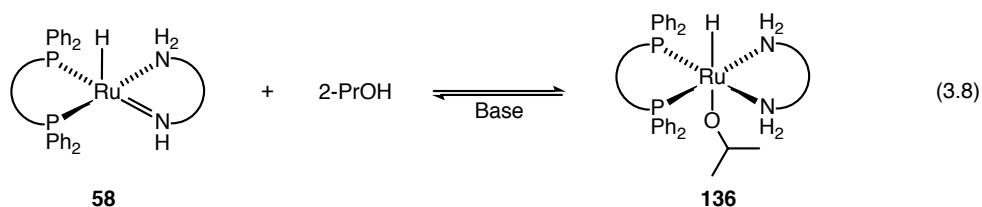
The reaction proceeded in high yield and *ee* with aromatic fluorides (entry 2), chlorides (entry 3), and even bromides (entry 4). There was little effect of steric crowding at the *para*-phenyl position on the reaction, as substitution of hydrogen (entry 1) by a *tert*-butyl group (entry 6) decreased the yield by only 3%, while the *ee* remained relatively unchanged. The methoxy amide (entry 5) was hydrogenated in low yield (78.1%) and in 97% *ee*, suggesting that electron-donating groups at the *para*-position partially hinder the reaction. Moving the fluoride from the *para* (entry 2) to the *meta*- position (entry 7) increased the yield from 87 to 99% with no change in *ee*. The (2-naphthoxy) amide (entry 8) reacted in comparable yield (93.5%) and *ee* (96%). The exchange of a methyl for a phenyl group alpha to the carbonyl (entry 9) did not significantly affect the yield (91.7%), but reduced the *ee* to 84%.

Replacing the methyl for an ethyl group (entry 10) reduced the yield (60%), but did not significantly affect the *ee* (95%). While replacing the phenoxy group for a methoxy group (entry 11) reduced both yield (66%) and *ee* (46%). 1-(*N*-phenylalanyl)-piperidine (entry 12) was hydrogenated to 2-anilino-1-propanol with 47.5% yield and 74% *ee*. This result demonstrates that the catalyst system can be used to prepare chiral β -amino alcohols. Chiral β -amino alcohols are important building blocks in the synthesis of chiral auxiliaries¹⁵⁵ and unnatural amino acids.¹⁵⁶⁻¹⁵⁹ To our surprise, exchanging the methyl with a 2-pyridyl group alpha to the carbonyl (entry 13) gave 1-formylpiperidine and 2-(phoxymethyl) pyridine (Eq. 3.7).

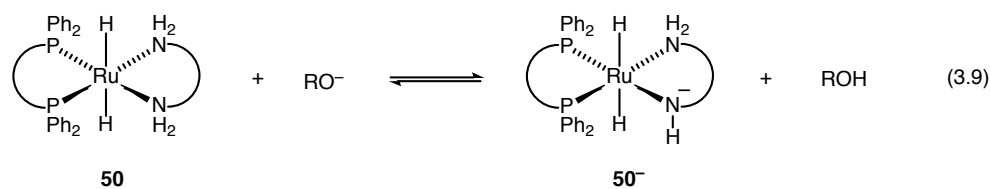


We recently reported a similar catalytic C–C cleavage reaction under these mild conditions.¹⁶⁰ Further research is required to investigate this phenomenon. 2-Phenylthio-1-(1-piperidinyl)-1-propanone (entry 14) was hydrogenated using 25 mol% of KO^tBu at room temperature under 30 atm H₂ to give the chiral β-thio alcohol in 16% yield and 74% *ee*.

The build up of secondary amine product may limit the turnover number of these reactions under these mild conditions. As well, the 2-PrOH and the buildup of primary alcohol product will also inhibit the catalyst. These alcohols will form secondary and primary Ru alkoxides by reaction with Ru amides such as **58**. This process is reversible in the presence of base (Eq. 3.8).⁸¹



We propose that 2-PrOH and product alcohols slow the hydrogenations by reducing the steady-state concentration of Ru-amides such as **58** during catalysis.⁸¹ We note that alkoxides such as **136** do not undergo net reactions with H₂, ketones, and nor do they hydrogenate ketones under mild conditions.¹⁶¹ A second potential mechanism in which 2-PrOH and the product alcohol may hinder the hydrogenation is by shifting the deprotonation equilibrium of **50** towards the dihydride (Eq. 3.9).



Although the basicity of both the RO^- and $\mathbf{50}^-$ would be affected by the presence of alcohol, Eq. 3.9 would still shift to the left with the increase in alcohol concentration that occurs as the hydrogenation proceeds. Both of these mechanisms predict that higher turnover numbers will be achieved if the pressure of H_2 is increased, which would increase the steady-state concentration of $\mathbf{50}$, but not significantly affect the *ee*.⁸³ Bergens and coworkers also showed that the hydrogenation of the ester, ethyl hexanoate is catalyzed by $\mathbf{50}$ at $-20\text{ }^\circ\text{C}$ under 4 atm H_2 in THF with KO^tBu , but slows as the concentration of *n*-hexanol builds up.⁸³ Therefore, we carried out the hydrogenation of 100 equivalents of 2-(4-fluorophenoxy)-1-(1-piperidiny)-1-propanone at 50 atm H_2 and, as predicted, the reaction proceeded in 92.6% yield in 95% *ee* (Table 2, entry 2, parenthesis). The product of this hydrogenation is an intermediate for a treatment of glaucoma in canines.^{162,163} The hydrogenation of 1-(*N*-phenyl-alanyl)-piperidine at 50 atm H_2 and $0\text{ }^\circ\text{C}$ increased the yield from 47.5 to 71% without significantly affecting the *ee* (Table 2, entry 12, parenthesis).

Figure 3.4 shows our proposed structure of the active catalyst $\mathbf{137}$ in the presence of 2-PrOH and 2-PrONa. This proposal is based upon our earlier observation that deprotonating one N-H group of the BINAP-dpen dihydride $\mathbf{50}$ substantially increased its activity towards amide reductions.⁸⁵ The mechanism(s) by which 2-PrOH increases the *ee* of these hydrogenations is not obvious.

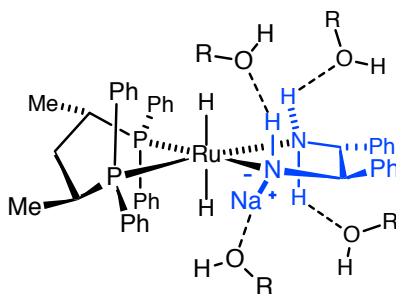


Figure 3.4: Proposed structure of the active catalyst **137** with possible interactions with 2-PrOH, primary alcohol products, etc. The skewphos is in the δ -skew configuration.

We recently published the solid-state structure of the dichloride **135** that contains (*S,S*)-skewphos in a chair conformation with one methyl group equatorially disposed, the other methyl group axial, and with the phenyl rings in a pseudo-achiral spatial disposition.^{160,164–166} (*S,S*)-Skewphos also adopts a C_2 -dissymmetric δ -skew conformation with both methyl groups in equatorial orientations and with the phenyl rings in a chiral spatial disposition.^{164–168} It is believed that the asymmetric induction of the skew conformation is higher than the chair. Skewphos adopts either the chair or skew conformation in Rh, Pd, and Pt compounds in the solid state,^{167,168} and the conformations of skewphos-Rh complexes are fluxional at room temperature in alcohol solutions.¹⁶⁷ Thus there is no obvious correlation between the conformation of (*S,S*)-skewphos in solid **135** and the active catalyst **137** in solution. One possible mechanism that 2-PrOH increases the *ee* of the amide hydrogenations, therefore, is by favoring the δ -skew conformation in **137**, thereby increasing the net asymmetric induction of the catalyst.

As discussed above, it is likely the active catalyst is the mono-deprotonated species **137**. Similar mono-deprotonated catalysts were first proposed by Chen

based upon rate studies of ketone hydrogenations.^{169,170} They were also investigated by computational studies on ketone hydrogenations.^{171,172} As well, there are many studies on the role of alcohols on the rate and selectivity of ketone bifunctional hydrogenations.¹⁷³⁻¹⁷⁵ Apart from our preliminary observations, we are aware of no detailed mechanistic studies on amide bifunctional hydrogenations. Figure 3.4 shows some of the hydrogen and ionic bonds that may form between 2-PrOH (R = 2-Pr) and the N-H or N⁻-Na⁺ groups in **137**. In principle, any of these interactions would influence the enantioselectivity of the hydrogenation. In principle, THF, *t*BuOH, the product alcohol, the various alkoxides present over the course of the amide reduction, and piperidine can engage in similar bonding with **137**. The system is complex, and a detailed study of the structure and reactivity of the putative intermediates would be required to unravel the stereochemical forces that lead to the major enantiomer of the product.

We note that the catalytic hydrogenation of the racemic ester *rac*-2-propyl 2-phenoxy-1-propanoate proceeded in 35% *ee*, confirming that the piperidine group in **134** does not undergo significant exchange with 2-propoxide during hydrogenation. Interestingly, the hydrogenation of the racemic aldehyde 2-phenoxypropanal produced 2-phenoxy-1-propanol after only 30 min, but in 9% *ee*. This low *ee* indicates that the aldehyde is either not an intermediate in the hydrogenation of the parent amide **134**, or that if it forms, it does not epimerize before it is reduced to the alcohol product.

Conclusion

In this chapter I have shown how high throughput screening and optimization reactions were used to discover the first asymmetric catalytic system for the hydrogenation of amides via DKR. The combination of the mechanistic observation that deprotonation of the N–H bonds in these bifunctional catalysts increases their reducing power, along with rapid screening and optimization lead to remarkably high *ee*'s for hydrogenation of a variety of functionalized amides via DKR under mild conditions. High *ee*'s are obtained by the addition of 2-PrOH. It is probable that 2-PrOH bonds to the diastereomeric transition states of the enantioselective step, favoring one pathway over the other. Further studies are required to investigate these mechanistic inferences and the origins of enantioselection.

Materials and methods

The rapid screening hydrogenation reactions were carried out in a 96-well plate (96 separate glass vials, each equipped with a magnetic stir bar) sealed within a brass reactor block at Center for Catalysis Research and Innovation (CCRI), Ottawa. All of the individual large-scale pressurized reactions were carried out in a stainless steel pressure reactor equipped with a magnetic stir bar at University of Alberta. The solvents tetrahydrofuran (Na/benzophenone), 2-propanol (Mg), methylene chloride (CaH₂) and hexanes (CaH₂) were dried by distillation from the appropriate drying agent under argon or N₂. Argon or N₂ was bubbled through all solvents for a minimum of 45 min before their use. The 2-bromopropanoic acid, 4-fluorophenol, 4-chlorophenol, 4-bromophenol, 4-methoxyphenol, and 2-phenoxypropionyl chloride

were all obtained from Alfa Aesar. The 3-fluorophenol and α -bromophenylacetic acid were obtained from TCI. The piperidine, 2,5-norbornadiene, morpholine, potassium *tert*-butoxide, and diisobutylaluminum hydride (1.0 M in toluene) were all obtained from Sigma-Aldrich. The thionyl chloride was obtained from Fluka, the sodium hydride from BDH, and the phenol from EM Science. LiAlH_4 was obtained from Anachemia. The liquid reagents were distilled before use. Table 3.3–3.5 lists the suppliers of the ligands used in this study. The ^1H NMR spectra were acquired using both 400 MHz and 500 MHz Varian Inova, and Varian DD2 M2 400 MHz NMR spectrometers. The ^{13}C NMR spectra were acquired using a Varian VNMRS 500 MHz NMR spectrometer. The chemical shifts are reported in parts per million relatives to TMS with the deuterated solvent as the internal standard. Abbreviations used in reporting of NMR data are s (singlet), d (doublet), t (triplet), q (quartet), dd (doublet of doublet), dq (doublet of quartet) and m (multiplet). Elemental Analysis data was acquired with a Carlo Erba EA1108 Elemental Analyzer. Optical rotation data was acquired at 591 nm with a Perkin Elmer 241 Polarimeter. HRMS spectra were acquired using either electrospray ionization in an Agilent 6220 ao TOF mass spectrometer or electron ionization on a Kratos Analytical MS50G double focusing sector mass spectrometer. GC-MS analysis was performed by using a Hewlett Packard 5890 chromatograph equipped with a 5970B mass selective detector and Supelco Beta DEX 225 capillary column (30 m \times 0.25 mm \times 0.25 μm film thickness). HPLC analysis was performed using a Waters 600E multi-solvent delivery system equipped with Waters 715 ultra WISP sample processor, Waters temperature control system, Waters 990 photodiode array detector, and a Daicel CHIRALPAK IB

(4.6 mm i.d. x 250 mm) chiral column. All of the *ee*'s were confirmed by comparing retention times and mass spectra or UV-Vis data to authentic racemic samples prepared separately.

Table 3.3–3.5: Sources, CAS number, and vial numbers for the ligands used in the rapid screening. Figures 3.19–3.22 show the structures of these ligands.

Vial	CAS	Supplier	Vial	CAS	Supplier	Vial	CAS	Supplier
A1			B1	71042-55-2	Strem	C1	96183-46-9	Strem
A2	256390-47-3	Strem	B2	610304-81-9	Strem	C2		
A3	505092-86-4	Strem	B3	503538-69-0	Strem	C3	184095-69-0	Solvias
A4			B4	866081-62-1	Strem	C4	360048-63-1	Solvias
A5	55739-58-7	Strem	B5			C5	292638-88-1	Solvias
A6	729572-46-7	Strem	B6	133545-24-1	Strem	C6	166172-63-0	Solvias
A7			B7	868851-47-2	Strem	C7	158923-11-6	Solvias
A8	917377-74-3	Strem	B8	1020670-88-5	Strem	C8	155830-69-6	Solvias
A9	917377-75-4	Strem	B9	244261-66-3	Strem	C9	167416-28-6	Solvias
A10	149968-36-5	Strem	B10	145214-57-9	Strem	C10	387868-06-6	Solvias
A11	255897-36-0	Strem	B11	192463-40-4	Strem	C11		
A12	37002-48-5	Strem	B12	261733-18-0	Strem	C12	77876-39-2	Strem

Vial	CAS	Supplier	Vial	CAS	Supplier	Vial	CAS	Supplier
D1	6737-42-4	TCI	E1	50777-76-9	Strem	F1	10150-27-3	Strem
D2			E2			F2	1493790-73-0	Strem
D3	13991-08-7	Strem	E3	452304-59-5	Strem	F3		Strem
D4	99646-28-3	Strem	E4	164858-78-0	Strem	F4	500103-26-4	Strem
D5	76858-94-1	Strem	E5	1237588-12-3	Strem	F5	736158-72-8	Strem
D6	137219-86-4	Strem	E6			F6	1150113-66-8	Strem
D7	76189-55-4	Strem	E7	422509-53-3	Strem	F7	174758-63-5	Strem
D8	64896-28-2	Strem	E8			F8	208248-67-3	Strem
D9	443150-11-6	Strem	E9	799297-44-2	Strem	F9		
D10			E10	192057-60-6	Strem	F10	494227-35-9	Solvias
D11	2622-14-2	Aldrich	E11	960128-64-7	Strem	F11		
D12	1259-35-4	Aldrich	E12	1091606-68-6	Strem	F12		Strem

Vial	CAS	Supplier	Vial	CAS	Supplier	Vial	CAS	Supplier
G1	1086138-36-4	Strem	H1					
G2	338800-13-8	Strem	H2	849923-88-2	Solvias			
G3	550373-32-5	Strem	H3	SL-J010-1	Solvias			
G4	851870-89-8	Strem	H4	494227-30-4	Solvias			

G5	1133149-41-3	Strem						
G6	1101230-28-7	Strem						
G7	1003012-96-1	Solvias						
G8	1357562-70-9	Strem						
G9	PNNP (J1)							
G10	PNNP (J2)							
G11	PP 1 (OP)							
G12	PP 2 ((<i>rac</i>)-ONP*)							

General procedure for DKR screening

Between 1.0 and 3.5 mg (2.4–6.2 μmol) of the P, P–P, P–N, P–N–P, and P–N–N–P ligands were weighed into separate wells (vials) of a 96-well plate inside a glove box (Refer the Table 3.3–3.5 and Figures 3.19–3.22 for ligand information). A standard solution of (*R,R*)-dpen in THF (50.6 mg in 5.00 mL of THF, 0.047 mol L⁻¹) was then added to the vials containing the monophosphines (0.5 equivalent of dpen per P) and the diphosphines (1 equivalent of dpen per P–P). Then a standard solution of the catalyst precursor **117** (0.12 mol L⁻¹, 250.6 mg of **117** in 0.20 mL of CH₂Cl₂ and 4.80 mL of THF) was added to each vial (0.5 equivalent per P or P–N ligands; and 1 equivalent for all the other ligands). The resulting solutions in the 96-well plate were covered, heated at 60 °C for 30 min under N₂, and then allowed to cool to room temperature. Five equivalents of KO^tBu in THF (268.3 mg dissolved in 4.00 mL of THF, 0.6 mol L⁻¹) and 10 equivalents of the amide substrate *rac*-**56** in THF (908.5 mg dissolved in 24.00 mL THF, 0.12 mol L⁻¹) were added to each vial. Finally, the appropriate volume of THF was added to each vial to bring the total volume to be 400 μL . All the standard solutions and THF were added using the Freeslate first-generation core module. The 96-well plate was encased in brass reactor block,

removed from the glove box, and then purged 3 × by evacuating and backfilling with hydrogen. The hydrogenation reactions were carried out under 4 atm H₂ for 4 hours at room temperature while being shaken. The hydrogenation was halted by depressurizing the reactor and exposing the wells to open air.

The reaction products were then analyzed with Agilent HPLC 1100 system equipped with DAD detector and a Daicel CHIRALPAK 1B chiral column (4.6 mm i.d. × 250 mm), solvent 2-PrOH:hexane of 2:98, flow rate 0.8 mL/min, temperature 30 °C. The retention times and UV-Vis spectra of the products were confirmed by comparison to those of authentic samples prepared independently (Figure 3.5).

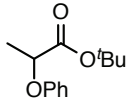
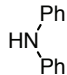
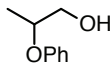
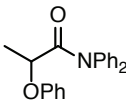
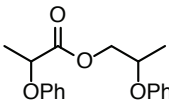
					
Average t_R in minutes	$t_R = 5.05$	$t_R = 9.99$	$t_{R1} = 17.41$ $t_{R2} = 23.92$	$t_{R1} = 18.51$ $t_{R2} = 36.16$	$t_{R1} = 8.27$ $t_{R2} = 8.27$ $t_{R3} = 25.88$ $t_{R4} = 44.20$

Figure 3.5: HPLC retention times of the reactants and products. Retention times are averaged over the chromatograms from the wells.

GC-MS analysis was performed on the products in well D7 ((*R*)-BINAP/((*R,R*)-dppe)-Ru system) to confirm the identities of diphenylamine, *tert*-butyl 2-phenoxypropanoate, and 2-phenoxypropyl 2-phenoxypropanoate. GC-MS analysis was performed by using Agilent GC 6890N coupled to Agilent 5975B MS in EI mode and to CTC GC-PAL autosampler and Agilent HP-5MS ((5% phenyl)-methylpolysiloxane) capillary column, (30 m × 250 μm × 0.25 μm film thickness, He 1.8 mL/min, temperature program of ([60 °C held for 3 min]–[20 °C/min to 175 °C

held for 0.25 min]–[25 °C/min to 275 °C held for 0.50 min]–[35 °C/min to 300 °C held for 1.0 min]).

Representative UV-Vis spectra of peaks in the HPLC chromatograms from the hydrogenation wells and of control, authentic samples

Figure 3.6: UV-Vis spectrum of authentic sample, tert-butyl 2-phenoxypropanoate, **127**, (left) vs. product mixture from rapid screening (right). The enantiomers of this compound did not separate under these conditions.

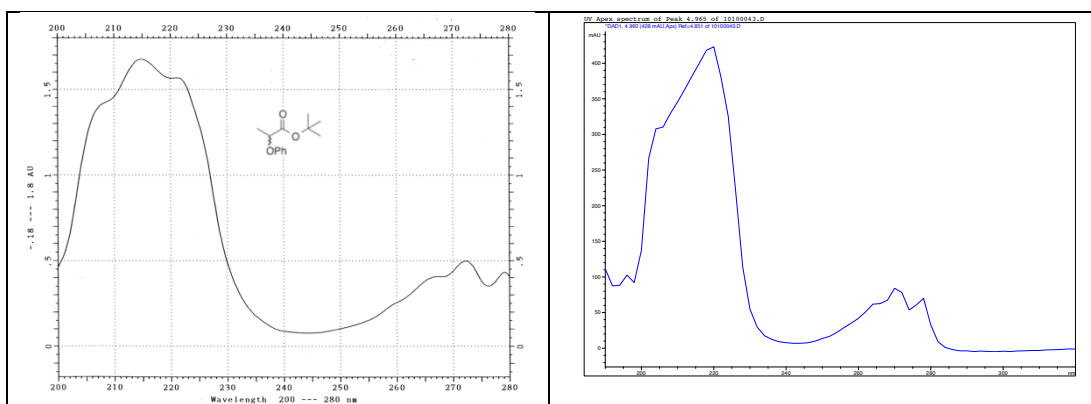


Figure 3.7: UV-Vis spectrum of authentic sample, diphenylamine (left) vs. product mixture from rapid screening (right).

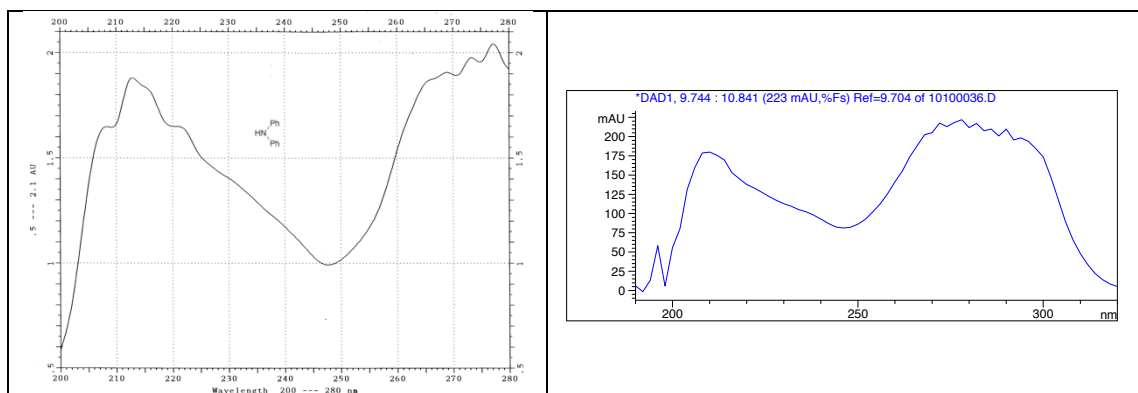


Figure 3.8: UV-Vis spectrum of authentic sample, *rac*-2-phenoxypropan-1-ol, both enantiomers separated (left) vs. product mixture from rapid screening (right).

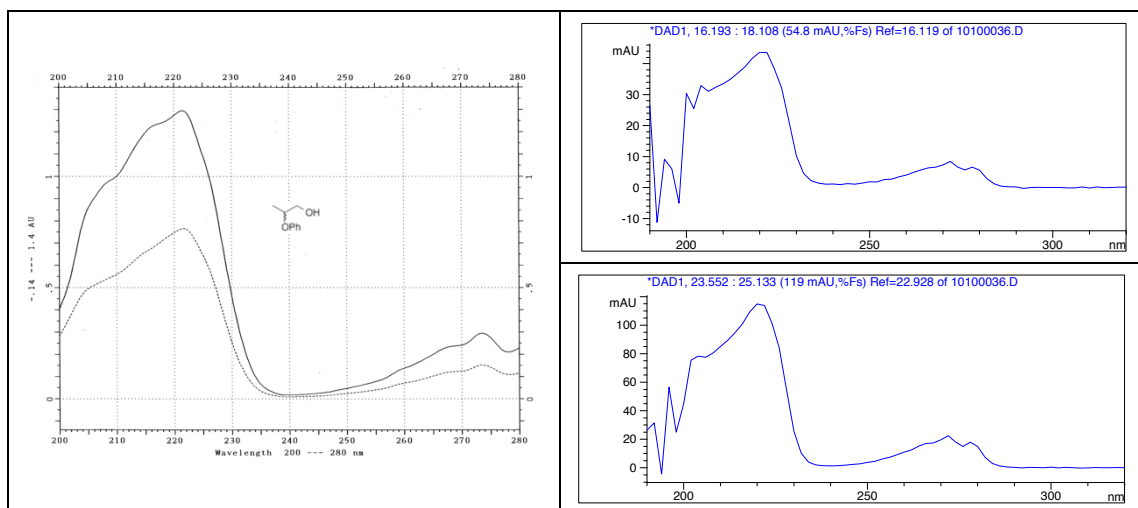


Figure 3.9: UV-Vis spectrum of authentic sample, *N,N*-diphenyl-2-phenoxypropionamide (left) vs. product mixture from rapid screening (right).

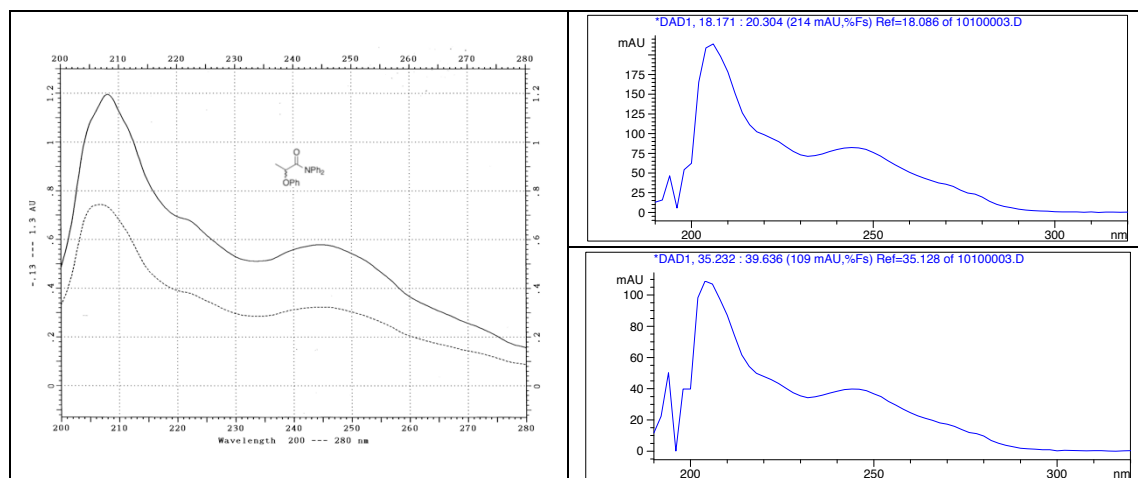


Figure 3.10: UV-Vis spectrum obtained from the authentic sample of 2-phenoxypropyl 2-phenoxypropanoate, showing three separated diastereomers.

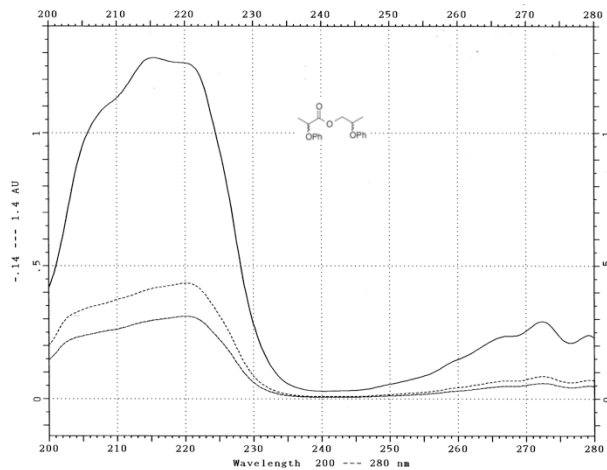


Figure 3.11: Representative UV-Vis spectrum of 2-phenoxypropyl 2-phenoxypropanoate from the rapid screening product mixture.

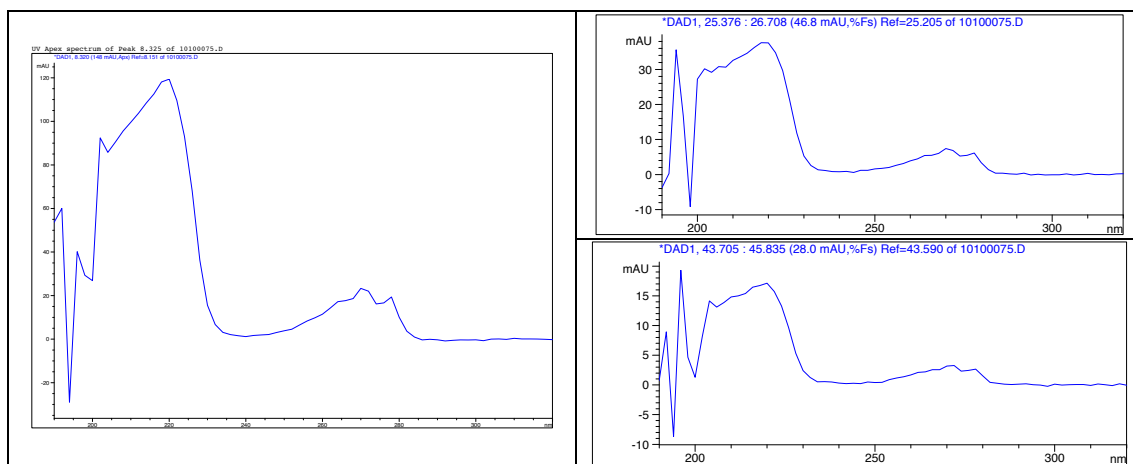


Figure 3.12: Gas chromatogram of the rapid screening hydrogenation product mixture from the reaction well D7.

File :C:\msdchem\1\DATA\Roxanne\1000D7.D
Operator :
Acquired : 17 Jun 2013 13:01 using AcqMethod RJune2013.M
Instrument : Instrument #1
Sample Name :
Misc Info :
Vial Number: 29

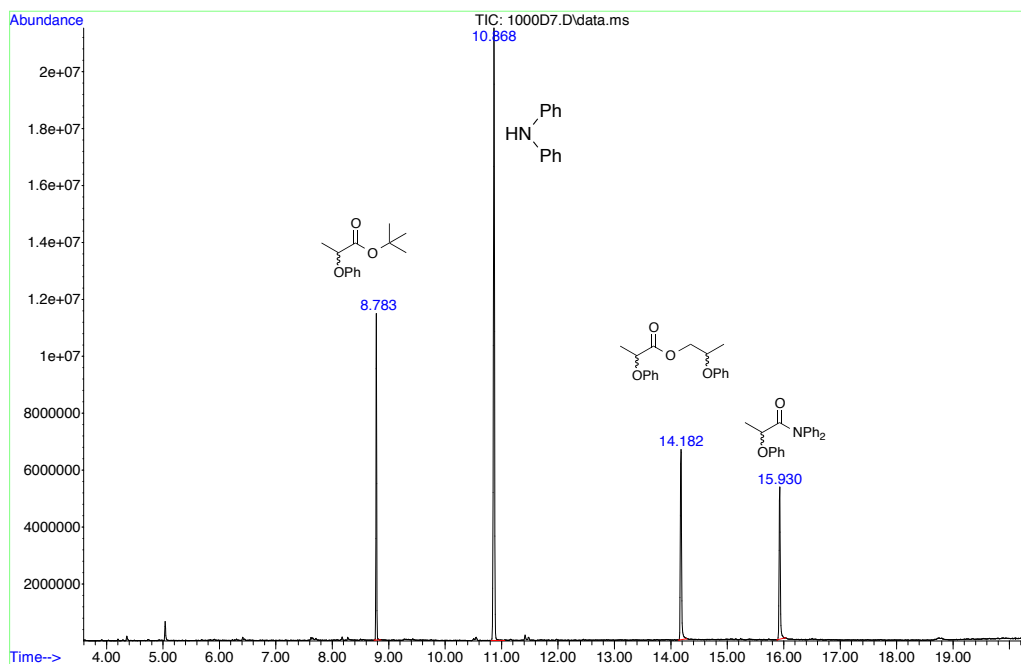


Figure 3.13: Mass spectrum for the peak at 8.794 minutes showing the presence of *tert*-butyl 2-phenoxypropanoate in the reaction product mixture.

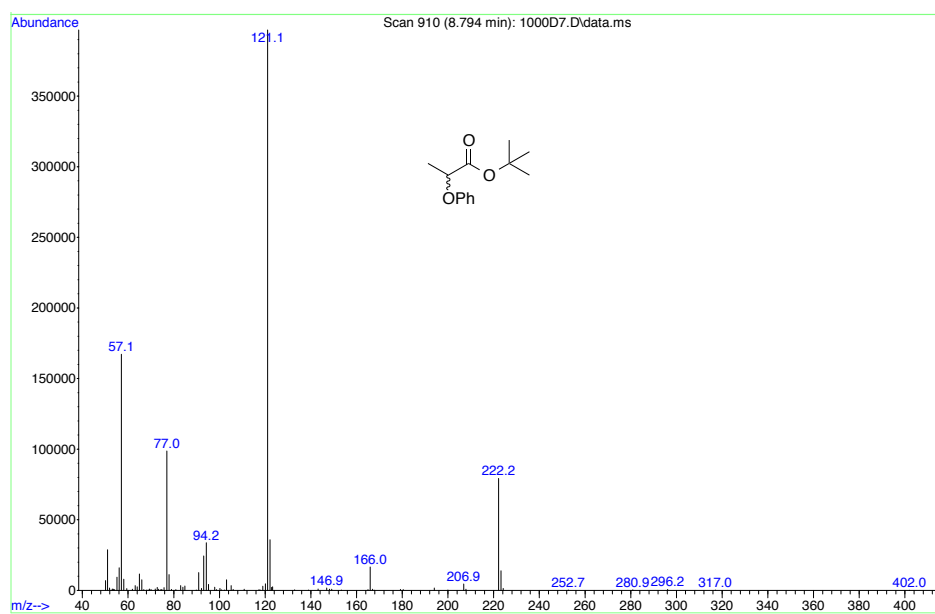
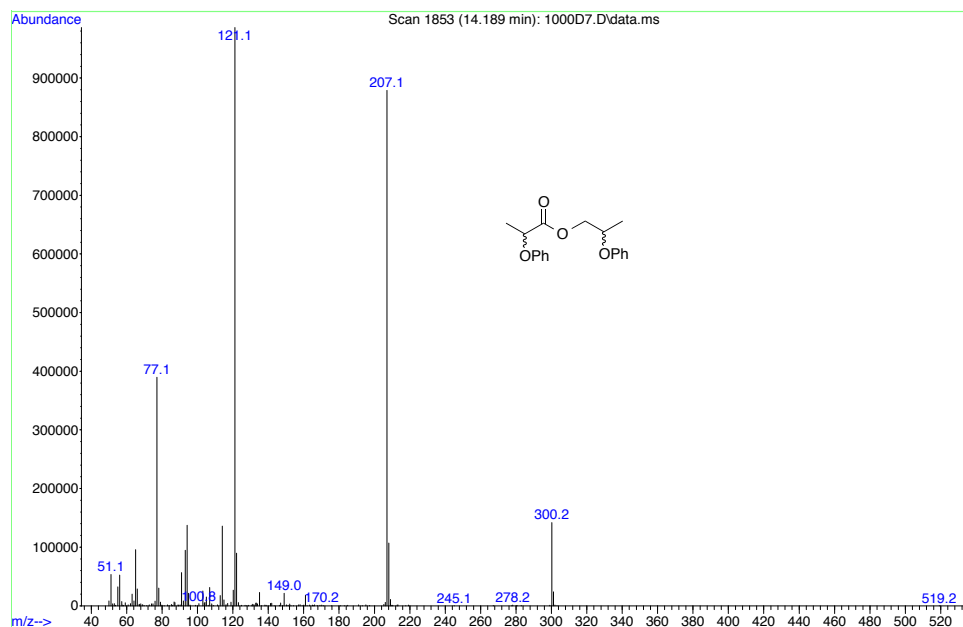


Figure 3.14: Mass spectrum for the peak at 14.189 minutes showing the presence of 2-phenoxypropyl 2-phenoxypropanoate in the reaction product mixture.



Representative HPLC chromatograms of product wells from the rapid screening

Figure 3.15: Representative chromatogram of well A2 for Category I ((R,R)-dpen and (R)-3,4,5-MeO-MeOBIPHEP).

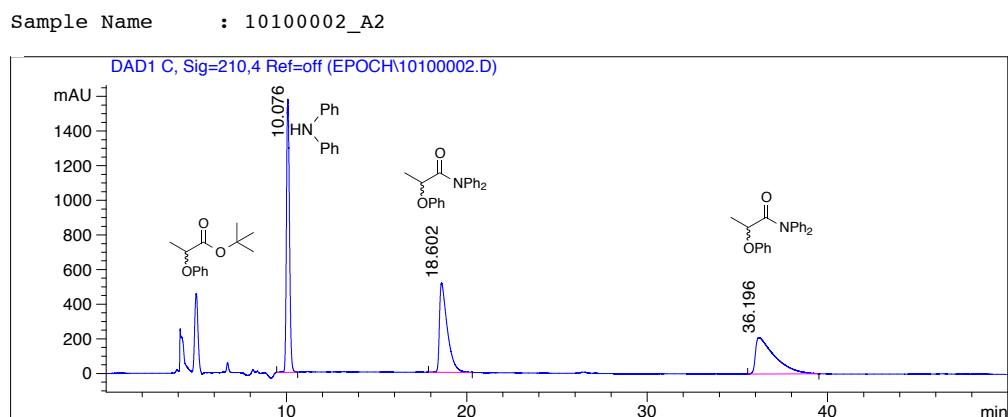


Figure 3.16: Representative chromatogram of well D7 for Category II ((*R,R*)-*dpen* and (*R*)-*BINAP*).

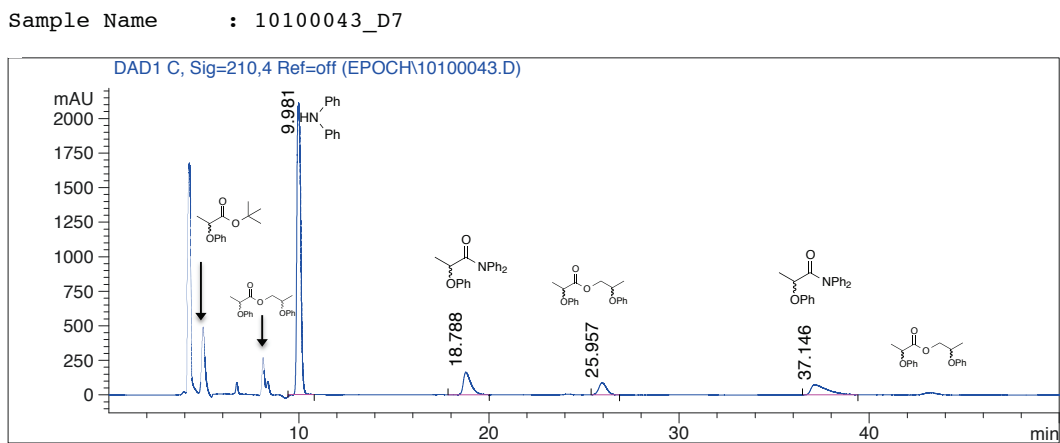


Figure 3.17: Representative chromatogram of well G3 for Category III (Bis[2-(dicyclohexylphosphino)ethyl]amine).

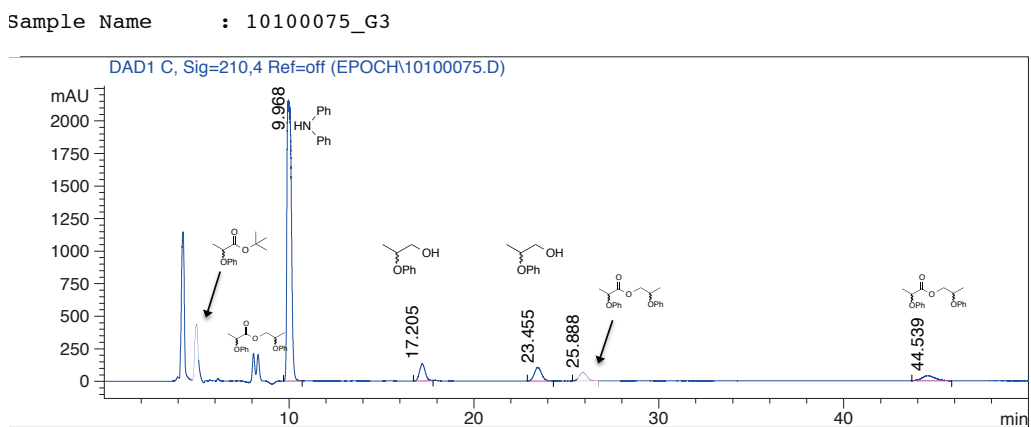
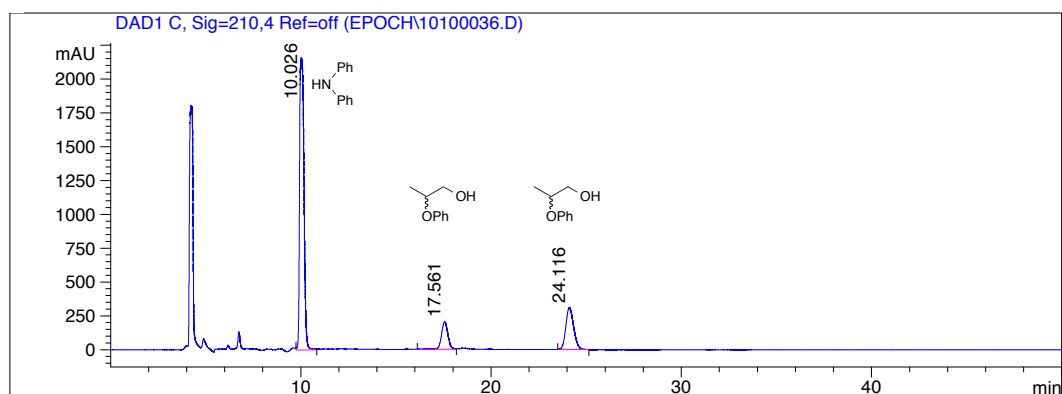


Figure 3.18: Representative chromatogram of well C12 for Category IV ((*R,R*)-*dpen* and (*S,S*)-*BDPP*).

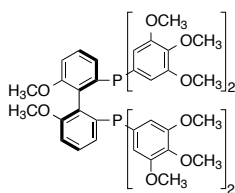
Sample Name : 10100036_C12



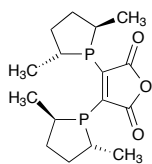
Categorization of ligands based upon their activity in the rapid screening

- I. Ligands showing little or no activity for the hydrogenation (38 ligands).*
 - II. Those with moderate to low amounts of starting materials remaining (12 ligands).*
 - III. No starting materials remaining but varying amounts of products and side products (7 ligands).*
 - IV. Complete conversion to diphenylamine and 2-phenoxy-1-propanol (17 ligands).*
-

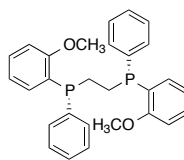
Figure 3.19: Structures of the ligands in category I



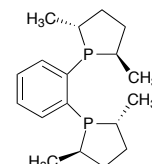
A2, CAS #: 256390-47-3



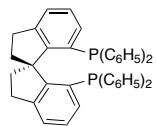
A3, CAS #: 505092-86-4



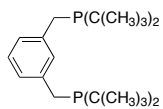
A5, CAS #: 55739-58-7



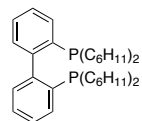
A7, CAS #: 147253-67-6



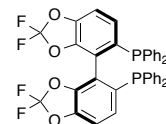
A8, CAS #: 917377-74-3



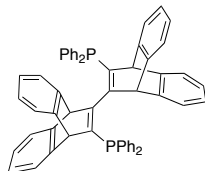
A10, CAS #: 149968-36-5



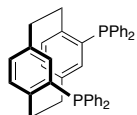
A11, CAS #: 255897-36-0



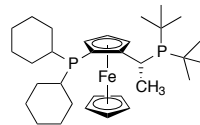
B3, CAS #: 503538-69-0



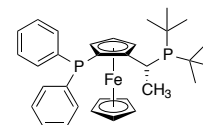
B8, CAS #: 1020670-88-5



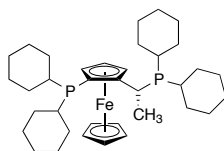
B11, CAS #: 192463-40-4



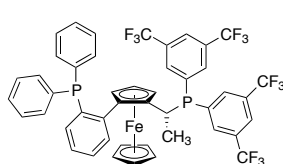
C7, CAS #: 158923-11-6
SL-J009-1



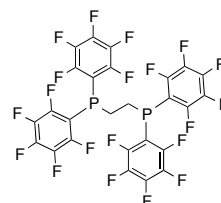
C8, CAS #: 155830-69-6
SL-J002-1



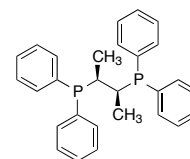
C9, CAS #: 167416-28-6
SL-J003-1



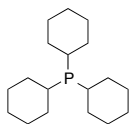
C10, CAS #: 387868-06-6
SL-W001-1



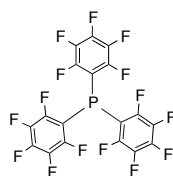
D5, CAS #: 76858-94-1



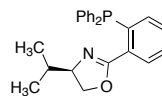
D8, CAS #: 64896-28-2



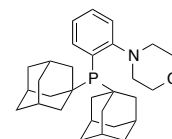
D11, CAS #: 2622-14-2



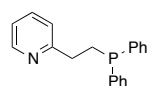
D12, CAS #: 1259-35-4



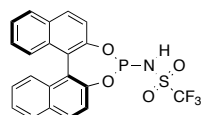
E4, CAS #: 164858-78-0



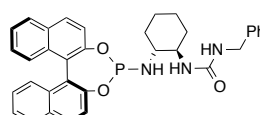
E5, CAS #: 1237588-12-3



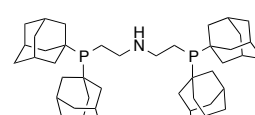
F1, CAS #: 10150-27-3



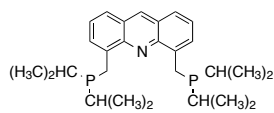
F2, CAS #: 1493790-73-0



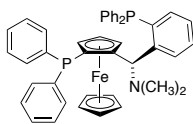
F12, CAS #: -----
15-2208 (Strem Chemicals)



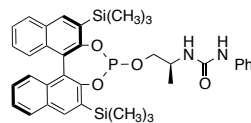
G1, CAS #: 1086138-36-4



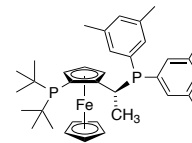
G6, CAS #: 1101230-28-7



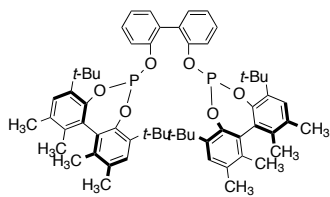
G7, CAS #: 1003012-96-1
SL-T001-1



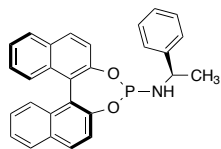
G8, CAS #: 1357562-70-9



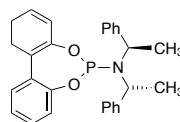
H3, CAS #:
SL-J010-1



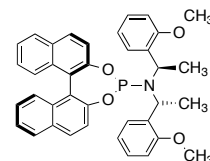
A6, CAS #: 729572-46-7



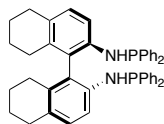
E7, CAS #: 422509-53-3



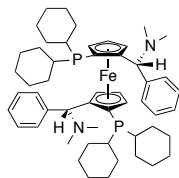
F4, CAS #: 500103-26-4



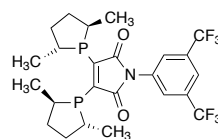
F5, CAS #: 736158-72-8



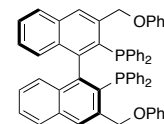
F8, CAS #: 208248-67-3



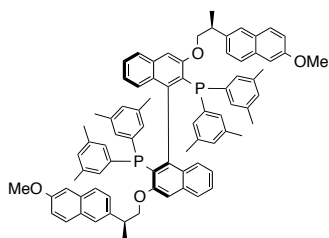
F10, CAS #: 494227-35-9
SL-M002-1



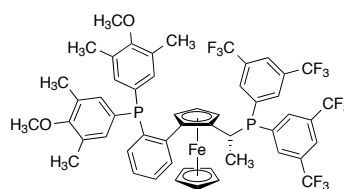
G5, CAS #: 1133149-41-3



G11, CAS #: XXX



G12, CAS #: XXX



H4, CAS #: 494227-30-4
SL-W005-1

Figure 3.20: Structures of the ligands in category II

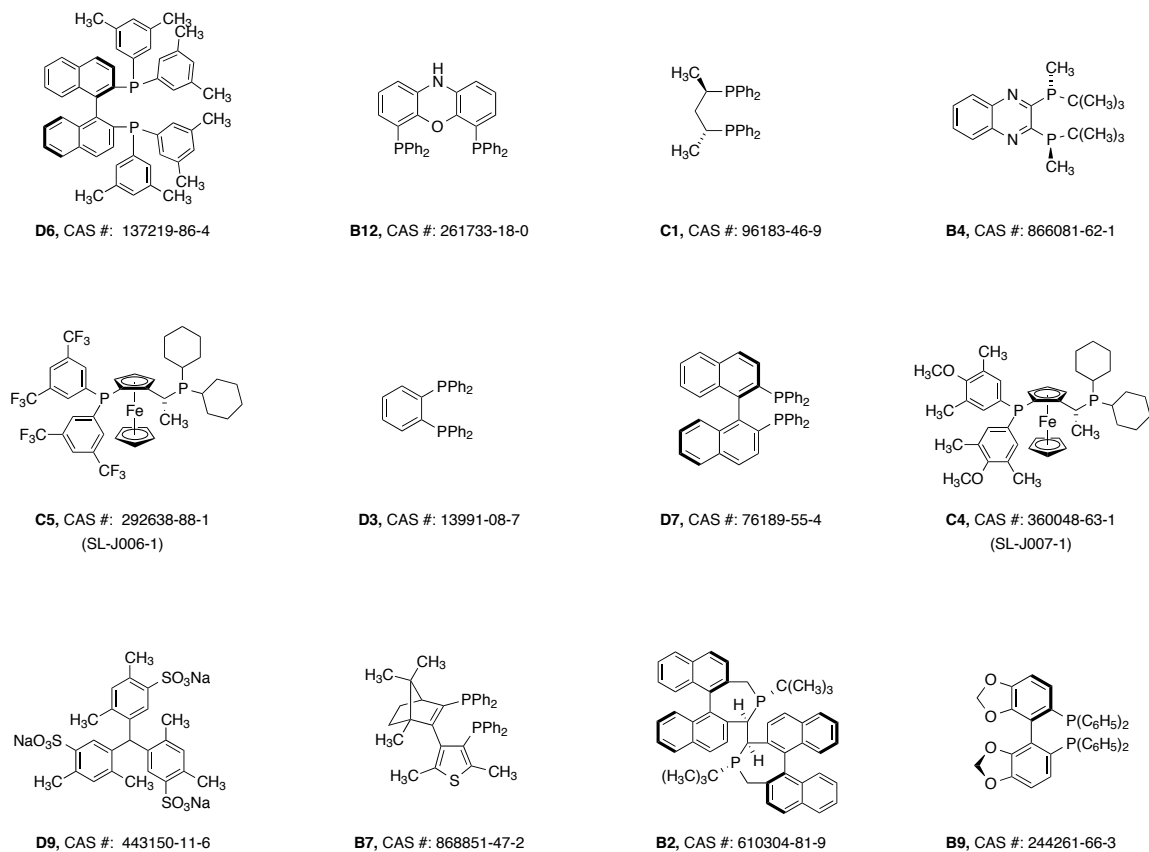


Figure 3.21: Structures of the ligands in category III

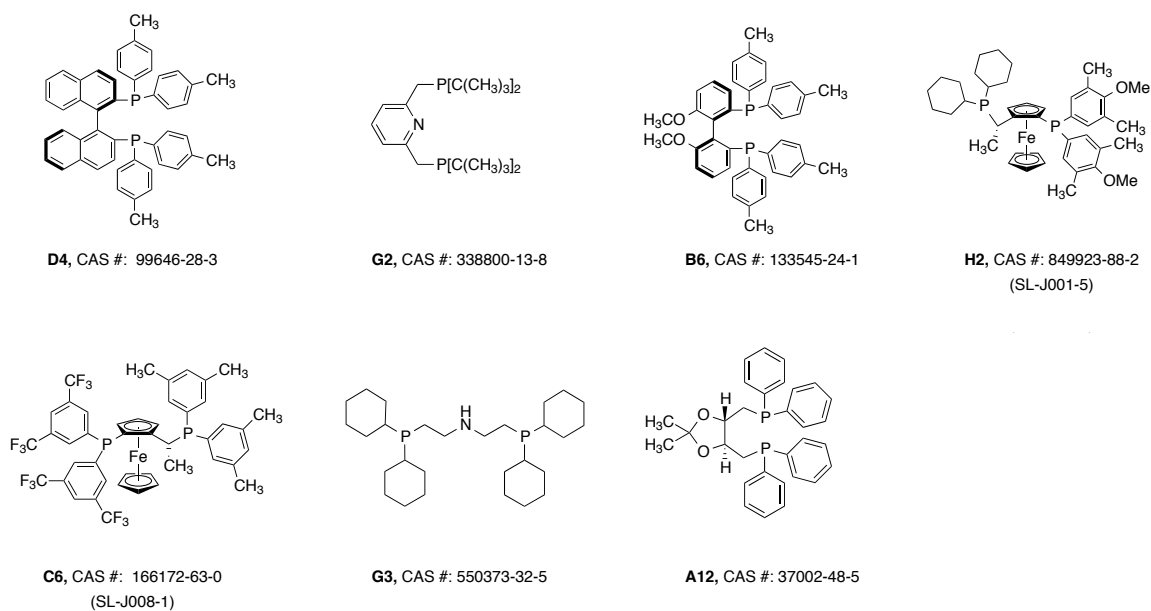
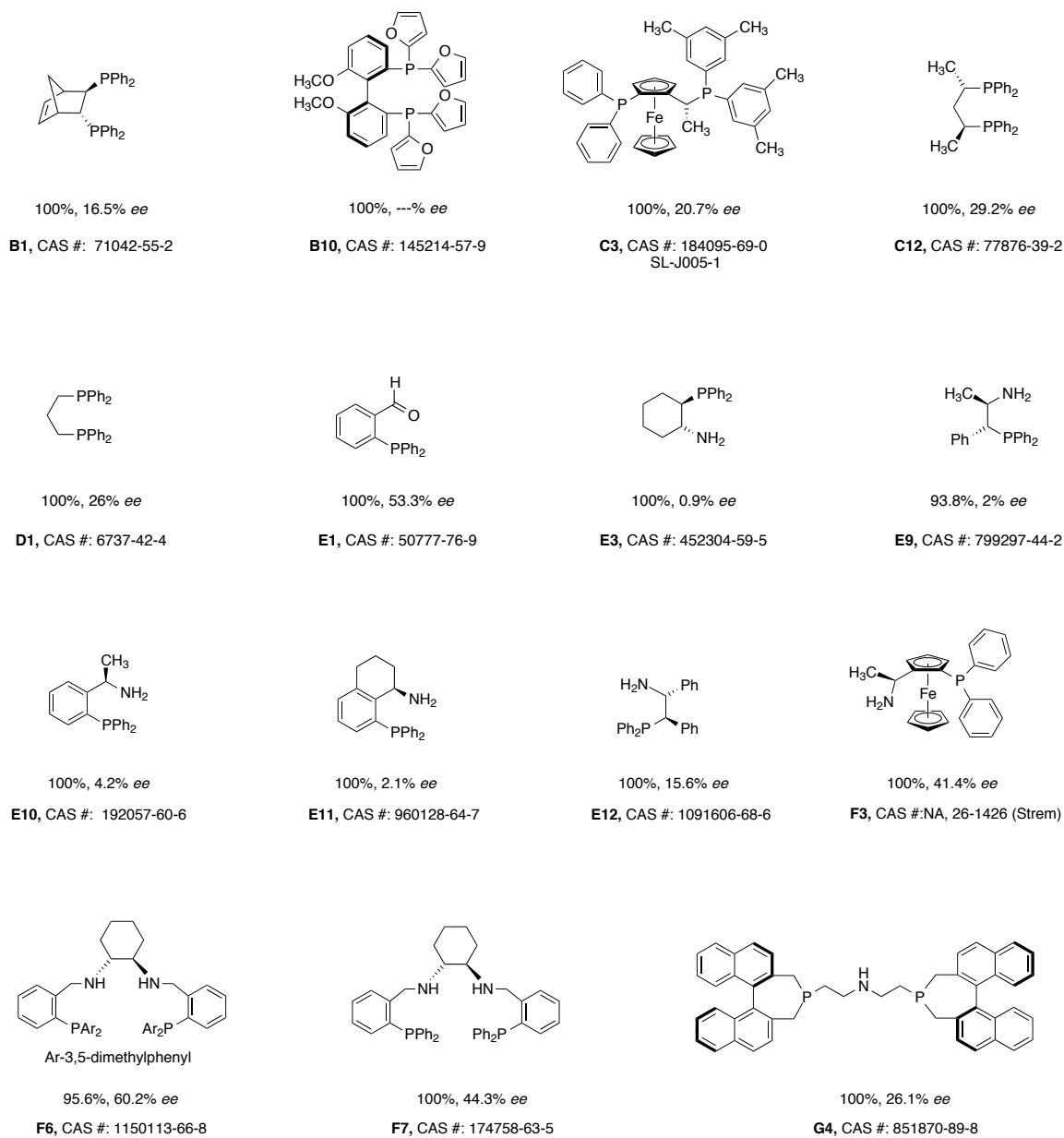
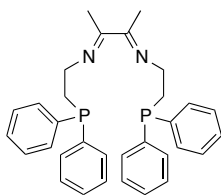


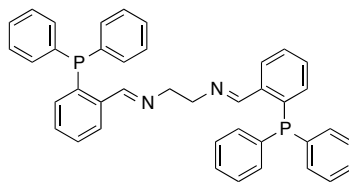
Figure 3.22: Structures of the ligands and *ee*'s for the hydrogenations of *rac*-56 in category IV.





100%, 0% *ee*

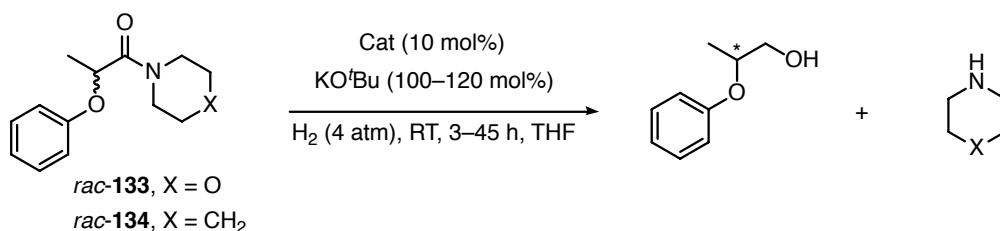
G9, CAS #: 36525-09-4



100%, 0.2% *ee*

G10, CAS #: 74684-87-0

Optimization experiments



General procedure for *in situ* catalyst preparation in lab-scale hydrogenations

[Ru($\eta^3\text{-C}_3\text{H}_5$)(COD)(MeCN)₂] BF_4 (**117**, 12.6 mg, 30 μmol), (*S,S*)-skewphos (13.2 mg, 30 μmol), (*R,R*)-dpen (6.4 mg, 30 μmol), and KO^tBu (40.4 mg, 360 μmol , 12 equivalents) were weighed into 4 separate NMR tubes inside a glove box. Freshly distilled THF was cannulated into the NMR tubes containing phosphine, diamine ligands (0.3 mL each), and the base (0.4 mL) under argon pressure. The THF solution of phosphine was then cannulated into the NMR tube containing the ruthenium precursor **117** under H₂ pressure, followed by the THF solution of the diamine. The resulting solution was allowed to react at 60 °C for 30 min with occasional shaking (at least five times during the heating process). During this time a clear, dark yellow solution formed. After 30 min, the THF solution of KO^tBu was

cannulated into the dark yellow solution under H₂ pressure. The mixture turned red in color and was then used for the subsequent hydrogenation.

General procedure for lab-scale hydrogenation (Table 3.1)

Solid amide, rac-2-phenoxy-1-(morpholine)-1-propanone (rac-133)

The amide (70.6 mg, 300 μmol, 10 equivalents) was added to the stainless steel autoclave equipped with a stir bar and purged with H₂ for 15–20 min. The prepared catalyst was then transferred to the autoclave under H₂ pressure using a cannula followed by 4.0 mL of freshly distilled THF wash. The autoclave was then sealed and pressurized to 4 atm H₂. The reaction mixture was stirred at room temperature for 3 to 45 hours. The reaction was stopped by depressurizing the autoclave and opening it to air. The catalyst was removed by passing the solution through a florisil plug using CH₂Cl₂ as the rinse solvent. The solvent was then removed under reduced pressure using a rotary evaporator. The reaction products were analyzed using NMR and GC-MS or HPLC.

Liquid amide, rac-2-phenoxy-1-(piperidine)-1-propanone (rac-134)

The stainless steel autoclave was purged with H₂ for 10 min. The amide (69.9 mg, 300 μmol, 10 equivalents) in freshly distilled THF (1.0 mL) was cannulated into the autoclave and purged with H₂ for another 10 min. The prepared catalyst was then transferred to the autoclave under H₂ pressure using a cannula followed by 3.0 mL of freshly distilled THF wash. The autoclave was then sealed and pressurized to 4 atm H₂. The reaction mixture was stirred at room temperature for 3.5–21 hours. The

reaction was stopped by depressurizing the autoclave and opening it to air. The catalyst was removed by passing the solution through a florisil plug using CH₂Cl₂ as the rinse solvent. The solvent was then removed under reduced pressure using a rotary evaporator. The reaction products were analyzed using NMR and GC-MS or HPLC.

Hydrogenation of rac-134 with low concentration of base (Table 3.1, entry 9)

The reaction was scaled up and performed by following the general procedure; **117** (25.2 mg, 60 μmol), (*S,S*)-skewphos (26.3 mg, 60 μmol), (*R,R*)-dpen (12.6 mg, 60 μmol), and KO^tBu (7.4 mg, 66 μmol, 1.1 equivalents) and *rac*-**134** (143 mg, 600 μmol, 10 equivalents). After 20 hours, the reaction was stopped by depressurizing the autoclave and opening it to air. The ¹H NMR spectrum (CDCl₃) was recorded by taking an aliquot from the reaction mixture (14% conversion by NMR).

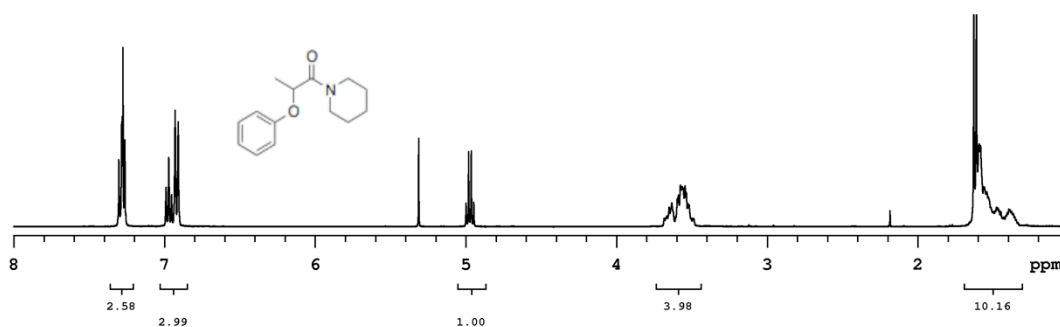
Separation of unreacted starting material from the hydrogenation of rac-134

The reaction mixture was passed through a florisil plug using CH₂Cl₂ (50 mL) as the rinse solvent. The solvent was then removed under reduced pressure using a rotary evaporator to give a reddish oily crude product. The crude product was purified by flash chromatography on a silica column with a 3:1 mixture of hexane:ethyl acetate eluent (R_f 0.12). The enantiomers of unreacted **134** were not separated by GC. The amide **134** was therefore reduced to the product alcohol, 2-phenoxypropan-1-ol by LiAlH₄ as follows to determine the *ee*.

Reduction of isolated amide **134** with LiAlH₄

LiAlH₄ (90 mg, 0.8 mmol, 3.1 equivalents) was weighed into a side arm flask inside a glove box. Freshly distilled THF (5 mL) was added to the flask under an N₂ atmosphere and cooled to 0 °C using an ice bath. The isolated substrate **134** (60 mg, 0.26 mmol) in THF (5 mL) was then cannulated into the flask containing LiAlH₄-THF. The resulting solution was allowed to warm to room temperature and stir overnight. After 16 hours, 2 mL of reaction mixture was transferred to another side arm flask. The reaction mixture was quenched with slow addition of water and stirred for 30 min under N₂ atmosphere. The resulting mixture was passed through a celite bed using CH₂Cl₂ (50 mL) as the eluent. The organic solvent was evaporated under reduced pressure to give the alcohol 2-phenoxypropan-1-ol. The resulting product was analyzed by both ¹H NMR and GC-MS.

Figure 3.23: The δ region from 8 to 1 ppm (top) corresponds to **134**. The δ region from 10 to 1 ppm (bottom) showing major products obtained from the reduction of isolated **134** by LiAlH₄ (Table 3.1, entry 9). Alcohol product denoted by (*), **134** denoted by (♦), Residual solvent denoted by (δ), aldehyde product denoted by (α)



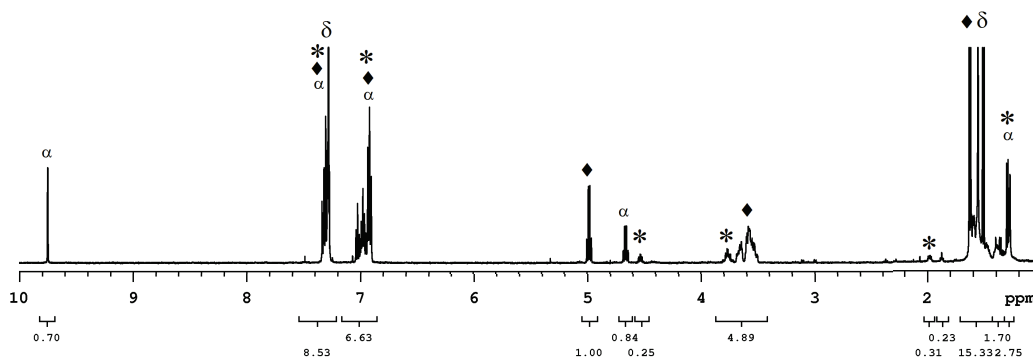
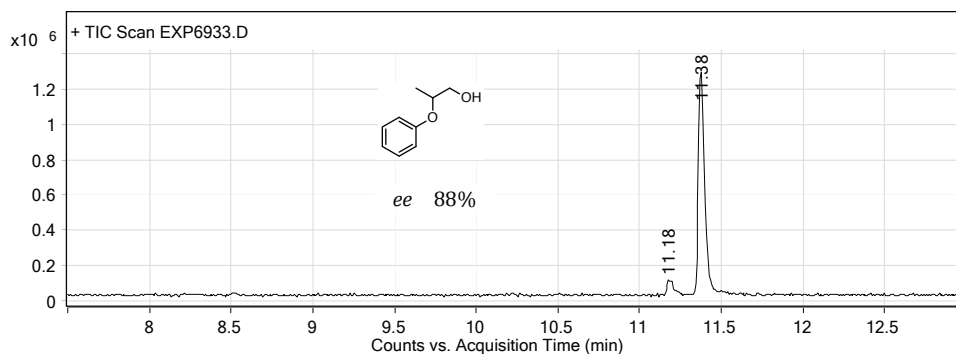


Figure 3.24: GC traces of the 2-phenoxypropan-1-ol; Top: obtained from the enantioselective hydrogenation of **134** with a low amount (1.1 equiv) of base (Table 3.1, entry 9). Bottom: Obtained from the reduction of isolated **134** by LiAlH_4 .

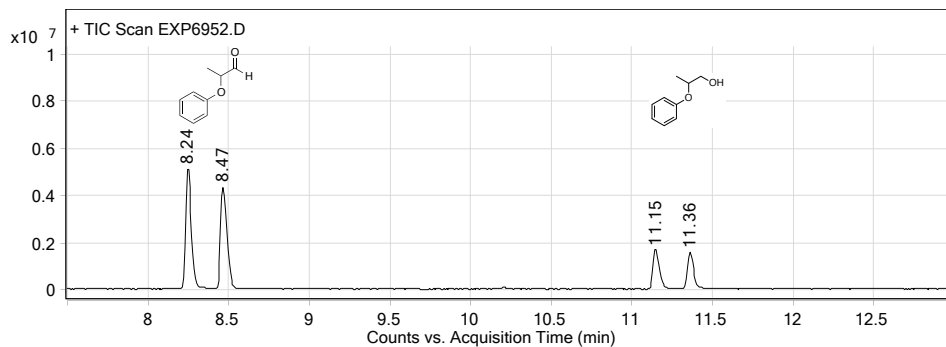
2-phenoxypropan-1-ol (hydrogenation product)



Integration Peak List

Peak	Start	RT	End	Height	Area	Area %
1	11.15	11.18	11.24	79011.05	195020.84	5.98
2	11.33	11.38	11.51	1249701.22	3262798.08	100

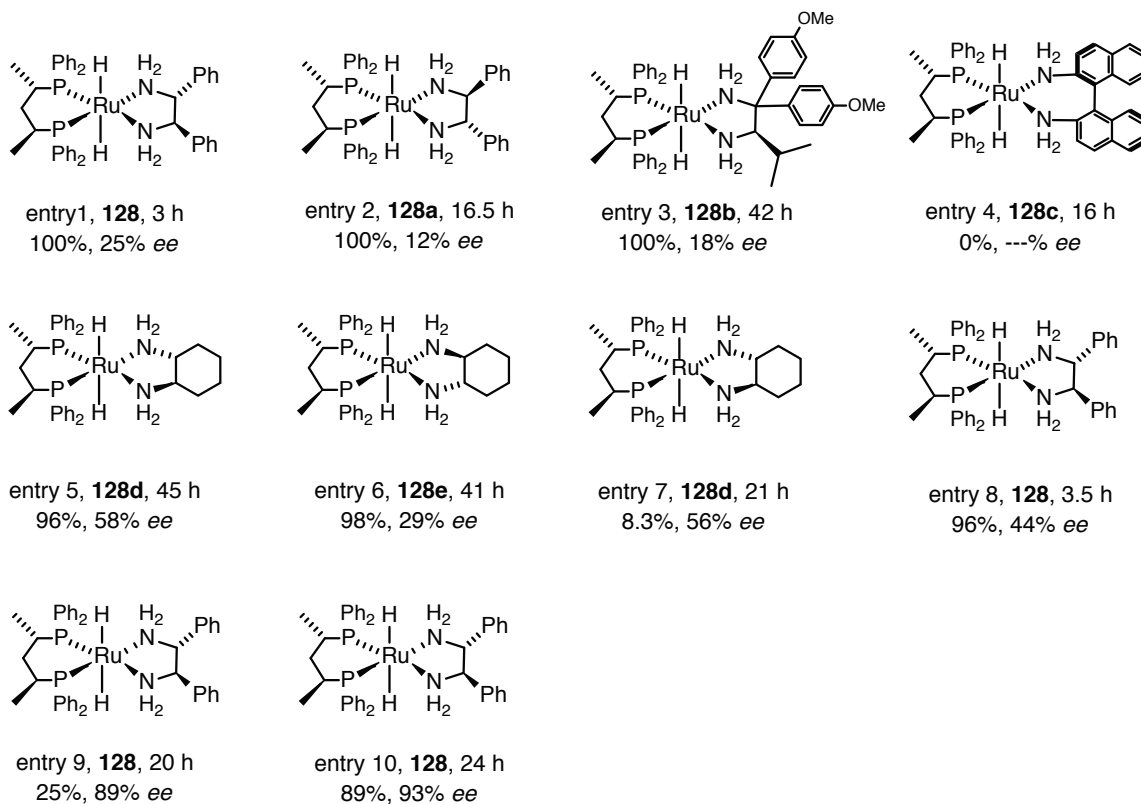
*Products from the LiAlH_4 reduction of unreactive **134** (2-phenoxypropan-1-ol and 2-phenoxypropanal)*



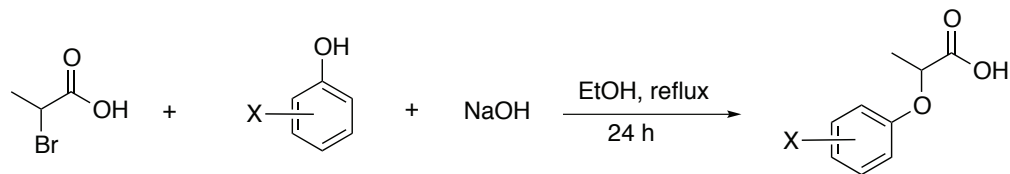
Integration Peak List

Peak	Start	RT	End	Height	Area	Area %
1	8.2	8.24	8.39	5073344.52	13092169.26	100
2	8.42	8.47	8.6	4282989.21	11528082.91	88.05
3	11.1	11.15	11.29	1651794.27	4491239.55	34.3
4	11.32	11.36	11.49	1520308.17	4052818.41	30.96

Figure 3.25: The putative dihydride catalysts (**128**, **128a–128e**) used for the optimization experiments (Table 3.1).



Synthesis of 2-phenoxy acids



General procedure:¹⁷⁶

94–111 mmol of phenol or naphthol and 2 equivalents of sodium hydroxide were dissolved in 150 mL of absolute ethanol. 1 equivalent of 2-bromopropanoic acid was then added while stirring vigorously. The mixture was refluxed at 80 °C for 24 hours. After cooling to room temperature, the ethanol was removed under reduced pressure and the resulting solid was dissolved in 150 mL of distilled water and acidified with 6 M HCl. The acidified mixture was extracted with 4 × 60 mL of diethyl ether. The combined ether layers were then extracted with 4 × 60 mL of saturated aqueous sodium carbonate. The aqueous layers were combined and then acidified with 6 M HCl and extracted again with 4 × 60 mL of ether. The final combined ether layers were washed with brine, then dried over sodium sulfate, and filtered. The solvent was evaporated under reduced pressure to give the crude product.

For known acids, only the ¹H NMR chemical shift information is reproduced here for convenience.

2-(4-fluorophenoxy)propanoic acid (CAS: 2967-70-6):¹⁷⁷ Crude yield 93%, off white powder. ¹H NMR (498.118 MHz, CDCl₃, 27.0 °C): δ 1.67 (3H, d, *J* = 7.0 Hz, CH₃), 4.75 (1H, q, *J* = 6.8 Hz, CH), 6.88 (2H, m, 2 aromatic CH), 7.00 (2H, m, 2 aromatic CH).

2-(4-chlorophenoxy)propanoic acid (CAS: 3307-39-9):¹⁷⁷ Crude yield 78%, off white powder, purified by crystallization using CH₂Cl₂/hexane, purified yield 61% white solid. ¹H NMR (399.794 MHz, CDCl₃, 26.5 °C): δ 1.68 (3H, d, *J* = 6.8 Hz, CH₃), 4.77 (1H, q, *J* = 6.8 Hz, CH), 6.85 (2H, d, *J* = 8.8 Hz, 2 aromatic CH), 7.26 (2H, d, *J* = 9.2 Hz, 2 aromatic CH).

2-(4-bromophenoxy)propanoic acid (CAS: 32019-08-2): Crude yield 90%, off white powder, purified by crystallization using CH₂Cl₂/hexane, purified yield 79% white solid. ¹H NMR (498.118 MHz, CDCl₃, 27.0 °C): δ 1.68 (3H, d, *J* = 7.0 Hz, CH₃), 4.77 (1H, q, *J* = 7.0 Hz, CH), 6.80 (2H, d, *J* = 9.0 Hz, 2 aromatic CH), 7.41 (2H, d, *J* = 9.0 Hz, 2 aromatic CH).

2-(4-methoxyphenoxy)propanoic acid (CAS: 13794-15-5):¹⁷⁸ Crude yield 99%, off white powder, purified by crystallization using CH₂Cl₂/hexane, purified yield 81%, colorless crystals. ¹H NMR (498.118 MHz, CDCl₃, 27.0 °C): δ 1.66 (3H, d, *J* = 7.0 Hz, CH₃), 3.79 (3H, s, OCH₃), 4.72 (1H, q, *J* = 7.0 Hz, CH), 6.86 (4H, m, 4 aromatic CH).

2-[4-(1,1-dimethylethyl)phenoxy]propanoic acid:¹⁷⁹ Crude yield 95%, off white powder, purified by crystallization using CH₂Cl₂/hexane, purified yield 62%, colorless crystals. ¹H NMR (498.118 MHz, CDCl₃, 27.0 °C): δ 1.32 (9H, s, 3CH₃), 1.67 (3H, d, *J* = 7.0 Hz, CH₃), 4.79 (1H, q, *J* = 6.8 Hz, CH), 6.86 (2H, d, *J* = 9.0 Hz, 2 aromatic CH), 7.31 (2H, d, *J* = 7.0 Hz, 2 aromatic CH).

2-(3-fluorophenoxy)propanoic acid (CAS: 91054-27-2): Crude yield 95%, off white powder, purified by crystallization using CH₂Cl₂/hexane, purified yield 60%, colorless crystals. ¹H NMR (498.118 MHz, CDCl₃, 27.0 °C): δ 1.69 (3H, d, *J* = 7.0 Hz,

CH₃), 4.80 (1H, q, *J* = 7.0 Hz, CH), 6.65 (1H, m, aromatic), 6.71 (2H, m, aromatic), 7.27 (1H, m, aromatic).

2-(2-naphthalenyloxy)propanoic acid (CAS: 10470-82-3):¹⁸⁰ Crude yield 90%, brown powder, purified by crystallization using CH₂Cl₂/hexane, purified yield 65%, white pink solid. ¹H NMR (498.118 MHz, CDCl₃, 27.0 °C): δ 1.75 (3H, d, *J* = 6.5 Hz, CH₃), 4.98 (1H, q, *J* = 7.0 Hz, CH), 7.12 (1H, d, *J* = 2.5 Hz, 1 aromatic CH), 7.23 (1H, dd, *J* = 2.5 Hz; *J* = 9.0 Hz, 1 aromatic CH), 7.39 (1H, t, *J* = 7.2 Hz, 1 aromatic CH), 7.47 (1H, t, *J* = 7.0 Hz, 1 aromatic CH), 7.74 (1H, d, *J* = 8.5, 1 aromatic CH), 7.80 (2H, d, *J* = 9.0 Hz, 2 aromatic CH).

2-phenoxy-2-phenylacetic acid (CAS: 3117-38-2): Prepared by a modified version of a literature procedure.¹⁸¹

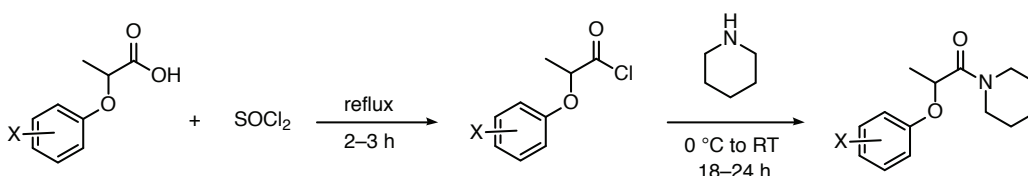
A mass of 7.5 g (~35 mmol) of α-bromophenylacetic acid was converted into an acid chloride (*vide infra*). The acid chloride was dissolved in 20 mL of DCM, and then freshly distilled 2-propanol (4 equivalents) was added drop wise with stirring. The reaction mixture was stirred overnight. The reaction mixture was evaporated under reduced pressure and then dissolved in 50 mL of DCM. The dissolved reaction mixture was then washed with 3 × 10 mL distilled H₂O, 3 × 10 mL of saturated aqueous sodium carbonate, and 20 mL of brine. The combined organic layer was then dried over sodium sulfate and filtered. The solvent was evaporated under reduced pressure to yield the isopropyl ester (89%, yellow oil).

The ester (4 g, 15.6 mmol) and 1.1 equivalents of phenol (1.6 g) were dissolved in 30 mL of distilled THF under N₂ atmosphere. Meanwhile, 1.1 equivalents of sodium hydride (0.6 g, 0.6 g/g) weighed into a flask equipped with a

stir-bar and immersed into an ice-bath. The resulting THF solution was then transferred slowly into the sodium hydride with stirring. The mixture was then allowed to warm to room temperature and stirred overnight. The reaction mixture was quenched by slowly adding water. The solvent was then removed under reduced pressure and the crude product dissolved in 50 mL of DCM. The mixture was washed with 3 × 10 mL of distilled H₂O, 3 × 10 mL of saturated aqueous sodium carbonate, 20 mL of brine, then dried over sodium sulfate, and filtered off. The product was then concentrated *in vacuo* to yield the product (67%, yellowish oil).

The resulting ester (2.8 g) was hydrolyzed by stirring with 10.3 g of NaOH in 90 mL of distilled H₂O. This mixture was refluxed overnight with stirring. The reaction mixture was then acidified with 6 M HCl and then extracted with 4 × 10 mL DCM. The organic layer was then washed with brine, dried over sodium sulfate, filtered, and then the solvent was evaporated under reduced pressure to yield α-phenoxyphenylacetic acid (>99%, off-white solid). ¹H NMR (499.806 MHz, CDCl₃, 27.0 °C): δ 5.69 (1H, s, CH), 7.02 (3H, m, 3 aromatic CH), 7.31 (2H, m, 2 aromatic CH), 7.44 (3H, m, 3 aromatic CH), 7.63 (2H, d, *J* = 6.5 Hz, 2 aromatic CH).

Synthesis of amides



General procedure

An acid (19–25 mmol) was placed into a three-neck flask under N₂ atmosphere and dissolved in 6 equivalents of thionyl chloride, which was added dropwise while stirring at room temperature. The mixture was refluxed for 2 hours at 74 °C. Excess thionyl chloride was removed using a water aspirator. Any additional thionyl chloride was removed by adding 20 mL of hexanes and removal by evaporation using the water aspirator. This hexane extraction was performed 3 times. The resulting acid chloride was dissolved in 30 mL of DCM and cooled to 0 °C. 2.2 molar equivalents of piperidine was added at a rate of 1 drop every 3 seconds with vigorous stirring. After addition was completed, the reaction mixture was allowed to warm to room temperature and stirred for 18–24 hours. The reaction mixture was extracted 4 times with water, washed with brine, dried over sodium sulfate and filtered. Finally, the organic solvent was removed under reduced pressure to yield an oily mixture, which was dried under high vacuum for 24 hours.

2-phenoxy-1-(1-piperidinyl)-1-propanone (Table 3.2, entry 1): Commercially available acid chloride was used for the synthesis. Viscous yellow-brown oil was obtained from passing the crude product through neutral alumina using CH₂Cl₂ as an eluent, 94% yield. ¹H NMR (499.806 MHz, CDCl₃, 27 °C): δ 1.66-1.37 (6H, m, 3 CH₂), 1.63 (3H, d, *J* = 7.0 Hz, CH₃), 3.68-3.50 (4H, m, 2 CH₂), 4.98 (1H, q, *J* = 6.8 Hz, CH), 6.95 (3H, m, 3 aromatic CH), 7.29 (2H, m, 2 aromatic CH). ¹³C{¹H} NMR (125.691 MHz, CDCl₃, 27 °C): δ 18.0 (CH₃), 24.5 (CH₂), 25.7 (CH₂), 26.5 (CH₂), 43.6 (CH₂), 46.0 (CH₂), 74.4 (CH), 114.9 (aromatic), 121.3 (aromatic), 129.6 (aromatic),

157.4 (aromatic), 169.4 (carbonyl). HRMS (EI) m/z : Calcd for $C_{14}H_{19}NO_2$ (M^+ , 33.62%) 233.1416; Found 233.1414. 140.1075 (45.69%), 121.0650 (100%), 112.0765 (64.78%), 84.0814 (53.79%).

2-(4-fluorophenoxy)-1-(1-piperidiny)-1-propanone (Table 3.2, entry 2): Viscous yellow-brown oil was obtained after passing the crude product through neutral alumina using CH_2Cl_2 as an eluent, 95% yield. 1H NMR (498.118 MHz, $CDCl_3$, 27 °C): δ 1.39-1.63 (6H, m, 3 CH_2), 1.60 (3H, d, J 6.8 Hz, CH_3), 3.47-3.67 (4H, m, 2 CH_2), 4.90 (1H, m, CH), 6.84-6.87 (2H, m, 2 aromatic CH), 6.95-6.98 (2H, m, 2 aromatic CH). $^{13}C\{^1H\}$ NMR (125.691 MHz, $CDCl_3$, 27 °C): δ 18.0 (CH), 24.5 (CH), 25.7 (CH), 26.5 (CH), 43.6 (CH), 46.0 (CH), 75.0 (CH) 115.9 (aromatic), 153.5 (aromatic), 156.6 (aromatic), 158.5 (aromatic), 169.3 (carbonyl). HRMS (EI) m/z : Calcd for $C_{14}H_{18}FNO_2$ (M^+ , 50.47%) 251.1322; Found 251.1328. 140.1071 (81.24%), (70.56%), 112.0762 (90.03%), 84.0811 (100%), 69.0704 (56.15%).

2-(4-chlorophenoxy)-1-(1-piperidiny)-1-propanone (Table 3.2, entry 3): A yellow brown oil that solidified to give a tan solid over the course of one week, 57% yield. 1H NMR (498.118 MHz, $CDCl_3$, 27 °C): δ 1.38-1.64 (6H, m, 3 CH_2), 1.62 (3H, d, J 6.8 Hz, CH_3), 3.48-3.65 (4H, m, 2 CH_2), 4.92 (1H, q, J 6.8 Hz CH), 6.85 (2H, d, J 9.1 Hz 2 aromatic CH), 7.23 (2H, d, J 9.1 Hz, 2 aromatic CH). $^{13}C\{^1H\}$ NMR (125.691 MHz, $CDCl_3$, 27 °C): δ 18.0 (CH), 24.5 (CH), 25.7 (CH), 26.5 (CH), 43.6 (CH), 46.0 (CH), 74.8 (CH) 116.1 (aromatic), 126.2 (aromatic), 129.5 (aromatic), 156.1 (aromatic), 169.0 (carbonyl). HRMS (EI) m/z : Calcd for $C_{14}H_{18}^{35}ClNO_2$ (M^+ , 45.31%) 267.1026; Found 267.1021. 140.1069 (83.33%), 128.0021 (45.07%), 112.0775 (74.74%), 84.0813

(100%). Anal. Calcd for C₁₄H₁₈ClNO₂: C, 62.80; H, 6.78; N, 5.23. Found: C, 62.53; H, 6.81; N 5.32.

2-(4-bromophenoxy)-1-(1-piperidinyl)-1-propanone (Table 3.2, entry 4): Brown solid, crude yield 95%, purified by flash chromatography on a silica column with 1:2.5 hexane:ethyl acetate as eluent (*R_f* 0.52). Isolated, purified yield: 47%, white solid. ¹H NMR (498.118 MHz, CDCl₃, 27.0 °C): δ 1.36-1.74 (6H, m, 3 CH₂), 1.61 (3H, d, *J* 6.5 Hz, CH₃), 3.47-3.65 (4H, m, 2CH₂), 4.96 (1H, q, *J* 6.8 Hz, CH), 6.80 (2H, d, *J* 9.0 Hz, 2 aromatic CH), 7.37 (2H, d, *J* 9.0 Hz, 2 aromatic CH). ¹³C{¹H} NMR (125.691 MHz, CDCl₃, 27.0 °C): δ 18.0 (CH₃), 24.5 (CH₂), 25.7 (CH₂), 26.5 (CH₂), 43.7 (CH₂), 46.0 (CH₂), 74.7 (CH), 113.6 (aromatic), 116.7 (aromatic), 132.4 (aromatic), 156.6 (aromatic), 169.0 (carbonyl). HRMS (EI) *m/z*: Calcd for C₁₄H₁₈⁸¹BrNO₂ (M⁺, 18.27%) 313.0501; Found 313.0502. Calcd for C₁₄H₁₈⁷⁹BrNO₂ (M⁺, 18.92%) 311.0521; Found 311.0515, 140.1073 (100%), 112.1126 (55.51%), 112.0761 (84.79%), 84.0811 (92.97%). Anal. Calcd for C₁₄H₁₈BrNO₂: C, 53.86; H, 5.81; N, 4.49. Found: C, 53.95; H, 5.84; N, 5.51.

2-(4-methoxyphenoxy)-1-(1-piperidinyl)-1-propanone (Table 3.2, entry 5): Brown solid, 79% crude yield. Purified twice by flash chromatography on a silica column with 1:2.5 hexane:ethyl acetate eluent (*R_f* 0.57). Isolated, purified yield: 21%. Off white solid. ¹H NMR (498.118 MHz, CDCl₃, 27.0 °C): δ 1.36-1.64 (6H, m, 3 CH₂), 1.59 (3H, d, *J* 7.0 Hz, CH₃), 3.48-3.68 (4H, m, 2CH₂), 3.77 (3H, s, CH₃), 4.89 (1H, q, *J* 6.8 Hz, CH), 6.84 (4H, m, 4 aromatic CH). ¹³C{¹H} NMR (125.691 MHz, CDCl₃, 27.0 °C): δ 18.1 (CH₃), 24.5 (CH₃), 25.7 (CH₂), 26.5 (CH₂), 43.6 (CH₂), 46.0 (CH₂), 55.7 (CH₂), 74.9 (CH), 114.7 (aromatic), 115.9 (aromatic), 151.5 (aromatic), 154.2 (aromatic),

169.6 (carbonyl). HRMS (ESI⁺) m/z: Calcd for C₁₅H₂₂NO₃ (M+H)⁺ 264.1594; Found 264.1594. Anal. Calcd for C₁₅H₂₁NO₃: C, 68.42; H, 8.04; N, 5.32. Found C, 68.51; H, 8.04, N 5.43.

2-[4-(1,1-dimethylethyl)phenoxy]-1-(1-piperidinyl)-1-propanone (Table 3.2, entry 6): Light brown solid, crude yield 81.7%, purified by recrystallization from CH₂Cl₂/hexane, off white solid. ¹H NMR (498.118 MHz, CDCl₃, 27.0 °C): δ 1.30 (9H, s, 3CH₃), 1.41-1.67 (6H, m, 3 CH₂), 1.60 (3H, d, *J* = 6.5 Hz, CH₃), 3.49-3.65 (4H, m, 2CH₂), 4.95 (1H, q, *J* = 6.6 Hz, CH), 6.84 (2H, d, *J* = 9.0 Hz, 2 aromatic CH), 7.29 (2H, d, *J* = 8.5 Hz, 2 aromatic CH). ¹³C{¹H} NMR (125.691 MHz, CDCl₃, 27.0 °C): δ 18.0 (C(CH₃)₃), 24.6 (CH₃), 25.7 (CH₂), 26.5 (CH₂), 31.5 (CH₃), 34.1 (CH₂), 43.6 (CH₂), 46.0 (CH₂), 74.1 (CH), 114.3 (aromatic), 126.3 (aromatic), 144.0 (aromatic), 155.2 (aromatic), 169.6 (carbonyl). HRMS (EI) m/z: Calcd for C₁₈H₂₇NO₂ (M⁺, 34.60%) 289.2042; Found 289.2039. 177.1279 (60.73%), 140.1074 (98.40%), 112.1127 (39.31%), 112.0762 (38.62%), 84.0809 (100%). Anal. Calcd for C₁₈H₂₇NO₂: C, 74.70; H, 9.40; N, 4.84. Found: C, 74.63; H, 9.49; N, 4.96.

2-(3-fluorophenoxy)-1-(1-piperidinyl)-1-propanone (Table 3.2, entry 7): A pale yellow oil that solidified into a tan solid over the course of a week, 86% yield. ¹H NMR (498.118 MHz, CDCl₃, 27.0 °C): δ 1.39-1.67 (6H, m, 3 CH₂), 1.62 (3H, d, *J* = 6.5 Hz, CH₃), 3.50-3.65 (4H, m, 2CH₂), 4.95 (1H, q, *J* = 6.8 Hz, CH), 6.62-6.71 (3H, m, 3 aromatic CH), 7.22 (1H, m, aromatic CH). ¹³C{¹H} NMR (125.691 MHz, CDCl₃, 27.0 °C): δ 17.9 (CH₃), 24.5 (CH₂), 25.7 (CH₂), 26.5 (CH₂), 43.6 (CH₂), 46.1 (CH₂), 74.5 (CH), 102.8 (d, *J* = 24.9Hz, aromatic), 108.2 (d, *J* = 24.1Hz, aromatic), 110.4 (aromatic), 130.4 (d, *J* = 10.1Hz, aromatic), 158.8 (d, *J* = 10.7Hz, aromatic), 163.6 (d, *J*

245.5Hz, aromatic), 168.9 (carbonyl). HRMS (EI) m/z: Calcd for C₁₄H₁₈FNO₂ (M⁺, 36.01%) 251.1322; Found 251.1322. 140.1068 (31.56%), 139.0553 (41.92%), 112.0758 (100%), 84.0811 (44.24%), 69.0685 (41.55%). Anal. Calcd for C₁₄H₁₈FNO₂: C, 66.91; H, 7.22; N, 5.57. Found: C, 67.00; H, 7.27; N, 5.70.

2-(2-naphthalenyloxy)-1-(1-piperidinyl)-1-propanone (Table 3.2, entry 8): Brown solid, 96% crude yield. Purified by flash chromatography on a silica column with a 1:2.5 mixture of hexane:ethyl acetate eluent (R_f 0.55), off white solid.

¹H NMR (498.118 MHz, CDCl₃, 27.0 °C): δ 1.36-1.74 (6H, m, 3 CH₂), 1.69 (3H, d, *J* 7.0 Hz, CH₃), 3.54-3.70 (4H, m, 2CH₂), 5.13 (1H, q, *J* 6.6 Hz, CH), 7.19 (2H, m, 2 aromatic CH), 7.36 (1H, m, aromatic CH), 7.45 (1H, m, aromatic CH), 7.74-7.79 (3H, m, aromatic CH). ¹³C{¹H} NMR (125.691 MHz, CDCl₃, 27.0 °C): δ 18.0 (CH₃), 24.5 (CH₂), 25.7 (CH₂), 26.5 (CH₂), 43.7 (CH₂), 46.1 (CH₂), 74.5 (CH), 107.6 (aromatic), 118.7 (aromatic), 123.9 (aromatic), 126.4 (aromatic), 127.0 (aromatic), 127.6 (aromatic), 129.2 (aromatic), 129.7 (aromatic), 134.5 (aromatic), 155.4 (aromatic), 169.3 (carbonyl). HRMS (EI) m/z: Calcd for C₁₈H₂₁NO₂ (M⁺, 21.67%) 283.1572; Found 283.1570. 112.1126 (43.21%), 112.0760 (33.84%), 62.0171 (100%). Anal. Calcd for C₁₈H₂₁NO₂: C, 76.29; H, 7.47; N, 4.94. Found: C, 76.06; H, 7.48; N, 5.00.

2-phenoxy-2-phenyl-1-(1-piperidinyl)-ethanone (Table 3.2, entry 9): Product was purified by flash chromatography on a silica column with a 50:1 ratio of silica to product, 4:1 hexane:ethyl acetate eluent, R_f 0.27. Product was dissolved in a minimum volume of DCM before injecting onto column. Purified yield, 88%, white

solid. ^1H NMR (499.806 MHz, CDCl_3 , 27.0 °C): δ 1.21-1.86 (6H, m, 3 CH_2), 3.40-3.61 (4H, m, 2 CH_2), 5.96 (1H, s, CH), 7.05 (3H, m, 3 aromatic CH), 7.38 (5H, m, 5 aromatic CH), 7.59 (2H, m, 2 aromatic CH). $^{13}\text{C}\{^1\text{H}\}$ NMR (125.691 MHz, CDCl_3 , 27.0 °C): δ 24.4 (CH_2), 25.6 (CH_2), 25.8 (CH_2), 43.8 (CH_2), 46.2 (CH_2), 80.7 (CH), 115.3 (aromatic), 121.7 (aromatic), 126.0 (aromatic), 128.2 (aromatic), 128.7 (aromatic), 129.7 (aromatic), 136.1 (aromatic), 157.8 (aromatic), 167.7 (carbonyl). HRMS (EI) m/z: Calcd for $\text{C}_{19}\text{H}_{21}\text{NO}_2$ (M^+ , 7.98%) 295.1572; Found 295.1568. 183.0808 (100%), 174.1287 (31.88%), 77.0383 (20.32%), 69.0700 (18.62%). Anal. Calcd for $\text{C}_{19}\text{H}_{21}\text{NO}_2$: C, 77.26; H, 7.17; N, 4.74. Found: C, 76.57; H, 7.18; N, 4.73.

2-(4-bromophenoxy)-1-(1-piperidinyl)-1-butanone (Table 3.2, entry 10): Viscous yellow-brown oil was obtained from passing the crude product through neutral alumina using CH_2Cl_2 as an eluent. 66% yield. ^1H NMR (498.118 MHz, CDCl_3 , 27.0 °C): δ 1.10-1.13 (3H, t, $J = 7.5$ Hz, CH_3), 1.59-1.62 (6H, m, 3 CH_2), 1.96-1.99 (2H, m, $J = 6.5$ Hz, CH_2), 3.42-3.70 (4H, m, 2 CH_2), 4.65-4.68 (1H, m, CH), 6.82 (2H, d, $J = 7.0$ Hz, 2 aromatic CH), 7.37 (2H, d, $J = 9.0$ Hz, 2 aromatic CH). $^{13}\text{C}\{^1\text{H}\}$ NMR (125.691 MHz, CDCl_3 , 27.0 °C): δ 10.4 (CH_3), 24.5 (CH_3), 25.8 (CH_2), 26.5 (CH_2), 26.5 (CH_2), 43.7 (CH_2), 46.0 (CH_2), 80.9 (CH), 113.6 (aromatic), 116.7 (aromatic), 132.4 (aromatic), 157.1 (aromatic), 169.0 (carbonyl). HRMS (ESI) m/z: Calcd for $\text{C}_{15}\text{H}_{21}\text{BrNO}_2$ ($\text{M}+\text{H}$) $^+$: 326.0750; Found 326.0753. Anal. Calcd for $\text{C}_{15}\text{H}_{20}\text{BrNO}_2$: C, 54.61; H, 6.09; N, 4.27. Found: C, 55.23; H, 6.18; N, 4.29.

2-bromo-1-(1-piperidinyl)-1-propanone: A colourless oil was obtained from passing through neutral alumina using CH₂Cl₂ as an eluent, 90% yield. ¹H NMR (499.797 MHz, CDCl₃, 27 °C): δ 1.75-1.55 (6H, m, 3 CH₂), 1.83 (3H, d, *J* = 6.5 Hz, CH₃), 3.73-3.38 (4H, m, 2 CH₂), 4.60 (1H, q, *J* = 6.5 Hz, CH), ¹³C{¹H} NMR (125.688 MHz, CDCl₃, 27 °C): δ 21.8 (CH₃), 24.4 (CH₂), 25.4 (CH₂), 26.1 (CH₂), 38.3 (CH), 43.5 (CH₂), 47.2 (CH₂), 167.3 (carbonyl). HRMS (ESI) *m/z*: Calcd for C₈H₁₄BrNNaO (M+Na)⁺: 242.0151; Found 242.0153. Anal. Calcd for C₈H₁₄BrNO: C, 43.65; H, 6.41; N, 6.36. Found: C, 43.78; H, 6.48; N, 6.39.

2-methoxy-1-(1-piperidinyl)-1-propanone (Table 3.2, entry 11): Sodium methoxide (0.96 g, 17.7 mmol, 1.3 equivalents) was dissolved in 30 mL of distilled MeOH. A solution of 2-bromo-1-(1-piperidinyl)-1-propanone (3.02 g, 13.6 mmol, 1 equivalent) in 30 mL of distilled MeOH was transferred to the sodium methoxide-MeOH under the N₂ atmosphere. The resulting solution was refluxed for 2 hours and cooled down to room temperature. The reaction mixture was diluted and excess sodium methoxide was quenched by slow addition of water (40 mL), extracted with DCM (3 × 50 mL). The combined organic layer was washed with brine (50 mL) dried over sodium sulfate, and filtered. The organic solvent was then removed under reduced pressure to yield the crude product as a colorless oil (94.3% crude yield). Purified by flash chromatography on a silica column with a 1:1 mixture of hexane:ethyl acetate as eluent (*R_f* = 0.16). The isolated, purified yield of the colorless oil was 70%. ¹H NMR (499.797 MHz, CDCl₃, 27 °C): δ 1.38 (3H, d, *J* = 6.5 Hz, CH₃), 1.67-1.56 (6H, m, 3 CH₂), 3.34 (3H, s), 3.59-3.55 (4H, m, 2 CH₂), 4.16 (1H, q, *J* = 6.5 Hz, CH), ¹³C{¹H} NMR (125.688 MHz, CDCl₃, 27 °C): δ 17.6 (CH₃), 24.6 (CH₂), 25.8

(CH₂), 26.6 (CH₂), 43.3 (CH₂), 45.9 (CH₂), 76.8 (CH), 170.2 (carbonyl). HRMS (ESI) m/z: Calcd for C₉H₁₈NO₂ (M+H)⁺ 172.1332; Found 172.1333.

1-(*N*-phenyl-alanyl)-piperidine (Table 3.2, entry 12): 2-bromo-1-(1-piperidinyl)-1-propanone (4.0 g, 18.2 mmol) and aniline (3.89 g, 36.4 mmol) were refluxed in benzene for 48 hours. After cooling to room temperature benzene was removed under reduced pressure and the resulting solid was dissolved in 60 mL of DCM. The organic layer was washed with 3 × 60 mL distilled H₂O, with 60 mL of brine, dried over sodium sulfate, and filtered. The organic solvent was then removed under reduced pressure to yield the crude product (95%, brownish solid). Purified by crystallization using CH₂Cl₂/hexane, purified yield 50%, light brown solid.

¹H NMR (499.797 MHz, CDCl₃, 27 °C): δ 1.38 (3H, d, *J* = 6.5 Hz, CH₃), 1.54-1.71 (6H, m, 3 CH₂), 3.64-3.48 (4H, m, 2 CH₂), 4.43 (1H, q, *J* = 6.5 Hz, CH), 4.7 (NH, br), 6.64-6.62 (2H, m, 2 aromatic CH), 6.73-6.69 (1H, m, 1 aromatic CH), 7.19-7.16 (2H, m, 2 aromatic CH). ¹³C{¹H} NMR (125.688 MHz, CDCl₃, 27.0 °C): δ 18.8 (CH₃), 24.5 (CH₂), 25.6 (CH₂), 26.5 (CH₂), 43.3 (CH₂), 46.4 (CH₂), 48.6 (CH), 113.5 (aromatic), 117.6 (aromatic), 129.3 (aromatic), 146.7 (aromatic), 171.7 (carbonyl). HRMS (ESI) m/z: Calcd for C₁₄H₂₁N₂O (M+H)⁺ 233.1648; Found 233.1645. Anal. Calcd for C₁₄H₂₀N₂O: C, 72.38; H, 8.68; N, 12.06. Found: C, 72.39; H, 8.77; N, 12.02.

2-phenoxy-2-(2-pyridyl)-1-(1-piperidinyl)-ethanone (Table 3.2, entry 13):

A solid substrate of 2-phenoxy-1-(piperidin-1-yl)ethanone (3.93 g, 17.9 mmol) was weighed into a side arm flask, evacuate and refilled with argon. The substrate was

then dissolved in 15 mL of freshly distilled THF and cooled to $-78\text{ }^{\circ}\text{C}$. A THF solution of lithium bis(trimethylsilyl)amide (3.3 g, 19.7 mmol dissolved in 15 mL of freshly distilled THF), in THF at $0\text{ }^{\circ}\text{C}$ was cannulated to the side arm flask containing 2-phenoxy-1-(piperidin-1-yl)ethanone under argon atmosphere over the course of 10 to 15 min. The resulting solution was stirred for another 30 min at $-78\text{ }^{\circ}\text{C}$. 2-Chloropyridine (2.04 g, 1.7 mL, 17.9 mmol) was added using a gastight syringe and the resulting reaction mixture was allowed to warm to room temperature and stirred for 48 hours. After the reaction time, saturated NH_4Cl was added, and stirred for another 15 min. The reaction mixture was extracted with ethylacetate ($4 \times 50\text{ mL}$) and the organic layers were combined, washed with brine (50 mL), dried over sodium sulfate, and filtered. The crude product (98% yield, off brown solid) was purified by flash chromatography on a silica column with a 3:2 mixture of hexane:ethyl acetate as eluent ($R_f = 0.12$). The isolated, purified yield of the white solid was 45%.

^1H NMR (499.797 MHz, CDCl_3 , $27.0\text{ }^{\circ}\text{C}$): δ 1.36-1.33 (1H, m, CH_2), 1.48-1.42 (2H, m, CH_2), 1.68-1.55 (3H, m, CH_2), 3.57-3.51 (2H, m, CH_2), 3.66-3.59 (2H, m, CH_2), 6.07 (1H, s, CH), 6.99-6.96 (1H, m, 1 aromatic CH), 7.04-7.02 (2H, m, 2 aromatic CH), 7.29-7.24 (3H, m, 3 aromatic CH), 7.75-7.66 (2H, m, 2 aromatic CH), 8.61-8.59 (1H, m, 1 aromatic CH). $^{13}\text{C}\{^1\text{H}\}$ NMR (125.688 MHz, CDCl_3 , $27.0\text{ }^{\circ}\text{C}$): δ 24.5 (CH_2), 25.5 (CH_2), 26.1 (CH_2), 43.6 (CH_2), 46.6 (CH_2), 79.8 (CH), 115.4 (aromatic), 121.7 (aromatic), 121.8 (aromatic), 123.2 (aromatic), 129.6 (aromatic), 137.0 (aromatic), 148.9 (aromatic), 156.7 (aromatic), 157.4 (aromatic), 166.5 (carbonyl). HRMS (ESI)

m/z: Calcd for $C_{18}H_{20}N_2NaO_2$ (M+Na)⁺ 319.1417; Found 319.1421. Anal. Calcd for $C_{18}H_{20}N_2O_2$: C, 72.95; H, 6.80; N, 9.45. Found: C, 72.93; H, 6.89; N, 9.39.

2-phenylthio-1-(1-piperidinyl)-1-propanone (Table 3.2, entry 14): ¹H NMR (499.118 MHz, CDCl₃, 27 °C): δ 1.49 (3H, d, *J* = 7.0 Hz, CH₃), 1.79-1.52 (6H, m, 3 CH₂), 3.50-3.37 (3H, m, CH₂), 3.68-3.63 (1H, m, CH₂) 4.05 (1H, q, *J* = 6.9 Hz, CH), 7.34-7.28 (3H, m, 3 aromatic CH), 7.48-7.46 (2H, m, 2 aromatic CH). ¹³C{¹H} NMR (125.691 MHz, CDCl₃, 27 °C): δ 18.5 (CH₃), 24.5 (CH₂), 25.6 (CH₂), 26.4 (CH₂), 42.6 (CH₂), 43.3 (CH₂), 47.1 (CH), 128.0 (aromatic), 128.8 (aromatic), 133.3 (aromatic), 133.5 (aromatic), 169.5 (carbonyl HRMS (ESI) m/z: Calcd for $C_{14}H_{20}NOS$ (M+H)⁺ 250.1260; Found 250.1261. Anal. Calcd for $C_{14}H_{19}NOS$: C, 67.43; H, 7.68; N, 5.62. Found: C, 67.59; H, 7.66; N, 5.59. *N,N*-diphenyl-2-phenoxypropionamide (CAS: 1021327-16-1): Prepared as previously reported.⁷⁹

Synthesis of esters and aldehyde

Isopropyl 2-phenoxypropanoate: 5 mL (5.9 g, 31.6 mmol) of 2-phenoxypropionyl chloride in 50 mL of DCM was cooled to 0 °C in an ice bath. 1.2 equivalents (5.3 mL) of triethylamine was then added, followed by a drop wise addition of 3 equivalents (7.2 mL) of isopropyl alcohol. The mixture was allowed to warm to room temperature and stirred overnight. The reaction mixture was washed with 4 × 25 mL of distilled H₂O and then washed with 30 mL of brine, dried over sodium sulfate, and filtered. The organic solvent was then removed under reduced pressure to yield the isopropyl ester (88%, yellow oil). ¹H NMR (499.806 MHz, CDCl₃, 27.0 °C): δ 1.20

(3H, d, J 6.2 Hz, CH₃), 1.29 (3H, d, J 6.2 Hz, CH₃), 1.63 (3H, d, J 6.8 Hz), 4.73 (1H, q, J 6.7 Hz, CH), 5.10 (1H, septet, J 6.2 Hz, CH), 6.90 (2H, d, J 8.1 Hz, 2 aromatic CH), 6.99 (1H, t, J 7.3 Hz, 1 aromatic CH), 7.29 (2H, dd, J 8.4 Hz, 7.5 Hz, 2 aromatic CH). ¹³C{¹H} NMR (125.691 MHz, CDCl₃, 27.0 °C): δ 18.5 (CH₃), 21.6 (CH₃), 21.7 (CH₃), 68.8 (CH), 72.7 (CH), 115.1 (aromatic), 121.5 (aromatic), 129.5 (aromatic), 157.7 (aromatic), 171.9 (carbonyl). HRMS (ESI) m/z : Calcd for C₁₂H₁₆NaO₃ (M+Na)⁺ 231.0993; Found 231.0993.

2-phenoxypropyl 2-phenoxypropanoate: The ester was prepared by reacting 2-phenoxypropionyl chloride (290 mg, 1.5 mmol) with racemic 2-phenoxypropan-1-ol (227.6 mg, 1.5 mmol) in DCM. The same procedure was followed as described above. Purified by flash chromatography on a silica column with a 9:1 mixture of hexane:ethyl acetate as eluent (R_f 0.23). The isolated, purified yield of the colorless oil was 70%. ¹H NMR (399.984 MHz, CDCl₃, 27.0 °C): δ 1.28 (3H, d, J 6.7 Hz, CH₃), 1.59 (3H, t, J 6.5 Hz, CH₃), 4.21-4.26 (1H, m, CH₂), 4.33-4.39 (1H, m, CH₂), 4.53-4.63 (1H, m, CH), 4.73-4.80 (1H, m, CH), 6.81-6.91 (4H, m, 4 aromatic CH), 6.92-6.99 (2H, m, 2 aromatic CH), 7.16-7.31 (4H, m, 4 aromatic CH). ¹³C{¹H} NMR (125.691 MHz, CDCl₃, 27.0 °C): δ 16.6 (CH₃), 18.6 (CH₃), 67.4 (CH₂), 71.6 (CH), 72.4 (CH), 115.0 (aromatic), 115.1 (aromatic), 116.0 (aromatic), 116.1 (aromatic), 121.3 (aromatic), 121.6 (aromatic), 129.6 (aromatic), 157.5 (aromatic), 157.6 (aromatic), 172.1 (carbonyl). HRMS (ESI) m/z : Calcd for C₁₈H₂₀NaO₄ (M+Na)⁺ 323.1254; Found 323.1252.

2-methoxypropyl benzoate: The ester was prepared by reacting the hydrogenation product of 2-methoxy-1-(1-piperidiny)-1-propanone (2-methoxypropanol, piperidine, isopropanol, unreacted starting material and THF) with excess benzoyl chloride (1.2 equivalents with respect to 2-methoxypropanol, piperidine, and isopropanol in the reaction mixture) in CH₂Cl₂ using the same procedure described above. ¹H NMR (499.118 MHz, CDCl₃, 27.0 °C): δ 1.29 (3H, d, *J* = 6.5 Hz, CH₃), 3.46 (3H, s), 3.75-3.70 (1H, m, CH), 4.38-4.29 (2H, m, CH₂).

2-phenoxypropanaldehyde: The aldehyde was prepared by a modified version of a procedure previously reported.¹⁸² 3.6 g (20 mmol) of methyl 2-phenoxypropanoate (prepared as described above) was dissolved in 50 mL of distilled anhydrous DCM under argon and cooled to -78 °C. 25 mL of 1 M diisobutylaluminum hydride (DIBAL) was added dropwise by a cannula. The resulting mixture was stirred for 30 min at -78 °C. Reaction was quenched with 0.5 mL of methanol and the reaction mixture was allowed to warm to room temperature. The mixture was poured into 130 mL of DCM in a separatory funnel. The mixture was washed with 26 mL of 1 M HCl, then 25 mL of brine, and then concentrated *in vacuo* to yield a colorless oil, crude yield >99%. The resulting clear oil was then purified by distillation at 50 °C under high vacuum.

¹H NMR (499.118 MHz, CDCl₃, 27.0 °C): δ 1.51 (3H, d, *J* = 7.0 Hz, CH₃), 4.66 (1H, dq, *J* = 1.8 Hz, 6.9 Hz, CH), 6.51 (2H, d, *J* = 8.0 Hz, 2 aromatic CH), 7.03 (1H, t, *J* = 7.4 Hz, aromatic CH), 7.32 (2H, dd, *J* = 7.7 Hz, 8.3 Hz, 2 aromatic CH), 9.75 (1H, d, *J* = 1.8 Hz, aldehyde). ¹³C{¹H} NMR (125.691 MHz, CDCl₃, 27.0 °C): δ 15.6 (CH₃), 77.8 (CH),

115.3 (aromatic), 121.9 (aromatic), 129.8 (aromatic), 157.3 (aromatic), 202.5 (carbonyl). HRMS (EI) m/z: Calcd for C₉H₁₀O₂ (M⁺, 27.29%) 150.0680; Found 150.0681. 121.0655 (100%), 97.1019 (22.13%), 93.0701 (29.61%), 69.0700 (18.62%).

Synthesis of ruthenium precursor

trans-RuCl₂((*S,S*)-skewphos)((*R,R*)-dpen) (**135**) was prepared as reported previously.¹⁸³

General procedure for the synthesis of racemic alcohol products from the parent amides

The racemic alcohols were prepared by a modified version of our previously reported hydrogenation procedure.⁸⁶ The achiral amide hydrogenation catalyst [Ru(η^3 -C₃H₅)(Ph₂PCH₂CH₂NH₂)₂]BF₄ (**51**, 6.8 mg, 0.010 mmol), and KO^tBu (11.2 mg, 0.1 mmol) were weighed out into two separate NMR tubes inside the glove box. Freshly distilled THF (1.0 mL) was then added to the NMR tube containing **51** by using a cannula under argon pressure. The argon was replaced by purging with H₂ gas. The solution of the ruthenium precursor **51** was then transferred by cannula into the tube containing the KO^tBu under H₂. The tube was then pressurized to ~2 psi gauge pressure. The resulting reddish-yellow solution was then transferred with a cannula under H₂ to the autoclave containing the amide substrate (0.5 mmol, 50 equivalents). A THF solution (4.0 mL) was used to rinse the NMR tube containing the catalyst into the autoclave. The autoclave containing the amide was purged with

H₂ gas for 15–20 min prior to transfer of the Ru catalyst. The autoclave was then pressurized to 50 atm H₂ and stirred at 80 °C overnight. After 24 hours, the reaction mixture was allowed to cool to room temperature and the autoclave was then slowly depressurized and opened to the atmosphere. The catalyst was removed by passing the solution through a florisil plug using CH₂Cl₂ as the rinse solvent. The solvent was then removed under reduced pressure using a rotary evaporator. The ¹H NMR spectra (CDCl₃) were identical to those of the 2-aryloxy propanols obtained from the asymmetric hydrogenations. The NMR yields of these racemic hydrogenations with **51** were 100%. The racemic products were also analyzed by GC-MS or HPLC.

Synthesis of sodium isopropoxide

0.1–0.2 g (4.35–8.7 mmol) of freshly cut sodium metal was placed into a side arm flask and purged with N₂ gas. Freshly distilled anhydrous isopropyl alcohol (20 mL) was then transferred to the flask containing the sodium, using a cannula under N₂. The solution was stirred at room temperature overnight. The resulting solution was decanted into another side arm flask and concentrated under reduced pressure using a schlenk line to yield a white powder. This powder was then dried under high vacuum overnight. The remaining sodium particles were deactivated by careful addition of isopropyl alcohol, ethanol, and water respectively under the N₂ atmosphere.

Note: the color of the sodium isopropoxide changed from white to pale pink over a period of time inside the glove box, so freshly prepared sodium isopropoxide was used for every hydrogenation reaction.

General procedure for lab-scale enantioselective hydrogenations (Table 3.2)

trans-135 (24.5 mg, 30 μmol) and the base 2-PrONa (123.0 mg, 1500 μmol , 2.5 equivalents to substrate) were weighed into 2 separate NMR tubes inside a glove box. Freshly distilled THF (1.0 mL each) was cannulated into the NMR tubes containing **135** and the base under argon pressure. 2-PrOH (1200 μmol , 90 μL , 2 equivalents to substrate) was also added to the NMR tube containing the base using a gas-tight syringe.

Solid amides: An amide (600 μmol , 20 equivalents) was added to a stainless steel autoclave equipped with a stir bar. The autoclave was then assembled and purged with H_2 (~ 1 atm) for 15–20 min. A THF solution of the catalyst precursor (prepared above) was transferred into the autoclave under H_2 pressure using a cannula. This was followed by the 2-PrONa /2-PrOH/THF. Freshly distilled THF (3.0 mL) was then used to rinse the NMR tubes to ensure quantitative transfers. The autoclave was then sealed and pressurized to 4 atm H_2 . The reaction mixture was stirred at room temperature for 24 hours. The reaction was stopped by depressurizing the autoclave and opening it to air. The catalyst was removed by passing the solution through a florisil plug using CH_2Cl_2 as the rinse solvent. The solvent was then removed under reduced pressure using a rotary evaporator. The reaction product was analyzed by NMR, GC-MS or HPLC spectroscopy.

Liquid amides: The autoclave was fitted with a magnetic stir bar and then purged with H₂ for 10 min. The pre-weighed amide (600 μmol, 20 equivalents) was dissolved in freshly distilled THF (1.0 mL) under argon. The amide was then transferred into the autoclave using a cannula. The autoclave was then purged with H₂ for another 10 min. The THF solution of the catalyst precursor **135** (prepared above) was then transferred into the autoclave under H₂ pressure using a cannula. This was then followed by the 2-PrONa/2-PrOH/THF solutions. Freshly distilled THF (2 mL) was then used to rinse the NMR tubes to ensure the quantitative transfers. The autoclave was then sealed and pressurized to 4 atm H₂. The reaction mixture was stirred at room temperature for 24 hours. The reaction was stopped by depressurizing the autoclave and opening it to air. The catalyst was removed by passing the solution through a florisil plug using CH₂Cl₂ as the rinse solvent. The solvent was then removed under reduced pressure using a rotary evaporator. The reaction product was analyzed by NMR, GC-MS or HPLC spectroscopy.

High turnover number enantioselective hydrogenation of 2-(4-fluorophenoxy)-1-(1-piperidiny)-1-propanone

The procedure for liquid amide was followed with 4.95 mg (6 μmol) of *trans*-**135** 123.0 mg of 2-PrONa (1500 μmol, 2.5 equivalents to substrate), 50 μL of 2-PrOH (600 μmol, 1 equivalent to substrate) and 150.8 mg of amide substrate (600 μmol, 100 equivalents to catalyst). The hydrogenation was performed at 50 atm H₂ and room temperature for 24 hours. The pressure was released and the reactor opened to air. The reaction mixture was then passed through the florisil plug using CH₂Cl₂ as

the rinse solvent. The solvent was then removed under reduced pressure using a rotary evaporator to give the crude product (99.5 mg, 97.4%) as the colorless oil. The NMR spectrum and GC-MS chromatogram were qualitatively identical those of the small-scale hydrogenation.

Purification of reaction product, 2-(3-fluorophenoxy)propan-1-ol by column chromatography (Table 3.2, entry 7)

The reaction was repeated with 34.5 mg (41.8 μmol) of *trans*-**135**, 173.0 mg of 2-PrONa (2109.5 μmol , 2.5 equivalents to substrate), 125 μL of 2-PrOH (1673 μmol , 2 equivalents to substrate) and 210.5 mg of 2-(3-fluorophenoxy)propan-1-ol (836.6 μmol , 20 equivalents to catalyst). The hydrogenation was performed at 4 atm H_2 and room temperature for 24 hours. The pressure was released and the reactor was opened to air. The reaction mixture was then passed through a florisil plug using CH_2Cl_2 (~75 mL) as the rinse solvent. The solvent was then removed under reduced pressure using a rotary evaporator to give the crude product (145 mg, >100%) as reddish oil. The ^1H NMR spectrum was recorded (in CDCl_3) by taking an aliquot from the reaction mixture. The ^1H NMR spectrum supported 100% conversion of the starting material. The crude product was purified, to yield a colorless oil, using flash chromatography on a silica column with a 4:1 mixture of hexane:ethyl acetate eluent (R_f 0.19). The purified yield of the colorless oil was 121 mg (~95%). The product turned to bluish purple color over time (in a day). However the NMR showed no decomposition. Anal. Calcd for $\text{C}_9\text{H}_{11}\text{FO}_2$: C, 63.52; H, 6.52. Found: C, 63.61; H, 6.55.

Spectroscopic identification of alcohol products

The following methods were used to determine the %ee of the product alcohols:

Method A: GC analysis using Supelco Beta DEX 225 capillary column (30 m × 0.25 mm × 0.25 μm film thickness, He 1 mL/min, temperature programmed from 100 °C to 220 °C at 5 °C/min).

Method B: HPLC analysis using Daicel CHIRALPAK IB (4.6 mm i.d. × 250 mm) chiral column, hexane:2-PrOH 97:3, 0.8 mL/min, at 30 °C.

2-phenoxypropan-1-ol (Table 3.2, entry 1):¹⁸⁴ Colorless oil, 87% yield, 97% *ee*. $[\alpha]_D^{22}$ -29.3 (c 1.87, g/100 mL, CHCl₃). ¹H NMR (498.118 MHz, CDCl₃, 27 °C): δ 1.29 (3H, d, *J* 6.0 Hz, CH₃), 2.12 (1H, br, OH), 3.70-3.81 (2H, m, CH₂), 4.50-4.54 (1H, m, CH), 6.94-7.01 (3H, m, aromatic CH), 7.28-7.37 (2H, m, aromatic CH). %*ee* was determined using method A, Retention times: *t*_R (minor) 11.24 min, *t*_R (major) 11.45 min.

2-(4-fluorophenoxy)propan-1-ol (Table 3.2, entry 2):¹⁵⁴ Colorless oil, 87% yield, 96% *ee*. $[\alpha]_D^{22}$ -25.7 (c 0.86, g/100 mL, CHCl₃). ¹H NMR (498.118 MHz, CDCl₃, 27 °C): δ 1.27 (3H, d, *J* 6.4 Hz, CH₃), 2.14 (1H, br, OH), 3.69-3.80 (2H, m, CH₂), 4.38-4.44 (1H, m, CH), 6.88-6.93 (2H, m, aromatic CH), 6.98-7.01 (2H, m, aromatic CH). %*ee* was determined using method A, Retention times: *t*_R (minor) 11.95 min, *t*_R (major) 12.12 min.

2-(4-chlorophenoxy)propan-1-ol (Table 3.2, entry 3):¹⁸⁴ Colorless oil, 91.7% yield, >99% *ee*. $[\alpha]_{\text{D}}^{22}$ -33.1 (*c* 1.11, g/100 mL, CHCl₃). ¹H NMR (498.118 MHz, CDCl₃, 27 °C): δ 1.28 (3H, d, *J* 6.4 Hz, CH₃), 2.01 (1H, br, OH), 3.69-3.80 (2H, m, CH₂), 4.43-4.50 (1H, m, CH), 6.86-6.90 (2H, m, aromatic CH), 7.23-7.27 (2H, m, aromatic CH). %*ee* was determined using method A, Retention times: t_{R} (minor) 17.05 min, t_{R} (major) 17.19 min.

2-(4-bromophenoxy)propan-1-ol (Table 3.2, entry 4):¹⁸⁵ Colorless oil, 94% yield, >99% *ee*. $[\alpha]_{\text{D}}^{22}$ -27.3 (*c* 1.88, g/100 mL, CHCl₃). ¹H NMR (498.118 MHz, CDCl₃, 27 °C): δ 1.28 (3H, d, *J* 7.4 Hz, CH₃), 2.05 (1H, br, OH), 3.69-3.80 (2H, m, CH₂), 4.43-4.50 (1H, m, CH), 6.83 (2H, d, *J* 6.4 Hz, aromatic CH), 7.40 (2H, d, *J* 6.4 Hz, aromatic CH). %*ee* was determined using method A, Retention times: t_{R} (minor) 19.38 min, t_{R} (major) 19.49 min.

2-(4-methoxyphenoxy)propan-1-ol (Table 3.2, entry 5):¹⁸⁶ Colorless oil, 78.1% yield, 97% *ee*. $[\alpha]_{\text{D}}^{22}$ -15.0 (*c* 1.32, g/100 mL, CHCl₃). ¹H NMR (498.118 MHz, CDCl₃, 27 °C): δ 1.25 (3H, d, *J* 6.4 Hz, CH₃), 2.17 (1H, br, OH), 3.68-3.78 (2H, m, CH₂), 3.78 (3H, s, CH₃), 4.36-4.40 (1H, m, CH), 6.83-6.86 (2H, m, aromatic CH), 6.88-6.91 (2H, m, aromatic CH). %*ee* was determined using method A, Retention times: t_{R} (minor) 17.25 min, t_{R} (major) 17.36 min.

2-(4-tert-butylphenoxy)propan-1-ol (Table 3.2, entry 6): Colorless oil, 84% yield, 97% *ee*. $[\alpha]_{\text{D}}^{22}$ -28.7 (*c* 1.01, g/100 mL, CHCl₃). ¹H NMR (498.118 MHz, CDCl₃, 27 °C): δ 1.29 (3H, d, *J* 6.5 Hz, CH₃), 1.32 (9H, s, CH₃), 2.08 (1H, br, OH), 3.70-3.80 (2H, m, CH₂), 4.45-4.55 (1H, m, CH), 6.89 (2H, d, *J* 8.9 Hz, aromatic CH), 7.32 (2H, d, *J* 8.9 Hz, aromatic CH). GC-HRMS, *m/z*: Calcd for C₁₃H₂₀O₂ (M⁺) 208.1463; Found

208.2000. %*ee* was determined using method A, Retention times: t_R (minor) 17.97 min, t_R (major) 18.07 min.

2-(3-fluorophenoxy)propan-1-ol (Table 3.2, entry 7): Colorless oil, 99% yield, 96% *ee*. $[\alpha]_D^{22}$ -42.5 (c 1.66, g/100 mL, CHCl₃). ¹H NMR (498.118 MHz, CDCl₃, 27 °C): δ 1.30 (3H, d, J 6.3 Hz, CH₃), 1.99 (1H, br, OH), 3.69-3.80 (2H, m, CH₂), 4.46-4.53 (1H, m, CH), 6.64-6.71 (2H, m, 2 aromatic CH), 6.72-6.75 (1H, m, aromatic CH), 7.21-7.27 (1H, m, aromatic CH). GC-HRMS, m/z : Calcd for C₉H₁₁FO₂ (M⁺) 170.0743; Found 170.1500. %*ee* was determined using method A, Retention times: t_R (minor) 11.88 min, t_R (major) 12.04 min.

2-(naphthalene-2-yloxy)propan-1-ol (Table 3.2, entry 8):¹⁸⁷ Colorless oil, 93.5% yield, 90% *ee*. $[\alpha]_D^{22}$ -34.3 (c 2.92, g/100 mL, CHCl₃). ¹H NMR (498.118 MHz, CDCl₃, 27 °C): δ 1.37 (3H, d, J 6.5 Hz, CH₃), 2.06 (1H, br, OH), 3.77-3.87 (2H, m, CH₂), 4.65-4.72 (1H, m, CH), 7.17-7.20 (1H, m, aromatic CH), 7.23-7.25 (1H, m, aromatic CH), 7.34-7.38 (1H, m, aromatic CH), 7.44-7.49 (1H, m, aromatic CH), 7.72-7.75 (1H, m, aromatic CH), 7.77-7.81 (2H, m, aromatic CH). %*ee* was determined using method A with the temperature gradient of 2 °C/min, Retention times: t_R (major) 48.14 min, t_R (minor) 47.85 min.

2-Phenoxy-2-phenylethyl alcohol (Table 3.2, entry 9):¹⁸⁸ White solid, 91.7% yield, 84% *ee*. $[\alpha]_D^{22}$ -19.1 (c 3.05, g/100 mL, CHCl₃). ¹H NMR (498.118 MHz, CDCl₃, 27 °C): δ 2.26 (1H, br, OH), 3.80-3.88 (1H, m, CH₂), 3.92-3.98 (1H, m, CH₂), 5.27-5.31 (1H, m, CH), 6.88-6.95 (3H, m, aromatic CH), 7.19-7.24 (2H, m, 2 aromatic CH), 7.29-7.33 (1H, m, aromatic CH), 7.35-7.41 (4H, m, 4 aromatic CH). %*ee* was determined using method B, Retention times: t_R (major) 20.68 min, t_R (minor) 27.45 min.

2-(4-bromophenoxy)butan-1-ol (Table 3.2, entry 10): Colorless oil, 60% yield, 95% *ee*. $[\alpha]_D^{22} +3.46$ ($c = 2.42$, g/100 mL, CHCl_3). $^1\text{H NMR}$ (498.118 MHz, CDCl_3 , 27 °C): δ 0.96 (3H, t, $J = 7.5$ Hz, CH_3), 1.64-1.77 (2H, m, CH_2), 1.80-1.90 (1H, br, OH), 3.75-3.85 (2H, m, CH_2), 4.25-4.30 (1H, m, CH) 6.80-6.87 (2H, m, aromatic CH), 7.38-7.41 (2H, m, aromatic CH). GC-HRMS, m/z : Calcd for $\text{C}_{10}\text{H}_{13}\text{BrO}_2$ (M^+) 244.0099; Found 244.2000 %*ee* was determined using method A, Retention times: t_R (minor) 20.64 min, t_R (major) 20.75 min.

2-methoxypropanol (Table 3.2, entry 11): The conversion was calculated using NMR recorded from the aliquot of the reaction mixture. The %*ee* was obtained from the benzoyl chloride derivative. %*ee* was determined using method A with the temperature gradient of 3 °C/min, Retention times: t_R (major) 20.32 min, t_R (minor) 20.39 min.

2-anilino-1-propanol (Table 3.2, entry 12):¹⁸⁹ 47.5% yield, 74% *ee*. $^1\text{H NMR}$ (498.118 MHz, CDCl_3 , 27.0 °C): δ 1.22 (3H, d, $J = 6.5$ Hz, CH_3), 3.56-3.49 (1H, m, CH), 3.70-3.65 (1H, m, CH), 3.77-3.73 (1H, m, CH), 6.80-6.70 (3H, m, aromatic CH), 7.23-7.18 (2H, m, aromatic CH). %*ee* was determined using method B, Retention times: t_R (major) 46.52 min, t_R (minor) 35.84 min.

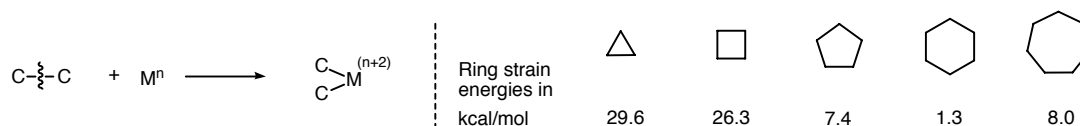
2-(phenylthio)-1-propanol (Table 3.2, entry 14): 16% yield, 74% *ee*. $^1\text{H NMR}$ (498.118 MHz, CDCl_3 , 27.0 °C): δ 1.33 (3H, d, $J = 7$ Hz, CH_3), 3.36-3.30 (1H, m, CH), 3.66-3.44 (2H, m, CH), 7.33-7.28 (3H, m, aromatic CH), 7.49-7.45 (2H, m, aromatic CH). %*ee* was determined using method A with the temperature gradient of 2 °C/min, Retention times: t_R (major) 25.86 min, t_R (minor) 25.45 min.

Chapter 4

A Fortuitous, Mild Catalytic Carbon-Carbon Bond Hydrogenolysis by a Phosphine-Free Catalyst³

Introduction

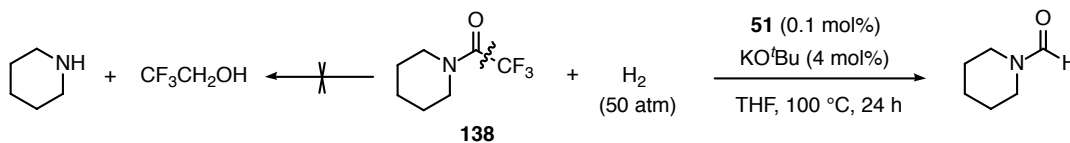
Carbon-carbon (C-C) bonds are ubiquitous. While there are a myriad of methods to prepare C-C bonds, relatively few methods exist to cleave them.¹⁹⁰⁻¹⁹² Oxidative addition is the most common transition metal-promoted C-C bond cleavage reaction. Transition metal-alkyl bonds, however, are relatively weak (ca. 30 kcal/mol), whereas C-C bonds in alkanes are typically stronger (ca. 90 kcal/mol), and they are sterically shielded by the groups on the carbon centers. Further, C-H bonds usually undergo oxidative addition more readily than C-C bonds.¹⁹³ The reported oxidative additions of C-C bonds are often driven by strain and/or they are assisted by chelation. For example, the ring strain energies of cyclopropane and cyclobutane are ~28 and ~25 kcal/mol higher than cyclohexane (Scheme 4.1).



Scheme 4.1: Transition metal assisted strain-driven C-C bond activation by oxidative addition.

³ A version of this chapter has been published. Rasu, L.; R.; Rennie, B.; Bergens, S. H. *Aust. J. Chem.* **2016**, *69*, 561-564.

As a result, the C–C activations of cyclopropane and cyclobutane by transition metal complexes are much more common than cyclohexane.¹⁹⁴ There are examples of transition metal catalyzed cleavage of unstrained C–C bonds in the literature. These unstrained C–C bond are, however, activated by an adjacent functional group such as C–CN, C–C(O)H, C–C–OR, etc.¹⁹⁵ The Bergens group recently reported the bifunctional catalysts $[\text{Ru}(\eta^3\text{-C}_3\text{H}_5)(\text{Ph}_2\text{PCH}_2\text{CH}_2\text{NH}_2)_2]\text{BF}_4$ (**51**)⁷⁹ and *trans*- $\text{Ru}(\text{H})(\eta^1\text{-BH}_4)(\text{Ph}_2\text{PCH}_2\text{CH}_2\text{NH}_2)_2$ (**61**)⁸⁶ for the hydrogenation of amides under basic and neutral conditions, respectively (Chapters 1 and 2). During the development of these catalysts, it was discovered that the hydrogenation of 2,2,2-trifluoro-1-(piperidin-1-yl)ethanone (**138**) unexpectedly produced the formylated amine, 1-formylpiperidine as the only detectable product (NMR) via a catalytic C–C bond cleavage reaction (Scheme 4.2).

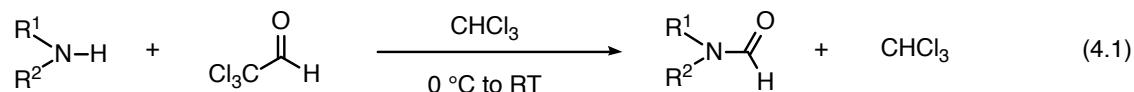


Scheme 4.2: Catalytic C–C bond hydrogenolysis of 2,2,2-trifluoro-1-(piperidin-1-yl)ethanone (**138**).

This chapter details the discovery and preliminary investigation of this unexpected catalytic hydrogenolysis of an $\text{sp}^3\text{-sp}^2$ C–C bond.

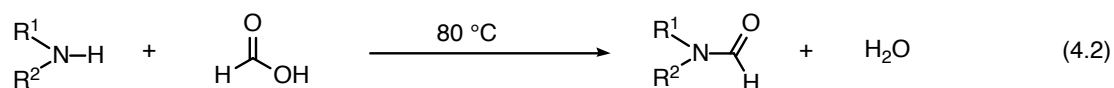
Formamides are used as solvents, protecting groups, and intermediates in the syntheses of pharmaceutically important compounds.^{196,197} They are typically prepared by formylation reactions catalyzed by acidic-, organic-, or transition metal compounds.¹⁹⁷

In 1952, Blicke and coworkers reported the formylation of amines by adding one equivalent of chloral to a precooled solution of the amine (Eq. 4.1).¹⁹⁸

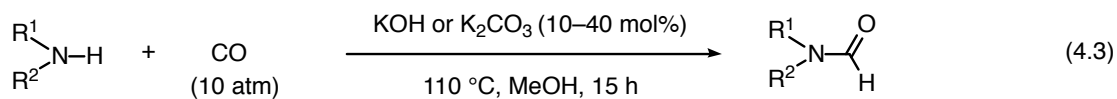


Formic acid is extensively used as a formylation reagent to prepare formamides.¹⁹⁷

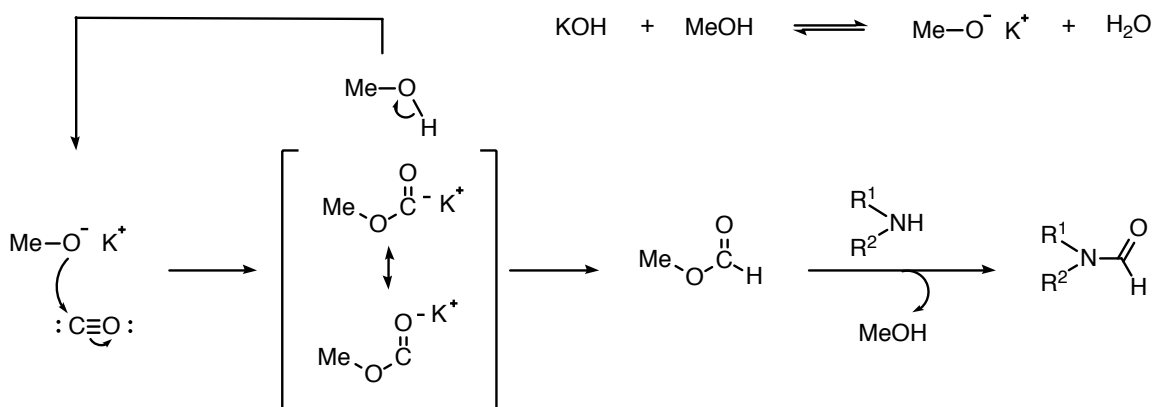
Recently, Majee and coworkers reported that formamides are prepared by heating formic acid and the amine at 80 °C (Eq. 4.2).¹⁹⁹ The reaction is low yielding below 80 °C, and impurities form above 100 °C, leaving a narrow temperature window for the preparation. Further, aliphatic amines formed the product in poor yields.



In 2015, Wu and coworkers reported an interesting base-catalyzed formylation with CO as the formylating reagent. Various amines were converted into their corresponding formylated products under 10 atm CO in the presence of 10–40 mol% of KOH or K₂CO₃ in MeOH (Eq. 4.3).²⁰⁰

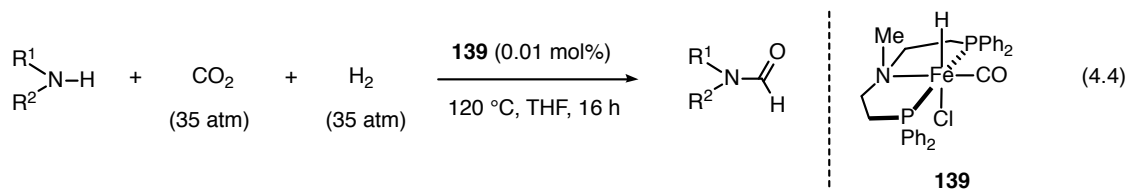


Secondary and primary amines were formylated in 70–90% yield. Aniline and related aromatic amines reacted in only ~12% yield. An optically pure amine, (*S*)-phenylethan-1-amine was formylated to the corresponding formamide without racemization. The authors proposed the following mechanism for these formylations in methanol solvent (Scheme 4.3).



Scheme 4.3: The proposed mechanism for base assisted formylation of amines by CO.

There are several reports of transition metal catalyzed formylation of amines using methanol, and CO₂/H₂ as the source of the formyl group.²⁰¹⁻²⁰³ Recently, Ding and co-workers reported such a formylation reaction using pincer type ruthenium or iron catalyst under 35 atm of CO₂ and H₂ at 120 °C. Various secondary and primary amines were formylated with yields ranging from 60 to 99% (TON up to 1000) (Eq. 4.4).²⁰⁴

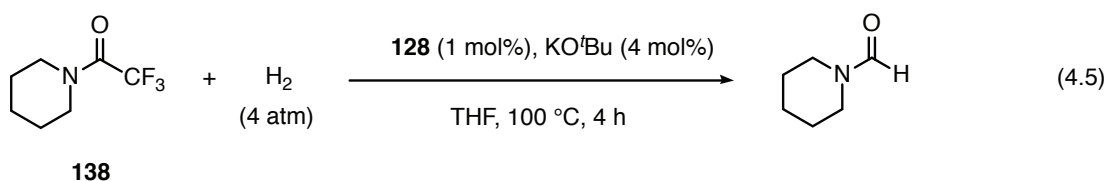


Results and discussion

As discussed in Chapters 2 and 3, the compound *cis*-[Ru(η^3 -C₃H₅)(MeCN)₂(COD)]BF₄ (**117**) is a useful starting material to prepare Ru-dihydride catalysts of the type *trans*-Ru(H)₂(P-P)(N-N).^{79,86} Typically, **117** is allowed to react with the P-P and N-N ligands at 60 °C for 30 min in THF to displace the MeCN and COD ligands. The

resulting cationic Ru-allyl complexes are then mixed with the base, substrate, and placed under H₂.

For this study, we chose Bosnich's ligand (*S,S*)-skewphos¹⁶⁵ ((*S,S*)-2,4-bis(diphenylphosphino)pentane) as the diphosphine, and (*R,R*)-dpen as the diamine. This combination of ligands formed a selective active catalyst for the enantioselective hydrogenation of α -chiral amides with DKR under mild conditions (Chapter 3). The putative dihydride catalyst, *trans*-Ru(H)₂((*S,S*)-skewphos)((*R,R*)-dpen) (**128**) was prepared as described above, and utilized for the hydrogenation of the trifluoroacetyl amide **138** under 4 atm H₂ at room temperature in THF (Eq. 4.5).



The reaction occurred in 100% yield after 4 hours (TON = 100) to form 1-formylpiperidine, the product of the net catalytic C–C bond cleavage reaction by H₂. A similar cyclic amide, 2,2,2-trifluoro-1-(morpholin-4-yl)ethanone also underwent the catalytic C–C bond cleavage in 4 hours to give the corresponding formyl amine in 100% yield. The related acyclic amide 2,2,2-trifluoro-1-(diethylaminy)ethanone formed diethylformamide as the sole detectable product in 69% yield.

Assuming the catalyst in this reaction is *trans*-Ru(H)₂((*S,S*)-skewphos)((*R,R*)-dpen) (**128**), we prepared the dichloride *trans*-Ru(Cl)₂((*S,S*)-skewphos)((*R,R*)-dpen) (**135**) as a structural model for the catalyst. Figure 4.1 shows the solid-state structure of **135** as determined by X-Ray diffraction. The backbone of the (*S,S*)-skewphos is in the chair conformation with one methyl group in the axial

orientation and the other equatorial. This conformation holds the phenyl rings on phosphorus in a pseudo achiral spatial array.

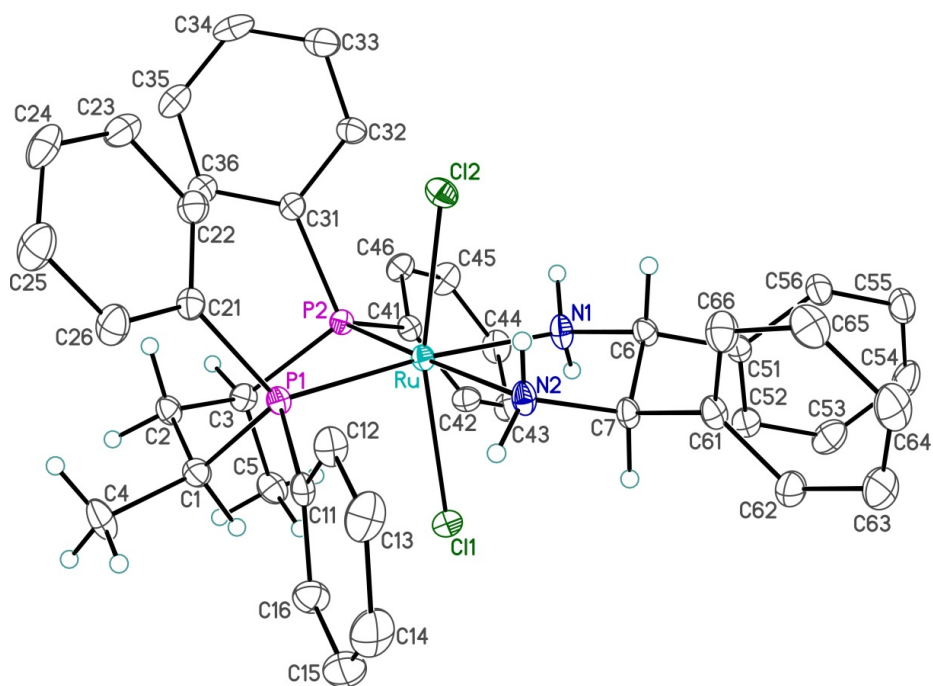


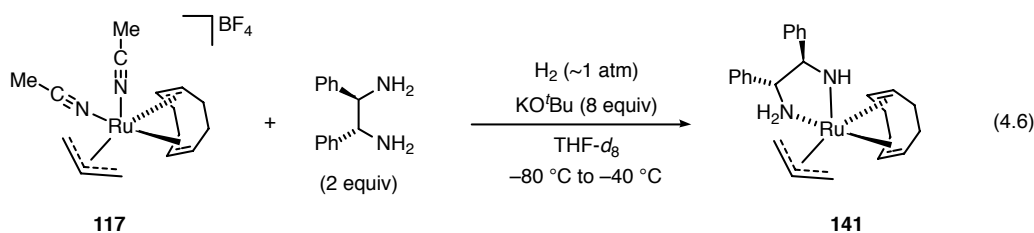
Figure 4.1: Solid state structure of *trans*-Ru(Cl)₂((*S,S*)-skewphos)((*R,R*)-dpen) (**135**) as determined by X-Ray diffraction with 30% probability of non-hydrogen atoms.

Perhaps the exigencies of crystal packing prevented the ligand from adopting the expected, more stable δ -skew conformation which would place both methyl groups equatorial and the phenyl rings in a chiral disposition.¹⁶⁵ As expected, the backbone of (*R,R*)-dpen is puckered in the λ -conformation with both phenyl rings equatorially disposed.

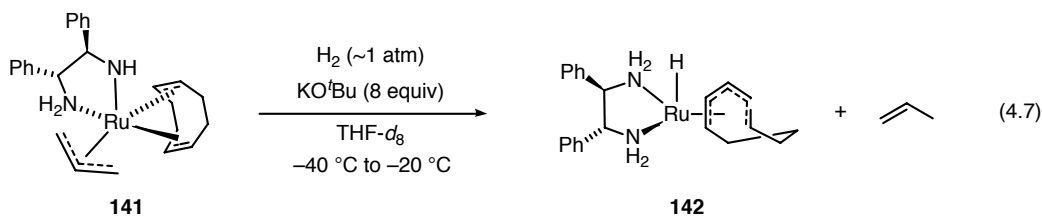
Remarkably, a phosphine-free catalyst, **140** could be prepared by replacing the (*S,S*)-skewphos with another equivalent of (*R,R*)-dpen. This putative bis(dpen) compound catalyzed the conversion of **138** into the formyl amine in 100% yield after 23 hours under the same mild conditions. The corresponding ethylenediamine

catalyst, made by reacting **117** with two equivalents of ethylenediamine, was also active, but with only 11% conversion after 15 hours.

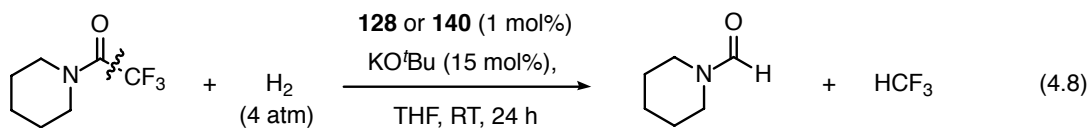
To investigate the nature of the catalyst and its reactivity, we monitored the reaction between the bis(acetonitrile) precursor **117** with two equivalents of (*R,R*)-dpen and 8 equivalents of KO^tBu under ~1 atm H₂ in THF-*d*₈ at -78 °C. At this temperature, the MeCN ligands were displaced by 1 equivalent of (*R,R*)-dpen to form the η³-C₃H₅ - amido complex **141**, with one NH₂ group in (*R,R*)-dpen deprotonated by the excess KO^tBu (Eq. 4.6). The compound was fully characterized in solution by ¹H NMR, ¹H-¹H gCOSY, ¹H-¹³C gHSQC, ¹H-¹⁵N gHSQC and TOCSY, ROESY NMR experiments (Figures 4.2 and 4.3).



Notably, the ¹H NMR chemical shift for the amido N-H group was -1.37 ppm. The shifts for the NH₂ protons were 4.87 and 5.13 ppm. The allyl, COD, and deprotonated diamine ligands in **142** were identified by the one spin system obtained in TOCSY NMR. Compound **141** loses propylene upon slow warming to ~ -20 °C. We tentatively propose that the transition metal product is the hydride **142**, with the C₈ ring bonded to Ru through an olefin and a η³-allyl group (Eq. 4.7). Bergens and coworkers showed a related pathway showing that the allylic activation of the COD ring followed by the elimination of propylene and the resulting C₈H₁₁ fragment is in part bonded to Ru as an η³-allyl.¹⁵²



The NMR peaks for **142** overlapped extensively, preventing its conclusive identification. The proposed structure would result from allylic activation of the 1-5 cyclooctadiene ring in **141**, followed by elimination of propylene. Further warming of the solution of **142** to room temperature resulted in the hydrogenation of propylene to propane, the hydrogenation of the acetonitrile to ethylamine, and the formation of unidentified ruthenium-containing products. All attempts to identify the ruthenium-containing products formed by warming the mixture **142** and (*R,R*)-dpen failed. The addition of the trifluoroacetyl amide **138** to this mixture, however, resulted in the formation of fluoroform, CHF_3 , as the major fluoride-containing product (identified by ^{19}F NMR and by a headspace analysis by GC-Mass Spectrometry). Thus the net catalytic reaction between **138** and the catalysts **128** and **140** is hydrogenolysis of the C–C bond to form 1-formylpiperidine and CHF_3 (Eq. 4.8).



While investigating the nature of **140**, we found that elemental mercury (200 equivalents) did not inhibit the hydrogenolysis catalyzed by **140**, and the activity of reduced Ru black was miniscule (~1% conversion) under these conditions. Taken together, these results suggest that **140** is a homogeneous Ru-H-dpen compound.

Conclusion

To our knowledge, the catalytic transformation of **138** into 1-formylpiperidine and fluoroform is the first catalytic hydrogenolysis of the sp^3 - sp^2 C-C bond in a trifluoro amide. The mild conditions, along with the absence of phosphine ligands are attractive features of this novel transformation. Efforts are underway in our laboratories to investigate the scope, the identity of the catalysts, and the mechanism of this reaction.

Materials and methods

Deuterated solvents were obtained from Aldrich and Cambridge Isotope Laboratories. Both THF- d_8 and THF were dried using Na/benzophenone just before each experiment. All pressurized reactions were carried out in a steel pressure reactor equipped with a magnetic stir bar. Potassium tert-butoxide was sublimed before use. Piperidine, potassium tert-butoxide, trifluoroacetic anhydride were obtained from Aldrich and (1*R*,2*R*)-1,2-diphenylethylenediamine was obtained from Alfa Aesar. ^1H , ^{13}C , and ^{19}F NMR spectra were recorded using 400 and 600 MHz Varian Inova, 500 MHz and 700 MHz Varian DirectDrive spectrometers. ^1H and ^{13}C NMR chemical shifts are reported in parts per million (δ) relative to TMS with the deuterated solvent as the internal reference. ^{19}F chemical shifts are reported in parts per million (δ) relative to CFCl_3 as the external references. NMR peak assignments were made using ^1H NMR, ^1H - ^1H gCOSY, ^1H - ^{13}C gHSQC, ^1H - ^{15}N gHSQC and TOCSY, ROESY NMR experiments. GC-MS analysis was performed by using a Hewlett Packard 5890 chromatograph equipped with a 5970B mass selective

detector and Supelco Beta DEX 225 capillary column (30 m × 0.25 mm × 0.25 μm film thickness). Elemental analysis data were obtained using a Carlo Erba CHNS-O EA1108 elemental analyzer.

Hydrogenation procedure

Cis-[Ru(η^3 -C₃H₅)(COD)(MeCN)₂]BF₄ (**117**, 0.025 mmol, 10.5 mg), 2 equivalents of (*R,R*)-dpen (0.05 mmol, 11.0 mg) (or 1 equivalent of (*R,R*)-dpen and 1 equivalent of (*S,S*)-skewphos) and KO^tBu (0.375 mmol, 42.1 mg) were weighed out into three NMR tubes in a glove box. Freshly distilled THF (0.8 mL) was then added by cannula under argon pressure into the tube containing (*R,R*)-dpen. The resultant solution was then cannulated into the NMR tube containing **117** under argon. It was then heated at 60 °C for 30 min with occasional shaking (pale brown, clear liquid). Meanwhile, the substrate (453 mg, 2.5 mmol, 100 equivalents) was dissolved in THF (1.0 mL) in an NMR tube, and added to a stainless steel autoclave under H₂ pressure and purged with hydrogen for 20 minutes. After 30 minutes KO^tBu in THF (0.7 mL) was added to the pre-heated NMR tube. The resulting orange/red solution was transferred to the autoclave under hydrogen pressure followed by a 2.5 mL THF wash. The autoclave was then pressurized to 4 atm H₂ and stirred at room temperature for 4 to 24 hours. The reaction was stopped by slowly depressurizing the autoclave and opening it to the atmosphere. The percent conversions were determined by ¹H NMR spectroscopy. The catalyst was removed by passing the solution through a florisil plug using CH₂Cl₂ as the rinse solvent. The solvent was

then removed under reduced pressure using a rotary evaporator and the NMR recorded using CDCl₃.

NMR study of the reaction between 117, ((R,R)-dpen), KO^tBu, H₂, and 138

Allylic precursor **117** (0.03 mmol, 12.6 mg), (*R,R*)-dpen (0.06 mmol, 12.7 mg) and KO^tBu (0.24 mmol, 26.9 mg) were weighed into three separate NMR tubes inside the glove box. Distilled THF-*d*₈ (0.5 mL) added to (*R,R*)-dpen by cannula under argon and ¹H NMR spectrum was recorded. Then the solution transferred to the NMR tube containing **117** under argon. Then the resulting solution was heated at 60 °C for 30 minutes with occasional shaking. After 30 minutes the ¹H and ¹⁹F NMR spectra were recorded. Then the solution temperature was decreased to -80 °C by immersing the NMR tube in dry ice/acetone mixture. The base in THF-*d*₈ (0.2 mL) was added to Ru-dpen mixture under hydrogen at -80 °C. The product was characterized by using ¹H, ¹⁹F, ¹H-¹⁵N HSQC, gTOCSY, gCOSY and gROESY NMR experiments in THF-*d*₈ at variable temperatures (-80 °C to room temperature). The *cis*-**117**/*(R,R)*-dpen/KO^tBu precatalyst was prepared again at -80 °C as described above and 10 equivalents of **138** was added at -60 °C. The reaction was monitored from -60 °C to room temperature.

Synthesis of 2,2,2-trifluoro-1-(piperidin-1-yl)ethanone (138).^{205,206} This is a modification of a literature procedure. 10.9 mL (7.9 g, 77.9 mmol) of triethylamine and 8.4 mL (7.3 g, 84.9 mmol) of piperidine were dissolved in 150 mL of stirred dichloromethane cooled in an ice/water bath. 10 mL (14.9 g, 70.8 mmol) of

trifluoroacetic anhydride was then added dropwise. The mixture was allowed to warm to room temperature and stirred overnight. The reaction mixture was washed with 2 × 50 mL of ~1 M HCl, with 2 × 50 mL distilled water and with 50 mL of brine. Then dried over sodium sulfate, and filtered. The organic solvent was removed under reduced pressure to yield **138** as a colorless oil (65%). The product purified by vacuum distillation (water aspirator) at 90 °C (boiling point 53 °C at 2.6 torr).²⁰⁵ ¹H NMR: (CDCl₃, 400 MHz, ppm): 3.54-3.64 (m, 4H); 1.65-1.71 (m, 6H).

N,N-Diethyl-2,2,2-trifluoroacetamide:²⁰⁷ Prepared as described above (60% yield, yellow oil). The product purified by passing through a neutral alumina plug. ¹H NMR: (CDCl₃, 498.118 MHz, ppm): 1.20-1.27 (m, 6H); 3.45-3.47 (m, 4H). The spectrum matches that reported for this compound.

Piperidine-1-carbaldehyde:²⁰⁸ ¹H NMR: (CDCl₃, 400MHz, ppm): 8.01(s, 1H); 3.29-3.50 (m, 4H); 1.52-1.78 (m, 6H).

N,N-Diethylformamide:²⁰⁹ ¹H NMR : (CDCl₃, 400 MHz, ppm): 8.05 (s, 1H); 3.37 (q, *J* 7.2 Hz, 2H); 3.27 (q, *J* 7.2 Hz, 2H); 1.19 (t, *J* 7.2 Hz, 3H); 1.13 (t, *J* 7.2 Hz, 3H).

trans-RuCl₂((*S,S*)-skewphos)((*R,R*)-dpen) (**135**) was prepared as reported previously.¹⁸³

Figure 4.2: ¹H NMR spectrum (δ 6.5 to -2.0 ppm) of [Ru(H₂NCH(Ph)CH(Ph)NH-)($\eta^{1,5}$ -C₈H₁₂)(η^3 -C₃H₅)]BF₄ (**141**) formed by the reaction of **117**, (*R,R*)-dpen, and KO^tBu in ~1 atm H₂ in THF-*d*₈ at -80 °C.

Residual solvent = δ ; coordinated (R,R)-dppe ligand, $\text{NH}_2 = \bullet$, $\text{NH}^- = \ominus$ $\text{CH} = \circ$; Non coordinated (R,R)-dppe ligand = \otimes , propylene = ϕ ; Free hydrogen gas = H ; ($\eta^3\text{-C}_3\text{H}_5$) = α ; ($\eta^{1,5}\text{-C}_8\text{H}_{12}$) = $*$

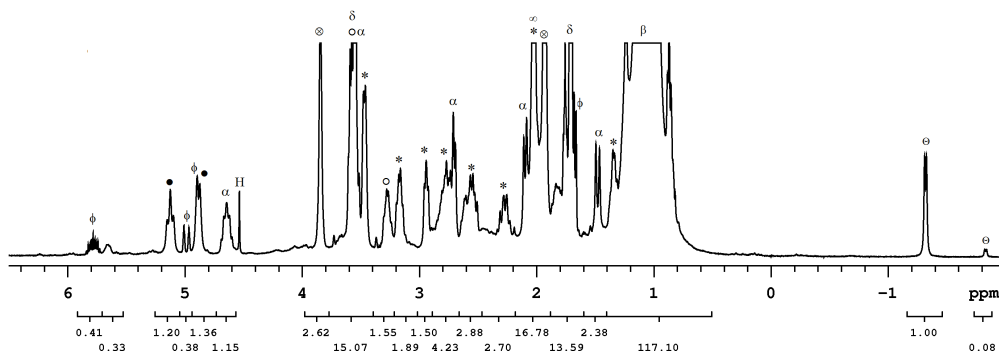


Figure 4.3a: ^1H NMR and zTOCSY1D spectrum (δ 6.5 to -2.0 ppm) of $[\text{Ru}(\text{H}_2\text{NCH}(\text{Ph})\text{CH}(\text{Ph})\text{NH}^-)(\eta^{1,5}\text{-C}_8\text{H}_{12})(\eta^3\text{-C}_3\text{H}_5)]\text{BF}_4$ (**141**) formed by the reaction of **117**, (R,R)-dppe, and KO^tBu in ~ 1 atm H_2 in $\text{THF-}d_8$ at -80 $^\circ\text{C}$. Spectrum top to bottom; Spectrum 1: zTOCSY1D, sel.excite @ -1.34 ppm. (Coordinated (R,R)-dppe ligand) Spectrum 2: zTOCSY1D, sel.excite @ 2.94 ppm. ($\eta^{1,5}\text{-C}_8\text{H}_{12}$) Spectrum 3: zTOCSY1D, sel.excite @ -1.34 ppm. ($\eta^3\text{-C}_3\text{H}_5$) Spectrum 4: ^1H NMR of $[\text{Ru}(\text{H}_2\text{NCH}(\text{Ph})\text{CH}(\text{Ph})\text{NH}^-)(\eta^{1,5}\text{-C}_8\text{H}_{12})(\eta^3\text{-C}_3\text{H}_5)]\text{BF}_4$

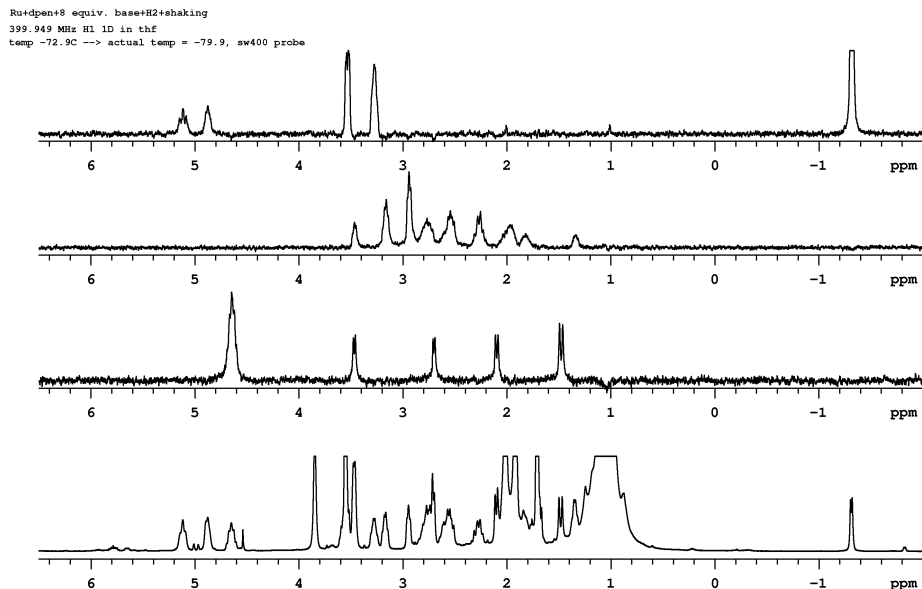
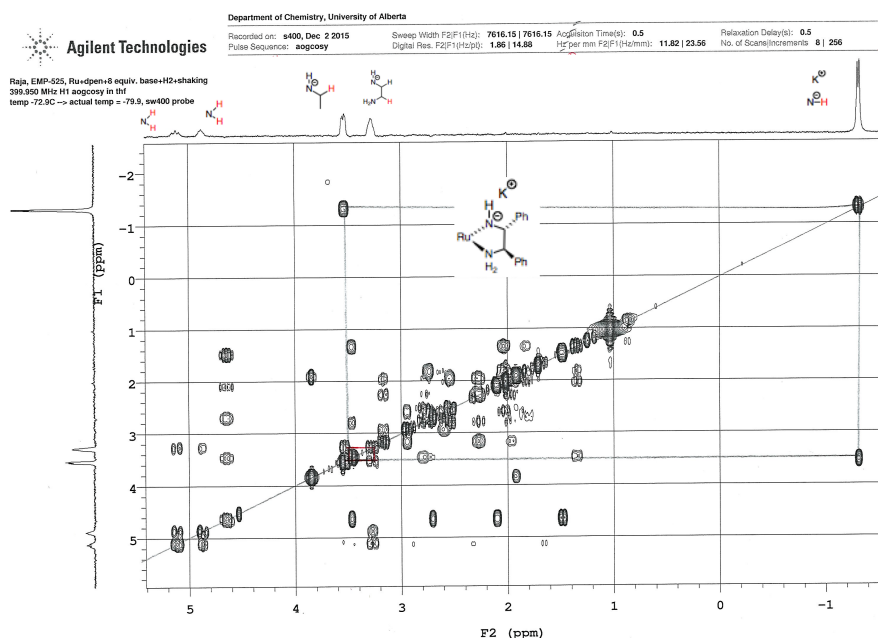


Figure 4.3b: ^1H - ^1H *g*COSY (vs. *z*TOCSY1D) of the product (**141**) formed by the reaction between **117**, (*R,R*)-*dppe*, and KO^tBu in ~ 1 atm H_2 in THF-d_8 .

Top: *g*COSY vs. *z*TOCSY1D of $\text{H}_2\text{NCH(Ph)CH(Ph)NH}^-$; middle: *g*COSY vs. *z*TOCSY1D of COD; bottom: *g*COSY vs. *z*TOCSY1D of $\eta^3\text{-C}_3\text{H}_5$



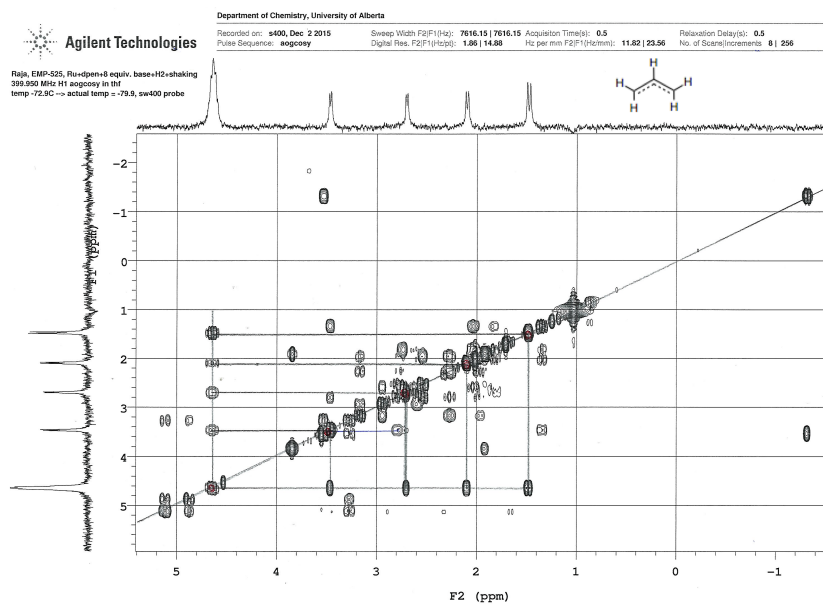
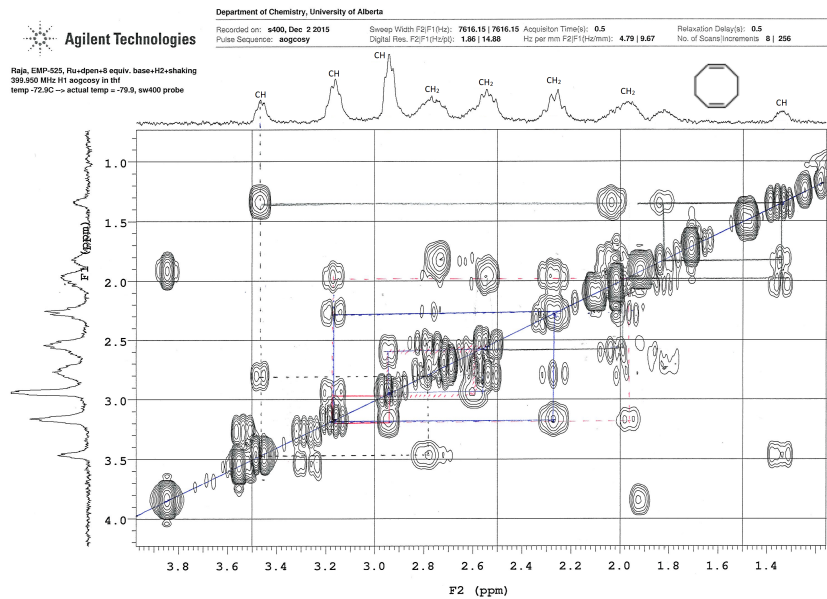


Figure 4.4: ¹H NMR spectrum (δ 6.5 to -2.0 ppm) of the product (**142**) formed by the reaction between **117**, (*R,R*)-dpen, and KO^tBu in ~ 1 atm H_2 in $THF-d_3$ at -20 °C.

Top: @ -20 °C; middle: @ -20 °C (after an hour); bottom: @ -20 °C (after 4 hours)

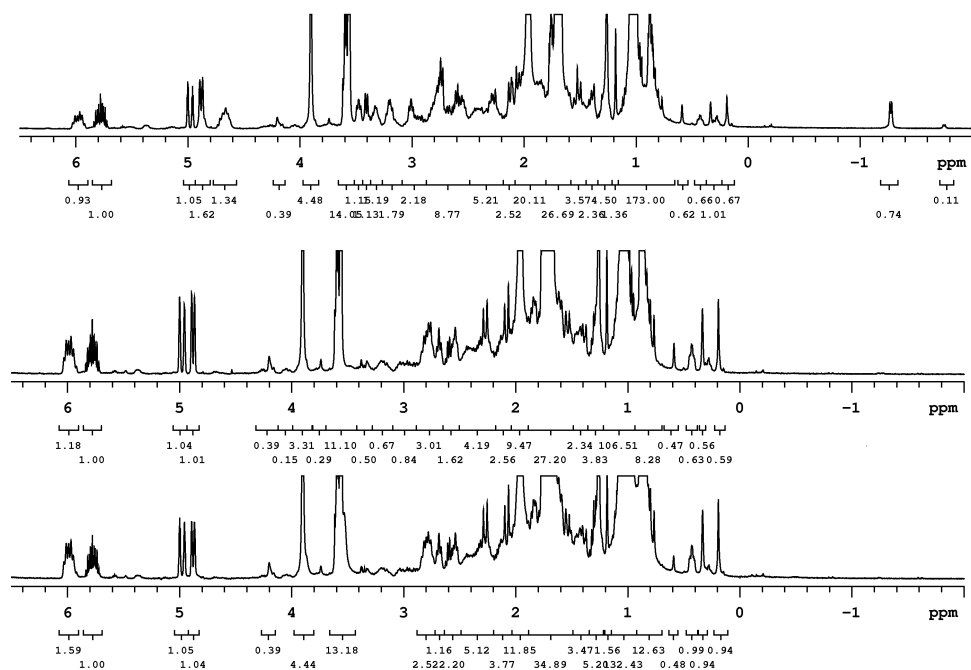


Figure 4.5: ¹H NMR spectrum (δ 9.0 to -12.0 ppm) of the product formed by the reaction between **117**, (*R,R*)-dpen, and KO^tBu in ~ 1 atm H_2 in $THF-d_8$ at RT.

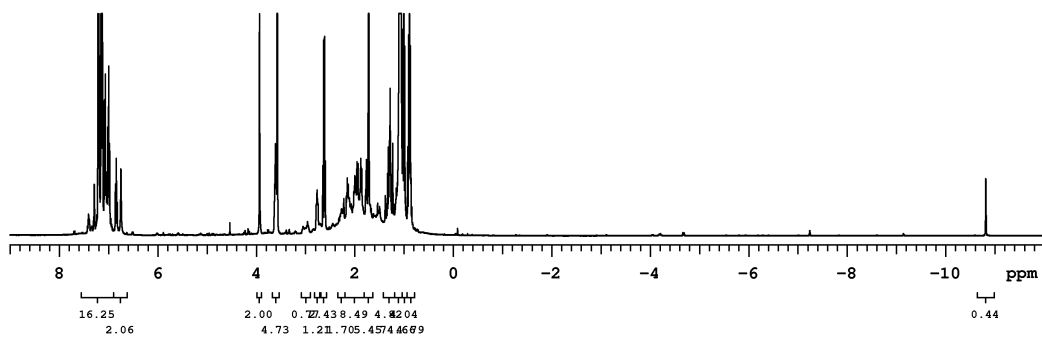


Figure 4.6: ¹H NMR spectrum (δ 5.0 to 0.0 ppm) of the product formed by the reaction between **117**, (*R,R*)-dpen, and KO^tBu in ~ 1 atm H_2 in $THF-d_8$ at RT.

Residual solvent = δ ; Non-coordinated (*R,R*)-dpen ligand = \otimes ; propane = P; Free hydrogen gas = H; Ethylamine = E

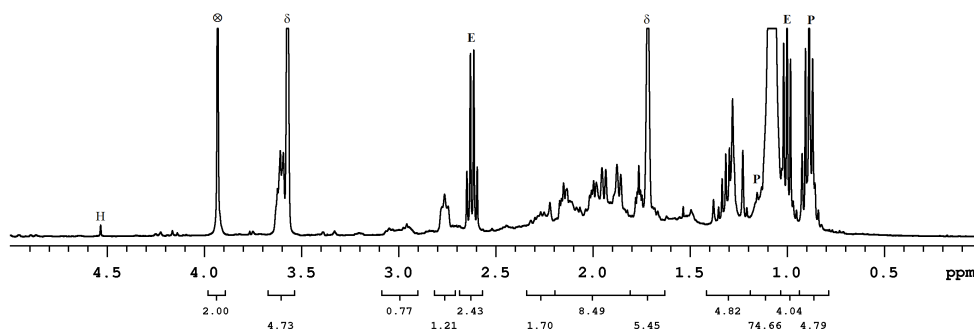


Figure 4.7: ^1H NMR and ^1H - ^{15}N NMR of a gHSQC spectrum (6 to -2 ppm) of $[\text{Ru}(\text{H}_2\text{NCH}(\text{Ph})\text{CH}(\text{Ph})\text{NH}-)(\eta^{1,5}\text{-C}_8\text{H}_{12})(\eta^3\text{-C}_3\text{H}_5)]\text{BF}_4$ (**141**) formed by the reaction of **117**, (*R,R*)-dpen, and KO^tBu in ~ 1 atm H_2 in THF-d_8 at -80 °C.

Coordinated (*R,R*)-dpen ligand, $\text{NH}_2 = \bullet$, $\text{NH}^- = \ominus$; Non coordinated (*R,R*)-dpen ligand = \otimes

Top: Only the first increment of ^1H - ^{15}N NMR of a gHSQC was recorded to show proton directly attached to nitrogen. The data were acquired at -80 °C using $^1J_{\text{H-}^{15}\text{N}} = 90$ Hz with the ^{15}N decoupler set at 90 ppm; Bottom: ^1H NMR of the mixture containing **141**.

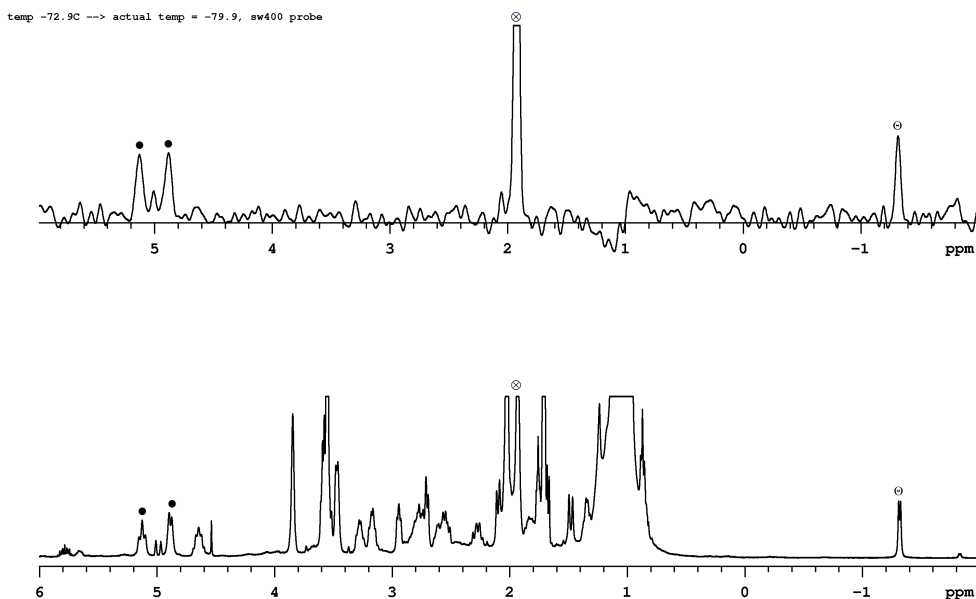
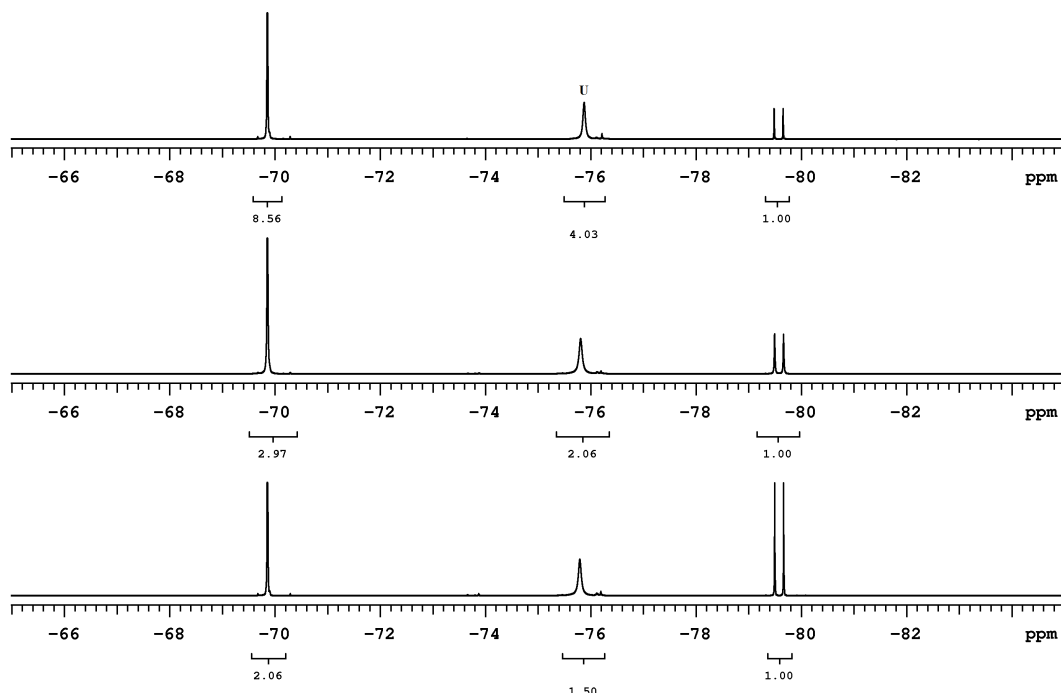


Figure 4.8: ^{19}F NMR spectrum (δ -65.0 to -85.0 ppm) of the product formed by the reaction between the catalyst and 10 equivalents of substrate **138** in THF-d_8 at room temperature at different times. (Unidentified intermediate = U)

Top: After 15 min; middle: after 16 hours; bottom: after 20 hours.



Control experiments

Hydrogenation using ruthenium nanoparticles

20.7 mg of Ruthenium black (0.014 mmol assuming 7% of Ru atoms are on the surface) were weighed into a test tube equipped with a magnetic stir bar and a rubber septum. After purging with hydrogen gas for 10 minutes the ruthenium black was reduced by heating at 60 °C for 30 minutes under hydrogen.²¹⁰ After 30 minutes the test tube placed inside the stainless steel autoclave equipped with the test tube holder and flushed with hydrogen using cannulas, needle lines, and

bubblers. **138** (1.25 mmol, 90 equivalents) in THF (1.0 mL) and KO^tBu (0.187 mmol, 14 equivalents) in THF (0.5 mL) were added using gas tight syringes under 1 atm H₂. Additional THF added to make the final volume to be 2.5 mL. Hydrogenated at 4 atm H₂ and stirred for 22 hours at room temperature.

Hydrogenations in the presence of Hg metal

117 (0.007 mmol, 3 mg), and 2 equivalents of (*R,R*)-dpen (0.014 mmol, 3.0 mg) were weighed out into a test tube equipped with stir bar and septum. Freshly distilled THF (0.5 mL) was then added by cannula under argon pressure into the test tube. It was then heated at 60 °C for 30 min while stirring (pale brown, clear liquid). After 30 minutes the resulting solution transferred to another test tube containing 200 equivalents of Hg (282.9 mg, 1.41 mmol) under 1 atm H₂ atmosphere. The substrate **138** (129.6 mg, 0.715 mmol, 100 equivalents) in THF (1.0 mL) and KO^tBu (0.107 mmol, 15 equivalents) in THF (0.5 mL) were added using gas tight syringe under 1 atm H₂ atmosphere. Additional THF added to make the final volume to be 2.5 mL. Hydrogenated at 4 atm H₂ and stirred for 22 hours at room temperature.

Table 4.1: *Crystallographic experimental details for trans-135*

A. Crystal Data

Formula	C ₄₅ H ₅₀ Cl ₆ N ₂ P ₂ Ru
Formula weight	994.58
Crystal dimensions (mm)	0.19 × 0.08 × 0.03
Crystal system	orthorhombic

Space group	$P2_12_12_1$ (No. 19)
Unit cell parameters ^a	
a (Å)	10.4622 (2)
b (Å)	17.2073 (3)
c (Å)	25.8113 (5)
V (Å ³)	4646.71 (15)
Z	4
ρ_{calcd} (g cm ⁻³)	1.422
μ (mm ⁻¹)	6.811
<i>B. Data Collection and Refinement Conditions</i>	
Diffractometer	Bruker D8/APEX II CCD ^b
Radiation (λ [Å])	Cu K α (1.54178) (microfocus source)
Temperature (°C)	-100
Scan type	ω and ϕ scans (1.0°) (5 s exposures)
Data collection 2θ limit (deg)	140.48
Total data collected	9431 ($-12 \leq h \leq 12$, $-20 \leq k \leq 21$, $-31 \leq l \leq 31$)
Independent reflections	9431 ($R_{\text{int}} = 0.1258$)
Number of observed reflections (NO)	8751 [$F_o^2 \geq 2\sigma(F_o^2)$]
Structure solution method	intrinsic phasing (<i>SHELXT-2014</i> ^c)
Refinement method	full-matrix least-squares on F^2 (<i>SHELXL-2013</i> ^c)

Absorption correction method	multi-scan (<i>TWINABS</i>)
Range of transmission factors	0.7533–0.5249
Data/restraints/parameters	9431 / 0 / 522
Flack absolute structure parameter ^d	-0.010(7)
Goodness-of-fit (<i>S</i>) ^e [all data]	1.051
Final <i>R</i> indices ^f	
$R_1 [F_o^2 \geq 2\sigma(F_o^2)]$	0.0415
wR_2 [all data]	0.1010
Largest difference peak and hole	0.822 and -0.971 e Å ⁻³

^aObtained from least-squares refinement of 9510 reflections with $6.84^\circ < 2\theta < 139.46^\circ$.

^bPrograms for diffractometer operation, data collection, data reduction and absorption correction were those supplied by Bruker.

^cSheldrick, G. M. *Acta Crystallogr.* **2008**, *A64*, 112–122.

^dFlack, H. D. *Acta Crystallogr.* **1983**, *A39*, 876–881; Flack, H. D.; Bernardinelli, G. *Acta Crystallogr.* **1999**, *A55*, 908–915; Flack, H. D.; Bernardinelli, G. *J. Appl. Cryst.* **2000**, *33*, 1143–1148. The Flack parameter will refine to a value near zero if the structure is in the correct configuration and will refine to a value near one for the inverted configuration.

^e $S = [\sum w(F_o^2 - F_c^2)^2 / (n - p)]^{1/2}$ (n = number of data; p = number of parameters varied; $w = [\sigma^2(F_o^2) + (0.0653P)^2 + 0.5429P]^{-1}$ where $P = [\text{Max}(F_o^2, 0) + 2F_c^2] / 3$).

$$fR_1 = \frac{\sum ||F_o| - |F_c||}{\sum |F_o|}; wR_2 = [\frac{\sum w(F_o^2 - F_c^2)^2}{\sum w(F_o^4)}]^{1/2}.$$

Table 4.2: Selected interatomic distances (Å) for **135**

(a) within the [RuCl₂{2,4-(Ph₂P)₂-pentane}{1,2-diphenylethylenediamine}] molecule

Atom1	Atom2	Distance	Atom1	Atom2	Distance
Ru	Cl1	2.4163(13)	C21	C22	1.392(9)
Ru	Cl2	2.4148(14)	C21	C26	1.397(8)
Ru	P1	2.2638(13)	C22	C23	1.389(9)
Ru	P2	2.2816(12)	C23	C24	1.373(11)
Ru	N1	2.170(5)	C24	C25	1.398(12)
Ru	N2	2.185(4)	C25	C26	1.386(10)
P1	C1	1.851(6)	C31	C32	1.401(8)
P1	C11	1.834(6)	C31	C36	1.406(8)
P1	C21	1.832(6)	C32	C33	1.380(9)
P2	C3	1.868(6)	C33	C34	1.384(10)
P2	C31	1.835(6)	C34	C35	1.388(10)
P2	C41	1.852(6)	C35	C36	1.387(9)
N1	H1NA	0.92(9)	C41	C42	1.400(8)
N1	H1NB	0.88(10)	C41	C46	1.394(8)
N1	C6	1.492(6)	C42	C43	1.387(8)
N2	H2NA	0.94(8)	C43	C44	1.375(10)

N2	H2NB	0.85(9)	C44	C45	1.384(10)
N2	C7	1.491(7)	C45	C46	1.390(8)
C1	C2	1.535(8)	C51	C52	1.389(8)
C1	C4	1.529(8)	C51	C56	1.389(7)
C2	C3	1.537(8)	C52	C53	1.404(9)
C3	C5	1.535(9)	C53	C54	1.384(11)
C6	C7	1.540(7)	C54	C55	1.387(11)
C6	C51	1.514(7)	C55	C56	1.377(9)
C7	C61	1.520(6)	C61	C62	1.380(8)
C11	C12	1.398(8)	C61	C66	1.390(9)
C11	C16	1.386(8)	C62	C63	1.393(8)
C12	C13	1.388(9)	C63	C64	1.372(11)
C13	C14	1.389(12)	C64	C65	1.390(10)
C14	C15	1.380(12)	C65	C66	1.388(8)
C15	C16	1.393(9)			

Table 4.3: Selected interatomic angles (deg) for **135**

(a) within the $[RuCl_2\{2,4-(Ph_2P)_2\text{-pentane}\}\{1,2\text{-diphenylethylenediamine}\}]$ molecule

Atom1	Atom2	Atom3	Angle	Atom1	Atom2	Atom3	Angle
Cl1	Ru	Cl2	163.58(5)	P1	C1	C2	110.4(4)
Cl1	Ru	P1	90.17(5)	P1	C1	C4	115.4(4)

Cl1	Ru	P2	94.35(5)	C2	C1	C4	109.5(5)
Cl1	Ru	N1	86.05(16)	C1	C2	C3	116.8(5)
Cl1	Ru	N2	83.17(15)	P2	C3	C2	111.4(4)
Cl2	Ru	P1	97.15(5)	P2	C3	C5	114.6(4)
Cl2	Ru	P2	100.20(5)	C2	C3	C5	112.1(5)
Cl2	Ru	N1	85.06(16)	N1	C6	C7	108.4(4)
Cl2	Ru	N2	81.55(15)	N1	C6	C51	112.5(5)
P1	Ru	P2	90.85(5)	C7	C6	C51	111.0(5)
P1	Ru	N1	172.98(14)	N2	C7	C6	108.1(4)
P1	Ru	N2	95.16(13)	N2	C7	C61	112.7(4)
P2	Ru	N1	95.32(13)	C6	C7	C61	110.7(4)
P2	Ru	N2	173.49(13)	P1	C11	C12	118.4(5)
N1	Ru	N2	78.53(18)	P1	C11	C16	122.5(4)
Ru	P1	C1	114.0(2)	C12	C11	C16	118.4(5)
Ru	P1	C11	109.75(16)	C11	C12	C13	120.6(6)
Ru	P1	C21	121.8(2)	C12	C13	C14	120.4(7)
C1	P1	C11	103.7(3)	C13	C14	C15	119.4(6)
C1	P1	C21	102.6(3)	C14	C15	C16	120.2(7)
C11	P1	C21	103.1(3)	C11	C16	C15	121.0(6)
Ru	P2	C3	117.49(18)	P1	C21	C22	119.1(5)
Ru	P2	C31	118.64(18)	P1	C21	C26	122.7(5)
Ru	P2	C41	115.23(17)	C22	C21	C26	118.1(6)

C3	P2	C31	102.2(3)	C21	C22	C23	121.0(6)
C3	P2	C41	100.6(2)	C22	C23	C24	120.1(7)
C31	P2	C41	99.7(2)	C23	C24	C25	120.3(7)
Ru	N1	H1NA	106(5)	C24	C25	C26	119.1(7)
Ru	N1	H1NB	113(6)	C21	C26	C25	121.4(7)
Ru	N1	C6	112.5(4)	P2	C31	C32	117.1(4)
H1NA	N1	H1NB	105(8)	P2	C31	C36	125.0(5)
C6	N1	H1NA	109(5)	C32	C31	C36	117.9(5)
C6	N1	H1NB	111(6)	C31	C32	C33	121.0(6)
Ru	N2	H2NA	105(4)	C32	C33	C34	120.5(6)
Ru	N2	H2NB	102(5)	C33	C34	C35	119.6(6)
Ru	N2	C7	111.3(3)	C34	C35	C36	120.2(6)
H2NA	N2	H2NB	114(7)	C31	C36	C35	120.7(6)
C7	N2	H2NA	111(4)	P2	C41	C42	119.5(4)
C7	N2	H2NB	114(6)	P2	C41	C46	122.5(4)
C42	C41	C46	117.9(5)	C53	C54	C55	119.2(6)
C41	C42	C43	121.4(6)	C54	C55	C56	120.8(6)
C42	C43	C44	119.9(6)	C51	C56	C55	120.8(6)
C43	C44	C45	119.6(6)	C7	C61	C62	120.5(5)
C44	C45	C46	120.9(6)	C7	C61	C66	121.2(5)
C41	C46	C45	120.2(6)	C62	C61	C66	118.3(5)
C6	C51	C52	120.8(5)	C61	C62	C63	120.9(6)

C6	C51	C56	120.4(5)	C62	C63	C64	120.1(7)
C52	C51	C56	118.8(5)	C63	C64	C65	120.1(6)
C51	C52	C53	120.3(6)	C64	C65	C66	119.2(6)
C52	C53	C54	120.0(7)	C61	C66	C65	121.4(6)

Chapter 5

Conclusion and Future Directions

Amide reduction without stoichiometric hydride reagents is one of the key areas of research that required improvement or a greener approach.¹ Significant improvements in the catalytic hydrogenation of amides have been achieved in the past decade. Several heterogeneous⁴²⁻⁵³ and homogeneous catalytic systems have been developed for the hydrogenation of amides. The heterogeneous catalysts favor net C–O cleavage and operates typically at $T > 130$ °C under 30–100 atm H₂. The drawbacks of these heterogeneous catalytic systems are the hydrogenation of aromatic, alkene, and alkyne groups as side reactions. Also, it has not been demonstrated that the heterogeneous catalysts tolerate a wide variety of functional groups. Homogeneous catalysts hydrogenate amides under acidic, basic, or neutral conditions. Acidic conditions favor net C–O cleavage^{54-58,62,66-71} while both basic and neutral conditions lead to net C–N cleavage^{72-80,85-95} products.

The research attending this dissertation developed a base-free catalyst system as described in Chapter 2.⁸⁶ Preliminary NMR studies showed that the reaction between the allyl-precursor **51** and 2 equivalents of NaBH₄ gives the *trans*-RuH(η^1 -BH₄)(Ph₂P(CH₂)₂NH₂)₂ (**61**) complex. This catalyst **61** hydrogenates amides to corresponding alcohol and the amine at 100 °C under 50 atm H₂ with up to a 100% yield (TON = 1000) in THF in the absence of added base. In particular, under similar conditions, **61** was more active towards the hydrogenation of 2° amides

than 3° amides. The hydrogenation of a less reactive oxazolidone (Evan's chiral auxiliaries) by **61** also showed that the absolute configurations are preserved at stereogenic carbon centres in groups attached to nitrogen, and in group alpha to the carbonyl group under base-free conditions.

Chapter 3 describes the high throughput screening (HTS) and optimization reactions performed to discover the first asymmetric catalytic system for the hydrogenation of α -chiral amides via DKR. Recently Bergens and coworkers found that mono or di deprotonation at the N-H groups of the **50** occurred with the excess base. They also found that the *trans*-K⁺[RuH₂((*R*)-BINAP)(*R,R*-H₂NCH(Ph)CH(Ph)NH⁽⁻⁾)] (**54-K**) is extremely active for the bifunctional addition as low as at -80 °C under ~2 atm H₂ towards cyclic imide and amide substrates.⁸⁵ These results showed that a racemic α -chiral amide (with acidic hydrogen at α -position) could be hydrogenated at low temperature and pressure in the presence of excess base via DKR. Motivated by these results, a high throughput screening (HTS) experiment was designed to find the catalysts candidates. With the results from the HTS and extensive lab-scale optimization reactions, a novel catalytic system, *trans*-RuCl₂((*S,S*)-skewphos)((*R,R*)-dpen) (**135**), was developed. The *trans*-**135** operates under only 4 atm H₂ pressure at room temperature to give the chiral primary alcohols by hydrogenation of amides with >99% *ee* in the presence of 2-PrONa and 2-PrOH. It is shown that high *ee*'s can be obtained with the addition of 2-PrOH. Previous studies show that alcohols inhibit the catalyst by forming secondary and primary Ru alkoxides by reacting with Ru amides such as **58**, but his process is reversible in the presence of the base.^{81,161} At low pressure, a higher amount of base

ensured both racemization of the substrate and activity of the catalyst. A large amount of base also probably deprotonate the N-H at **135** to form an active deprotonated species. A higher turnover numbers reaction (TON~93) was demonstrated by increasing the H₂ pressure from 4 atm to 50 atm without affecting the *ee* significantly.

Chapter 4 describes an unforeseen hydrogenolysis of sp³-sp² C-C bond with a phosphine-free homogeneous catalyst under mild conditions.¹⁶⁰ During the development of the amide hydrogenation catalytic system, we observed an unusual reaction. Hydrogenation of an amide, 2,2,2-trifluoro-1-(piperidine-1-yl)ethanone produced 1-formylpiperidine and fluoroform via hydrogenolysis of sp³-sp² C-C bond instead of the expected C-N cleavage products. Preliminary mechanistic studies ensured a homogeneous 'Ru-H' complex is responsible for this hydrogenolysis. However, all the attempts for the definitive identification of the Ru-H species responsible for this transformation were unsuccessful.

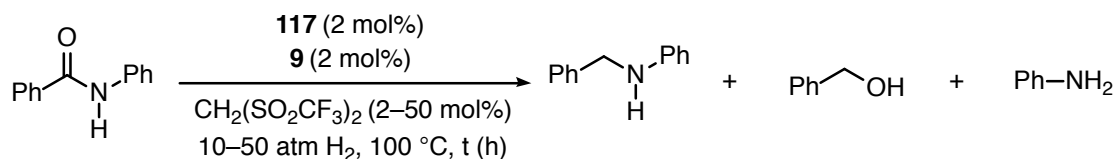
Future work

Green Chemistry is a key theme in the current era and catalysis often provides greener strategies over conventional approaches. Indeed, the recent advances in catalytic hydrogenation of amides allow the reduction of amides under ≤50 atm H₂ and at 100 °C. There are however many challenges, and questions need to be addressed to make this reaction a viable pilot process. Traditional reduction of amides using stoichiometric reagents generally gives the C-O cleavage products. The current catalytic systems, however, produce both C-O and C-N cleavage

products. The catalytic selectivity for these products needs to be studied in detail. Although, heterogeneous catalysts favor net C–O cleavage, a system with functional group tolerance and that operates under mild conditions is yet to be developed. [Ru(Triphos)] catalyst do hydrogenate amides with a preference for C–O cleavage. However, the actual catalytic species that participate in these hydrogenations are yet to be identified. The identification and understanding of this active species will help to develop catalytic systems with higher activity and utility.

I performed some preliminary experiments to develop a catalytic system for the hydrogenation of amides via C–O cleavage. I used the catalytic system containing **117/9**/bis(trifluoromethanesulfonyl)methane with benzanilide as the model substrate. Table 5.1 shows the reaction conditions and selectivity for the hydrogenation of benzanilide.

Table 5.1: Screening studies for the hydrogenation of benzanilide under acidic condition.^(a)



entry	Cat:acid:sub	P/atm	t/h	THF:IPA	%Conv ^(b)	%Conv	%Conv	Selectivity for C–O
						C–O	C–N	
1	1:3:50	30	18	8:0	63.4	13.8	49.5	21.8
2	1:10:50	10	20	8:0	54.8	21.2	33.6	38.6
3	1:20:50	10	22	8:0	54.8	20	34.8	36.5

4	1:10:50	30	24	1:5	65.6	48.8	16.8	74.4
5 ^(c)	1:10:50	50	16	0.5:5.5	50	39	11	78
7 ^(d)	1:10:50	30	18	0.5:5.5	68	58.6	9.9	85.5

(a) Reaction conditions: Hydrogenation was performed at 100 °C unless otherwise noted. (b) Determined using ¹H NMR spectroscopy. (c) Reaction performed at 80 °C (d) Ph-NH₂ (100 mol%) added; Cat:acid:sub:Ph-NH₂ 1:10:50:50.

Increasing the amount of acid (entry 2 and 3) didn't improve the yield or selectivity. Selectivity was increased in 2-PrOH/THF solvent mixture (entries 4–7) than in THF alone. Significantly, the hydrogenation was carried out at under 50 atm H₂ at 80 °C with 50% conversion (TON = 50) in 16 hours (entry 5). Interestingly, the addition of the aniline into the reaction mixture increased the selectivity for C–O cleavage. This result indicates that the hydrogenation of benzanilide may proceed to give C–N cleavage products (aniline and benzyl alcohol), which then form the imine by condensation. The hydrogenation of imine then provides the net C–O cleavage products. These preliminary results are promising but require additional experiments to develop a catalytic system for the hydrogenation of amides via C–O cleavage under mild conditions.

General procedure for acid-assisted hydrogenations of benzanilide

Catalyst preparation: **117** (12.6 mg, 30.0 μmol), **9** (18.7 mg, 30.0 μmol), and CH₂(SO₂CF₃)₂ (30.0–750 μmol) were weighed out into three separate NMR tubes in a glove box. THF (0.5 mL) was then added by cannula under argon pressure into the NMR tube containing **9** at room temperature. This solution was then transferred by

cannula under argon into the NMR tube containing **117** at room temperature. The mixture was then heated at 60 °C for 30 min under with periodic mixing. After 30 min, the mixture was then added to the NMR tube containing the acid and was then used for the hydrogenations described below.

General procedures for hydrogenation: The benzanilide (1500 μmol , 50 equivalents) was added to a stainless steel autoclave equipped with a magnetic stir bar. The autoclave was then purged with H_2 for 20 min at room temperature. The catalyst, **117/9/acid** prepared above was then added by cannula under H_2 pressure followed by a THF or 2-PrOH washes using a gas tight syringe. The autoclave was then pressurized to 10–50 atm H_2 . The reaction mixture was stirred at 70–100 °C for 16–24 hours. The autoclave was then allowed to cool over the course of 1 hour before venting at room temperature. The % conversions were determined by ^1H NMR spectroscopy.

In Chapter 2, the alcohols from the hydrogenation could inhibit the catalytic activity. Developing a catalytic system that could be used in a flow reactor may help to reduce the build-up of alcohol during the hydrogenation and thus allow high turnovers. Preliminary NMR studies showed the clean formation of *trans*- $\text{RuH}(\eta^1\text{-BH}_4)(\text{Ph}_2\text{P}(\text{CH}_2)_2\text{NH}_2)_2$ from the reaction between the allyl-precursor **51** and NaBH_4 . Isolation of **61** and the characterization of its stability could allow the preparation of several pre-catalyst analogs.

In Chapter 3, the addition of 2-PrOH increased the *ee* of the alcohol products but also inhibit the catalytic activity by forming the Ru-alkoxide. Another possible

role of the 2-PrOH is increasing the polarity of the reaction medium and thus the rate of racemization of the amides substrates. Understanding the role of the 2-PrOH will help to choose the proper type (e.g. a bulky alcohol) of alcohol that doesn't compete with the active catalyst. The minimum quantity of alcohol required will reduce the amount of base for the hydrogenation.

Chapter 4 describes hydrogenolysis of an sp^3 - sp^2 C-C bond with a phosphine-free homogeneous catalyst. Understanding the active catalyst and the mechanism will help to widen the application of the challenging C-C bond cleavage.

References:

1. Busacca, C. A.; Fandrick, D. R.; Song, J. J.; Senanayake, C. H. Transition Metal Catalysis in the Pharmaceutical Industry. In *Application of Transition Metal Catalysis in Drug Discovery and Development: An Industrial Perspective*; Crawley, M. L., Trost, B. M., Eds.; John Wiley & Sons, Inc.: Hoboken, NJ, 2012; p 2.
2. North American Catalysis, Society. Available at <http://nacatsoc.org/above/what-is-catalysis/> accessed on 28th March 2017.
3. Ranade, V. V.; Joshi, S. S. Catalysis and Catalytic Process In *Industrial Catalytic process for Fine and Specialty Chemicals*; Ranade, V. V.; Joshi, S. S., Eds.; Elsevier: 2016; p1
4. Green, S. J. *Industrial Catalysis*; E. Benn Limited: London, 1928; pp1–2.
5. van Leeuwen, P. W. N. M. *Homogeneous Catalysis: Understanding the art*; Kluwer Academic Publishers: Dordrecht, Netherlands, 2004; pp 1, 75.
6. Laidler, K. J. *Pure Appl. Chem.* **1996**, *68*, 149–192.
7. Chatterjee, S. *Phys. Chem. Chem. Phys.* **2016**, *18*, 20033–20046.
8. Nutman, A. P.; Bennett, V. C.; Friend, C. R. L.; Van Kranendonk, M. J.; Chivas, A. R. *Nature* **2016**, *537*, 535–538.
9. Buchholz, K.; Collins, J. *Appl. Microbiol. Biotechnol.* **2013**, *97*, 3747–3762.
10. Recent example: Milton, R. D.; Cai, R.; Abdellaoui, S.; Leech, D.; De Lacey, A. L.; Pita, M.; Minter, S. D. *Angew. Chem. Int. Ed.* **2017**, *56*, 2680–2683.

11. Review example: Jahangiri, H.; Bennett, J.; Mahjoubi, P.; Wilson, K.; Gu, S. *Catal. Sci. Technol.* **2014**, *4*, 2210–2229.
12. Review example: Palo, D. R.; Dagle, R. A.; Holladay, J. D. *Chem. Rev.* **2007**, *107*, 3992–4021.
13. Review example: Iulianelli, A.; Liguori, S.; Wilcox, J.; Basile, A. *Catal. Rev.* **2016**, *58*, 1–35.
14. Review example: Vogt, E. T. C.; Weckhuysen, B. M. *Chem. Soc. Rev.* **2015**, *44*, 7342–7370.
15. Miller, E. L. *J. Midwifery Womens Health* **2002**, *476*, 426–434.
16. Eisch, J. J. *Organometallics* **2012**, *31*, 4917–4932.
17. Keith, J. A.; Henry, P. M. *Angew. Chem. Int. Ed.* **2009**, *48*, 9038–9049.
18. Osborn, J. A.; Jardine, F. H.; Young, J. F.; Wilkinson, G. J. *Chem. Soc. A*, **1966**, 1711–1732.
19. Albini, A.; Protti, S. *Paradigms in Green Chemistry and Technology; Springer Briefs in Green Chemistry for Sustainability*; Springer: New York, 2015; pp 1–8.
20. Constable, D. J. C.; Dunn, P. J.; Hayler, J. D.; Humphrey, G. R.; Leazer, J. L.; Linderman, R. J.; Lorenz, K.; Manley, J.; Pearlman, B. A.; Wells, A.; Zaks, A.; Zhang, T. Y. *Green Chem.* **2007**, *9*, 411–420.
21. Smith, A. M.; Whyman, R. *Chem. Rev.* **2014**, *114*, 5477–5510.
22. Allen, F. H.; Kennard, O.; Watson, D. G.; Brammer, L.; Orpen, A. G.; Taylor, R. J. *Chem. Soc. Perkin Trans.* **1987**, *2*, S1–S19.

23. Jones, J. *Core Carbonyl Chemistry*; Oxford Primer Series No. 47; Oxford University Press: New York, 1997; pp 48–49.
24. Clayden, J.; Greeves, N.; Warren, S. *Organic Chemistry*, 2nd ed.; Oxford University Press: New York, 2012; p 155.
25. Volkov, A.; Tinnis, F.; Slagbrand, T.; Trillo, P.; Adolfsson, H. *Chem. Soc. Rev.* **2016**, *45*, 6685–6697.
26. Carey, J. S.; Laffan, D.; Thomas, C.; Williams, M. T. *Org. Biomol. Chem.* **2006**, *4*, 2337–2347.
27. Magano, J.; Dunetz, J. R. *Org. Process Res. Dev.* **2012**, *16*, 1156–1184.
28. Bannister, R. M.; Brookes, M. H.; Evans, G. R.; Katz, R. B.; Tyrrell, N. D. *Org. Process Res. Dev.* **2000**, *4*, 467–472.
29. Alimardanov, A.; Nikitenko, A.; Connolly, T. J.; Feigelson, G.; Chan, A. W.; Ding, Z.; Ghosh, M.; Shi, X.; Ren, J.; Hansen, E.; Farr, R.; MacEwan, M.; Tadayon, S.; Springer, D. M.; Kreft, A. F.; Ho, D. M.; Potoski, J. R. *Org. Process Res. Dev.* **2009**, *13*, 1161–1168.
30. Tao, J.; Kazlauskas, R. J. *Biocatalysis for Green Chemistry and Chemical Process Development, First ed.*; Wiley-VCH: Weinheim, Germany, 2011.
31. Jimenez-Gonzales, C.; Curzons, A. D.; Constable, D. J. C.; Cunningham, V. L. *Int. J. Life Cycle Assess* **2004**, *9*, 115–121.
32. US Department of Commerce, Economics and Statistic Administration, US Census Bureau, US Department of Transportation, Bureau of Transportation statistics (1999); 1997 Economic Census, Transportation. 1997 Commodity Flow Survey (Issued 1999), EC97TFC-US.

33. Smith, M. B. *Organic Synthesis*, 3rd ed.; Academic Press: Boston, 2010; p 422.
34. Kubas, G. J. *Chem. Rev.* **2007**, *107*, 4152–4205.
35. Nishimura, S., Ed. *Heterogeneous Catalytic Hydrogenations for Organic Synthesis*; John Wiley & Sons, Inc.: New York, 2001.
36. Ohkuma, T.; Ooka, H.; Hashiguchi, S.; Ikariya, T.; Noyori, R. *J. Am. Chem. Soc.* **1995**, *117*, 2675–2676.
37. Ohkuma, T.; Koizumi, M.; Doucet, H.; Pham, T.; Kozawa, M.; Murata, K.; Katayama, E.; Yokozawa, T.; Ikariya, T.; Noyori, R. *J. Am. Chem. Soc.* **1998**, *120*, 13529–13530.
38. Ohkuma, T.; Koizumi, M.; Ikehira, H.; Yokozawa, T.; Noyori, R. *Org. Lett.* **2000**, *2*, 659–662.
39. Chaplin, D.; Harrison, P.; Henschke, J. P.; Lennon, I. C.; Meek, G.; Moran, P.; Pilkington, C. J.; Ramsden, J. A.; Watkins, S.; Zanotti-Gerosa, A. *Org. Process Res. Dev.* **2003**, *7*, 89–94.
40. Blaser, H. -U.; Pugin, B.; Spindler, F. Asymmetric Hydrogenation. In *Organometallics as Catalysts in the Fine Chemical Industry*; Beller, M.; Blaser, H. -U., Eds.; Springer-Verlag: Berlin, 2012; Vol. 42, p 65.
41. Goto, M.; Konishi, T.; Kawaguchi, S.; Yamada, M.; Nagata, T.; Yamano, M. *Org. Process Res. Dev.* **2011**, *15*, 1178–1184.
42. Wojcik, B.; Adkins, H. *J. Am. Chem. Soc.* **1934**, *56*, 2419–2424.
43. Sauer, J. C.; Adkins, H. *J. Am. Chem. Soc.* **1938**, *60*, 402–406.
44. Galinovsky, F.; Stern, E. *Ber. dtsh. Chem. Ges. A/B* **1943**, *76*, 1034–1038.
45. Guyer, A.; Bieler, A.; Gerliczy, G. *Helv. Chim. Acta* **1955**, *38*, 1649–1654.

46. Hirosawa, C.; Wakasa, N.; Fuchikami, T. *Tetrahedron Lett.* **1996**, *37*, 6749–6752.
47. Beamson, G.; Papworth, A. J.; Phillips, C.; Smith, A. M.; Whyman, R. *Adv. Synth. Catal.* **2010**, *352*, 869–883.
48. Beamson, G.; Papworth, A. J.; Phillips, C.; Smith, A. M.; Whyman, R. *J. Catal.* **2010**, *269*, 93–102.
49. Beamson, G.; Papworth, A. J.; Phillips, C.; Smith, A. M.; Whyman, R. *J. Catal.* **2011**, *278*, 228–238.
50. Stein, M.; Breit, B. *Angew. Chem. Int. Ed.* **2013**, *52*, 2231–2234.
51. Coetzee, J.; Manyar, H. G.; Hardacre, C.; Cole-Hamilton, D. J. *ChemCatChem* **2013**, *5*, 2843–2847.
52. Nakagawa, Y.; Tamura, R.; Tamura, M.; Tomishige, K. *Sci. Technol. Adv. Mater.* **2015**, *16*, 014901.
53. Shimizu, K.; Onodera, W.; Touchy, A. S.; Siddiki, S. M. A. H.; Tayao, T.; Kon, K. *ChemistrySelect.* **2016**, *4*, 736–740.
54. Kilner, M.; Tyers, D. V.; Crabtree, S. P.; Wood, M. A. Davy Process Technology Limited, UK; Patent WO03093208A1, 2003.
55. Magro, A. A. N.; Eastham, G. R.; Cole-Hamilton, D. *Chem. Commun.* **2007**, 3154–3156.
56. Eastham, G. R.; Cole-Hamilton, D. J.; Magro, A. A. N. Lucite International UK Limited, UK; Patent WO2008035123A2, 2008; p 36.

57. Dodds, D. L.; Coetzee, J.; Klankermeyer, J.; Brosinski, S.; Leitner, W.; Cole-Hamilton, D. J. *Chem. Commun.* **2012**, *48*, 12249 (Published additions and corrections to Reference 55).
58. Coetzee, J.; Dodds, D. L.; Klankermeyer, J.; Brosinski, S.; Leitner, W.; Slawin, A. M. Z.; Cole-Hamilton, D. J. *Chem. Eur. J.* **2013**, *19*, 11039–11050.
59. Barbaro, P.; Bianchini, C.; Meli, A.; Moreno, M.; Vizza, F. *Organometallic*, **2002**, *21*, 1430–1437.
60. Hasanayn, F.; Morris, R. H. *Inorg. Chem.* **2012**, *51*, 10808–10818.
61. Geilen, F. M. A.; Engendahl, B.; Hölscher, M.; Klankermeyer, J.; Leitner, W. *J. Am. Chem. Soc.* **2011**, *133*, 14349–14358.
62. vom Stein, T.; Meuresch, M.; Limper, D.; Schmitz, M.; Hölscher; Coetzee, J.; Cole-Hamilton, D. J.; Klankermeyer, J.; Leitner, W. *J. Am. Chem. Soc.* **2014**, *136*, 13217–13225.
63. Cui, X.; Li, Y.; Topf, C.; Junge, K.; Beller, M. *Angew. Chem. Int. Ed.* **2015**, *54*, 5196–5200.
64. Crabtree, R. H. *Chem. Rev.* **2016**, *116*, 8750–8769.
65. Perutz, R. N.; Sabo-Etienne, S. *Angew. Chem. Int. Ed.* **2007**, *46*, 2578–2592.
66. Ito, T.; Horino, H.; Koshiro, Y.; Yamamoto, A. *Bull. Chem. Soc. Jpn.* **1982**, *55*, 504–512.
67. Cabrero-Antonino, J. R.; Alberico, E.; Junge, K.; Junge, H.; Beller, M. *Chem. Sci.* **2016**, *7*, 3432–3442.
68. Yuan, M.-L.; Xie, J.-H.; Zhou, Q.-L. *ChemCatChem.* **2016**, *8*, 3036–3040.

69. Parks, D. J.; Piers, W. E.; Parvez, M.; Atencio, R.; Zaworotko, M. J. *Organometallic* **1998**, *17*, 1369–1377.
70. Meuresch, M.; Westhues, S.; Leitner, W.; Klankermayer, J. *Angew. Chem. Int. Ed.* **2016**, *55*, 1392–1395.
71. Yuan, M.-L.; Xie, J.-H.; Zhu, S.-F.; Zhou, Q.-L. *ACS Catal.* **2016**, *6*, 3665–3669.
72. Ito, M.; Koo, L. W.; Himizu, A.; Kobayashi, C.; Sakaguchi, A.; Ikariya, T. *Angew. Chem. Int. Ed.* **2009**, *48*, 1324–1327.
73. Ikariya, T.; Ito, M.; Ootsuka, T.; Hashimoto, T. Tokyo Institute of Technology, Japan; Central Glass Company Limited; Patent WO2010073974A1, 2010; p 31.
74. Ito, M.; Ootsuka, T.; Watari, R.; Shiibashi, A.; Himizu, A.; Ikariya, T. *J. Am. Chem. Soc.* **2011**, *133*, 4240–4242.
75. Balaraman, E.; Gnanaprakasam, B.; Shimon, L. J. W.; Milstein, D. *J. Am. Chem. Soc.* **2010**, *132*, 16756–16758.
76. Milstein, D.; Gunanathan, C.; Ben-David, Y.; Balaraman, E.; Gnanaprakasam, B.; Zhang, H. Yeda Research and Development Company Limited, Israel; Patent US2012253042A1, 2012.
77. Barrios-Francisco, R.; Balaraman, E.; Diskin-Posner, Y.; Leitner, G.; Shimon, L. J. W.; Milstein, D. *Organometallics* **2013**, *32*, 2973–2982.
78. Cantillo, D. *Eur. J. Inorg. Chem.* **2011**, *19*, 3008–3013.
79. John, J. M.; Bergens, S. H. *Angew. Chem. Int. Ed.* **2011**, *50*, 10377–10380.
80. Bergens, S. H.; John, J. M. University of Alberta, Canada; Patent WO2013010275A1, 2013; p 95.

81. Hamilton, R. J.; Bergens, S. H. *J. Am. Chem. Soc.* **2006**, *128*, 13700–13701.
82. Hamilton, R. J.; Bergens, S. H. *J. Am. Chem. Soc.* **2008**, *130*, 11979–11987.
83. Takebayashi, S.; Bergens, S. H. *Organometallics* **2009**, *28*, 2349–2351.
84. Takebayashi, S.; John, J. M.; Bergens, S. H. *J. Am. Chem. Soc.* **2010**, *132*, 12832–12834.
85. John, J. M.; Takebayashi, S.; Dabral, N.; Miskolzie, M.; Bergens, S. H. *J. Am. Chem. Soc.* **2013**, *135*, 8578–8584.
86. John, J. M.; Loorthuraja, R.; Antoniuk, E.; Bergens, S. H. *Catal. Sci. Technol.* **2015**, *5*, 1181–1186.
87. Miura, T.; Held, I. E.; Oishi, S.; Naruto, M.; Saito, S. *Tetrahedron Lett.* **2013**, *54*, 2674–2678.
88. Kita, Y.; Higuchi, T.; Mashima, K. *Chem. Commun.* **2014**, *50*, 11211–11213.
89. Cabrero-Antonino, J. R.; Alberico, E.; Drexler, H.-J.; Baumann, W.; Junge, K.; Junge, H.; Beller, M. *ACS Catal.* **2016**, *6*, 47–54.
90. Shi, L.; Tan, X.; Long, J.; Xiong, X.; Yang, S.; Xue, P.; Lv, H.; Zhang, X. *Chem. Eur. J.* **2017**, *23*, 546–548.
91. Garg, J. A.; Chakraborty, S.; Ben-David, Y.; Milstein, D. *Chem. Commun.* **2016**, *52*, 5285–5288.
92. Assmann, M.; Balmer, M.; Harms, K.; Langer, R. *Organometallics* **2016**, *35*, 1931–1943.
93. Rezayee, N. M.; Samblanet, D. C.; Sanford, M. S. *ACS Catal.* **2016**, *6*, 6377–6383.
94. Jajarathne, U.; Zhang, Y.; Hazari, N.; Bernskoetter, W. H. *Organometallics*

- 2017**, 36, 409–416.
95. Papa, V.; Cabrero-Antonino, J. R.; Alberico, E.; Spanneberg, A.; Junge, K.; Junge, H.; Beller, M. *Chem. Sci.* **2017**, 8, 3576–3585.
 96. Clayden, J.; Greeves, N.; Warren, S. *Organic Chemistry*, 2nd ed.; Oxford University Press: New York, 2012.
 97. Rachwalski, M.; Vermue, N.; Rutjes, F. P. J. T. *Chem. Soc. Rev.* **2013**, 42, 9268–9282.
 98. Matthews, S. J.; McCoy, C. *Clin. Ther.* **2003**, 25, 342–395.
 99. Minnaard, A. J.; Feringa, B. L.; Lefort, L.; de Vries, J. G. *Acc. Chem. Res.* **2007**, 40, 1267–1277.
 100. Sakai, K.; Hirayama, N.; Tamura, R. *Novel Optical Resolution Technologies*; Springer-Verlag Berlin, Heidelberg, 2007; *Top. Curr. Chem.*, Vol. 269/2006
 101. Fogassy, E.; Nogradi, M.; Kozma, D.; Egri, G.; Palovics, E.; Kiss, V. *Org. Biomol. Chem.* **2006**, 4, 3011–3030.
 102. Harrington, P. J.; Lodewijk, E. *Org. Process Res. Dev.* **1997**, 1, 72–76.
 103. Lorenz, H.; Seidel-Morgenstern, A. *Angew. Chem. Int. Ed.* **2014**, 53, 1218–1250.
 104. Faber, K. *Biotransformations in Organic Chemistry*, 6th ed.; Springer: Heidelberg, 2011; p 7.
 105. Scott, J. W. Readily Available Chiral Carbon Fragments and their use in Synthesis. In *Asymmetric Synthesis*; Morrison, J. D., Ed.; Academic Press: New York, 1984; vol. 4, pp 1–226.
 106. Knowles, W. S.; Sabacky, M. J. *Chem. Commun.* **1968**, 24, 1445–1446.

107. Horner, L.; Siegel, H.; Buthe, H. *Angew. Chem. Int. Ed.* **1968**, *12*, 942.
108. Knowles, W. S. *Angew. Chem. Int. Ed.* **2002**, *41*, 1998–2007.
109. Knowles, W. S. Asymmetric Hydrogenations–The Monsanto L-Dopa Process. In *Asymmetric Catalysis on Industrial Scale: Challenges, Approaches and Solutions*; Blaser, H. -U., Schmidt, E., Eds.; Wiley-VCH Verlag GmbH & Co. KGaA: Weinheim, 2004; pp 21–38.
110. Selke, R. The Other L-Dopa Process. In *Asymmetric Catalysis on Industrial Scale: Challenges, Approaches and Solutions*; Blaser, H. -U., Schmidt, E., Eds.; Wiley-VCH Verlag GmbH & Co. KGaA: Weinheim, 2004; pp 39–53.
111. Ager, D. J.; de Vries, A. H. M.; de Vries, J. G. *Chem. Soc. Rev.* **2012**, *41*, 3340–3380.
112. Blaser, H. -U.; Buser, H. -P.; Jalett, H. -P.; Pugin, B.; Spindler, F. *Synlett.* **1999**, 867–868.
113. Blaser, H. -U.; Lotz, M.; Spindler, F. Asymmetric Catalytic Hydrogenation Reactions with Ferrocene-Based Diphosphine Ligands. In *Handbook of Chiral Chemicals*, 2nd ed; Ager, D. J., Eds. CRC-Taylor Francis: Boca Raton, 2006; pp 294–296.
114. Blaser, H. -U.; Spindler, F.; Studer, M. *Appl. Catal., A* **2001**, *221*, 119–143.
115. Noyori, R. *Angew. Chem. Int. Ed.* **2002**, *41*, 2008–2022.
116. Miyashita, A.; Yasuda, A.; Takaya, H.; Toriumi, K.; Ito, T.; Souchi, T.; Noyori, R. *J. Am. Chem. Soc.* **1980**, *102*, 7932–7934.
117. Noyori, R.; Ohkuma, T.; Kitamura, M.; Takaya, H.; Sayo, N.; Kumobayashi, H.; Akutagawa, S. *J. Am. Chem. Soc.* **1987**, *109*, 5856–5858.

118. Laneman, S. A. Transition Metal Catalyzed Hydrogenation, Isomerizations, and Other Reactions. In *Handbook of Chiral Chemicals*, 2nd ed; Ager, D. J., Eds. CRC-Taylor Francis: Boca Raton, 2006; p 186.
119. Akutagawa, S. *Appl. Catal., A* **1995**, *128*, 171–207.
120. Moss, G. P. *Pure Appl. Chem.* **1996**, *68*, 2193–2222.
121. Vedejs, E.; Jure, M. *Angew. Chem. Int. Ed.* **2005**, *44*, 3974–4001.
122. Seeman, J. I. *Chem. Rev.* **1983**, *83*, 83–134.
123. Gawley, R. E. *J. Org. Chem.* **2006**, *71*, 2411–2416.
124. Balcells, D.; Maseras, F. *New J. Chem.* **2007**, *31*, 333–343.
125. Scalone, M.; Waldmeier, P. *Org. Process Res. Dev.* **2003**, *7*, 418–425.
126. Sun, Y.; Krska, S.; Shultz, C. S.; Teller, D. M. Enabling Asymmetric Hydrogenation for the Design of Efficient Synthesis of Drug Substrates. In *Asymmetric Catalysis on Industrial Scale: Challenges, Approaches and Solutions*, 2nd ed.; Blaser, H. -U., Federsel, H. -J., Eds.; Wiley-VCH Verlag GmbH & Co. KGaA: Weinheim, 2010; p 333.
127. de Vries, J. G.; Lefort, L. *Oil & Gas Science and Technology-Rev. IFP Energies nouvelles*, **2013**, *68*, 519–528.
128. Shultz, C. S.; Krska, S. W. *Acc. Chem. Res.* **2007**, *40*, 1320–1326.
129. McWilliams, C. J.; Sidler, R. D.; Sun, Y.; Mathre, D. J. *J. Assoc. Lab. Auto.* **2005**, *10*, 394–407.
130. Rubin, A. E.; Tummala, S.; Both, D. A.; Wang, C. C.; Delaney, E. J. *Chem. Rev.* **2006**, *106*, 2794–2810.

131. Chen, C. -Y.; Frey, L. F.; Shultz, S.; Wallace, D. J.; Marcantonio, K.; Payack, J. F.; Vazquez, E.; Springfield, S. A.; Zhou, G.; Liu, P.; Kieczkowski, G. R.; Chen, A. M.; Phenix, B. D.; Singh, U.; Strine, J.; Izzo, B.; Krska, S. W. *Org. Process Res. Dev.* **2007**, *11*, 616–623.
132. Hansen, K. B.; Hsiao, Y., Xu, F.; Rivera, N.; Clausen, A.; Kubryk, M.; Krska, S.W.; Rosner, T.; Simmons, B.; Armstrong, J.D.III. *J. Am. Chem. Soc.* **2009**, *131*, 8798–8804.
133. Ohkuma, T.; Koizumi, M.; Muñiz, K.; Hilt, G.; Kabuto, C.; Noyori, R. *J. Am. Chem. Soc.* **2002**, *124*, 6508–6509.
134. Sandoval, C.; Ohkuma, T.; Muñiz, K.; Noyori, R. *J. Am. Chem. Soc.* **2003**, *125*, 13490–13503.
135. *Examples of carbonyl hydrogenation catalysts containing $\eta^1\text{-BH}_4^-$* (Ref 30–34): Guo, R.; Chen, X.; Elpelt, C.; Song, D.; Morris. *Org. Lett.* **2005**, *7*, 1757–1759.
136. Zhang, J.; Balaraman, E.; Leitun, G.; Milstein, D. *Organometallics* **2011**, *30*, 5716–5724.
137. Langer, R.; Iron, M. A.; Konstantinovski, L.; Diskin-Posner, Y.; Leitun, G.; Ben-David, Y.; Milstein, D. *Chem. Eur. J.* **2012**, *18*, 7196–7209.
138. Ino, Y.; Yoshida, A.; Kuriyama, W. Takasago International Corporation, Japan; Patent EP1970360A1, 2008; p 26.
139. Ino, Y. Kuriyama, W.; Ogata, O.; Matsumoto, T. *Top. Catal.* **2010**, *53*, 1019–1024.

140. Green, T. W.; Wuts, P. G. M. *Protective Groups in Organic Synthesis*, Wiley-Interscience, New York, **1999**, 550–555, 740–743.
141. (a) Evans, D. A.; Ennis, M. D.; Mathre, D. J. *J. Am. Chem. Soc.* **1982**, *104*, 1737–1739. (b) Das, S.; Addis, D.; Zhou, S.; Junge, K.; Beller, M. *J. Am. Chem. Soc.* **2010**, *132*, 1770–1771. (c) Hong, G.; Wu, S.; Zhu, X.; Mao, D.; Wang, L. *Tetrahedron* **2016**, *72*, 436–441. (d) Mai, W.-P.; Song, G.; Yuan, J.-W.; Yang, L.-R.; Sun, G.-C.; Xiao, Y.-M.; Mao, P.; Qu, L.-B. *RSC Adv.* **2013**, *3*, 3869–3872. (e) Zhu, Y.-P.; Sergeyev, S.; Franck, P.; Orru, R. V. A.; Maes, B. U. W. *Org. Lett.* **2016**, *18*, 4602–4605. (f) Xie, W.; Zhao, M.; Cui, C. *Organometallics* **2013**, *32*, 7440–7444.
142. Abdur-Rashid, K.; Guo, R.; Lough, A. J.; Morris, R. H.; Song, D. *Adv. Synth. Catal.* **2005**, *347*, 571–579.
143. M. J. Hass, M.Sc. Thesis, University of Alberta, **2011**.
144. Shibasaki, T.; Komine, N.; Hirano, M.; Komiya, S. *J. Organomet. Chem.* **2007**, *692*, 2385–2394. (b) A modified procedure to prepare **115** is reported herein.
145. Ohkuma, T. *Proc. Jpn. Acad. Ser. B*, **2010**, *86*, 202–219.
146. Klingler, F. D. *Acc. Chem. Res.* **2007**, *40*, 1367–1376.
147. Noyori, R.; Tokunga, M.; Kitamura, M. *Bull. Chem. Soc. Jap.* **1995**, *68*, 36–56.
148. Xie, J.-H.; Zhou, Z.-T.; Kong, W.-L.; Zhou, Q.-L. *J. Am. Chem. Soc.* **2007**, *129*, 1868–1869.
149. Zhou, Z.-T.; Xie, J.-H.; Zhou, Q.-L. *Adv. Synth. Catal.* **2009**, *351*, 363–366.
150. Li, X.; List, B. *Chem. Commun.* **2007**, 1739–1741.

151. Saudan, L, A. Hydrogenation of Esters. In *Sustainable Catalysis: Challenges and Practices for the Pharmaceutical and Fine Chemical Industries*; Dunn, P. J., Hii, K. K., Krische, M. J., Williams, M. T., Eds.; Wiley: Weinheim, 2013; pp 42–45.
152. A related pathway is allylic activation of the COD ring to eliminate propylene and the resulting C₈H₁₁ fragment is bonded to Ru as a π -allyl in [Ru(η^3 -C₈H₁₁)(P–P)(N–N)]BF₄. See; Wiles, J. A.; Daley, C. J. A.; Hamilton, R. J.; Leong, C. G.; Bergens, S. H. *Organometallics* **2004**, *23*, 4564–4568.
153. Control reactions showed the precursor **117** is inactive in the absence of added P or N ligands under these conditions.
154. Miyazawa, T.; Yukawa, T.; Koshiha, T.; Sakamoto, H.; Ueji, S.; Yanagihara, R.; Yamada, T. *Tetrahedron: Asymmetry* **2001**, *12*, 1595–1602.
155. Ager, D. J.; Prakash, I.; Shaad, D. R. *Chem. Rev.* **1996**, *96*, 835–875.
156. Bedore, M. W.; Zaborenko, N.; Jensen, K. F.; Jamison, T. F. *Org. Process. Res. Dev.* **2010**, *14*, 432–440.
157. Yadav, J. S.; Reddy, A. R.; Narsaiah, A. V.; Reddy, B. V. S. *J. Mol. Catal. A.* **2007**, *261*, 207–212.
158. Bose, D. S.; Narsaiah, A. V. *Bioorg. Med. Chem.* **2005**, *3*, 627–630.
159. Corey, E. J.; Zhang, F. *Angew. Chem. Int. Ed.* **1999**, *38*, 1931–1934.
160. Rasu, L.; Rennie, B.; Miskolzie, M.; Bergens, S. H. *Aust. J. Chem.* **2016**, *69*, 561–564.
161. Hamilton, R. J.; Leong, C. G.; Bigam, G.; Miskolzie, M.; Bergens, S. H. *J. Am. Chem. Soc.* **2005**, *127*, 4152–4153.

162. Kador, P. F.; Wyman, M.; Betts, D. M. US Pat. 8158667 B2, Apr. 17, **2012**.
163. Dirlam, N. L.; Moore, B. S.; Urban, F. J. *J. Org. Chem.* **1987**, *52*, 3587–3591.
164. Boucher, H.; Bosnich, B. *Inorg. Chem.* **1976**, *15*, 1471–1477.
165. MacNeil, P. A.; Roberts, N. K.; Bosnich, B. *J. Am. Chem. Soc.* **1981**, *103*, 2273–2280.
166. Bosnich, B.; Roberts, N. K. *Adv. Chem. Ser.* **1982**, *196*, 337–354.
167. Bakos, J.; Toth, I.; Heil, B.; Szalontai, G.; Párkányi, L.; Fülöp, V. *J. Organomet. Chem.* **1989**, *370*, 263–276.
168. Jánosi, L.; Kollár, L.; Macchi, P.; Sironi, A. *J. Organomet. Chem.* **2006**, *691*, 2846–2852.
169. Hartmann, R.; Chen, P. *Angew. Chem. Int. Ed.* **2001**, *40*, 3581–3585.
170. Hartmann, R.; Chen, P. *Adv. Synth. Catal.* **2003**, *345*, 1353–1359.
171. Dub, P. A.; Henson, N. J.; Martin, R. L.; Gordon, J. C. *J. Am. Chem. Soc.* **2014**, *136*, 3505–3521.
172. Dub, P. A.; Gordon, J. C. *Dalton Trans.* **2016**, *45*, 6756–6781.
173. For examples see Ref 173–175: Hedberg, C.; Kallstrom, K.; Arvidsson, P. I.; Brandt, P.; Andersson, P. G. *J. Am. Chem. Soc.* **2005**, *727*, 15083–15090.
174. Hadzovic, A.; Song, D.; MacLaughlin, C. M.; Morris, R. H. *Organometallics* **2007**, *26*, 5987–5999.
175. Wylie, W. N. O.; Lough, A. J.; Morris, R. H. *Organometallics* **2012**, *31*, 2137–2151.

176. Gualtieri, F.; Bottalico, C.; Calandrella, A.; Dei, S.; Giovannoni, M. P.; Mealli, S.; Romanelli, M. N.; Scapecchi, S.; Teodori, E.; Galeotti, N.; Ghelardini, C.; Giotti, A.; Bartolini, A. *J. Med. Chem.* **1994**, *37*, 1712–1719.
177. Watanabe, K.; Koshiha, T.; Yasufuku, Y.; Miyazawa, T.; Ueji, S. *Bioorganic Chemistry*, **2001**, *29*, 65–76.
178. Deffieux, D.; Fabre, I.; Courselle, C.; Quideau, S. *J. Org. Chem.* **2002**, *67*, 4458–4465.
179. Yasufuku, Y.; Ueji, S. *Bioorganic Chemistry*, **1997**, *25*, 88–99.
180. Koul, S.; Koul, J. L.; Singh, B.; Kapoor, M.; Parshad, R.; Manhas, K. S.; Taneja, S. C.; Qazi, G. N. *Asymmetry* **2005**, *16*, 2575–2591.
181. Tessier, P.; Ajamian, A.; Dominguez, C.; Chantigny, Y. A.; Deziel, R.; Leit, S.; Smil, D. METHYLGENE INC. Canada, Patent WO2008/122115A1, 2008, p.46.
182. Preti, L.; Attanasi, O. A.; Caselli, E.; Favi, G.; Ori, C.; Davoli, P.; Felluga, F.; Prati, F. *Eur. J. Org. Chem.* **2010**, *22*, 4312–4320.
183. Akotsi, O. M.; Metera, K.; Reid, R. D.; McDonald, R.; Bergens, S. H. *Chirality* **2000**, *12*, 514–522.
184. Sutter, M.; Sotto, N.; Raoul, Y.; Méfay, E.; Lemaire, M. *Green Chem.* **2013**, *15*, 347–352.
185. Cheshire, D.; Cladingboel, D.; Hirst, S.; Manners, C.; Stocks, M.; AstraZeneca AB; Patent US 6300352B1, **2001**.
186. van der Zeijden, A. A. H.; Mattheis, C. *J. Organomet. Chem.* **1999**, *584*, 274–285.
187. Lin, Y-S.; Lin, C-Y.; Liu, C-W.; Tsai, T. Y. R. *Tetrahedron* **2006**, *62*, 872–877.

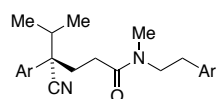
188. Lu, H-f.; Zhou, J-t .; Cheng, H-l.; Sun, L-l.; Yang, F-f.; Wu, R-Z.; Gao, Y-h.; Luo, Z. *B. Tetrahedron* **2013**, *69*, 11174–11184.
189. Antonio, A.; Romina, C.; Gianni, P.; Samuele, R.; Sergio, S. *Tetrahedron* **2001**, *57*, 4039–4043.
190. Jones, W, D. Mechanistic Studies of Transition Metal-Mediated C-C Bond Activation. In *C-C Bond Activation*; Dong, G., Eds.; Springer: Berlin, 2014; Vol. 346, pp 1–2.
191. Ruhland, K. *Eur. J. Org. Chem.* **2012**, *14*, 2683–2706.
192. Souillart, L.; Cramer, N. *Chem. Rev.* **2015**, *115*, 9410–9464.
193. Halpern, J. *Acc. Chem. Res.* **1982**, *15*, 238–244.
194. Khoury, P. R.; Goddard, J. D.; Tam, W. *Tetrahedron* **2004**, *60*, 8103–8112.
195. Chen, F.; Wang, T.; Jiao, N. *Chem. Rev.* **2014**, *114*, 8613–8661.
196. Sarkar, A.; Santa, S.; Kundu, S. K.; Hajra, A.; Zyryanov, G. V.; Chupakhin, O. N.; Charushin, V. N.; Majee, A. *Green Chem.* **2016**, *18*, 4475–4525.
197. Gerack, G. J.; McElwee-White, L. *Molecules* **2014**, *19*, 7689–7713.
198. Blicke, F. F.; Lu, C.-J. *J. Am. Chem. Soc.* **1952**, *74*, 3933–3934.
199. Rahman, M.; Kundu, D.; Hajra, A.; Majee, A. *Tetrahedron Lett.* **2010**, *51*, 2896–2899.
200. Li, W.; Wu, X.-F. *Chem. Eur. J.* **2015**, *21*, 14943–14948.
201. Kothandaraman, J.; Kar, S.; Sen, R.; Goepfert, A.; Olah, G. A.; Surya Prakash, G. K. *J. Am. Chem. Soc.* **2017**, *139*, 2549–2552.
202. Daw, P.; Chakraborty, S.; Leitus, G.; Diskin-Posner, Y.; Ben-David, Y.; Milstein, D. *ACS Catal.* **2017**, *7*, 2500–2504.

203. Tlili, A.; Blondiaux, E.; Frogneux, X.; Cantat, T. *Green Chem.* **2015**, *17*, 157–168.
204. Zhang, L.; Han, Z.; Zhao, X.; Wang, Z.; Ding, K. *Angew. Chem. Int. Ed.* **2015**, *54*, 6186–6189.
205. Schenck, H. A.; Lenkowski, P. W.; Choudhury-Mukherjee, I.; Ko, S.-H.; Stables, J. P.; Patel, M. K.; Brown, M. L. *Bioorg. Med. Chem.* **2004**, *12*, 979–993.
206. Lu, X.; Cseh, S.; Byun, H.-S.; Tigyi, G.; Bittman, R. *J. Org. Chem.* **2003**, *68*, 7046–7050.
207. Smith, D. P.; Anderson, J.; Plante, J.; Ashcroft, A. E.; Radford, S. E.; Wilson, A. J.; Parker, M. J. *Chem. Commun.* **2008**, *11*, 5728–5730.
208. Ortega, N.; Richter, C.; Glorius, F. *Org. Lett.* **2013**, *15*, 1776–1779.
209. Chong, C. C.; Kinjo, R. *Angew. Chem. Int. Ed.* **2015**, *54*, 12116–12120.
210. Markiewicz, M. E. P, *PhD Thesis*, University of Alberta, 2011.

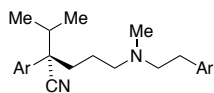
Appendices

Compound Numbers and Structures

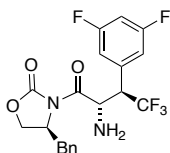
Chapter 1



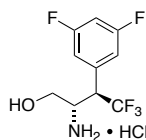
1



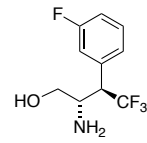
2



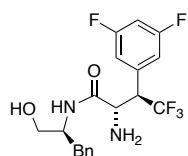
3



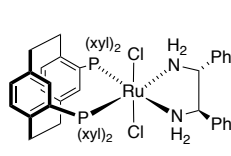
4



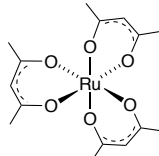
5



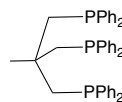
6



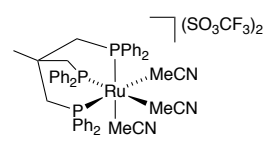
7



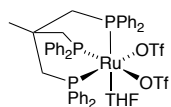
8



9



10



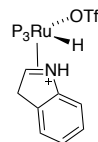
11



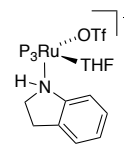
12



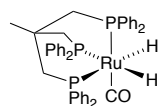
13



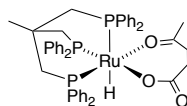
14



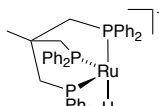
15



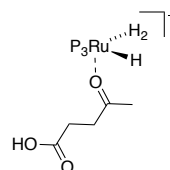
16



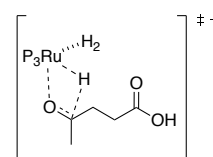
17



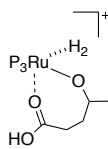
18



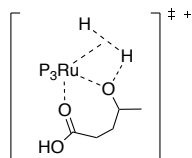
19



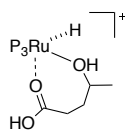
20



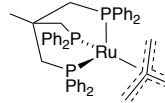
21



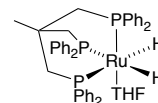
22



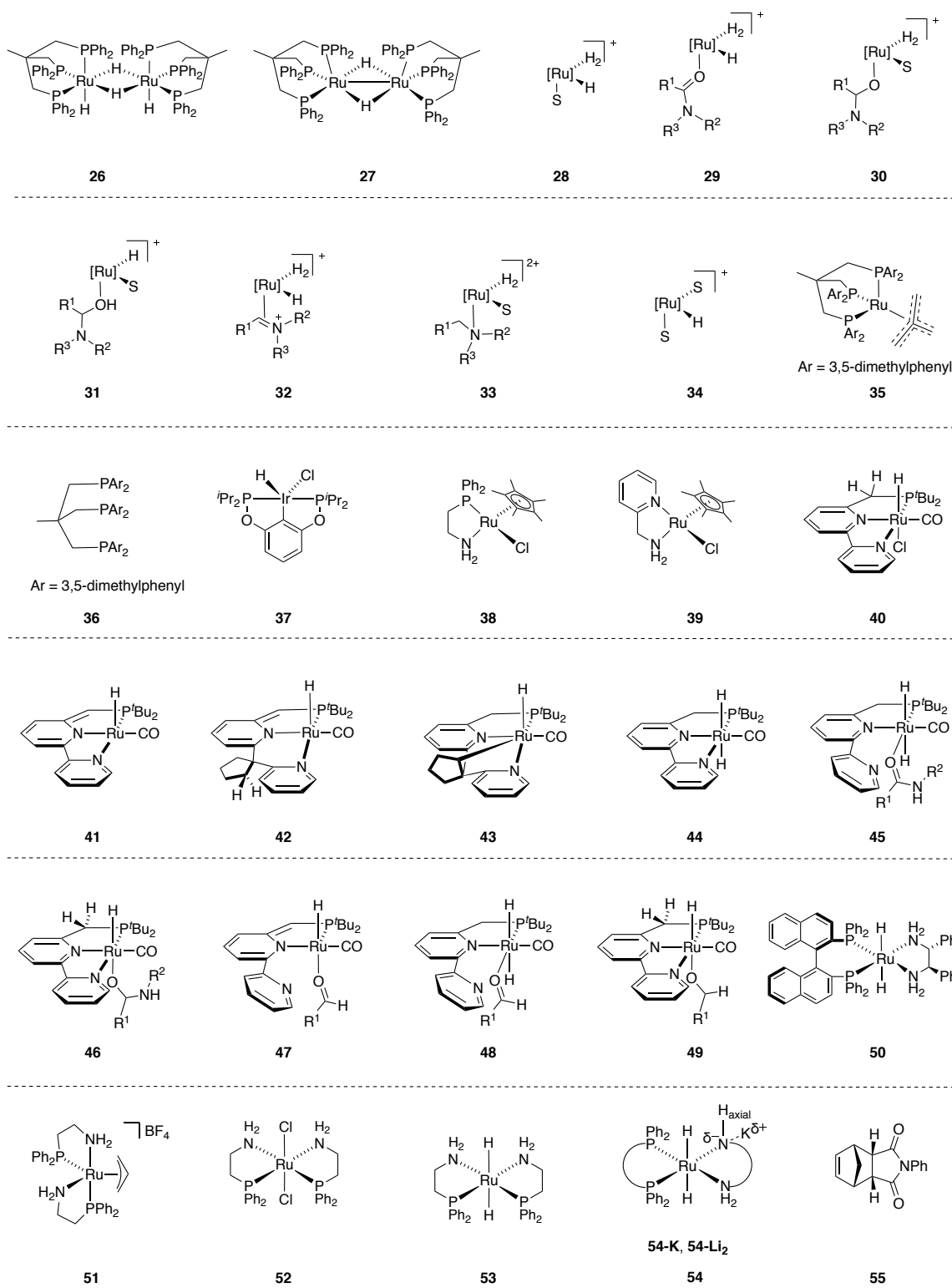
23

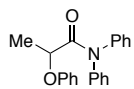


24

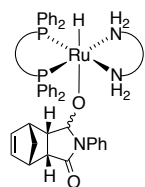


25

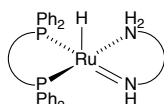




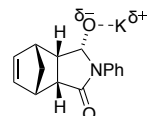
56



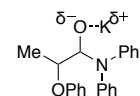
57



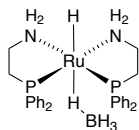
58



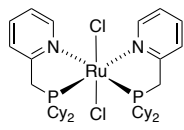
59



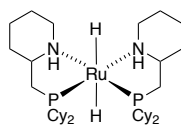
60



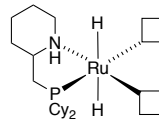
61



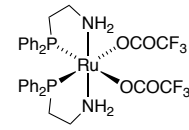
62



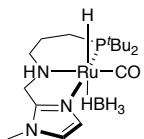
63



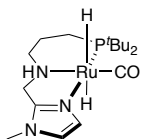
64



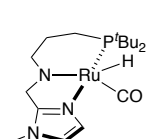
65



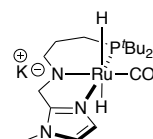
66



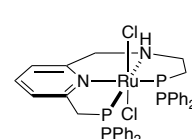
67



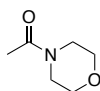
68



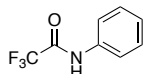
69



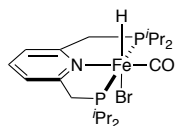
70



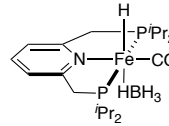
71



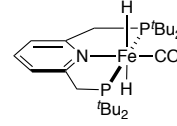
72



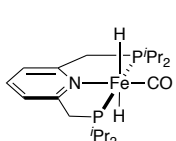
73



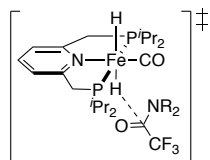
74



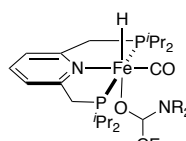
75



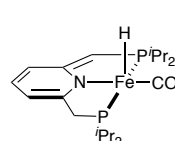
76



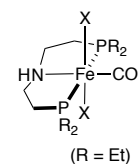
77



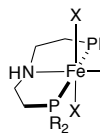
78



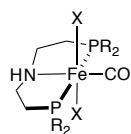
79



80

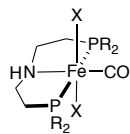
(R = *i*Pr)

81



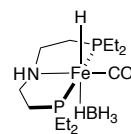
(R = Cy)

82

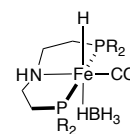


(R = Ph)

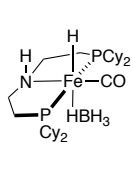
83



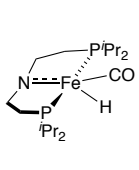
84

(R = *i*Pr)

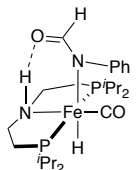
85



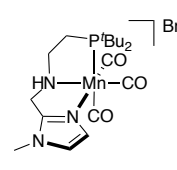
86



87



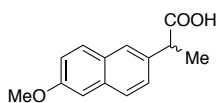
88



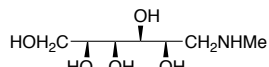
89

Mn(CO)₅Br

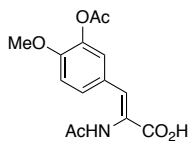
90



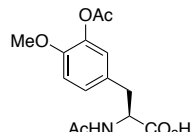
91



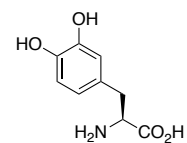
92



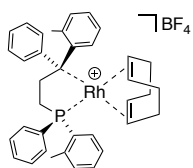
93



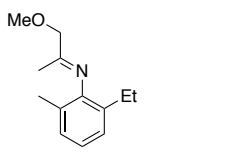
94



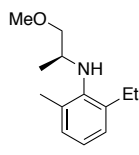
95



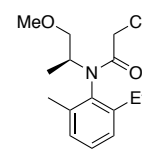
96



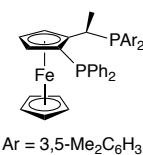
97



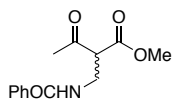
98



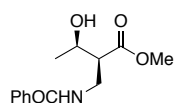
99



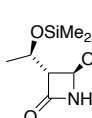
100

Ar = 3,5-Me₂C₆H₃

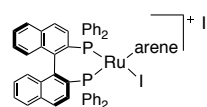
101



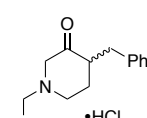
102



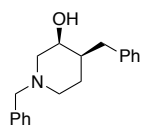
103



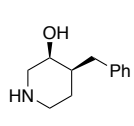
104



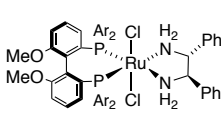
105



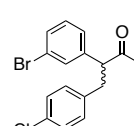
106



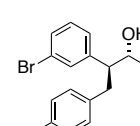
107



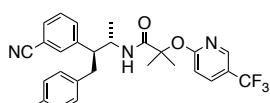
108

Ar = 3,5-ⁱPr₂C₆H₃⁻

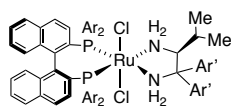
109



110



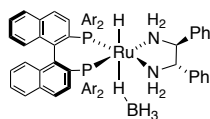
111



112

Ar = 3,5-MeC₆H₃
Ar' = 4-OMeC₆H₄

Chapter 2

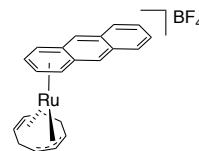


Ar = 3,5-MeC₆H₃

113



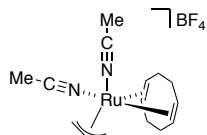
114



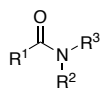
115



116

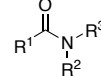


117



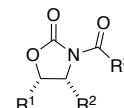
(118a-118f)

118



(119a-119h)

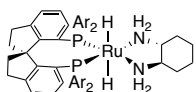
119



(120a, 120b)

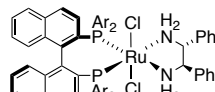
120

Chapter 3



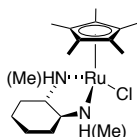
Ar = 3,5-Me₂-4-MeOC₆H₂
(DMM-SDP)

121

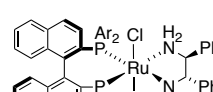


Ar = 3,5-Me₂C₆H₃

122

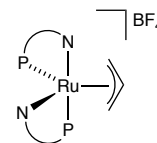


123

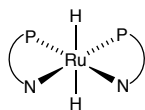


Ar = 3,5-Me₂C₆H₃

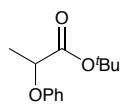
124



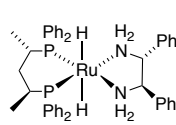
125



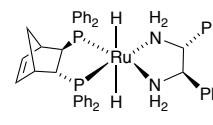
126



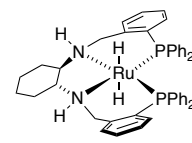
127



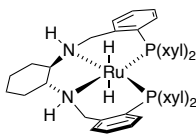
128



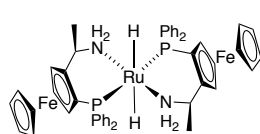
129



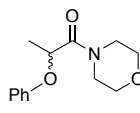
130



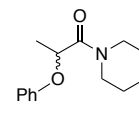
131



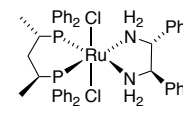
132



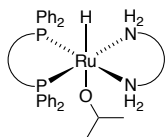
133



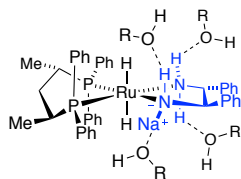
134



135

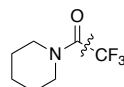


136

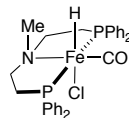


137

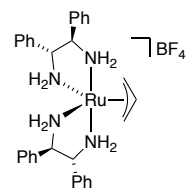
Chapter 4



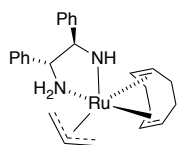
138



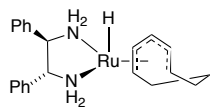
139



140



141



142